

Université du Québec
Institut National de la Recherche Scientifique
Centre Énergie, Matériaux et Télécommunications

**INVESTIGATION OF
CARBON NANOTUBE/5-ETHYLIDENE-2-NORBORNENE AS
MICRO-ENCAPSULATED HEALING AGENT FOR SELF-HEALING
EPOXY FOR AEROSPACE APPLICATIONS**

by

Hasna Hena Zamal

Dissertation submitted for the partial fulfillment of the requirements of the degree,
Doctor of philosophy, Ph.D.
in science of energy and materials

Jury d'évaluation

Director of Research

Federico Rosei
Professor, INRS-EMT, Université du Québec

President of the jury and
Internal Examiner

Andreas Ruediger
Professor, INRS-EMT, Université du Québec.

External Examiner

Marco Amabili
Professor, Department of Mechanical Engineering
McGill University

External Examiner

Fabio Cicoira
Professor, Department of Chemical Engineering
Polytechnique Montréal

ACKNOWLEDGEMENT

I would like to express my sincere gratitude to my supervisor Professor Federico Rosei for giving me the opportunity to pursue my PhD study under his supervision at Institut national de la recherche scientifique (INRS), University of Quebec, Quebec, Canada. His judicious guidance and supports have ensured my work to be of high quality. I would also like to express my gratitude to Dr. David Barba, for being very patient and kind and for his continuous guidance provided throughout the duration of my PhD studies.

I am also grateful to Dr. Brahim Aïssa for having shared his knowledge and idea, for arranging labs and facilities to start my initial research works and his continuous supports and guidance. His friendly guidance and expert advice have been invaluable throughout all stages of my work.

I would like to give thanks to Prof. Daniel Therriault and Dr. Emile Haddad for providing lab access for performing some of my research works at Polytechnique Montréal and MPB Technologies Inc., respectively. I would like to acknowledge funding from the Natural Science and Engineering Research Council (NSERC) of Canada, for a Collaborative Research and Development project in partnership with MPB.

I am also thankful to all NFL group members, lab technicians, administrative staffs, and all professors and students of EMT-INRS for their direct and indirect supports.

Special thanks are due to my soul mate, my dearest husband, Dr. Mohammad Asgar Khan who has been always there for me in every situation. There is no word to express my gratitude for his unconditional love, encouragement, patience, and support throughout my Ph.D. journey. I also want to express my pride and joy of my life, my son, Warsi Azam Khan and daughter Warisa Nastarin Khan's contribution for cheering me up every situation during my study when I downhearted.

Last but certainly not least, I would like to extend my appreciation to my parents; my father, Dr. Hame Zamal and my mother Shahanara Zamal for their emotional support and believing in me in all aspects of my education. Their prayer for me is what sustained me thus far.

Above all, I owe it all to Almighty Allah for granting me the wisdom, health, and strength to undertake this hard research task and enabling me to its completion.

ABSTRACT

Self-healing polymers based on ring-opening metathesis polymerization (ROMP) incorporating second generation Hoveyda-Grubbs' (HG2) catalyst as polymerization initiator and 5-ethylidene-2-norbornene (5E2N) as healing monomer are promising for self-healing applications. This is particularly true at low temperatures that may persist in the internal environment of an operating space vehicle. In this work, a detailed quantitative analysis of the ROMP reaction kinetics of 5E2N/HG2 system has been conducted from room temperature down to -30°C by using a systematic micro-Raman spectroscopy measurement. The analysis is based on measuring the changes in peak intensity and integrated area of Raman phonons related to the characteristic (C=C) functional groups indicating the progression of the reaction with time. The apparent rate constants for the reactions at different low temperatures were determined for the first order kinetics using the Arrhenius principle. The calculated values of the rate constants and activation energies are found consistent with values found in the literature for similar reactions. Our experiments and methodology were specifically designed to enable an efficient monitoring of the ROMP reaction below 0°C . This provides an opportunity for studying the effects of various factors on the polymerization kinetics of different self-healing system and optimizing them accordingly to make them suitable for specific applications.

Considering the recent interest in the use of carbon nanotubes in advanced polymers for enhancing their structural and electrical performance, microencapsulation of carbon nanotubes in a self-healing monomer like 5E2N can open unique opportunities to impart electro-mechanical self-healing functionalities to the mechanical structures and electronic parts/devices used in modern aerospace vehicles. In our work, we successfully microencapsulated multiwalled carbon nanotubes (referred simply as CNTs in this work) suspended in 5E2N into polymeric shells using *in-situ* polymerization method. To ensure their suitability for self-healing applications, the thermo-physical characteristics of the microcapsules, including their average size, shape, uniformity, shell wall structural integrity and thickness, thermal stability and core content are extensively investigated by optical and scanning electron microscopy as well as thermogravimetric (TGA) and differential scanning calorimetric (DSC) analyses. The presence of CNTs inside the core liquid content of the microcapsules, as well as their efficient release upon breaking event and the subsequent polymerization of the core monomers inside the damaged zone of the materials are confirmed by microscopy, spectroscopic and fractographic analyses.

Structural polymers like epoxy-based polymers are extensively used in various aerospace parts, structures, and devices. They, however, are subjected to various forms of damages under different loading conditions, which can accumulate over time leading to major structural failure. We report on a comparative investigation of the self-healing properties of epoxy-based polymer incorporated with microencapsulated CNT/5E2N under two different types of mechanical failure.

Healing efficiencies of the epoxy systems incorporated with the two types of microencapsulated healing agents (5E2N and CNT/5E2N) were evaluated and compared under lap shear and mode I fracture loading. When implemented the microcapsules inside epoxy, we demonstrated that excellent self-healing capabilities incurred by the epoxy polymer under these two different loading modes within the system containing CNT/5E2N microcapsules. For both lap shear mode and mode I fracture tests, the use of CNT/5E2N suspension inside the core of the microvessels is found to improve the properties of the pristine composites, as well as their healing properties much better than the case of microcapsules containing only 5E2N. 97% of the fracture toughness and 78% of the lap shear strength is restored with microencapsulated CNT/5E2N after their complete mechanical failure compared to 76% and 39%, respectively, with microencapsulated 5E2N alone. Our results suggest that epoxies incorporated with CNT/5E2N microcapsules can serve both as very efficient self-healable matrix material for implementation in high performance laminated composites and self-healable structural adhesives in advanced aerospace engineering.

When implemented inside conductive polymer, we also show that 82% of the electrical conductivity of the samples can also be autonomically restored using the CNT/5E2N microcapsules. This makes the CNT/5E2N healing agent suitable for self-healing applications for key aerospace structural parts as well as advanced electronic components and devices.

Keywords: Self-healing; polymerization; epoxy; microencapsulation; carbon nanotubes; aerospace; electrical conductivity; ROMP; fracture; adhesive

RÉSUMÉ

Les polymères auto-réparants à l'aide d'une polymérisation par ouverture de cycle par métathèse (ROMP, de l'anglais Ring-Opening Metathesis Polymerization) où les catalyseurs Hoveyda-Grubbs (HG2) de seconde génération jouent le rôle d'initiateur et les monomères d'éthylidène-5-norbornène-2 (5E2N) celui d'agents réparateurs, sont des matériaux très prometteurs. Ceci est particulièrement vrai à basse température, dans un environnement correspondant à celui rencontré à l'intérieur d'un véhicule spatial en opération. Cependant, pour pouvoir les rendre apte à des applications dans l'espace, il existe encore de nombreux obstacles à surmonter, tels que ceux associés aux effets de la température sur la cinétique de réaction ROMP et son efficacité. Dans ce travail, une étude quantitative détaillée de la cinétique de réaction ROMP de systèmes 5E2N/HG2 a été menée en recourant à la spectroscopie Raman, pour des températures comprises entre la température de la pièce et -30°C . Cette analyse repose sur l'observation de pics phononiques associés au groupe fonctionnel caractéristique des liaisons C=C, et la mesure de leurs variations d'intensité spectrales et de leur surface intégrée, qui révèlent la progression de la réaction chimique au fil du temps. En utilisant le principe d'Arrhenius, les coefficients de variations apparentes ont été déterminés pour chaque température de réaction donnée, au moyen d'une relation cinétique de premier ordre. Les valeurs extraites des taux de variation observés et des énergies d'activation correspondantes sont en accord avec celles rapportées dans la littérature pour des réactions similaires. Nos expériences et notre méthodologie ont été spécialement mis au point pour permettre un contrôle efficace la réaction ROMP en dessous de 0°C . Ceci nous a donné la possibilité d'étudier les effets de certains facteurs sur la vitesse de polymérisation au sein de différents systèmes auto-réparants, mais aussi de les optimiser en conséquent pour les adapter à des applications spécifiques.

Considérant l'intérêt actuellement suscité par l'utilisation de nanotubes de carbone dans la réalisation de polymères avancés afin d'augmenter leurs performances structurelles et électriques, la micro-encapsulation de nanotubes de carbone au sein de monomères auto-réparants comme le 5E2N peut potentiellement ouvrir de nouvelles voies technologiques très intéressantes, en conférant des propriétés d'auto-guérison électro-mécanique à des structures mécaniques et des équipements électroniques utilisés dans les véhicules aérospatiaux modernes. Dans notre travail, nous sommes parvenus à incorporer des nanotubes de carbone multi-parois (simplement notés CNTs dans la suite du texte) dans des micro-capsules contenant une solution de 5E2N liquide, enrobée d'une paroi en polymère, au moyen d'une méthode de polymérisation *in-situ*. Afin de s'assurer que ces matériaux étaient adaptés pour des applications

réelles, les caractéristiques thermo-physiques de ces micro-capsules, incluant leurs tailles moyennes, formes, uniformités, l'intégrité structurelle et l'épaisseur de leurs parois, leur stabilité thermique et la nature de leur contenu ont été étudiés de manière intensive, en recourant aux techniques de microscopies optique et électronique, ainsi qu'aux analyses thermogravimétriques (TGA) et par calorimétrie différentielle à balayage (DSC). La présence de CNTs à l'intérieur du cœur liquide des microcapsules, leur dispersion effective une fois la paroi de la microcapsule déchirée, ainsi que leur capacité à se polymériser rapidement ont pu être constatés par analyses microscopiques, spectroscopiques et fracto-graphiques.

Les polymères à base d'époxy servent à la fois de matériau matriciel aux composites laminés et d'adhésif ultra-performant dans les jointures collées, qu'on retrouve dans les pièces, structures et dispositifs employés dans l'industrie aérospatiale. L'époxy peut être sujet à plusieurs types d'endommagement, dépendamment des contraintes subies par le matériau, lesquels peuvent s'accumuler avec le temps jusqu'à entraîner une défaillance complète du système. Nous présentons une étude comparative des propriétés d'auto-guérison de polymères à base d'époxy auxquels des micro-capsules contenant un mélange CNT/5E2N ont été intégrés, pour deux différentes catégories de bris mécanique.

Le rétablissement de systèmes dans lesquels ont été incorporées des capsules à base d'agents 5E2N et CNT/5E2N a été évalué et comparé sous l'effet d'un cisaillement laminaire et d'une charge de rupture verticale (mode I). Une fois les micro-capsules introduites dans l'époxy, nous démontrons que le système contenant des micro-capsules de CNT/5E2N possède d'excellentes capacités auto-curatives pour chacune de ces contraintes. Pour les tests effectués en mode de cisaillement laminaire et de charge de rupture verticale, l'utilisation d'un mélange CNT/5E2N à l'intérieur de micro-réservoir permet d'augmenter la résistance naturelle du milieu, ainsi que ses propriétés auto-réparatrices, bien mieux qu'en utilisant seulement un agent de 5E2N. Après rupture complète, 97% de la ténacité et 78% de la résistance au cisaillement du système sont restaurés avec des micro-capsules de CNT/5E2N, contre seulement 76% et 39% avec des micro-capsules de 5E2N. Nos résultats suggèrent qu'en ingénierie spatiale avancée, un polymère structurel tel que celui réalisé à base d'époxy contenant des micro-capsules de CNT/5E2N peut servir à la fois de matrice auto-réparante très efficace dans les composites laminés de haute performance et de structure réparante adhésive dans les jointures collées.

Lorsqu'elles sont employées dans les polymères conducteurs, nous montrons aussi que 82% de la conductivité électrique des échantillons est restituée de manière autonome à l'aide des micro-capsules de CNT/5E2N. Ce résultat fait du mélange CNT/5E2N un agent auto-réparateur adapté

pour une utilisation au sein de structures aérospatiales principales, ainsi qu'à l'intérieur de composants et de dispositifs électroniques avancés.

Mots-clés : Auto-réparants; polymérisation; epoxy ; microencapsulation ; nanotubes de carbone ; aérospatial; conductivité électrique; ROMP; fracture; adhésif

TABLE OF CONTENTS

ACKNOWLEDGEMENT	II
ABSTRACT	III
RÉSUMÉ	V
TABLE OF CONTENTS	VIII
LIST OF FIGURES	XI
LIST OF TABLES	XV
LIST OF ABBREVIATIONS	XVI
CHAPTER 1: INTRODUCTION, OBJECTIVES AND METHODOLOGY	1
1.1 INTRODUCTION.....	1
1.2 OBJECTIVES	4
1.3 METHODOLOGY.....	4
1.4 CHALLENGES	8
1.5 DISSERTATION ORGANIZATION	10
CHAPTER 2: BACKGROUND AND LITERATURE REVIEW	13
2.1 BACKGROUND AND SELF-HEALING APPROACHES OF POLYMERS	13
2.2 SELF-HEALING DESIGN WITH VASCULAR NETWORK	15
2.3 SELF-HEALING WITH MICROCAPSULES	21
2.3.1 <i>Choice of healing agents for the recovery of mechanical properties</i>	22
2.3.2 <i>General characteristics and chemical configurations of DCPD and 5E2N</i>	27
2.3.3 <i>Comparison of DCPD and 5E2N as healing agents</i>	28
2.3.4 <i>Comparison of rheological properties of DCPD Vs ENB</i>	29
2.3.5 <i>Comparison of heat flow characteristics of DCPD Vs ENB</i>	33
2.3.6 <i>Suggestions to improve the properties of ROMP-active healing agents</i>	34
2.3.7 <i>Microencapsulation of healing agent monomers and the desired characteristics of the microcapsules</i>	35
2.3.8 <i>Factors affecting the microencapsulation process and the quality of microcapsules</i>	41
2.3.9 <i>Choice of catalyst</i>	43
2.3.10 <i>Comparative evaluation of Ruthenium catalysts</i>	44
2.4 RESTORATION OF MECHANICAL PROPERTIES OF MATERIALS USING MICROCAPSULES AND EVALUATION OF HEALING EFFICIENCIES	48
2.5 RESTORATION OF ELECTRICAL PROPERTIES OF MATERIALS USING MICROCAPSULES.....	53
CHAPTER 3: INVESTIGATION OF THE POLYMERIZATION KINETICS OF 5E2N INITIATED BY HG2 CATALYST AT LOW TEMPERATURES USING MICRO-RAMAN SPECTRAL ANALYSIS	57
3.1 APPLICATIONS AND ADVANTAGES OF RAMAN SPECTROSCOPY FOR OUR INVESTIGATION	57

3.2 ROMP REACTION OF 5E2N	58
3.3 EXPERIMENTAL	61
3.3.1 <i>Materials</i>	61
3.3.2 <i>Equipment and methods</i>	61
3.4 RESULTS AND DISCUSSION	62
3.4.1 <i>Identification of the key Raman phonon peaks</i>	62
3.4.2 <i>Monitoring the ROMP reaction of 5E2N</i>	64
3.4.3 <i>Determination of the kinetic parameters of the reaction</i>	66
3.5 CONCLUDING REMARKS	69
CHAPTER 4: MICROENCAPSULATION OF CNT/5E2N SUSPENSION, THEIR CHARACTERIZATION AND RECOVERY OF ELECTRICAL CONDUCTIVITY	71
4.1 INTRODUCTION.....	71
4.2 EXPERIMENTAL	72
4.2.1 <i>Materials</i>	72
4.2.2 <i>Fabrication of microcapsules</i>	72
4.2.3 <i>Characterization</i>	73
4.2.4 <i>Fabrication of self-healing polymer samples for electrical conductivity restoration tests</i>	74
4.2.5 <i>Measurement principle and determination of self-healing efficiency:</i>	75
4.3 RESULTS AND DISCUSSION	76
4.3.1 <i>Fabrication of microcapsules</i>	76
4.3.2 <i>Microscopic investigations</i>	79
4.3.3 <i>Thermal stability analysis</i>	82
4.3.4 <i>Qualitative analysis of the core suspension of the microcapsules</i>	83
4.3.5 <i>Restoration of electrical conductivity</i>	84
4.4 CONCLUDING REMARKS	86
CHAPTER 5: FAILURE ANALYSIS OF SELF-HEALING EPOXY USING MICROENCAPSULATED CNT/5E2N	87
5.1 EVALUATION OF MECHANICAL SELF-HEALING OF EPOXY	87
5.2 EXPERIMENTAL	88
5.2.1 <i>Materials, procedures, and equipment</i>	88
5.2.2 <i>Preliminary investigation of the effects of CNTs on the ROMP products of 5E2N</i>	89
5.2.3 <i>Production of microcapsules and preparation of epoxy mixtures</i>	90
5.2.4 <i>Preparation of adhesive joint samples and lap shear test</i>	91
5.2.5 <i>Preparation of TDCB samples and mode I fracture test</i>	94
5.3 RESULTS AND DISCUSSION	98
5.3.1 <i>Preliminary investigation of the effects of CNTs on the mechanical properties of poly (CNT/5E2N)</i>	98

5.3.2 <i>Microcapsules</i>	101
5.3.3 <i>Results and analysis of lap shear and mode I fracture tests</i>	102
5.4 CONFIRMATION OF SELF-HEALING PROCESS AND CONTRIBUTION OF CNTs.....	107
5.5 CONCLUDING REMARKS.....	112
CHAPTER 6: CONCLUSIONS, PERSPECTIVES AND RECOMMENDATIONS FOR FUTURE WORKS	113
6.1 CONCLUSIONS AND PERSPECTIVES	113
6.2 RECOMMENDATIONS FOR FUTURE WORKS	117
AUTHOR CONTRIBUTIONS.....	118
REFERENCES.....	120
ANNEX.....	133
SOMMAIRE RÉCAPITULATIF.....	137

LIST OF FIGURES

FIGURE 2.1	EXTRINSIC SELF-HEALING APPROACH BASED ON MICROCAPSULES CONTAINING A LIQUID SUSPENSION OF CNT/5E2N.	14
FIGURE 2.2	SCHEMATIC OF SELF REPAIRING STRATEGY FOR POLYMER MATRIX WITH HOLLOW TUBES/FIBERS [62]	16
FIGURE 2.3	ROBOTIC DEPOSITION OF A FUGITIVE ORGANIC INK THROUGH A NOZZLE ONTO A MOVING X-Y STAGE, B) 3D MICROVASCULAR NETWORK SCAFFOLD (BLUE) WITH VERTICAL SPIRAL TOWER STRUCTURE (YELLOW) EMBEDDED INTO IT [72].	17
FIGURE 2.4	SELF-HEALING COATING-SUBSTRATE STRUCTURE AFTER CRACKS ARE FORMED IN THE COATING REVEALING THE PRESENCE OF EXCESS HEALING LIQUID ON THE COATING SURFACE [71].	17
FIGURE 2.5	HOLLOW CHANNELS BUILT IN FRPC BY A 'LOST-WAX- TYPE PROCESS USING LOW MELTING SOLDER WIRE PREFORM [80].	19
FIGURE 2.6	SCHEMATIC DIAGRAM OF GLASS FIBER PREFORM WOVEN INTO A 3D STRUCTURE. SACRIFICIAL PLA FIBERS ARE SHOWN IN RED [82].	19
FIGURE 2.7	CHEMICAL STRUCTURE OF ENDO-DCPD [15].	27
FIGURE 2.8	5-ETHYLIDENE-2-NORBORNENE [17]	28
FIGURE 2.9	EVOLUTION OF STORAGE MODULUS WITH CURE TIME FOR UNREACTED SAMPLES WITH CATALYST OF 1.0 WT% FOR DCPD AND 0.1 WT.% FOR ENB (DIRECT MIXING) [17].	30
FIGURE 2.10	EVOLUTION OF STORAGE MODULUS WITH CURE TIME AT RT FOR DIFFERENT ROMP ACTIVE MONOMERS WITH CATALYST PARTICLES EXPOSED TO THE EPOXY FILM SURFACE (INDIRECT MIXING METHOD REPRESENTING REAL APPLICATION SCENARIO) [131]	32
FIGURE 2.11	DSC THERMOGRAMS OF DCPD AND 5E2N FOR SAMPLES CURED FOR 5 MIN AT ROOM TEMPERATURE WITH DIFFERENT AMOUNT OF G1 CATALYST [17].	33
FIGURE 2.12	GENERAL PROCESS OF MICROENCAPSULATION OF A HYDROPHOBIC CORE BY <i>IN-SITU</i> POLYMERIZATION OF UREA AND/OR MELAMINE AND FORMALDEHYDE.	37
FIGURE 2.13	SURFACE MORPHOLOGY AND SHELL THICKNESS OF UF MICROCAPSULES [133]	40
FIGURE 2.14	MEAN DIAMETER OF THE MICROCAPSULES VS AGITATION SPEED [133]	43
FIGURE 2.15	TAPERED DOUBLE-CANTILEVER BEAM (TDCB) GEOMETRY (DIMENSIONS IN MM) [12].	48
FIGURE 2.16	TYPICAL LOAD-DISPLACEMENT CURVE FOR THE FRACTURE TESTS OF TDCB EPOXY SAMPLES FOR DETERMINING HEALING EFFICIENCY [12].	49

FIGURE 2.17	EFFECTS OF AVERAGE DIAMETER OF MICROCAPSULES CONTAINING DCPD ON FRACTURE TOUGHNESS OF EPOXY AND THE HEALING EFFICIENCY [12].....	51
FIGURE 2.18	EFFECTS OF MICROCAPSULE CONCENTRATION CONTAINING DCPD ON INITIAL (VIRGIN) AND HEALED FRACTURE TOUGHNESS OF EPOXY [12].....	52
FIGURE 2.19	AUTONOMIC CONDUCTIVITY RESTORATION CONCEPT USING MICROENCAPSULATED GA-IN LIQUID METAL ALLOY [99]	53
FIGURE 2.20	OPTICAL MICROGRAPH OF MICROCAPSULES CONTAINING SWCNT (0.05 WT%) SUSPENDED IN EPA [168]	54
FIGURE 2.21	EXPERIMENTAL SETUP SHOWING PROBE TIPS SUBMERGED INTO THE SOLUTION DROPLET CONTAINING SWCNT. (B) CURRENT–VOLTAGE PLOTS SHOWING CONDUCTIVITY MEASUREMENTS OF SOLUTIONS OF CAPSULES CONTAINING SWCNT IN EPA [168]	55
FIGURE 3.1	ROMP REACTION OF 5E2N AT THE PRESENCE OF HG2 CATALYST.....	59
FIGURE 3.2	A) SCHEMATIC OF THE <i>IN-SITU</i> OBSERVATION OF THE ROMP REACTION OF 5E2N INITIATED BY HG2 CATALYST BY RAMAN SPECTROSCOPY. B) RAMAN SPECTROMETER EQUIPPED WITH A THERMOELECTRICALLY COOLED CCD (CHARGE COUPLED DEVICE). COOLING STAGE EQUIPPED WITH LIQUID NITROGEN IS USED TO MAINTAIN THE DESIRED TEMPERATURE FOR THE REACTION. C) SAMPLE IS PLACED INSIDE THE COOLING STAGE.	61
FIGURE 3.3	RAMAN SPECTRA RECORDED FOR THE REACTANT 5E2N MONOMER AND DURING THE POLYMERIZATION REACTION.	63
FIGURE 3.4	RAMAN SPECTROSCOPIC OBSERVATION OF THE EVOLUTION OF THE POLYMERIZATION REACTION OF 5E2N ACTIVATED BY HG2 CATALYST AT -30°C.	64
FIGURE 3.5	SPECTRAL DECONVOLUTION OF THE RAMAN SIGNAL BETWEEN 1635 AND 1705 cm^{-1}	65
FIGURE 3.6	CHANGES IN THE NORMALIZED PEAK INTENSITIES WITH TIME FOR EACH POLYMERIZATION TEMPERATURE	67
FIGURE 3.7	ARRHENIUS PLOT CORRELATING THE APPARENT RATE CONSTANTS WITH ABSOLUTE REACTION TEMPERATURES FOR THE ROMP REACTION OF 5E2N/HG2.	68
FIGURE 4.1	ELECTRICAL CIRCUITS MADE WITH CONDUCTIVE SILVER/EPOXY INCORPORATED WITH MICROCAPSULES CONTAINING CNT/5E2N AND GRUBBS' CATALYST FOR THE ELECTRICAL CONDUCTIVITY RESTORATION TEST. BRIDGE VOLTAGES WERE MEASURED FOR THE NEAT (NO MICROCAPSULES) AND SELF-HEALING SAMPLES (WITH MICROCAPSULES) WITH A) AND C) UN CUT CONDUCTIVE PATH; AND B) AND D) CUT BETWEEN POINT 1 AND 2 AND AFTER ALLOWING FOR HEALING FOR 24 HOURS.....	74
FIGURE 4.2	CIRCUIT DIAGRAM OF THE WHEATSTONE BRIDGE, THE SAMPLES WERE CONNECTED IN THE POSITION OF THE R3 RESISTOR [99]	75

FIGURE 4.3	PROCESS FLOW CHART FOR SUCCESSFUL MICROENCAPSULATION OF CNT/5E2N IN PMUF SHELLS. THE PROCESS IS ADAPTED FROM REF [20]	77
FIGURE 4.4	CNT/5E2N SUSPENSION A) RIGHT AFTER THE SONICATION AND B) AFTER 1 MONTH	78
FIGURE 4.5	(A) FREE FLOWING MICROCAPSULES OBSERVED UNDER OM (5X). (B) RELEASED CNT PARTICLES (ENCIRCLED) AS OBSERVED ON THE GLASS SLIDE AFTER CRUSHING THE MICROCAPSULES (OM 50X). THE INSET SHOWS THE HIGH MAGNIFICATION (25000X) IMAGE OF CNTs RELEASED.	79
FIGURE 4.6	SEM OBSERVATIONS OF (A) INDIVIDUALLY SEPARATED SPHERICAL MICROCAPSULES (B) SHELL THICKNESS (C) CORE-SHELL STRUCTURE (D) CNTs INSIDE THE CORE OF THE MICROCAPSULES.	80
FIGURE 4.7	TYPICAL DISTRIBUTION OF SIZES OF MICROCAPSULES.	81
FIGURE 4.8	TEM OBSERVATION OF CNTs IN THE CORE LIQUID OF THE MICROCAPSULES.	82
FIGURE 4.9	A) COMPARISON OF WEIGHT LOSS VS. TEMPERATURE IN TGA FOR MICROCAPSULES CONTAINING LIQUID 5E2N ONLY, AND MICROCAPSULES CONTAINING CNT/5E2N SUSPENSION WITH 0.1 WT. % CNTs. B) COMPARISON OF HEAT FLOW VS. TEMPERATURE OF LIQUID 5E2N AND CNT/5E2N SUSPENSION WITH 0.1 WT.% CNTs IN DSC	82
FIGURE 4.10	COMPARISON OF RAMAN SPECTRA GENERATED FOR THE CORE LIQUID EXTRACTED FROM 5E2N MICROCAPSULES AND CNT/5E2N MICROCAPSULES, BEFORE (A) AND AFTER (B) POLYMERIZATION.	84
FIGURE 4.11	COMPARISON OF THE RESTORATION OF ELECTRICAL CONDUCTIVITY OF THE DAMAGED CONDUCTIVE POLYMER SAMPLES WITH AND WITHOUT CNT/5E2N MICROCAPSULES.	85
FIGURE 5.1	SINGLE LAP JOINT CONFIGURATION USED IN EXPERIMENT [218]	91
FIGURE 5.2	ARRANGEMENTS (NOT TO THE SCALE) FOR THE PREPARATION OF LAP SHEAR SAMPLES TO ENSURE UNIFORM BONDLINE THICKNESS IN THE SAME BATCH.	92
FIGURE 5.3	EXPERIMENTAL SET-UP FOR SINGLE LAP SHEAR TEST	93
FIGURE 5.4	A) TAPERED DOUBLE-CANTILEVER BEAM (TDCB) GEOMETRY (DIMENSIONS IN MM), [12] B) PLACEMENT OF HEALING AGENTS AND LOADING DIRECTION RELATIVE TO PRE-CRACK.	95
FIGURE 5.5	A) A CURED SELF-HEALING TDCB EPOXY SAMPLE INCORPORATED WITH MICROCAPSULES AND CATALYST AT THE MID-REGION, AND B) LOADING OF THE SAMPLE FOR THE MODE I FRACTURE TEST	96
FIGURE 5.6	CURING AND ESTIMATION OF T _g OF EPOXY SAMPLES.	98
FIGURE 5.7	EFFECT OF CNT CONCENTRATION (WT. %) ON THE HARDNESS OF POLY (CNT/5E2N) PRODUCED BY ROMP REACTION INITIATED BY HG ₂ . THE LINE IS A GUIDE TO THE EYE.	99
FIGURE 5.8	REPRESENTATIVE LOAD-DISPLACEMENT CURVES FOR THE POLY (CNT/5E2N) SAMPLES CONTAINING DIFFERENT CONCENTRATIONS OF CNTs (0.05, 0.10 AND 0.20 WT.%)	100

FIGURE 5.9 SEM MICROGRAPHS OF THE TWO TYPES OF MICROCAPSULES, CONTAINING 5E2N MONOMER ONLY: A) 100X, B) 500X; CONTAINING A SUSPENSION OF CNT/5E2N: C) 100X AND D) 500X, CNTs AT THE SURFACE OF THE MICROCAPSULES SHOWN IN THE INSET..... 101

FIGURE 5.10 (A) REPRESENTATIVE LOAD-DISPLACEMENT CURVES OBTAINED BY LAP SHEAR TESTS CONDUCTED ON LS (R), LS (5E2N) AND LS (CNT/5E2N) SAMPLES, AND (B) MODE I FRACTURE TESTS CONDUCTED ON TDCB (R), TDCB (5E2N) AND TDCB (CNT/5E2N) SAMPLES..... 103

FIGURE 5.11 AVERAGE LAP SHEAR STRENGTHS OF THREE TYPES OF SAMPLES IN (A) FIRST LOADING AND (B) SECOND LOADING (AFTER HEALING)..... 104

FIGURE 5.12 ENHANCEMENTS OF ORIGINAL MECHANICAL RESISTANCE [$\Delta T_v(\%)$ AND $\Delta [K_{Ic}]_v(\%)$] DUE TO THE INCORPORATION OF TWO TYPES OF MICROCAPSULES (5E2N-ONLY AND CNT/5E2N MICROCAPSULES) INTO THE LAP SHEAR AND TDCB SAMPLES. 105

FIGURE 5.13 COMPARISON OF HEALING EFFICIENCIES OF THE FOUR TYPES OF HEALED SAMPLES, LS (5E2N) (EPOXY ADHESIVE SAMPLES CONTAINING 5E2N-ONLY MICROCAPSULES), LS (CNT/5E2N WITH 0.1 WT.% CNT) (EPOXY ADHESIVE SAMPLES CONTAINING CNT/5E2N MICROCAPSULES), TDCB (5E2N) (TDCB EPOXY SAMPLES CONTAINING 5E2N-ONLY MICROCAPSULES) AND TDCB (CNT/5E2N WITH 0.1 WT.% CNT) (TDCB EPOXY SAMPLES CONTAINING CNT/5E2N MICROCAPSULES)..... 107

FIGURE 5.14 REPRESENTATIVE SEM MICROGRAPHS OF THE FRACTURE SURFACE OF THE SELF-HEALED SAMPLES, (A) LAP SHEAR SAMPLE AND (B) TDCB SAMPLE. THE PRESENCE OF A SELF-HEALED POLYMER LAYER (POLY-5E2N) IS HIGHLIGHTED IN BLUE..... 108

FIGURE 5.15 (A) REPRESENTATIVE RAMAN SPECTRA GENERATED BY THE FRACTURE SURFACE OF THE SELF-HEALED EPOXY SAMPLES. (B) PRESENCE OF CNTs AT THE FRACTURE SURFACE ARE INDICATED BY ARROWS AND SHOWN IN THE INSET, WITH MAGNIFICATION OF 50000X. THE INSET SHOWS A SLIGHT SHIFT OF G-BAND OF THE CNTs 109

FIGURE 5.16 REPRESENTATIVE SEM MICROGRAPH OF FRACTURE SURFACE OF TDCB SAMPLES AFTER THE MODE I FRACTURE TEST. CNT AGGREGATES AT THE FRACTURE SURFACE ARE SHOWN IN THE INSET. PRESENCE OF CRACK-TAILS INDICATE CRACK PINNING MECHANISM OF TOUGHENING BY THE CNT AGGREGATES. 111

LIST OF TABLES

TABLE 2.1	OVERVIEW OF THE WORKS FOR THE MECHANICAL RECOVERY OF EPOXY-BASED HOST MATERIALS FOR DIFFERENT MICROENCAPSULATED HEALING AGENT SYSTEMS	24
TABLE 3.1	SATURATION TIMES FOR THE REACTION AT DIFFERENT TEMPERATURES.....	66
TABLE 4.1	CONTROLLING PARAMETERS FOR SUCCESSFUL MICROENCAPSULATION OF CNT/5E2N	79

LIST OF ABBREVIATIONS

<u>Acronym</u>	<u>Description</u>
5E2N	5-Ethylidene-2-Norbornene
BHT	Butylated hydroxytoluene
CNTs	(Multiwalled) Carbon Nanotubes
CCD	Charge-coupled device
DCPD	Dicyclopentadiene
DSC	Differential scanning calorimetry
DETA	Diethylenetriamine
DMA	Dynamic mechanical analysis
EPA	Ethyl phenylacetate
EMA	Ethylene maleic anhydride
FRPC	Fiber reinforced polymer composites
FESEM	Field emission scanning electron microscope
G1	First-generation Grubbs' catalyst
G2	Second-generation Grubbs' catalyst
GMA	Glycidyl methacrylate
G'	Storage modulus
HG1	First-generation Hoveyda-Grubbs' catalyst
HG2	Second generation Hoveyda-Grubbs' catalyst
ILSS	Inter laminar shear strength
IPDI	Isophorone diisocyanate
MNC	Methyl 5-norbornene-2- carboxylate
Nicl ₂	Imidazole
NMR	Nuclear magnetic resonance

OCP	Open circuit potential
PMUF/MUF	(Poly) melamine urea formaldehyde
PVA	Poly vinyl alcohol
PhCl	Chlorobenzene
PLA	Poly lactide
P3HT	3- hexylthiophene-2, 5-diyl
RT	Room temperature
ROMP	Ring opening metathesis polymerization
SEM	Scanning electron microscope
SDS	Sodium dodecyl sulphate
SWCNT	Single walled carbon nanotube
SLS	Sodium lauryl sulphate
TETA	Triethylenetetramine
TEM	Transmission electron microscope
TDCB	Tapered double cantilever beam
T _g	Glass transition temperature
TGA	Thermogravimetric analysis
UF	Urea formaldehyde
VaSC	Vaporisation of sacrificial components

CHAPTER 1: INTRODUCTION, OBJECTIVES AND METHODOLOGY

1.1 Introduction

Polymers, specially, the epoxy-based materials and their composites are used in key structures and devices and serve many useful functions in modern civil and military applications ranging from civil infrastructure to aerospace, automotive and electronics applications. Examples of their applications include in geostationary satellites, space modules and spacecrafts, fuselage, and wings of modern passenger airplane models like Boeing 787, airbus 380 etc. [1-3] [4]. Further, the environment in which they are operated may subject them to very low temperatures (down to -150°C) such as in space or in the colder regions of the earth. During their operations, the parts of the airplanes and spacecrafts made of these materials are also subjected to damage which can be caused by various mechanical loadings, collisions with space debris or any foreign objects (like bird strikes) or other environmental factors like thermal cycling. One of the major concerns for the parts made of epoxies and their composites is that even a minor damage or microcracks in the internal sites of these materials can seriously compromise [5] their structural integrity, intended functionalities and performance. The microcracks in the epoxies can propagate during the operation and it can ultimately lead to failure of the parts if those minor cracks are not repaired in due time.

Proper real time detection of these minor, and often hidden damage in epoxies and their manual on-site repair is often immensely difficult and expensive. This is mainly due to the lack of access to the internal damage sites of the parts and the limitations associated with the current available damage detection technologies. The remote locations of the parts, such as in space or at the high altitudes (for the airplanes) also make them extremely difficult for manual on-site repair of the damage. One of the smart solutions can be to self-heal those minor damage without requiring any manual intervention. Technically, the self-healing of the epoxies should also be capable of being carried out at their exposed low temperatures prevailing in their operating environment.

Any material, when subjected to some form of damage, loses some of its original properties such as its strength, toughness, structural integrity and electrical conductivity. Self-healing is a process through which a damaged material can undergo total or partial repair to restore its original properties and functionalities after degradation due to its ageing or accidental events [6-8]. Conceptually, the self-healing ability is quantified by 'self-healing efficiency', which provides the

percentage value of the physical property lost by the material that can be successfully restored through the self-healing process. Self-heal capability of epoxies used in modern space and aerospace structures and devices can mitigate the difficulties, complexities and higher costs associated with remote repair of different types of damage. Self-healing functionality of epoxies at their operating environment can also ensure the safety and the reliability of advanced equipment and extend thereby their lifetime functioning.

The concept of self-healing polymers includes healing reagents stored in micro storage vessels (microcapsules) which are embedded into the polymeric materials. This class of materials has been widely studied after the pioneering work of White and Sottos [9], who showed the efficient recovery of the mechanical properties of structural epoxy by using microencapsulated liquid Dicyclopentadiene (DCPD) monomers as healing agent. The monomer is capable of undergoing ring opening metathesis polymerization (ROMP) reaction initiated by the Ruthenium Grubbs catalyst [10]. The invention of the Ruthenium Grubbs catalysts capable of undergoing different types of metathesis reactions, by Grubbs and co-workers [11] (which led them to the awarding of Nobel Prize in 2005), opened and advanced a wide variety of applications in the field of polymer chemistry including self-healing.

Several early works [9, 12-14], demonstrated recovery of fracture toughness of epoxy samples incorporated with first-generation Grubbs' catalyst (G1) and microcapsules containing DCPD. Up to 85% mechanical healing efficiency was demonstrated for the samples incorporated with 5-20 wt.% microcapsules with 2.5-5 wt.% of G1 with a healing time of 48h at RT (room temperature). However, for practical applications, there are few obstacles with the DCPD/Grubbs' healing agents' system that need to be addressed.

Firstly, long period of healing time, such as 48h in the above works, is not desirable. This is because, in the meantime, damage may propagate further with continuous operation of the part. The DCPD monomer released from the broken microcapsules, during the long period of healing time, can also evaporate or diffuse into the matrix reducing its self-healing effectiveness.

Secondly, the requirement of large amount of catalyst, up to 5 wt.% in the above works, for effective healing is also not desirable [15]. Dispersion of large amount of catalyst into the epoxies may degrade their virgin/original properties. Further, Ruthenium is scarce in nature and as such, Ruthenium catalysts are expensive. Thus, it is essential to develop healing agents that can react much faster with low catalyst requirements [15, 16].

Finally, the freezing point of DCPD is around 15°C [17] which strongly limits its use at low temperatures where aerospace vehicles often operate [18].

Such constraints of DCPD prompts for the investigation of alternative healing agent monomers that can be microencapsulated suitably for various self-healing applications. 5 ethylidene-2-nobornone (5E2N) is one of them which has a freezing point around -80°C [19]. It undergoes a much faster ROMP reaction with the Grubbs catalyst (of the order of few seconds at room temperature) with much less catalyst loading (as low as 0.1 wt.%) compared to DCPD, [17] this makes it an attractive alternative healing agent candidate especially suitable for aerospace applications at low temperatures.

5E2N monomer alone is microencapsulated into poly melamine urea formaldehyde (PMUF) shells using *in-situ* polymerization technique [17, 20]. However, unlike DCPD, 5E2N produces a mechanically weaker polymer upon ROMP reaction which limits its ability to significantly recover the mechanical properties of the self-healing epoxies. The incorporation of carbon nanotubes into 5E2N has been suggested to overcome this drawback [19]. To this end, in this work, we aim to microencapsulate multi-walled carbon nanotubes (CNTs) dispersed in 5E2N and investigate the microencapsulated CNT/5E2N suspension as healing agent for epoxy with self-healing electro-mechanical properties for aerospace applications.

Apart from mechanical strengths of epoxies, polymers in general can become suitable for advanced electronic applications by imparting appropriate electrical properties to them. A small amount of CNTs (0.1 - 6 wt.%) in epoxies was found to significantly increase their mechanical strength and shear modulus [21-23], as well as their electrical conductivity by several orders of magnitude [24], and their thermal conductivity by up to 300% [25-29]. In addition to making polymers more resistant mechanically [30-37], the integration of CNTs [28, 32, 34, 38-40], into polymers can also be used to improve the overall electrical conductivity of the polymer structures, act as sensors for monitoring damages [41, 42], improve effective lifetime of high performance batteries [43] or develop innovative electronic devices, such as circuits printed on flexible sheets [44]. As such, the successful microencapsulation of CNT/5E2N, instead of 5E2N monomer alone, can not only overcome its limitation of forming weaker polymer for mechanical self-healing, it can also impart additional electrical self-healing functionalities to the conductive polymer by restoring its electrical network after complete failure. Incorporation of CNT/5E2N microcapsules in epoxies can thus make them suitable for efficient recovery of either or both mechanical and electrical properties after damage, even at low temperatures. The successful microencapsulation

of CNTs dispersed in a self-healing monomer, such as 5E2N, can, thus open multiple opportunities for self-healing applications in aerospace environment.

In recent years, CNTs have been increasingly tested in various components of future generation aircrafts in which polymers such as epoxies and their composites are already extensively used to make a majority of their components/structures [4]. For example, some of the most recent models of commercial passenger airplanes like Boeing 787, Airbus A350 and Bombardier C series models employ polymer composites for up to 50% of their total weight [4]. The increasing use of these materials in modern aerospace structures suggests that successful microencapsulation of CNT/5E2N suspension will make it a serious healing agent candidate for many self-healing applications. Per se, the ultimate purpose of this work is to investigate the CNT/5E2N as microencapsulated healing agent for self-healing epoxy for aerospace applications.

1.2 Objectives

The key objectives of this work are

- i) Investigating the polymerization (or cure) kinetics of 5E2N initiated by selected Ruthenium Grubbs catalyst at low temperatures using non-destructive analyses
- ii) Developing procedures for enabling microencapsulation of a CNT/5E2N suspension and the quality characterization of the produced microcapsules
- iii) Testing the mechanical self-healing efficiency of the microencapsulated CNT/5E2N under different stress conditions when incorporated into epoxy
- iv) Testing the electrical self-healing efficiency of the microencapsulated CNT/5E2N
- v) Investigating the effects of CNTs present in the microencapsulated monomer on the self-healing efficiency

1.3 Methodology

Investigation of CNT/5E2N as microencapsulated healing agent for self-healing epoxy for aerospace applications requires thorough understanding and implementation of some key aspects that strongly influence the self-healing behavior and its effectiveness. The methodology that is followed to achieve the major objectives of this work is discussed as follows:

i) Understanding the thermo-chemical characteristics and behaviour of 5E2N, specially, the ROMP reaction and the kinetics of its polymerization initiated by suitable Grubbs' catalyst at low temperatures

5E2N, as the healing agent monomer is the principal liquid that flows to the cracks, as they appear in the materials, which is subsequently polymerized by suitable catalysts to fill, close, and repair the crack. Understanding the thermo-chemical characteristic of the monomer and its ROMP reaction mechanism, is thus, critical for their applications as healing agent monomer. The fundamentals of this important features are first studied thoroughly through literature reviews. However, to make them suitable for applications at low temperatures such as in space environment, understanding the polymerization kinetics of 5E2N at low sub-zero temperatures represent a key step.

To this end, experiments and methodology are specifically designed to enable an efficient monitoring of the ROMP reaction of 5E2N initiated by 2nd generation Hoveyda-Grubbs' catalyst (HG2) system below 0°C. A detailed quantitative analysis of the ROMP reaction kinetics of 5E2N/HG2 system has been conducted from room temperature down to -30°C by using a systematic micro-Raman spectroscopic measurement. Using this method, the kinetic parameters of the reaction and activation energies are determined based on the typical Arrhenius equation showing the temperature dependence of the reaction rates.

ii) Proof of concept

CNTs in the range of 0-6 wt.% [21-23] are known to improve the mechanical properties of polymer, such as epoxies, significantly. However, how the CNTs affect the properties of poly-5E2N produced through the ROMP reaction when they are already integrated into the liquid monomer phase is important to understand. The key idea of microencapsulating CNT/5E2N instead of 5E2N alone as self-healing agent was derived from the expectation that the CNT/5E2N suspension when polymerized through ROMP reaction would produce polymer with improved mechanical properties.

To verify this, poly (CNT/5E2N) samples were produced through the ROMP reaction of CNT/5E2N monomer suspension with varying concentration of CNTs. Poly-5E2N samples were also produced, as reference, through the ROMP reaction of 5E2N monomer alone. Microhardness tests and three-point bending tests were then performed on the samples and the resulting mechanical properties were compared.

iii) Microencapsulation of CNT/5E2N suspension

One of the most challenging part of this work is to determine and establish the suitable process parameters to enable successful microencapsulation of CNT/5E2N. To address this, the method of microencapsulation of the similar healing agent monomers such as the microencapsulation of DCPD [13] and 5E2N [20] are thoroughly understood through literature reviews. The standard method of microencapsulation is then adapted for the microencapsulation of our intended core monomer (CNT/5E2N) according to its requirements on a trial-and-error basis.

iv) Quality control tests of the microcapsules

The quality characteristics of the microcapsules can significantly affect their intended self-healing performance. The key quality characteristics of the produced microcapsules that can affect their self-healing performance include formation of continuous core-shell structures that are free from clustering, their size (diameters) and size distributions, shell morphology and thickness, thermal stability, core content, release of the core materials upon their breaking etc. These features of the microcapsules were investigated using a variety of characterization methods including optical and scanning electron microscopy (SEM), transmission electron microscopy (TEM), thermogravimetric analysis (TGA), differential scanning calorimetry (DSC) and Raman spectral analysis.

v) Choice of the epoxy system/catalyst and integration of healing agents

When the selected healing agent monomer (CNT/5E2N, in our case) is successfully microencapsulated, their self-healing efficiency needs to be evaluated. To this end, the healing agents, i.e., the microcapsules and the catalysts are required to be integrated into an epoxy system to manufacture samples.

Effective integration of the healing agents into the samples requires that the microcapsules and catalyst particles remain intact and active throughout the processing stages and can serve their intended purpose during operation.

Especially, exposure to the thermo-chemical processing required for the curing of some epoxy precursors are known to degrade and damage the activity of Grubbs catalysts [12, 45], which, can ultimately lead to poor or unsuccessful healing of damage.

A variety of aerospace grade epoxy precursors and curing agents as well as a few types of Grubbs catalysts are commercially available for various applications. To minimize the complexity in our work, the epoxy system (the precursors and curing agent) is chosen such that it needs relatively

low temperature treatment for their complete curing. At the same time, the Grubbs catalyst type that has high resistance to thermo-chemical degradation as well as can remain active at very low sub-zero temperatures is chosen. With these in mind, the combination of commercially available EPON 828 precursor and epicure 3046 curing agent are selected as the base matrix materials and HG2 catalyst is selected as catalyst, for the evaluation of healing efficiency of the microencapsulated CNT/5E2N.

Apart from the choice of the materials, the other key process variables that are carefully considered for the fabrication of self-healing epoxy samples are i) average size of the microcapsules to be integrated into the samples, ii) concentration (wt.%) of microcapsules to be used iii) concentration of catalyst to be used, iv) choosing suitable curing cycles to ensure complete and uniform curing of the samples etc. The choice of these process variables, which can affect the self-healing efficiency significantly, was based on extensive literature review of the relevant works.

vi) Evaluation of healing efficiency of microencapsulated CNT/5E2N integrated into the epoxy samples subjected to different stress fields

Mechanical self-healing efficiency of the microencapsulated CNT/5E2N monomer is evaluated by performing several mechanical tests on the epoxy samples incorporated with the healing agents. Widely accepted testing protocols used in self-healing literature for evaluating the self-healing efficiency are followed in this work. Accordingly, cured self-healing epoxy samples incorporated with the microencapsulated healing agents are first damaged to complete failure in a controlled way under a specific stress field. The failure event is then followed by resting the samples at pre-specified temperature for a predetermined time period allowing for the self-healing of damage. A selected mechanical property is measured for the undamaged samples as well as for the same samples self-healed after the damage. Mechanical self-healing efficiency is determined as the extent of the recovered property as a fraction or percentage of the same property of the undamaged samples. In our work, self-healing efficiencies are evaluated for the samples exposed to two different stress situations, one being under mode I fracture stress field and the other under adhesive shear stress field. Mode I fracture stress is related to the tensile stress, experienced by the formation of cracks and their propagation, normal to the crack plane, pulling the crack faces apart. On the other hand, the adhesive shear stress is associated to the stress felt by the adhesive bond when it is pulled (loaded) parallel to the adhesive bond, thus forcing the substrates to slide over each other. Fractographic analyses and Raman measurements conducted on the fractured

surfaces of mode I fracture stress samples and adhesive shear stress samples were also performed to support the test results.

In addition, electrical self-healing efficiency of microencapsulated CNT/5E2N incorporated into the samples were also evaluated using the same principles of the self-healing testing protocols.

To extract the effect of CNTs on the self-healing efficiencies, self-healing samples are fabricated, separately with the microcapsules containing 5E2N alone as well as with the microcapsules containing CNT/5E2N. The self-healing efficiencies of the microencapsulated monomers, as determined by the electro-mechanical tests performed on the samples separately incorporated with both types of microcapsules, are then compared to extract the effect of CNTs. The additional effect of incorporating the microcapsules into the samples on the original properties of neat samples that does not contain any healing agents are also evaluated in these tests.

1.4 Challenges

Two of the major challenges of this work was, first to establish suitable reaction process parameters to successfully enable the formation of microcapsules containing CNT/5E2N suspension in PMUF shells and, second, to recover individually separated free flowing microcapsules from the reaction process. Determining the process parameters for successful microencapsulation of CNT/5E2N, was a long tedious process. Many of the trials were unsuccessful for yielding any microcapsule output at the end of the microencapsulation reaction process. Each of the trials involves adjusting slightly the process parameters and run the full microencapsulation reaction process, and finally trying to recuperate microcapsules from it. Starting the reaction process, monitoring it throughout the completion, recuperation efforts involving filtration, drying etc., and finally checking and analysing the outputs in each trial requires substantial time and efforts. The final product of the microencapsulation trials ranged from the formation of completely gelled emulsion to completely separated oil and water phase after the reactions were finished. Selected process parameters were needed to be slowly adjusted in each trial, finally leading to the repeatable successful microencapsulation of CNT/5E2N.

The main challenges of this work are

i) Adapting the established method for the microencapsulation of a one component liquid healing agent like 5E2N to the current requirements of enabling the microencapsulation of two component liquid-solid suspension (CNT/5E2N), in PMUF shells.

ii) Recuperation of cluster free, individually separated microcapsules

The filtration process used to recuperate microcapsules from the product of microencapsulation reaction, is, often, very slow. A vacuum is usually used to speed up the process. However, even with the help of vacuum (vacuum assist), the filtration process might get stuck if the microcapsule clusters or sticky residues were formed in the reaction process. Multiple washing process before filtration of the reaction product, often, did not work. More research is necessary to dig into the causes and speed up the filtration process and increase the output of microcapsules containing CNT/5E2N.

iii) Ensuring that the microcapsules satisfy the key quality characteristics requirements for successful self-healing applications.

This include analyzing the key characteristics of the microcapsules such as the size and architecture of the microcapsules, distribution of their sizes, shell thickness, thermal stability etc., as well as, confirming the expected key features like presence of CNTs with sufficient aspect ratio dispersed in 5E2N inside the core of the microcapsules and their subsequent release as the microcapsules break etc. These are done by various characterization techniques and tools using OM, SEM, TGA, TEM, and Raman analysis.

iv) Demonstrating significant recovery of mechanical and electrical properties of the self-healing epoxy incorporated with the microencapsulated CNT/5E2N.

Different types of samples were needed to be fabricated and tested using standard testing methods. For each test, we used three-five samples of each type. In each step of this manufacturing and testing process of the samples, the guidelines of the standards were needed to be followed accurately to obtain repeatable results. For all the mechanical tests, the results were mostly reproducible within 5-10% of their average values. This is another major challenge of this work.

v) Extracting and evidencing the effects and contributions of CNTs in monomer on self-healing efficiency.

This needed additional efforts to microencapsulate 5E2N alone and manufacture different sets of samples with microencapsulated 5E2N. These samples needed to be tested similarly as done for the samples incorporated with microencapsulated CNT/5E2N to differentiate and highlight the difference in self-healing efficiencies achieved by the two different microcapsules containing different core monomers. Fractographic and Raman analysis were also done to support and evidence the contribution of CNTs on self-healing efficiency.

vi) Investigating the cure kinetics of the monomer at low temperatures using Raman analysis.

The design of experiment and methodology to monitor the kinetics of polymerization at low temperatures using Raman spectral analysis required a considerable understanding both of the ROMP reaction mechanism and Raman spectral responses.

1.5 Dissertation organization

The structure of the dissertation is outlined as follows:

The first chapter of the dissertation is the introduction, objectives, and methodology. Here, the importance of epoxy-based polymers and their composites in the modern advanced structures and devices in various fields including aerospace industries are highlighted. The complexities associated with minor damages in polymer composites during their operation and the difficulties with their manual on-site repairs are discussed briefly. The definition of self-healing material with a brief background of the self-healing studies of polymers are given. The motivation of studying alternative healing agents like 5E2N for applications at low temperatures, its limitations, and the possibilities to overcome the limitations with integration of CNTs are discussed. Specially, the opportunities associated with successful microencapsulation of CNTs dispersed in a self-healing monomer is emphasised. The key objectives of this work are then listed. Following this, a summary of the methodology followed in this work to achieve the key objectives are discussed. The major challenges of this research work are then pointed out with a brief description. Finally, the organization of the dissertation is given at the end of this chapter.

Chapter 2 refers to the different types of self-healing approaches for polymers to understand the basic strategies associated with them. In this chapter, the different extrinsic self-healing systems involving storage of liquid healing agents in polymers which are widely investigated in recent literatures are discussed in detail. Theoretically, besides microencapsulation method, the liquid healing agent CNT/5E2N that is investigated in our work can be utilized effectively in those self-healing systems as well. The advantages and limitations of different self-healing strategies for their practical applications are also highlighted.

After the initial discussion of different self-healing strategies, chapter 2 continues with the extensive comparison of the thermo-chemical characteristics of ROMP-active DCPD monomer, possibly the most widely investigated liquid healing agent in literature, with another ROMP-active 5E2N monomer which is the principal healing agent component in the current investigation. The

comparison offers a good insight of the potential of using 5E2N as an alternative liquid healing agent for various self-healing applications.

The chapter 2 is then dedicated to discussing the general method of microencapsulation of liquid healing agents like DCPD and 5E2N in polymeric shells, the desired quality characteristics of the produced microcapsules for efficient self-healing and the key process parameters that affect the success and quality of the microcapsules.

Finally, the recovery of mechanical and electrical properties of host materials using microencapsulated healing agents, common methods of evaluating the self-healing efficiency and the key factors that affect the self-healing efficiency are discussed in chapter 2 in detail.

Chapter 3 reports the current investigation of the cure kinetics of 5E2N initiated by HG2 catalyst at low temperatures using micro-Raman spectral analysis. It gives an overview of the Raman spectroscopy and discusses the advantages of using this over other relevant methods for such study. It then describes the detailed procedures and discusses the method developed in this work for the investigation. Finally, it offers the analysis of the results in detail.

Chapter 4 describes the experimental procedures for the synthesis of microcapsules containing CNT/5E2N at their core, and their quality characterization. The key process parameters that led to the successful microencapsulation of 5E2N/CNT are revealed. It then discusses the different important characteristics of the microcapsules analyzed by different characterizing techniques including DSC, TGA, TEM, SEM, and Raman spectroscopy. Finally, the electrical self-healing efficiency of the microcapsules is evaluated and the design of experiments, methods and the result of the evaluation is presented at the end of this chapter.

Chapter 5 describes different mechanical testing performed both for the preliminary proof of concepts and for the final evaluation of mechanical self-healing efficiency of the microencapsulated CNT/5E2N incorporated into epoxy. In this chapter, a detailed assessment of the mechanical self-healing efficiency of the microcapsules for epoxy samples subjected to different stress conditions are presented through comparative analysis of results.

Finally, chapter 6 outlines the conclusions and perspectives of the work and provides recommendations for future works.

CHAPTER 2: BACKGROUND AND LITERATURE REVIEW

2.1 Background and self-healing approaches of polymers

The concept of self-healing has come from the observation of nature where the injuries to animal or plant bodies are healed automatically through biological processes. Scientists also observed the autogenous healing mechanism in synthetic materials like concrete few hundred years ago [46]. From those observations, scientists in the last century tried to impart healing capability to other synthetic materials like ceramics and polymers. Self healing is defined as a process by which a material can undergo the repair and restoration of the original functionality at a damage event by using only the materials that are inherently available to them [47].

Researchers followed different approaches and strategies to develop polymers with self-healing functionality. These approaches can be broadly categorized into two basic classes [18, 48-52]. These are: (i) intrinsic self-healing and ii) extrinsic self-healing. In intrinsic healing, the polymer structure is modified itself at the molecular scale to include new chemical groups that bond reversibly or dynamically. The cracks are also healed with the application of external stimuli, often in the form of heat, but may need other stimuli like pressure and light to complete the healing process [48-52]. In extrinsic healing, external healing agents (e.g., monomer, catalyst, resins etc.) are embedded and dispersed into the polymer matrix, either directly or using breakable storage vessels (e.g., microcapsules, hollow fibers, microvascular networks) [18, 48, 50-52]. In this case, cracks are intended to be healed at room temperature without requiring additional external stimuli.

Most of the reported studies in intrinsic self-healing experiments are limited to thermoplastic polymers [53, 54], which limits its implementation (especially for heavy-duty applications) due to their weaker strength, stiffness and glass transition temperature (T_g) properties [55], compared to the thermoset polymers. The studies of intrinsic self-healing of thermosets such as epoxies are strongly limited [56, 57]. In addition, external intervention such as heating the materials after damage is generally required to activate the intrinsic self-healing process [54, 56], which makes the systems integrating this functionality non-autonomic.

While the main focus of extrinsic self-healing studies has been on the recovery of mechanical properties for heavy-duty structural applications, this concept has been applied to impart other functionalities and to prepare interesting smart materials such as self-healing anti-corrosion coating, self-healing electrical conductive coating, thermosensitive composites, sensors etc. [55].

In our work, we utilize extrinsic approach to investigate CNT/5E2N as microencapsulated healing agent for self-healing epoxy with the ability to autonomously recover its electro-mechanical properties after damage for advanced aerospace applications.

The majority of the extrinsic self-healing approaches employ liquid healing agents (e.g., monomers, resins, hardeners) in breakable containers (like hollow tubes, microcapsules) or in pre-designed microvascular hollow network which are embedded into the host polymer matrix to store the healing agent and timely deliver it to the damage site as the damage occurs in the material. Based on the storage and delivery system of the healing agents into the host polymer, major extrinsic self-healing designs can be broadly divided into two main categories. These are:

- a) Self-healing with vascular network
- b) Self-healing with microcapsules

The key idea of the designs is, when a crack inside the host polymer matrix generates and propagates through the material, it breaks the embedded microcapsules or vascular network and thereby releasing the liquid healing agents between the two opened faces of the crack. Figure 2.1 shows the conceptual route of the extrinsic self-healing process for polymer originally introduced by White *et al.* [9], using CNT/5E2N suspension as microencapsulated healing agents.

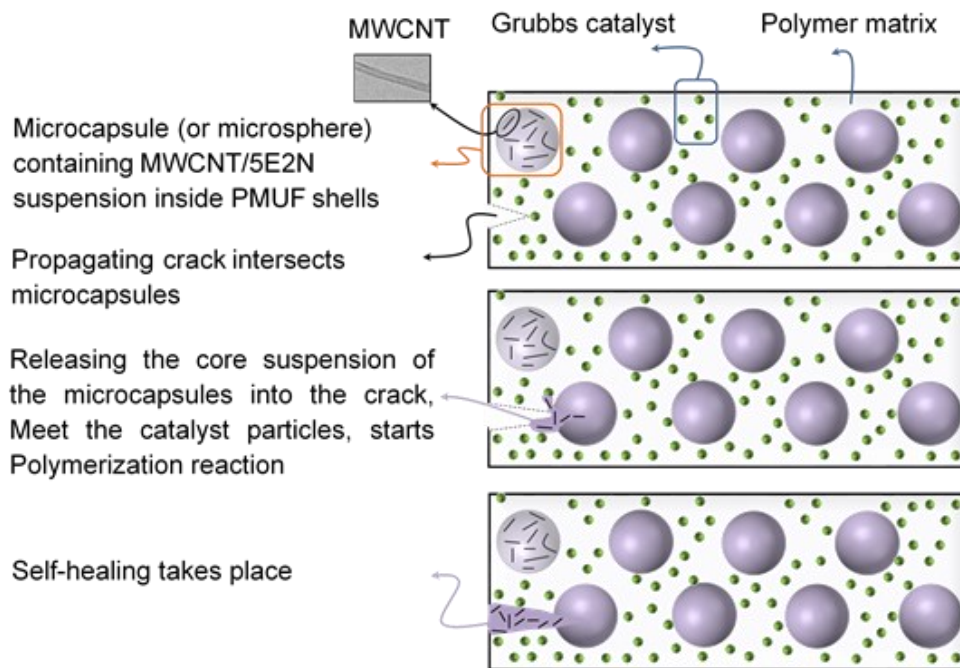


Figure 2.1 Extrinsic self-healing approach based on microcapsules containing a liquid suspension of CNT/5E2N

Here, the liquid healing agent (CNT/5E2N suspension in this case) released from the broken microcapsules fills the gaps between the two crack faces and is solidified/polymerized with the aid of a pre-dispersed catalyst (or a curing agent) to close the gaps between the two crack faces. The autonomous gluing of the crack contributes to the recovery of the lost properties of the material.

Self-healing strategies with vascular networks in the host polymer matrix has few variations studied by different group of researchers. The basic principles of these variations, their advantages, limitations, and the main factors that affect the healing effectiveness are discussed below.

2.2 Self-healing design with vascular network

Self-healing design of engineering materials, especially, with vascular network, was inspired by the natural wound-healing capabilities of living organisms. For example, a simple cut or a scratch in the skin is healed autonomically, multiple times as needed, triggered by the activation of vascular system in human. Dry [58-61] originally introduced the 'bioinspired' design of self-healing of concrete material where a liquid healing agent is stored in hollow glass tubes (diameters in mm scale) which are pre-embedded in the concrete. The concept of healing with vascular network was later expanded for polymers [5, 61-70].

In the initial designs [61], self-repairing of polymer was demonstrated by employing single part cyanoacrylate and two-part epoxy adhesives as healing agents contained inside hollow tubes which were embedded into the polymer matrix. As shown in Figure 2.2.[62], for imparting the self-healing capabilities to the polymer, the healing agents were first infiltrated into the glass tubes using vacuum and then, the tubes were embedded into the polymer matrix during the manufacturing stage of the part.

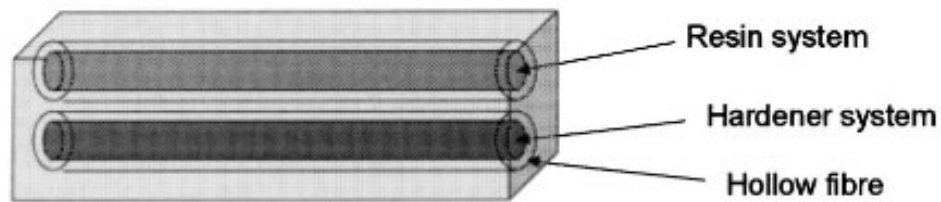


Figure 2.2 Schematic of self repairing strategy for polymer matrix with hollow tubes/fibers [62]

Later, researchers investigated the development of self-healing polymers using microvascular channel network design [71-85]. In this design, instead of embedding hollow tubes/fibers into the polymer matrix, hollow channels or a network of channels are built or excavated into the bulk polymer or into FRPC. Liquid healing agents are then injected into the hollow network of channels for imparting self-healing functionality to it.

Researchers employed different techniques to build networks of hollow channels into polymer or FRPC. Toohey *et al.* [71], demonstrated healing of a coating-substrate polymer specimens incorporated with a three-dimensional (3D) interconnected microvascular network fabricated through direct-write assembly, a technique refined by Therriault *et al.* [72]. In the work [71], first a 3D tubular framework, similar as shown in Figure 2.3, was built with fugitive organic ink using a robotic apparatus. The fugitive ink is composed of a mixture of microcrystalline wax with lower molecular weight organic constituents. Such materials are suitable for the 2D and 3D patterning of sacrificial layers, which can be subsequently removed using an external stimulus such as heat [86].

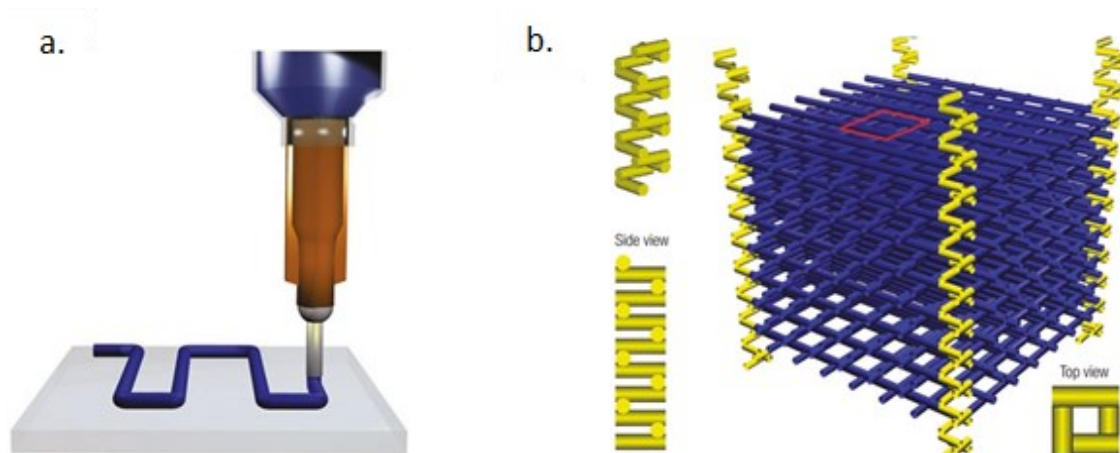


Figure 2.3 Robotic deposition of a fugitive organic ink through a nozzle onto a moving x-y stage, b) 3D microvascular network scaffold (blue) with vertical spiral tower structure (yellow) embedded into it [72]

The 3D scaffold was then infiltrated with epoxy and cured to make a substrate. Subsequently, the fugitive ink framework was removed by heating the substrate leaving there an interconnected network of hollow channels. This approach yielded a pervasive network of smooth cylindrical channels of diameter $\sim 10\text{--}300\mu\text{m}$ with defined connectivity. The channels were then filled with liquid healing agent DCPD. An epoxy coating, approximately $700\ \mu\text{m}$ thick, containing Grubbs' catalyst particles was applied to the top surface of the microvascular substrate. Repeated healing of the cracks under four-point bending load and release of healing agents was demonstrated for the coating-substrate specimens as shown in Figure 2.4 [71].

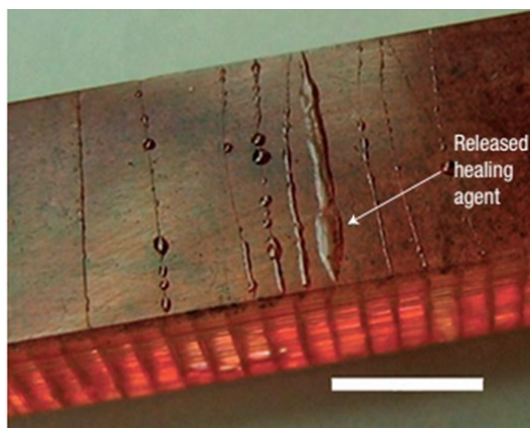


Figure 2.4 Self-healing coating-substrate structure after cracks are formed in the coating revealing the presence of excess healing liquid on the coating surface [71]

The same group of researchers [73-75] investigated the effect of different architectures of the 3D network of hollow channels, created by direct write assembly, on the delivery of healing agents to the damaged sites and their self-healing performance. With the 3D network of hollow channels built into polymer coating-substrate specimens, multiple healing cycles was demonstrated using two-part epoxy/hardener healing agent system. The vascular system, in these works, was however, required to be placed away from the location of damage to preserve the integrity of the network during a damage event. The hollow channels were also needed to be terminated where the cracks were most likely to occur, which, according to ref.[87], requires prior knowledge of the probability of damage throughout a structure. Preservation of the hollow channel network built in the structure in a damage event and the requirement of the prior knowledge of the likely locations of damage are two of the major challenges of the self-healing design with microvascular network.

Some researchers [76] studied the incorporation of a pressure-delivery system of two-part healing agents into the polymer structure to speed up the delivery of healing agents to the crack sites through the microchannels and to promote their mixing for effective polymerization. Separate pressurized reservoirs of healing agents and, in a case, computer-controlled pumps were employed to accomplish multiple high efficiency healing. With these requirements, the self-healing system, however, might get bulky and complex for real applications.

Compared to bulk polymers, incorporating vascular networks in FRPC is much more difficult due to the presence of reinforcement fibers inside in ordered arrays and in the form of plies stacked and glued together in a multiple layer arrangement. The inclusion of vascular channel networks in the FRPC can easily disrupt the position, arrangement, continuation, and the intimate formation of the reinforcement fibers around the matrix, potentially compromising the mechanical properties of the FRPC.

Few techniques have been employed by researchers to incorporate the hollow channel networks into the FRPC. Bond and co-workers [77-81] incorporated vascular network into FRPC using wire preforms. Low melting solder wire preforms, or high melting teflon-coated steel wire preforms were used for this purpose. The wire preforms were placed on the layers of the fibres during lay-up of the manufacturing process and subsequently removed after curing of the FRPC, leaving behind hollow channels within the plies, as shown in Figure 2.5, in the finally manufactured part. The removal of the wires after curing of the FRPC were performed either mechanically for the teflon-coated steel wire preforms [77], or in a 'lost-wax' type process for the low melting solder wire preforms by applying heat and vacuum [77-81]. The hollow channels thus created in the FRPC can be connected to external reservoir of pressurized healing agents and large volumes of

liquid healing agents can be pumped through the damaged sites for multiple healing of damage [80].

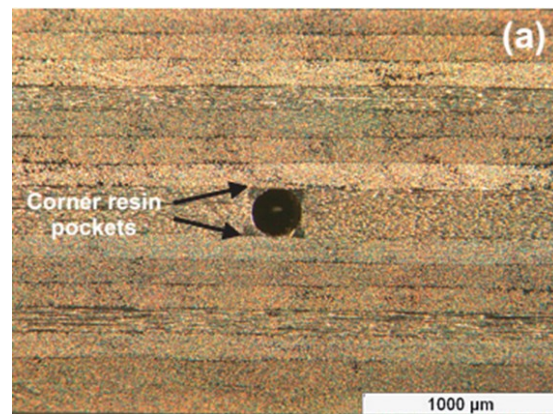


Figure 2.5 Hollow channels built in FRPC by a ‘lost-wax- type process using low melting solder wire preform [80]

Other researchers built 3D microvascular channel network into bulk polymer [82] and into FRPC [83] using a process called vaporisation of sacrificial components (VaSC). In this process, sacrificial polylactide (PLA) fibers treated with a catalyst to accelerate their thermal decomposition are first stitched into a 3D carbon or glass fabric preform as shown in Figure 2.6. The fiber preform is then infused with epoxy and cured. After curing, the PLA fibers are removed by vaporisation of the sacrificial fibers at high temperature, leaving a hollow 3D channel network in the composite. These channels can be subsequently filled with a variety of liquids which can circulate throughout the composite structure [82].

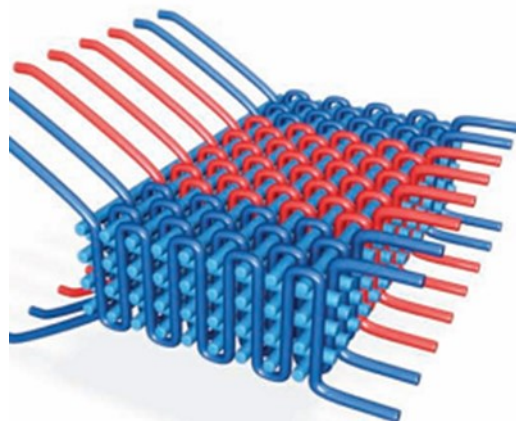


Figure 2.6 Schematic diagram of glass fiber preform woven into a 3D structure. Sacrificial PLA fibers are shown in red [82]

With the 3D microvascular channels, multiple healing of crack (up to 3 healing cycles) under mode I fracture loading was demonstrated using a two-part epoxy/hardener healing agent system,[83] However, to achieve multiple healing of damage at the same location, fracture of materials in new location was required to rupture previously undamaged vasculature which allows the healing agents to continually deliver to the previous damage location [83]. Network architecture of the hollow channels in the material which ensures the availability of healing agents to a damage site was found to play a large part in achieving healing after the first healing cycle [87]. Optimization of the network architecture of the hollow channels in the material as well as developing fabrication techniques that allow for fabricating complex, branched network of channels is thus essential to benefit from the multiple healing option of the vascular network design of self-healing.

Major issues in developing self-healing polymers with microvascular networks are listed below:

- i) Rupture of the vascular network at one location during a first damage event can create discontinuity of flow of the healing agents preventing their transportation to damage sites during the subsequent damage events.
- ii) At present, damage can only be repaired in relatively close proximity to the vasculature. Further, preserving the integrity of the vascular network during a damage event requires prior knowledge of the likely locations of damage in the host material [87].
- iii) Possible blockage of the vascular network with polymerised healing agents can hamper further release of healing agent reducing multiple healing ability of the vascular self-healing system [87].
- iv) The presence of hollow network of channels inside the host polymer part might affect the original structural properties (strength and stiffness) of the part [88].
- v) Fabrication issues like deformation of the 3D scaffold made by fugitive ink [71], difficulties in producing branched network of hollow channels using VaSc process [82] etc. need to be resolved.
- vi) Need to optimize the locations of the vasculature in the host material, their diameters, numbers, orientations, spacing, connectivity etc. for optimum healing effects with minimum loss of structural properties of the host material.
- vii) Most of these methods are not suitable for rapid large-scale production of self-healing polymers and their composites with complex vasculatures, mainly due to incompatibility with existing manufacturing methods and materials [82].

Recent advancement of 3D printing technologies [84] that allow making objects from 3D model data, and development of novel ink materials [85] makes the design and fabrication of complex,

highly branched 3D network structure possible. This can ultimately provide a mechanism for the optimization of vascular network design for efficient multiple self-healing of polymers [87].

Overall, self-healing of polymers with vascular network design is an excellent and promising route for future self-healing applications. However, some issues, as listed above, still need to be addressed and improved significantly before their real large-scale applications.

2.3 Self-healing with microcapsules

In microcapsule-based self-healing, the storage and delivery of the healing chemical is accomplished by microcapsules which are embedded into the host material. Microcapsule-based self-healing system reduced the manufacturing issues which are experienced in the vascular network approach [89]. Also, the microcapsules, the carriers of the liquid healing agents, as opposed to the other design with microvascular network, usually forms a good bonding with the host material which is essential for developing efficient self-healing polymers without compromising their original structural properties [13]. These key differences along with its easy scalability [90] and relative ease of manufacturing make the self-healing design with microcapsules very attractive and preferable in many cases.

Research group of White *et al.* [9], first demonstrated significant recovery of strengths of epoxy after damage using microencapsulated DCPD and Grubbs catalyst system as healing agents. Since then, extensive research is carried out investigating various aspects of microcapsule-based self-healing of polymer. Most of these research works are focused on the recovery of mechanical properties of polymer for structural applications. Side-by-side, numerous research works on microcapsule-based self-healing were carried out for some non-structural applications such as corrosion protective self-healing or, more precisely, self-sealing polymer coating applications [91-96]. Only a few of these works were also dedicated to the investigation of recovery of electrical properties of materials [43, 92, 97-99]. Most of these works, however, were designed for the investigation of recovery of either a targeted single mechanical property or a single functional property of material. In modern aerospace applications, polymers such as epoxies are extensively used for various critical purposes [100], that require a continuous maintenance of not only their mechanical properties, but also of their other functional properties, especially their electrical properties, simultaneously during their operation. However, investigations on the possibility of simultaneous recovery of two or more properties of materials for the applications in low

temperature aerospace environment are scarce in self-healing literature. The current work aims to contribute to this area of self-healing research.

Epoxy-based polymers and their fiber reinforced composites are extensively used in many key structures, parts and devices of modern aeroplanes and spacecrafts [1, 101]. They are used as matrix materials for high-strength laminated FRPC, high-performance structural adhesives,[1-3][100] as coating materials that require electrical conductivity [100] and for many other advanced aerospace applications. Consistent electrical and mechanical response of these structures and device with the variations of different types of external loads, especially, during their in-flight operation is critical. In addition to susceptibility to mechanical failure, any inconsistencies in their electrical response during their in-flight operation can lead to severe consequences such as electrical interference to the sensitive circuitry, explosion, radio-communication interference, jamming of radio navigation etc. leading to flight safety hazards [100]. Rapid self-healing of electro-mechanical properties of epoxies under in-flight operating conditions can greatly contribute to avoid this type of flight safety hazards. In this context, the current work investigates CNT/5E2N as microencapsulated healing agent for the recovery of electro-mechanical properties of epoxy-based polymer for aerospace applications.

The healing agents used, their microencapsulation process, the properties of the microcapsules, their effects on the properties of the host material, their self-healing efficiencies as well as the methods of evaluation and the targeted applications are some of the key aspects of different earlier investigations that are found most relevant to the current work. Among the numerous works on microcapsule-based self-healing of polymers, the works that investigate these aspects for the targeted recovery of either mechanical or electrical properties of materials are reviewed in detail in the following sections.

2.3.1 Choice of healing agents for the recovery of mechanical properties

The healing agents are the active chemical species incorporated into the host material that help it regaining its original properties and functionalities after a damage event. To do this, the healing agent acts to mend the discontinuities in the host material caused by the damage event. Researchers investigated different healing agents for different microcapsule-based self-healing applications. For the intended recovery of mechanical properties for structural applications, the healing agents chosen are usually monomers or prepolymers that can undergo polymerization reaction when initiated by a suitable catalyst, solvent or a curing agent.

To be selected as a healing agent for the structural applications, the monomers or the prepolymers should possess some desired characteristics [68] such as:

- i) It must remain sufficiently fluid at the intended operating temperature until the polymerization reaction is initiated.
- ii) It should be capable of being readily polymerized, initiated by a catalyst or a curing agent at the operating temperature without any external assistance.
- iii) Their polymerization reaction should be initiated and progress fast, preferably, for example, in a few minutes at the operating temperature.
- iv) it should be capable of producing strong enough polymer upon their curing reaction to efficiently repair the initial microcracks generated in the host material.
- v) The produced polymer should bond or connect well with the host material.
- vi) it should enable its microencapsulation with suitable microcapsule characteristics.

The extent of mechanical recovery of host material after damage depends mainly on the nature and properties of the healing agents used. Besides the ROMP-active healing agents like DCPD/Grubbs' catalyst system, researchers encapsulated other healing agent monomer/prepolymer and evaluated their mechanical healing efficiencies. The healing efficiencies largely depend on the strength of their polymer and their compatibility with the host matrix. The healing agents used also dictates their cure kinetics, requirement of external trigger, applicable operating conditions etc. Applied healing conditions, specially, the temperature at which the healing is carried out and the time duration allowed for healing also has significant effect on the extent of recovery of mechanical properties and the healing efficiencies depending on the healing agents used.

Table 2.1 provides an overview of some of the relevant works for the mechanical recovery of epoxy-based polymers incorporated with different microencapsulated healing agent systems.

Table 2.1 Overview of the works for the mechanical recovery of epoxy-based host materials for different microencapsulated healing agent systems

Healing agent	Catalyst /Initiator	Temp. (°C)	Time (hr)	Healing Efficiency (%)	Ref.
DCPD	G1	RT	48	Up to 90%	[12, 102]
DCPD	G1	RT	48	97%	[103]
DCPD	G1	RT 80°C	48	45% 80%	[104]
DCPD	G1	RT	24	44%	[105]
DCPD	G1	RT	48 h	Up to 96%	[106]
DCPD	G1	RT	24 h	56%	[107]
Epoxy	Solvent Ethyl phenylacetate (EPA)	RT	24h	35%	[108]
Epoxy	Solvent (EPA)	RT	24h	83%	[109]
Epoxy	Amine	RT	48h	(89 ± 13%)	[110]
Epoxy	Polyether amine	RT	24h	84.5%	[111]
Epoxy	Solvent (EPA)	80°C	48h	68%	[90]
Isophorone diisocyanate IPDI	-	25°C	7 Days	Up to 107%	[112]
Epoxy	Solvent (EPA)	RT	24h	52%	[113]
Polydimethylsiloxane PDMS-a	Triethylenetetramine TETA	RT 80°C	48h	82-100% 110%	[114]
Epoxy	Mercaptan	RT	24h	80%	[115]
DCPD	Tungsten hexachloride (WCL ₆)	RT	24h	91.8%	[116]
Epoxy	EPA	RT	24h	100%	[117]

Table 2.1 Overview of the works for the mechanical recovery of epoxy-based host materials for different microencapsulated healing agent systems, cont'd

Healing agent	Catalyst /Initiator	Temp. (°C)	Time (hr)	Healing Efficiency (%)	Ref.
Epoxy	Alginate AG	40 °C	48h	86% 76%	[118]
Epoxy	Mercaptan	55 °C	17h	171%	[119]
Epoxy	Mercaptan	RT	24h	28%	[120]
ENB/DCPD (5%)	HG1	RT	-	69 ± 3%	[121]
ENB	HG1	RT	-	Up to 124%	[122, 123]
Chlorobenzene	-	RT	24h	82%	[124]
Epoxy/chlorobenzene Epoxy/ethyl phenylacetate, Epoxy/phenylacetate	-	RT	24h	Up to 100%	[125]
Glycidyl methacrylate (GMA)	-	25°C	72h	Up to 100%	[126]
ENB/methyl 5-norbornene-2-carboxylate (MNC)	G2	50°C	-	Up to 88±13%	[127]
Epoxy	NiCl ₂ (imidazole)	130°C	60 min	ILSS: 97.5% Tensile: 144.5%	[128]

As table 2.1 indicates, researchers investigated a few different monomers/prepolymers as healing agent candidates for various microcapsule-based self-healing structural applications. They include DCPD, different epoxy-based prepolymers, glycidyl methacrylate, styrene, and few others that possess some of the desired characteristics listed before.

Among them, A two-component liquid healing agent systems, e.g. an epoxy-hardener healing agent system, is often highly sensitive to stoichiometric mixing.[70] As a consequence, it is important to ensure that they are adequately mixed at a specific mixing ratio for their proper curing and, consequently, for effective healing of damage. It also requires that the two types of microvessels containing the two components of the healing agents are broken simultaneously by the propagating crack in the host material and release the two components at least at a stoichiometric ratio. This might be difficult to ensure in practice hampering effective healing of damage. Healing agents with less sensitivity to mixing ratios of resin and initiator (or catalyst) is, thus, desirable for practical self-healing applications. The CNT/5E2N monomer and Grubbs' catalyst healing agent system investigated in this work is envisaged to be less sensitive to this mixing ratio requirement.

Further, for complete curing at RT for some healing agent systems, such as an epoxy/hardener system, active mixing and sufficient healing time in the range of 5-7 days, for example, might be required.[68] Duration of a few days and the requirement of active mixing of healing agent components for achieving significant self-healing of damage is not desirable for practical applications.

Again, poor healing efficiency (limited recovery of properties) was reported at room temperature for some healing agent systems [70, 120]. Good recovery of strength was only achieved with the assistance of external heat after the damage event which makes the system non-autonomic.

For this, Williams *et al.* [68], recommended development of new healing agent resin formulation to meet the requirement of autonomic self-healing which include low viscosity, long shelf-life, insensitivity to stoichiometry, faster curing etc. The CNT/5E2N healing agent system investigated in our work is envisaged to satisfy many of these essential requirements of autonomic self-healing system.

Among the different extrinsic healing agent systems investigated in literature, ROMP-active DCPD is most widely investigated healing agent monomer for structural applications. However, because of its physical limitation of having a freezing point at 15°C [15], it is not suitable for self-healing applications at low temperatures such as prevailing in space environment. Like DCPD, 5E2N can also undergo similar ROMP reaction when initiated by Grubbs' catalyst but is less explored as a healing agent for self-healing applications. This is mainly because 5E2N produces weaker polymer after polymerization reaction compared to DCPD, that limits its recovery efficiency of mechanical properties for structural applications. We envisioned that incorporating CNTs in 5E2N monomer would not only overcome this limitation of 5E2N, but also provide an additional electrical self-healing ability to it thanks to the excellent electro-mechanical properties of CNTs. Further, unlike DCPD, 5E2N remains liquid at sub-zero temperatures down to -80°C [19] which makes it a potential healing agent candidate for low temperature self-healing aerospace applications. In our work, we investigate CNT/5E2N as a microencapsulated healing agent for the recovery of electro-mechanical properties of epoxy-based polymer for aerospace applications.

To adapt CNT/5E2N as a healing agent for microcapsule-based self-healing applications, it is imperative to understand the physical, chemical, thermal and mechanical characteristics of 5E2N in comparison to DCPD because of their similarities in nature. These properties also greatly affect their microencapsulation process and the self-healing efficiency. From the available literatures, a detailed comparison of the characteristics of DCPD and 5E2N is drawn in the following sections.

2.3.2 General characteristics and chemical configurations of DCPD and 5E2N

Pure DCPD is a colourless, waxy solid at room temperature. However, some commercially available DCPD, with DCPD content below 95 wt.% are liquid at room temperature and freezes at around 15°C [19]. The commercially available high purity DCPD (DCPD content around 95 wt.%) are typically used as the self-healing monomer.

DCPD exists in two stereoisomers: endo-DCPD and exo-DCPD. Their chemical configurations are shown in Figure 2.7. Typically, more than 90% of the DCPD molecules present in commercially grades of DCPD are in the endo form [15, 17]. As shown in the figure, DCPD molecules consist of two sites of unsaturation (carbon-carbon double bonds termed as alkenes or olefins). As can be seen in the figure, one unsaturation exists in the highly strained cyclic norbornene ring and the other exists in the less strained (and cyclic) cyclopentane ring attached to each other.

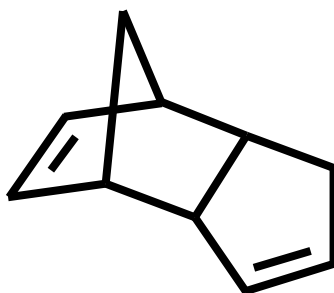


Figure 2.7 Chemical structure of Endo-DCPD [15]

Poly DCPD, the resulting polymer of DCPD, is extensively crosslinked when made under typical manufacturing conditions and results in a very high impact resistance, good resistance to chemical corrosion and a high heat-deflection temperature [129].

5E2N, also referred to as ethylidene norbornene (ENB) in literature, on the other hand, is a colourless liquid with a freezing point around -80°C [19]. As in DCPD, the ENB molecules consist of two sites of unsaturation (carbon-carbon double bond), as shown in Figure 2.8. As in the figure, one unsaturation exists in the norbornene ring and unlike DCPD, the other unsaturation exists in the acyclic ethylidene group attached to cyclic norbornene.

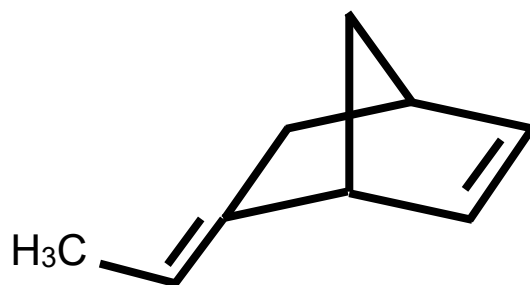


Figure 2.8 5-ethylidene-2-norbornene [17]

When polymerized, 5E2N produces mostly linear polymer with less strength than poly DCPD [130].

Both DCPD and 5E2N are ROMP-active monomers. Principally, the unsaturation in the higher strained norbornene ring takes part in the ROMP reaction. The crosslinking reactions happen at the site of other unsaturation [129].

2.3.3 Comparison of DCPD and 5E2N as healing agents

Lee and co-workers [15, 17, 131], characterized and compared DCPD and ENB as healing agents. For effective healing of materials, it is necessary to understand how the healing agents behave during and after the cure (polymerization) reaction [15]. The researchers in refs. [15, 17, 131, 132], investigated and compared the gelation and vitrification time during the cure of the two monomers (DCPD and ENB) when initiated by first generation Grubbs' catalyst (G1) at room temperature. For better understanding of the comparative behaviour of the healing agents and due to the high relevance to our investigation, the works of refs. [15, 17, 131, 132], are discussed in detail in the following sections.

Thermosetting resins normally transform from liquid state to rubbery state and finally to glassy state during their cure. Gelation time, vitrification time and glass transition temperatures (T_g) are the important characterizing parameters of the cure process. Transformation from liquid to rubbery state during the cure is known as gelation and is defined by the incipient formation of infinite size of molecule (at the molecular level) and abrupt increase in viscosity (at a macroscopic level). Beyond this point, processability decreases and resin flow is retarded greatly. After the

very initiation of the polymerization reaction of the healing monomer, the gelation time estimates the time before which the healing agent can flow into the crack planes to fill the cracks. Transformation from rubbery to glassy state during the cure is known as vitrification which usually indicates the end of the cure reaction. During the process of vitrification, a stiff glassy solid is formed through further chemical reactions (crosslinking) and/or chain entanglement. The vitrification time indicates the time duration (starting from the very initiation of the polymerization reaction) after which the polymerized healed material starts to reveal substantial stiffness. Glass transition temperature, on the other hand, is defined as the temperature (or a range of temperature) at which the transformation from liquid to glassy state occurs. Gelation time, vitrification time and glass transition temperature are important parameters to characterize monomers and their corresponding polymers and, thus, to understand and optimize the self-healing behavior of healing agents [15, 17].

2.3.4 Comparison of rheological properties of DCPD Vs ENB

Researchers in refs. [15, 17, 131, 132] employed rheological measurements, dynamic mechanical analysis (DMA) and DSC for investigating the polymerization behaviour of DCPD and 5E2N and the development of their inherent thermo-mechanical properties.

They employed two methods for their investigation. In the first method (direct mixing method) [17], [15, 131], the monomers and a predetermined concentration (wt.% of the monomer) of catalysts were mixed directly, and rheological measurements were made dynamically (with time). In the second method (indirect mixing method) [131], predetermined amount of catalyst was first mixed with epoxy/amine system and cured into a film that was later polished to expose some catalyst particles. The healing agent monomer was then introduced on the epoxy film surface for the dynamic rheological measurements. The indirect mixing method was a simulative experiment, representing actual application scenario where, instead of directly mixing the monomer and catalysts, the microcapsules and the catalysts are incorporated into the host epoxy polymer and the healing agents are allowed to undergo self-healing process [15, 131].

With the direct mixing method, the evolution of storage modulus (G') with cure time for DCPD cured with 1wt.% G1 at RT and for ENB cured with only 0.10 wt.% G1 at RT is shown in Figure 2.9.

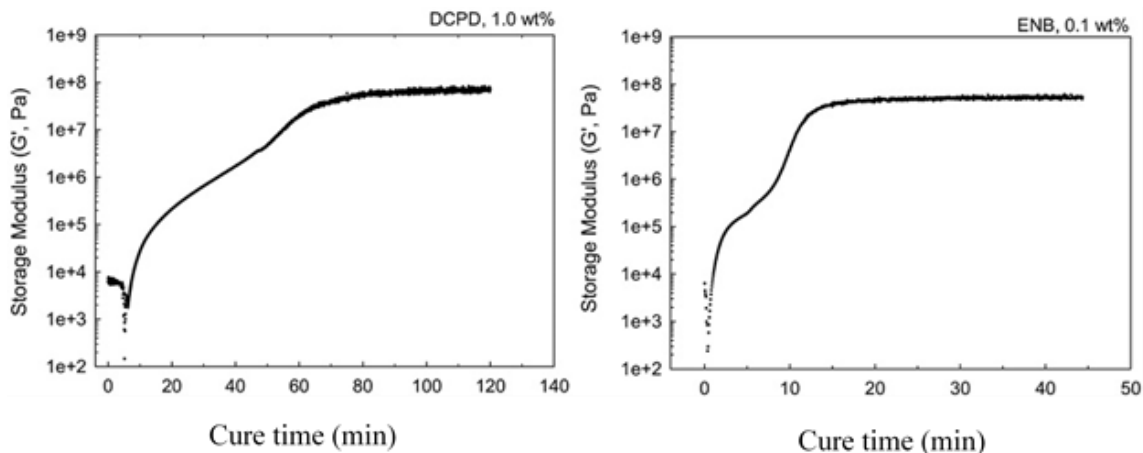


Figure 2.9 Evolution of storage modulus with cure time for unreacted samples with catalyst of 1.0 wt% for DCPD and 0.1 wt.% for ENB (direct mixing) [17]

Materials with viscoelastic properties like many polymers, do not follow a strict proportional relationship between stress and strain (Hooke's law) as perfect elastic materials. Under cyclic load, even within the linear elastic region, the stiffness observed during the loading part of the cycle does not remain constant during the unloading time. The energy stored during the loading is partly lost during unloading. The modulus obtained during the initial loading of such viscoelastic materials is called the 'storage modulus'. For polymers, this type of behaviour is caused by the flow behavior of polymer chains and their entanglement during their loading cycles [133].

From the figure, typically, the storage modulus G' initially increased rapidly, slowed down for a while, and then increased rapidly again, levelling off thereafter [15]. For DCPD cured with 1 wt.% G1 at RT, the gel time and vitrification time were found to be 5min and 50 min, respectively. On the other hand, for ENB cured with only 0.10 wt.% G1 at RT, the gel time and vitrification time were found to be only 0.8 min and 8 min, respectively. This indicates that, the cure reaction of ENB proceeds much faster compared to DCPD with much lower amount of catalyst [17]. Further, with direct mixing, the steady state storage modulus ($G'_{\text{level-off}}$) value for the DCPD (cured with 1 wt.% G1) and ENB (cured with 0.1 wt.% i.e., 1/10 of the amount of G1 used in DCPD) were found in proximity (8.0×10^7 Pa for DCPD Vs 5.5×10^7 Pa for ENB) as shown in Figure 2.9 above. As noted by ref.[15], the rigidity or stiffness after cure can be estimated from the G' value. The results suggest that healed materials with ENB monomer as healing agent might effectively recover the stiffness of damaged host material as much as DCPD.

Further, with direct mixing method, ref. [15], observed that the gelation time and vitrification time shortens with increase of the amount of catalyst. The effect of catalyst was much greater in vitrification than gelation. The vitrification time of DCPD cured with 5 wt.% G1 was reduced to about 21 min compared to 50 min when it was cured with 1 wt.% G1. On the other hand, the vitrification time of ENB cured with only 0.030 wt.% of G1 at RT was 19 min which is reduced to only 8 min with a little 0.10 wt% of G1 [15]. The results suggest that the vitrification time at RT might be reduced even more with only a little increase of the catalyst amount for ENB whereas DCPD would require large increase of catalyst amount to further reduce the vitrification time at RT.

For the indirect mixing method, much larger quantity of catalyst in epoxy was necessary for curing the monomer samples and the ROMP reaction was much slower than in direct mixing method. This is because the effective contact of monomer to the solid catalyst, in this method, is limited only to the exposed catalyst particles available on the surface of the epoxy coating film. The storage modulus value after 60 min reaction time was reached to only 1×10^5 Pa for DCPD even with 9 wt.% of catalyst in the epoxy film. On the other hand, ENB with only 3 wt.% catalyst in the epoxy film achieved the storage modulus 5 times more (5×10^5 Pa) than DCPD after the same (60 min) reaction time [15]. The result suggests that, in the real application scenario ENB monomer as healing agent can recover the mechanical properties of damaged host polymer much more quickly and effectively with much less amount of expensive Grubbs' catalyst.

However, as their results suggest [15], if substantial healing time is allowed, DCPD might reach slightly better storage modulus but at the cost of much high amount of catalyst which is often not desirable in practical applications.

In a subsequent work, Mauldin *et al.* [131] investigated several ROMP active monomers using the same rheological measurements with the indirect mixing method. Among the five ROMP-active monomers tested including DCPD and ENB, with 2.5 wt.% G1 catalyst embedded in the epoxy film, ENB monomer achieved the highest storage modulus, almost 2 orders of magnitude higher than DCPD, after about 2h of reaction time at RT as shown in Figure 2.10.

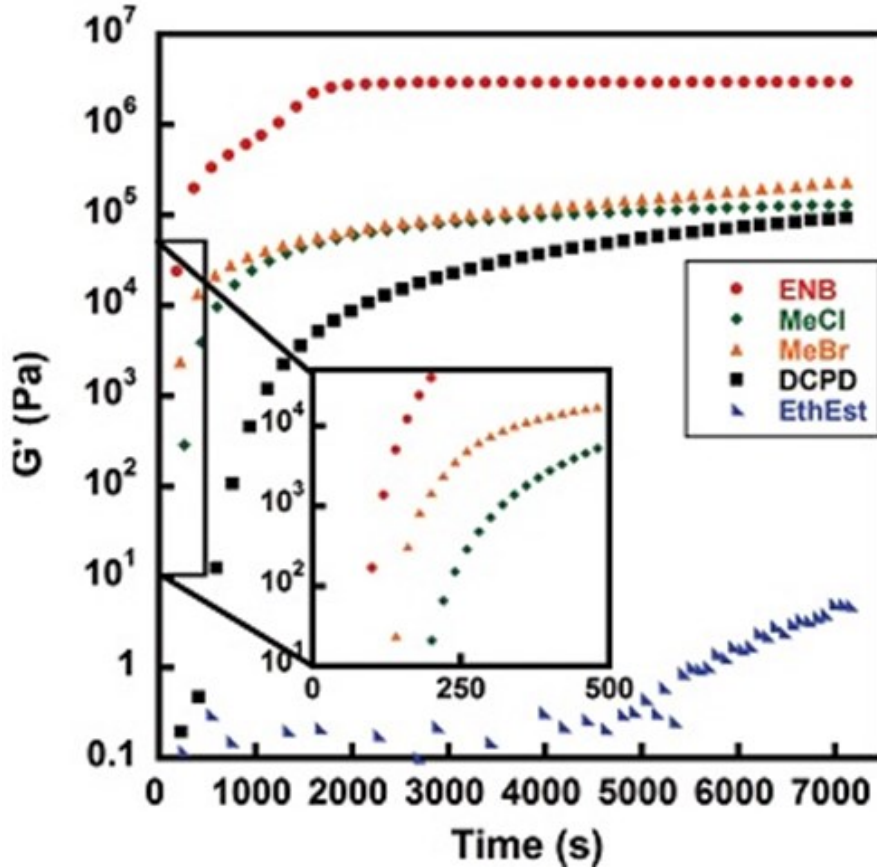


Figure 2.10 Evolution of storage modulus with cure time at RT for different ROMP active monomers with catalyst particles exposed to the epoxy film surface (indirect mixing method representing real application scenario) [131]

Not only achieving the highest value of the storage modulus, ENB achieves this value only in 30 min (about 1800 sec in Figure 2.10) at RT after reaction with catalyst in a real application scenario. On the contrary, Figure 2.10 indicates that DCPD would require much greater time, probably days to catch up, if at all, the steady state rigidity of ENB. The study again confirms that ENB can be a highly potential healing agent monomer with the desired healing agent characteristics such as very fast reaction, low catalyst requirement, good rigidity and low temperature capabilities for effective self-healing of epoxies, especially, for aerospace applications.

2.3.5 Comparison of heat flow characteristics of DCPD Vs ENB

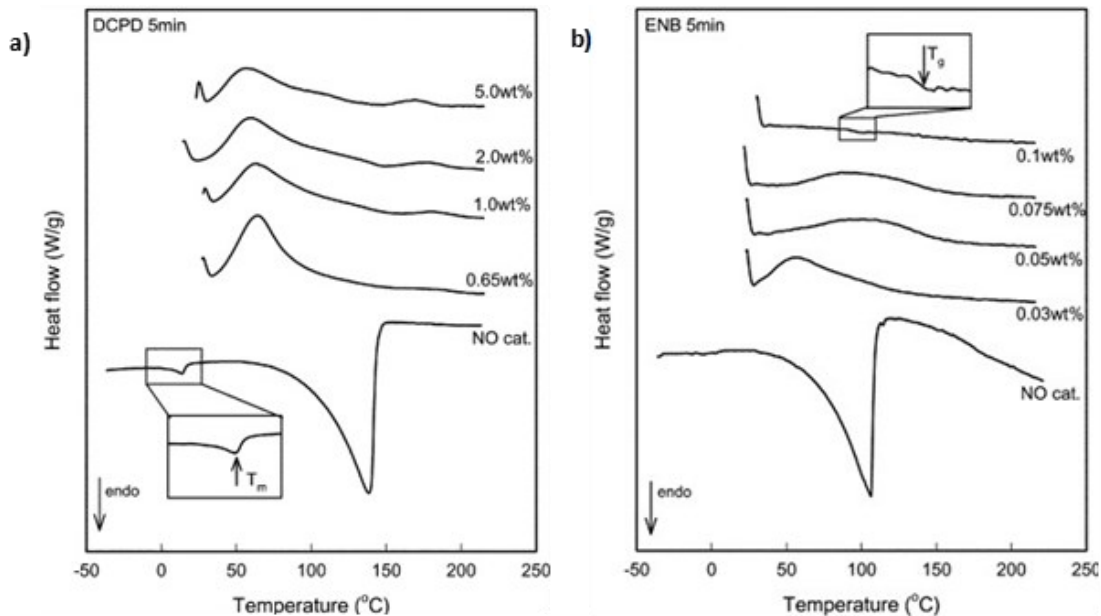


Figure 2.11 DSC thermograms of DCPD and 5E2N for samples cured for 5 min at room temperature with different amount of G1 catalyst [17]

A comparison of DSC analysis of solidified samples of DCPD and 5E2N cured with different amount of G1 for 5 min at room temperature is shown in Figure 2.11. The DSC analysis further confirms the earlier rheological observations that 5E2N can be cured much faster than DCPD with much less amount of catalyst requirement.

The DCPD samples, in Figure 2.11 (a), show exothermic peaks which, as noted by the authors [17], appears in the DSC curve due to the further reaction of remaining active functional groups in the samples. The authors further observed distinct exothermic peaks due to residual reactions for the solidified DCPD samples cured for 120 min (not shown in the figure) at room temperature with up to 5 wt.% of G1. This implies that, 120 min of cure time is not enough for complete curing of DCPD at room temperature even with high concentration (5 wt.%) of G1.

In comparison, Figure 2.11 (b) shows that the exothermic peak disappeared for the solidified ENB sample cured for 5 min at room temperature with only 0.1 wt.% G1. This indicates that the ENB can be completely cured at RT within 5 min with only 0.1 wt.% of G1 [17]. The glass transition temperatures of fully cured samples were also found higher for 5E2N (90°C) than DCPD (50°C) [17]. This implies that, 5E2N can operate at a wider temperature range as healing agent.

Much lower freezing temperature, much faster reaction rates and much lower catalyst requirements of ENB, compared to DCPD, indicates that it can be a potential healing agent candidate for applications at low temperature environment such as in space structures. This is particularly true at low temperatures that may persist in the internal environment of an operating space vehicle. However, there are still some important challenges related to the temperature effects on the cure kinetics and efficiency, to make them suitable for applications in space environment. In our work, we have studied the cure kinetics of 5E2N at low temperatures down to -30°C, using micro-Raman spectroscopic analysis.

2.3.6 Suggestions to improve the properties of ROMP-active healing agents

The researchers in ref. [15], suggested a blend of ENB and DCPD as healing agent to combine the benefit of high reactivity of ENB and higher rigidity of DCPD. They showed that if DCPD is blended with ENB at the proportion of (ENB: DCPD) 3:1 by weight, it can achieve highest rigidity after 120 min in the indirect mixing method. The suggestion of blending ENB with DCPD might allow to achieve higher rigidity contributing to effective recovery of mechanical properties of damaged composite. However, the possible changes in the molecular level of ENB affected by the blending with other reactive chemical like DCPD, might reduce the reactivity of the ENB itself. Thus, the potential benefits of ENB as healing agent might not be fully exploited. Further, the formation of two types of polymers from two different monomers (DCPD and ENB), their compatibility, coherence and the combined mechanical properties achieved through ROMP reaction with Grubbs' catalyst as well as the reaction mechanism itself must be studied thoroughly before such suggestions can be implemented in practice. Further, no attempt of microencapsulating a blend of DCPD/5E2N is found in literature.

Kessler *et al.* [37] demonstrated a huge increase in mechanical properties of poly-5E2N incorporated with ENB-functionalized CNTs. In our work, instead of a blend of 5E2N with other reactive chemicals and their subsequent microencapsulation, we propose a CNT/5E2N suspension as healing agent and its microencapsulation. The incorporation of CNTs in 5E2N is likely to enhance its mechanical self-healing capability as well as to impart an additional electrical self-healing capability to it. In this way, the reactivity of ENB would be preserved and its other comparative advantages over DCPD as demonstrated in refs. [15, 17, 131], can fully be utilized as healing agent.

2.3.7 Microencapsulation of healing agent monomers and the desired characteristics of the microcapsules

One of the major challenges of microcapsule-based self-healing is to enable the microencapsulation of selected healing agent monomer with some desired characteristics of the produced microcapsules for efficient self-healing. The desired characteristics of the microcapsules include:

- i) There should be sufficient amount of liquid content in the core of the individual microcapsule with respect to its total weight/volume. In other words, the major portion of the weight/volume of the individual microcapsules should be the liquid core [102].
- ii) The liquid healing agent would remain intact inside the core of the microcapsules until the microcapsules are broken. There should not be much diffusion or loss of core content over time from the microcapsules [133].
- iii) The shells of the microcapsules should be strong enough (mainly depends on the shell material and thickness of the shells) to survive handling and manufacturing of self healing material. On the contrary, the shells of the microcapsules must be weak enough so that they can easily break during an event of damage that generates microcracks inside the self-healing materials [9, 133].
- iv) The microcapsule shells should facilitate strong bonding to the host material [133].
- v) The microcapsules should also be thermally stable, at least up to the temperature to which they are exposed to during manufacturing and operation of the self-healing material [20].

In-situ polymerization [90] is one of the most widely used methods of microencapsulation of oil-based hydrophobic healing agent monomer like DCPD and 5E2N in suitable polymeric shells. In this method, tiny droplets of a hydrophobic liquid is encapsulated into polymeric shells in a hydrophilic aqueous medium [134]. The formation of the shell walls takes place at the aqueous /organic interface of the healing agent droplets in an oil-in-water type emulsion, through the polymerization of polymeric shell materials [90]. Commonly used shell materials are amino resins which are principally composed of urea and/or melamine and formaldehyde [135] that satisfy many of the desired characteristics of the produced microcapsules as listed above. They provide adequate chemical and mechanical stability of the microcapsules, long shelf-life, good adhesion strengths to polymeric matrixes and higher compatibility with most matrixes [136].

Various core materials are reported to be successfully encapsulated using *in-situ* polymerization of amino resins. However, being a purely chemical reaction process, *in-situ* polymerization

requires precise control of the properties of the reactive solutions made of the core healing agent monomer, shell materials, supporting chemical agents etc. for successful microencapsulation. Simultaneously, it requires precise control of a variety of processing parameters that affect the chemical reaction. While the principle of *in-situ* polymerization remains the same, the process control for each combination of core/shell materials was found to be largely empirical due to the highly complex nature of the chemical process of microencapsulation.

Brown *et al.* [133] microencapsulated DCPD monomer in urea-formaldehyde (UF) shells using *in-situ* polymerization. In later works, Liu *et al.* [20] microencapsulated 5E2N in melamine-urea-formaldehyde (MUF) shells using the same principle. Subsequently, Noh and Lee [137] microencapsulated DCPD as well as 5E2N containing a fluorescent dye in MUF shells. However, they needed to develop specific procedures to match the requirements of the process to enable formation of microcapsules with desired characteristics. The general process of microencapsulation by in-situ polymerization of urea and/or melamine and formaldehyde can be depicted as in Figure 2.12 below.

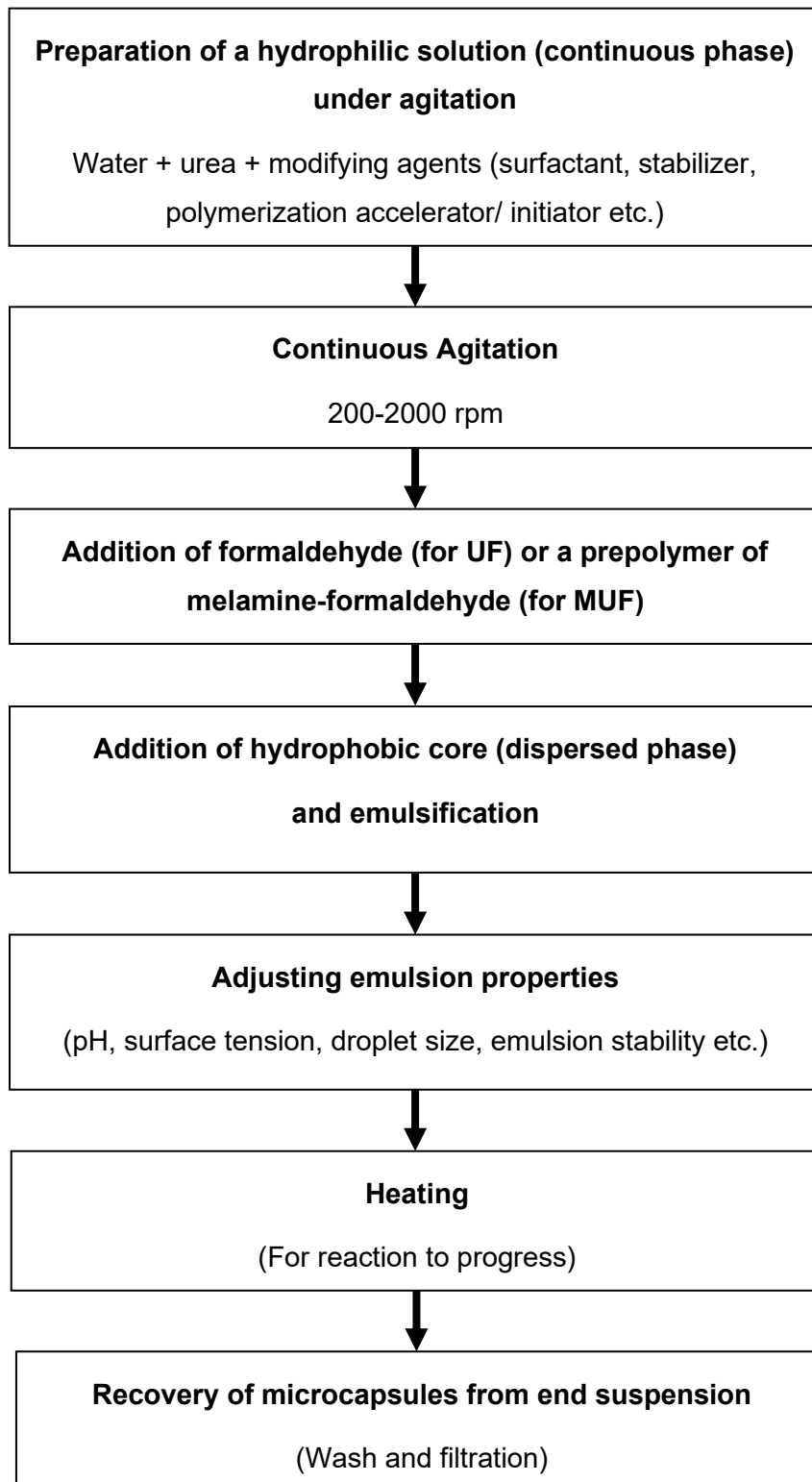


Figure 2.12 General process of microencapsulation of a hydrophobic core by *in-situ* polymerization of urea and/or melamine and formaldehyde

As in the refs. [20, 133, 137], amino resin microcapsules containing a hydrophobic core are generally prepared by *in-situ* polymerization in an oil-in-water type emulsion. The microencapsulation reaction is carried out in a beaker suspended in a temperature-controlled water bath. At the beginning, urea is dissolved into deionized water along with some modifying chemical agents to constitute the hydrophilic continuous phase of the emulsion. The modifying agents are different types of chemical agents that aid in the microencapsulation process. They include, for example, different surfactants, stabilizers, polymerization initiators/accelerators, cross-linking agents etc. They are added sequentially under continuous agitation using a mechanical mixer. The remaining part of the shell material, formaldehyde for the UF microcapsule or a melamine-formaldehyde prepolymer in the case of MUF microcapsules, is then added to the urea solution. In the case of MUF microcapsules, a prepolymer of melamine and formaldehyde is prepared beforehand by dissolving and heating them to a specified temperature. For UF microcapsules, formaldehyde is added directly to the urea solution. At this stage, the hydrophobic core healing agent monomer, the dispersed phase, is added to the solution to form an oil-in-water type emulsion. At this stage, different properties of the formed emulsion are required to be precisely adjusted based on the requirements of the core/shell material combination before initiating the *in-situ* polymerization reaction of the amino resin shell materials. The different emulsion properties that are found critical for the successful microencapsulation by this method include the average droplet size of the emulsion, its pH, surface tension, viscosity, stability of the emulsion etc. The already added modifying agents play crucial roles in controlling the emulsion properties and stabilizing the emulsion making it suitable for successful encapsulation of the core material. After forming a stable emulsion, the final stage of the process is heating the emulsion to the specified temperature to initiate and progress the microencapsulation reaction. After finishing the reaction, the produced microcapsules are recovered by washing and filtering the end suspension.

Brown *et al.* [133] investigated and discussed the key steps that takes place during the microencapsulation of DCPD in UF shells by *in-situ* polymerization in an oil-in-water emulsion. As the current work involves microencapsulation of CNT/5E2N in MUF shells using the same method, understanding these key steps of microencapsulation and their effects on the characteristics of the produced microcapsules is critical. The key findings of their work are discussed below.

In their work, [133] the oil phase or the hydrophobic phase was DCPD which was intended to remain at the core of the microcapsule shells and the medium of the emulsion was aqueous phase

in which the key reaction of UF polymerization took place. During the microencapsulation process, the urea and formaldehyde reacts in the aqueous phase to form a low molecular weight prepolymer. As the molecular weight of the prepolymer increases with progression of the reaction, it deposits at the oil-water interface. The UF ultimately becomes highly crosslinked and forms strong shell walls around the microdroplets of the oil phase, in this case, DCPD, leading to the microencapsulation of DCPD in UF shells [133].

They [133] identified four distinct stages in the microencapsulation process. At the first stage, the temperature of the emulsion was increased continuously to a set point and the agitation speed remained low. At this stage, individual droplets of the oil phase of the emulsion, DCPD in this case, are formed. If agitation is stopped in this quarter of the process, these droplets rapidly coalesce to form a distinct second phase which floats above the aqueous phase of the emulsion. A transition to a cloudy appearance of the emulsion was identified as the beginning of second stage of the process. If agitation is stopped at this stage, the droplets remain as distinct microcapsules. However, at this stage, the microcapsules clump was too fragile to isolate. During this stage, soluble oligomeric species forms and deposits at the core/water interface. The interfacial tension between the hydrophobic core and aqueous continuous phase acts as the driving force for the deposition of polymer as a smooth layer. A transition to milky white solution was identified as the start of the third stage of the microencapsulation process. At this stage, the temperature of the emulsion is stabilized. If agitation is stopped at this region, separable microcapsules appear. The shell thickness of the microcapsules reaches its maximum at this region. The surface morphology also transitions from smooth to rough. The milky white appearance of the emulsion resulting from the light scattering of large aggregates was found to directly correlate to the development of UF nanoparticles in suspension at this stage. This stage is driven by the decreased solubility of the formed higher molecular weight polymer and colloidal species present in the solution. Finally, at the last stage, the suspension becomes clear indicating the completion of the curing reaction [133, 135]. At this time, the agitation is stopped, and microcapsules produced are easily separable.

The UF microcapsules produced in ref. [133] were characterized by two membranes of the shell wall. The inner membrane was smooth, continuous, and free of voids whereas the outer membrane was rough and porous as shown in Figure 2.13.

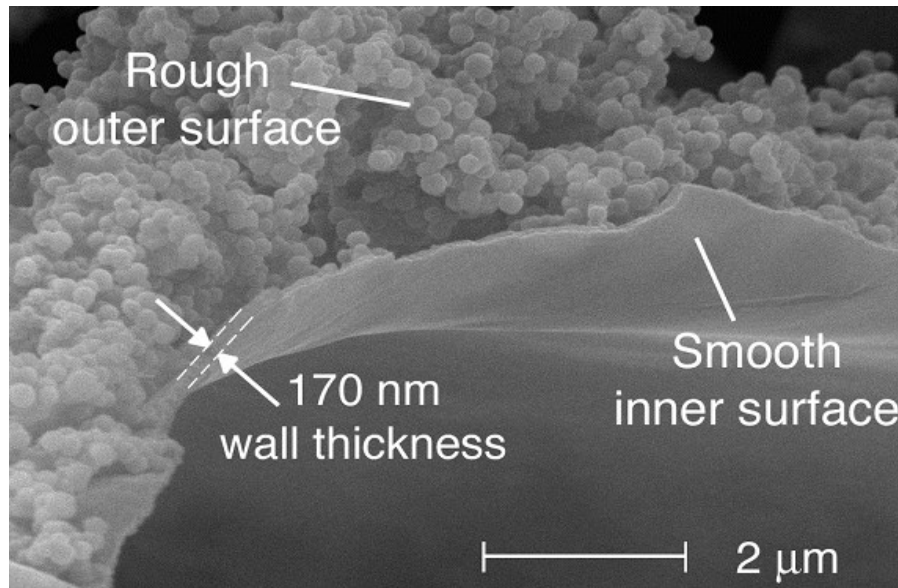


Figure 2.13 Surface morphology and shell thickness of UF microcapsules [133]

According to the authors [133], the smooth, non-porous inner membrane of the microcapsules was the result of deposition of low molecular weight of UF prepolymer at the DCPD-water interface while the prepolymer remains soluble. The rough porous structure on the outer surface of the microcapsules was the result of the deposition and agglomeration of UF nanoparticles that precipitated from the higher molecular weight of prepolymer in the aqueous solution and attached to the microcapsule shells during the microencapsulation process [133]. It is to be noted that roughness of the microcapsule surface to some extent is desirable as it enhances their mechanical adhesion when embedded in the host polymer and improves self-healing performance [133].

The shell thickness of the microcapsules that ref. [133], obtained were in the range of 160-220 nm which was also found to be largely independent of the manufacturing process parameters. According to the authors, the microcapsules in this range of shell thickness is sufficiently robust to survive handling and manufacturing of self-healing polymer composites [133].

In contrast to UF microcapsules, MUF capsules were more resilient to the formation of nanoparticles and displayed a smooth and relatively thicker shell up to 700-900 nm [20, 135]. Hu *et al.* [138] observed that MF microcapsules are stronger and ruptures at larger deformations than UF for a given size and shell thickness. They [138] also observed that mechanical strengths of the MF microcapsules vary with in-situ polymerization reaction time and size of the

microcapsules. In our work, CNT/5E2N suspension is microencapsulated in MUF shells using the *in-situ* polymerization method.

2.3.8 Factors affecting the microencapsulation process and the quality of microcapsules

Various factors were found to affect the success and yield of the microencapsulation process by *in-situ* polymerization method and the quality of the produced microcapsules. The major factors, as found in literature, are discussed below.

i) Reaction temperature

As discussed above, the capsule shells are formed by the deposition of the polymer and nanoparticles at the core droplet surface during the encapsulation process. Formation of the amino resin polymer and the nanoparticle in solution is dependent on their rate of reaction which is principally controlled by the reaction temperature. For example, an increase in reaction temperature from 50°C to 70°C during the encapsulation of palm oil by UF increased the nanoparticle formation and severely affected the encapsulation efficiency. Similarly, low reaction temperature of 40 °C and 60 °C also resulted in poor encapsulation efficiency for the encapsulation of epoxy in UF shells [135, 139]. Poorer dispersion of the core material at lower reaction temperature and the resulting polymer precipitation in solution rather than at the core droplet surface was presumed to be the cause behind this. According to ref. [140], the reaction temperature also strongly influences the thickness, roughness and porosity of the microcapsule shells. Reaction temperature of 55°C and 85°C were used, for the microencapsulation of DCPD in UF [133] and 5E2N in MUF [20], respectively.

ii) Molar ratio of the shell materials

The molar ratio of the shell materials, i.e., the molar ratio of urea and formaldehyde, determine the properties of the capsule wall. Low formaldehyde/urea molar ratio can lead to the production of weaker shells of the microcapsules due to lower crosslinking of the shell materials. [136]

iii) Ratio of core/shell material

It affects the dispersion process and determines the surface area available to shell material. Dispersion of large amount of core material is expected to be more difficult as the droplets coalesces more readily. It affects the formation of nanoparticles in solution and the shell thickness of the produced microcapsules [135].

iv) Use of suitable modifying agents

Successful formation of microcapsules relies on the efficient phase separation of the core and shell materials during the encapsulation process. The balance of hydrophobicity of the core material and the hydrophilicity of the shell materials dictates this partitioning process for this type of microencapsulation of an oil-in-water type emulsion. Interfacial interactions of the core and shell materials play a crucial role in this regard. The use of various modifying agents including the surfactants and stabilizers provide control over the interfacial interactions and limits Ostwald ripening and droplets coalescence [135]. The surfactant is selected to promote the chemical compatibility between the hydrophilic and hydrophobic part of the emulsion.

The use of various modifying agents is found to be empirical in literature depending on the characteristics of the encapsulant core and shell materials combination. For the encapsulation of DCPD in UF shells, Brown *et al.* [133] used ammonium chloride as a polymerization initiator, and resorcinol as a crosslinking agent. They also employed reactive Ethylene maleic anhydride (EMA) as surfactant. On the other hand, Liu *et al.* [20] and Noh and Lee [137] did not employ initiators and cross-linking agents for the encapsulation of 5E2N in MUF shells. Instead of reactive surfactants, they used inert surfactants like sodium dodecyl sulphate (SDS) and poly vinyl alcohol (PVA) for the 5E2N/MUF system. For DCPD/UF system, control of pH of the emulsion at different stages of the microencapsulation process was found to be critical [133] whereas for the 5E2N/MUF system, pH of the emulsion was not a controlling parameter [20, 137].

v) Stirring speed

Mixing and dispersion of the core hydrophobic phase into the oil-in-water emulsion is primarily achieved by mechanical stirring. The stirring provides the required kinetic energy to the system for the formation of the core droplets in the emulsion. The average size of the droplets produced in the emulsion is inversely related to the stirring energy. Brown *et al.* [133] reported an exponential relationship between the average diameter of the produced UF microcapsules and stirring speed as shown in Figure 2.14.

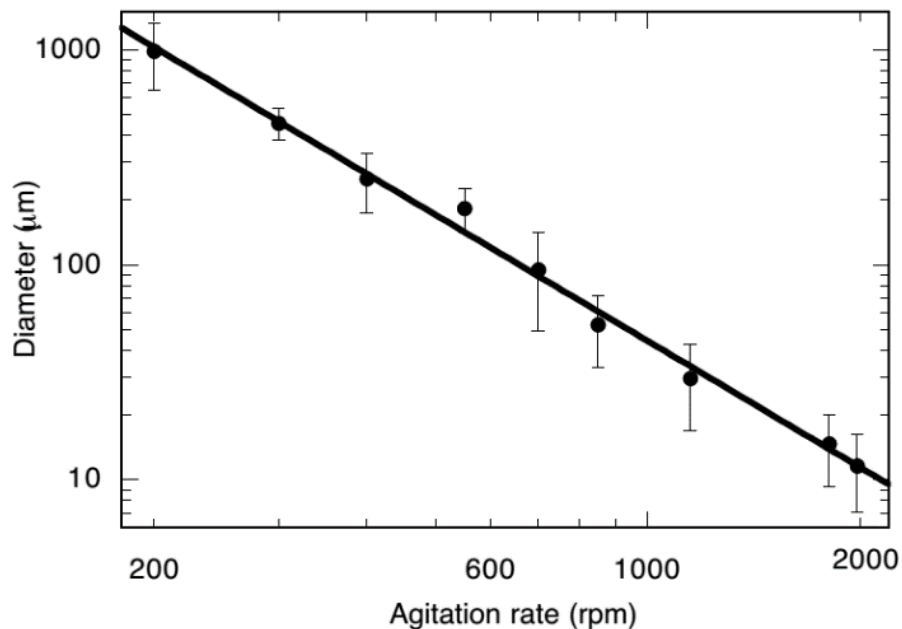


Figure 2.14 Mean diameter of the microcapsules vs agitation speed [133]

Besides the above factors, the design of the reactor, stirrer type, agitation process, heating rate and duration of reaction etc. were found to have significant impact on the success and outcome of the microencapsulation process.

2.3.9 Choice of catalyst

Aside from the healing agent monomer, the incorporated catalyst/initiator plays the second most important role in achieving self-healing of the host polymer. Without a suitable catalyst/initiator for the polymerization reaction of the healing agent, self-healing might not be possible to achieve. Specially, for the ROMP-based self-healing system, the importance of choosing a suitable catalyst type is crucial. It dictates the ROMP mechanism and the cure kinetics of the healing agent monomer and ultimately determines how fast and efficiently the self-healing can be proceeded in the surrounding operating environment.

In the last decade, ROMP initiators have made immense developments in constructing many polymers of industrial importance [11, 141]. ROMP reactions and in general, olefin metathesis can be accomplished using a number of different transition metal catalysts (e.g., Ru, Mo, W, Ti) [10, 129, 142-149]. Stability in ambient environment (with air and moisture), activity and tolerance

to different functional groups are the major concerns for these catalysts for many practical applications [129, 142, 149-151]. For example, molybdenum- or tungsten-based Schrock catalysts display high metathesis activities and stabilities but are sensitive to ambient air and moisture and are relatively intolerant of polar functionalities [152]. Ruthenium-based Grubbs' catalyst, on the other hand, is known to show high metathesis activity while being tolerant of a wide range of functional groups such as esters, amides, ketones, aldehydes, alcohols, acids as well as oxygen and water [141, 153-158].

During fabrication of high-performance self-healing polymers based on ROMP reaction of healing agents, catalysts are required to be dispersed into the polymer matrix where it is often exposed to a variety of chemical groups present in the matrix, its diluents, curing agents/cross-linkers, inhibitors etc. The fabrication process or a substantial part of it often undergoes in ambient environment with air and moisture present. The characteristics of the Ruthenium-based Grubbs' catalyst including their high metathesis activity, excellent tolerance to different chemical functional groups and insensitivity to ambient air and moisture, thus, suits best for the development of high-performance self-healing polymers. On the contrary, Ruthenium catalysts are also known for their sensitivity to exposure to high temperatures and amine functional groups [144, 159, 160] of different curing agents to which high performance polymers are often exposed to, especially, during their fabrication process. Commercial Ruthenium catalysts are also expensive. Thus, a comparative evaluation of their thermo-chemical stabilities and activities is necessary for their proper selection for the targeted low temperature self-healing aerospace applications.

2.3.10 Comparative evaluation of Ruthenium catalysts

Several versions of Ruthenium based Grubbs' catalysts are commercially available. Among them G1, G2, HG1 and HG2 are utilized/investigated in self-healing literatures with G1 used in most of the investigations for ROMP-based self-healing at room temperature and above.

Grubbs' catalysts are based on Ruthenium atoms with five ligands. These ligands play a key role in stabilizing and activating the central metal atom of such catalysts. For example, the Ruthenium metal center remains the same in both G1 and HG2 catalysts. The key difference in Grubbs' and Hoveyda-Grubbs' catalysts is related to the type of ligands involved in their chemical structure. These chemical bonds have a profound impact on the reaction activity and kinetic at different temperatures, and dictate the properties of the materials, like its stability and its tolerance to different functional groups [161].

i) Effect of morphologies

Jones *et al.* [45] investigated the effect of different morphologies/crystal polymorphs of G1 on their thermal stability. The thermal stability of the catalysts was investigated by DSC measurements and ROMP trials after their thermal exposure at different temperatures. The as-received G1 obtained from Sigma Aldrich was composed of relatively large crystals roughly 150 μm long and 40 X 50 μm in cross section. The as-received G1 obtained from Strem chemicals was in the form of crystalline rods about 100 μm in length and only 2 μm in diameter partially fused together in lumps. Smaller crystal dimensions were obtained by grinding the as-received catalyst or through recrystallization processes like solvent evaporation, addition of non-solvent and freeze drying [45].

ROMP trials after thermal exposure showed that G1 of Sigma-Aldrich remained active after heating under nitrogen to 190°C while Strem catalyst lost reactivity after 180°C. Similarly, under air, Sigma-Aldrich catalyst retained their activity up to 140°C while the Strem catalyst began to decompose at 90°C [45]. According to the DSC traces of different crystal polymorphs of the catalysts, they [45] suggested that the crystal polymorphs of G1 influence their thermal stability.

Further, in their fracture test of polymer samples, they observed that the ground Grubbs' catalyst did not provide any better healing capability than the as received Sigma-Aldrich Grubbs' catalyst. When the catalyst was mixed with uncured epoxy matrix, it was exposed to amine curing agent DETA (Diethylenetriamine) which deactivated the catalyst [45]. Similarly, the micrometer thick disk morphology of freeze-dried catalyst was also deactivated by the amine curing agent [45]. They observed that if the catalyst particles are too small, more exposure to the amine curing agents, such as DETA, would significantly reduce the reactivity of the catalyst due to their higher surface area [45]. To avoid the deactivation of catalyst during mixing, Brown *et al.* [12] suggested to choose the mixing order such that the curing agent does not come into direct contact with the catalyst.

ii) Comparison of activity and thermo-chemical stabilities

Wilson *et al.*, [161] the same research group, later investigated and compared chemical stabilities and initial polymerization kinetics of three variations of catalysts (G1, G2 and HG2). For the evaluation, they employed a freeze-drying technique to transform the highly crystalline solid particle forms of all three as-received catalysts into their amorphous polymorphs with higher-surface area morphologies [161].

ROMP activity both in solution and in bulk were compared for the three catalysts. Solution ROMP activity of the catalysts were investigated by *in-situ* NMR experiments in which each catalyst was dissolved first in benzene and later adding DCPD into it at 25°C. Bulk ROMP activity of the catalysts was evaluated by DSC measurements. The stability of the catalysts (in solution of methylene chloride) to DETA was evaluated by ¹H NMR at 25°C. The chemical compatibility of the three catalysts with DETA was also evaluated by measuring healing performance of an EPON 828/DETA matrix via self-activated fracture tests of TDCB samples [161].

Initial polymerization rates of catalysts in solution at 25°C was found to be significantly higher for G2 than G1. The rate constants for G1 and G2 in solution of benzene were measured to be 1.45×10^{-4} and $4.3 \times 10^{-3} \text{ s}^{-1}$, respectively. G2, on the contrary, showed slower ROMP activity than G1 in bulk reaction condition. Attempted similar experiments with HG2 catalyst both in solution and bulk polymerization of DCPD was failed due to too fast reaction at 25°C and caused the required measurements impossible to make [161]. This suggests a much higher polymerization rate of HG2 at RT, which, in fact, implies that HG2 catalyst might be suitable for ROMP reaction at very low sub-zero temperatures.

For the chemical compatibility tests of the three catalysts to DETA, the authors casted TDCB epoxy samples by mixing each catalyst to EPON 828 and DETA prior to curing them at 25°C and post-curing them at 35°C for 24 hours and later performed self-activated healing tests with the samples. Both freeze-dried and as-received catalysts were tested for evaluating their effect upon exposure to DETA. For the freeze-dried morphologies of the catalysts, upon adding G1 to the curing mixture of the EPON 828 resin and DETA, the purple G1 catalyst turned brown immediately. This color change is the indicative of the deactivation of the catalyst, as they mentioned and indicated in ref. [12, 161, 162], A color change from brown to green was also observed for G2 while no obvious color change was observed for HG2. This implies that, HG2, even in its amorphous form was not deactivated upon exposure to the DETA curing agent when at 25°C. The as received forms of the catalysts did not, however showed such immediate color change. The authors [161], argued that the as-received catalysts having more robust morphology were more capable of resisting deactivation by amine curing agents like DETA.

Further, in the work [161], ¹H-NMR spectra were analyzed for each catalyst dissolved in methylene chloride solution when DETA was added. The analysis implied that unstable DETA-ruthenium complex was formed with G1 that undergoes decomposition [148]. For G2 and HG2, more stable ruthenium complex was formed when DETA was added. The authors suggested that the ruthenium catalysts that contain N-heterocyclic ligands (such as in G2 and HG2), instead of

phosphine ligand (such as in G1), might have greater ability to stabilize new ruthenium complexes with primary amines, such as DETA, resisting deactivation of catalyst [161]. Further, for self-healing applications, catalyst is embedded into polymer matrix as solid particles which, compared to in solution, is expected to impart more resistance to deactivation by amine curing agents. Their DSC experiments also confirmed that the thermal stability of as-received catalyst morphology both under air and N₂ is higher than freeze-dried morphology.

Guadagno *et al.* [163] employed ¹H NMR and infrared spectroscopy to investigate the thermal and chemical stability of HG2 in self-healing epoxy. In their investigation, free HG2 was found to have exceptional stability even after thermal treatment at 180°C in air atmosphere. However, the HG2 catalysts was found to be deactivated in the self-healing epoxy system when cured at high temperature up to 150°C or 180°C. Their infrared analysis revealed that the HG2 gives rise to a reaction with the oxirane rings of the epoxy precursors if directly treated at high temperatures (150-180°C). The formation of chemical bonds with the epoxy functionality at high temperatures changes the reactivity of HG2 irreversibly and therefore, the catalyst was not subsequently able to promote polymerization of healing monomer, thus losing its self-healing ability [163].

They [163] recommended and verified a two-stage curing process for the epoxy system in which the self-healing epoxy formulation is first cured at lower temperature (up to 70°C for 7h) and then treated in a second stage at higher temperature (150°C for 2h). The idea was to anticipate opening of all oxirane rings at lower temperature in which the catalyst was not reactive enough to form chemical bonds with them. They verified that HG2 does not react with the oxirane rings of the epoxy precursor even for an extended period of time at low temperature (70°C). The temperature of 70°C, on the other hand, is high enough for the curing of a liquid epoxy formulation with appropriate curing agents. Their experiments showed that with the pre-treatment at lower temperatures, the catalytic activity of HG2 powder embedded in epoxy formulation can be preserved up to a temperature between 150-160°C [163]. The findings of the study are important for self-healing epoxy formulations that require high temperature cure processing.

Based on the findings of the above studies, HG2 is chosen for our work for the investigation of CNT/5E2N as micro-encapsulated healing agent for self-healing epoxy for targeted low temperature aerospace applications.

2.4 Restoration of mechanical properties of materials using microcapsules and evaluation of healing efficiencies

Numerous works have been carried out to demonstrate and optimize the recovery of mechanical properties of host material using microcapsules containing different healing agents. White *et al.* [9] established a testing protocol for evaluating the mechanical healing efficiency of structural polymer such as cured epoxies incorporated with healing agents. The protocol for evaluating the healing efficiency of self-healing polymer is widely adopted by scientific community [12-14, 102, 164, 165] in this field. In this protocol, healing efficiency of self-healing polymer is measured by controlled fracture of the samples with a tapered double cantilever beam (TDCB) geometry. The TDCB geometry of the polymer samples, developed by Mostovoy *et al.* [12, 166], provides a crack-length independent measure of fracture toughness of the samples [12]. Figure 2.15 shows the typical geometry of tapered double-cantilever beam (TDCB) used by different authors [12-14, 102, 164, 165] for measuring the self-healing efficiency of epoxies incorporated with healing agents.

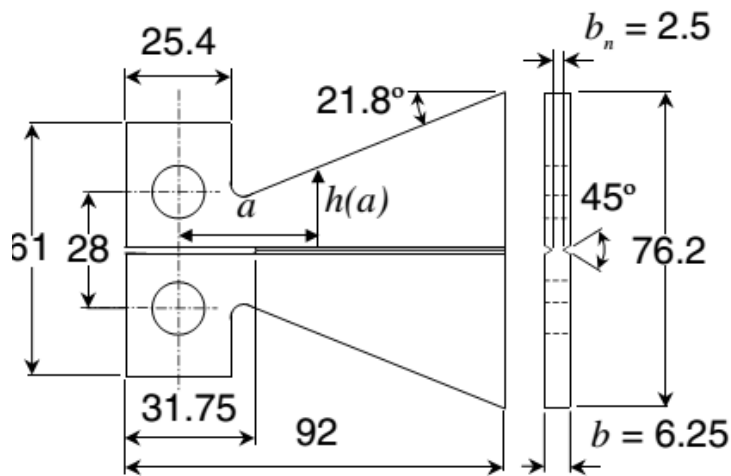


Figure 2.15 Tapered double-cantilever beam (TDCB) geometry (dimensions in mm) [12]

For the TDCB sample geometry, the healing efficiency is given as [12],

$$\eta = \frac{K_{Ic_{heated}}}{K_{Ic_{virgin}}} = \frac{P_{c_{heated}}}{P_{c_{virgin}}} \text{ ----- [Eq.2.1]}$$

where $K_{Ic_{virgin}}$ is the fracture toughness of the virgin specimen and $K_{Ic_{healed}}$ fracture toughness of the healed specimen and P_c are the corresponding critical fracture loads.

According to Eq. (2.1), the healing efficiency can be directly calculated just by knowing the critical loads of fracture. With the sample geometry, there is no need to control or monitor the crack lengths during the tests, which is difficult to do accurately, and measure the individual fracture toughness of samples, to determine the healing efficiency.

According to the protocol, the polymer samples with TDCB geometry is first fabricated by incorporating the healing agents (microcapsules and catalysts) into it. The samples are initially fractured along their centre line into two halves. The two halves of the samples are then kept in close contact for specified healing conditions. The healed samples are then fractured again for the second time. The critical loads during the initial fracture and second fracture after healing are measured during the tests to determine the healing efficiency according to Eq. (2.1).

A typical load-displacement curve for the fracture tests of TDCB epoxy samples for the measurement of healing efficiency is shown in Figure 2.16.

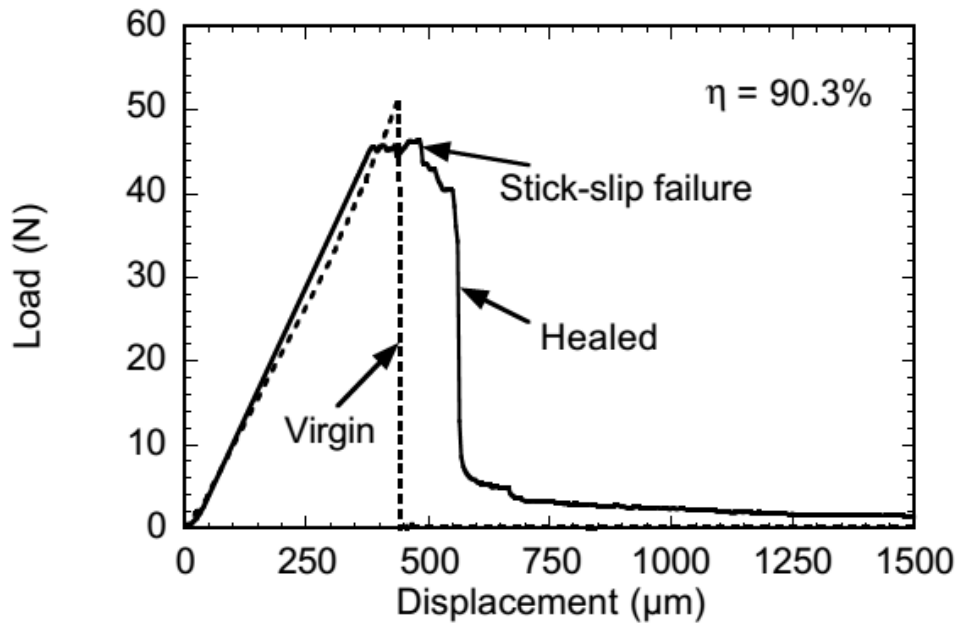


Figure 2.16 Typical load-displacement curve for the fracture tests of TDCB epoxy samples for determining healing efficiency [12]

According to Figure 2.16, the critical failure load of the healed test is about 90.3% of the critical failure load of the initial (virgin) test giving a 90.3% healing efficiency. In our work, we followed this protocol for evaluating the mechanical healing efficiency of the microcapsules containing CNT/5E2N incorporated into epoxy samples.

2.3.12 Factors affecting mechanical healing efficiencies

Apart from the choice of the healing agents and suitable catalyst/initiator for targeted applications, some other major factors affect their mechanical self-healing performance. As found in literature, the major factors are the physical and mechanical properties of the microcapsules themselves, their interaction with the host polymer and the average size (diameter) and concentration (wt.%) of microcapsules incorporated into the host polymer.

i) Physical and mechanical properties of the microcapsules and their interaction with the host polymer

Keller *et al.* [167] observed that for efficient healing agent delivery, the elastic stiffness and failure strength of the microcapsules, as well as the percentage of the capsule core volume occupied by the liquid reactants are important parameters. They [167] measured the elastic modulus of PUF shelled microcapsules containing DCPD to be 3.7 ± 0.2 GPa which was also found to be independent of the microcapsule diameters. They noticed that the capsule-to-matrix stiffness ratio influences the path of crack propagation in close proximity to the microcapsules in the polymer matrix. A microcapsule with a higher elastic modulus than the surrounding matrix creates a stress field that deviates the crack path away from the microcapsule. On the other hand, a more amenable shell wall material produces a stress field that attracts the crack toward the microcapsule facilitating the rupture of the microcapsules [167].

It is also important that the microcapsule shells possess sufficient strength to remain intact during processing of polymer matrix [89]. For this, the shell walls of the microcapsules should have to be optimally thick. If the shell walls are too thick, for example, it will not rupture during encountering an approaching crack in the sample. Without the rupture of microcapsules, no healing is possible. If the shell wall is too thin, on the other hand, it will be fragile and diffusion of healing agent will hinder the healing process [89, 167].

Brown *et al.* [13] observed that good adhesion between the microcapsules and epoxy matrix is essential for the rupture of microcapsules for efficient healing and for any positive effect on the initial mechanical properties. If there are poor bonding between microcapsules and epoxy, the

fracture behavior resembles the fracture behavior of epoxy with a similar concentration of voids. Thus, good matrix-microcapsule adhesion is one of the important requirements for efficient self-healing.

ii) Average size (diameter) and concentration of the microcapsules incorporated in the host polymer

The dependence of the average microcapsule size on the healing efficiency of epoxy for the DCPD/G1 healing agent system [12] is depicted in Figure 2.17.

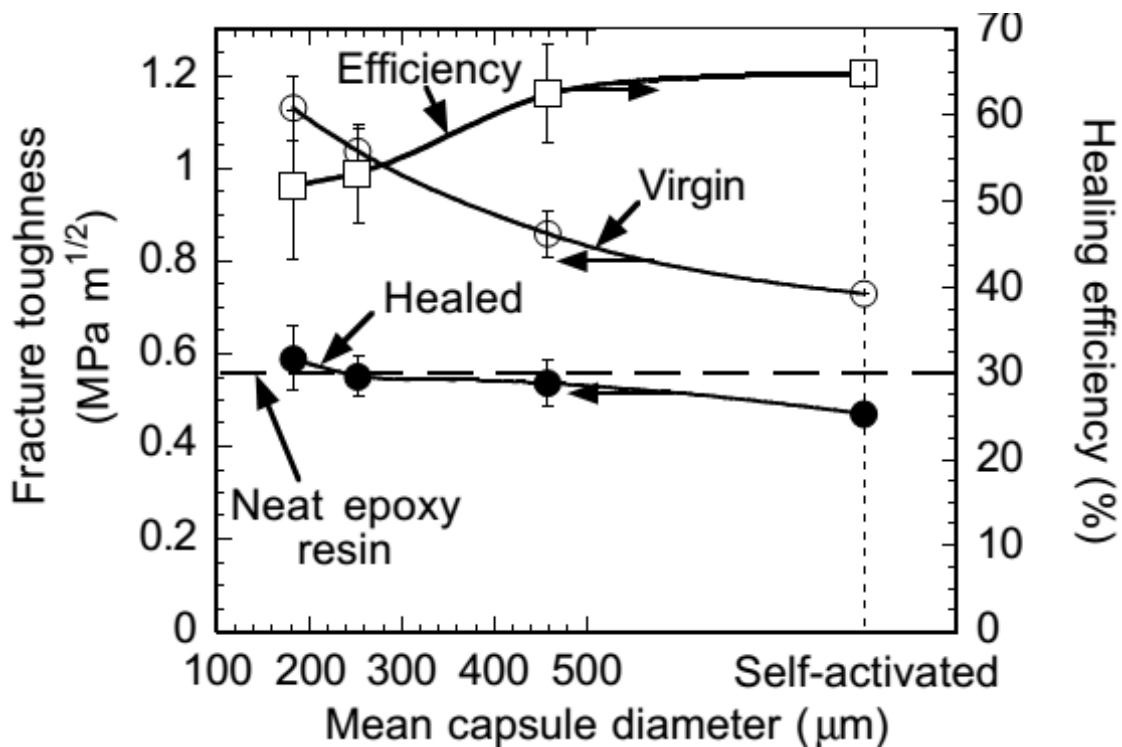


Figure 2.17 Effects of average diameter of microcapsules containing DCPD on fracture toughness of epoxy and the healing efficiency [12]

Figure 2.17 shows that healing efficiency is increased with the increase of average diameter of the microcapsules containing DCPD. However, increasing the size of the microcapsules from around 180 µm to 460 µm decreased the initial (virgin) fracture toughness of epoxy significantly. Significant reduction of initial mechanical properties due to the incorporation of healing agents into the host material defeats the ultimate purpose of self-healing. For this, the average diameter

of the microcapsules should be chosen to minimize the reduction of initial mechanical properties of the host material.

Figure 2.18, on the other hand, shows the effect of concentration of microcapsules containing DCPD on initial and healed fracture toughness of the epoxy.

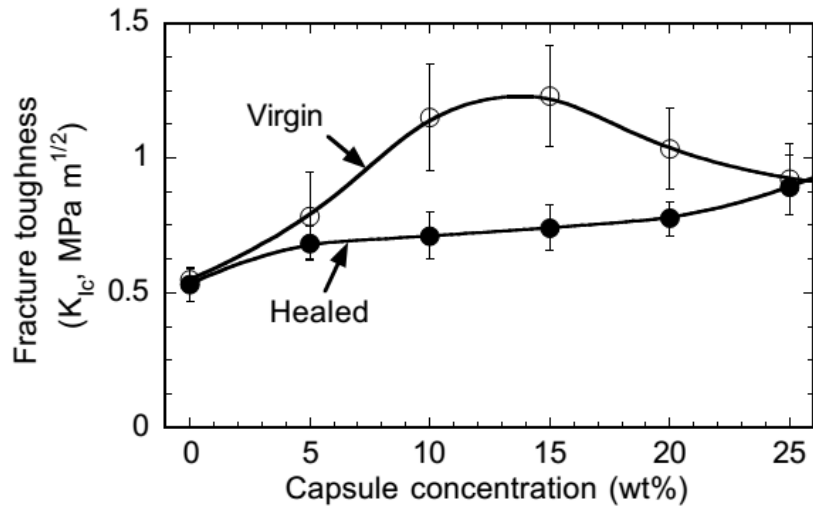


Figure 2.18 Effects of microcapsule concentration containing DCPD on initial (virgin) and healed fracture toughness of epoxy [12]

Figure 2.18 shows that the initial fracture toughness of epoxy increases up to a concentration of 10-15 wt.% of microcapsules after which it decreases. The healed fracture toughness, on the other hand remains more or less same between 5-15 wt.% of microcapsules with slight increase above 15 wt.%. Increasing the concentration of microcapsules, however, also increase the viscosity of the uncured resin which makes the manufacturing of samples difficult [12].

Rule *et al.* [102] established a simple relationship to determine the total mass of healing agent delivered per unit crack area (volume), as well as the average size and concentration of microcapsules incorporated into resin samples, as follows [102]:

$$\bar{m} = \rho_s \varphi d_c \text{ ,----- [Eq. 2.2]}$$

where, \bar{m} is the mass per unit crack area of healing agent available for delivery, ρ_s is the density of the sample, φ is the mass fraction of the microcapsules and d_c is the diameter of the microcapsules.

According to Eq. (2.2), the total mass of available healing agent per unit crack area is proportional to both the microcapsule weight fraction and their diameter. The amount of healing agent that the microcapsules release into the crack sites is found to vary linearly with the microcapsule diameter for a given weight fraction of the microcapsules. They also demonstrated that the self-healing performance reaches its maximum levels only when sufficient healing agent is available to fill the crack entirely. Based on the observations made in refs. [12, 102], and the relationships developed in ref. [102], the size and concentration of microcapsules can be rationally chosen for optimal healing efficiencies in a great variety of polymer-based samples.

2.5 Restoration of electrical properties of materials using microcapsules

Minor mechanical damage in electronic devices such as in integrated circuits or in lithium-ion batteries disrupts their integrity and performance due to the disruption in the electrical conductivity and limits their lifetime. Aside from the efforts for the recovery of mechanical properties of materials after damage, some efforts were made to impart electrical self-healing functionality to materials [43, 97, 99, 168, 169].

Blaiszik *et al.* [99] microencapsulated an eutectic gallium–indium (Ga–In) liquid metal alloy which has a melting point below room temperature (16°C) and possesses relatively high conductivity ($3.40 \times 10^4 \text{S}\cdot\text{cm}^{-1}$) in UF shells. They demonstrated self-healing of an electrical circuit with nearly full recovery (99%) of conductance in less than one millisecond after damage. The microcapsules containing the liquid metal alloy were dispersed in a dielectric epoxy formulation which was deposited on a conductive line in a microelectronic device as shown in Figure 2.19, [99].

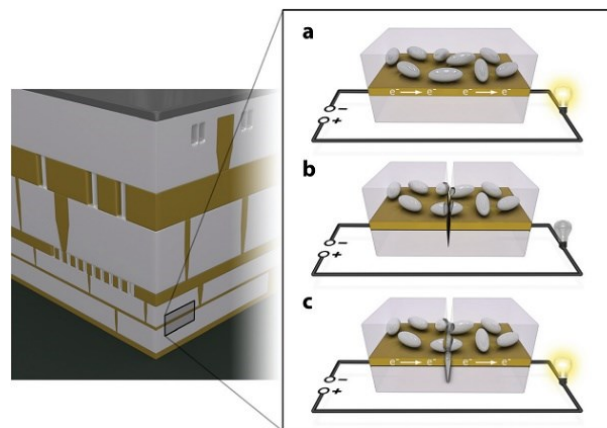


Figure 2.19 Autonomous conductivity restoration concept using microencapsulated Ga-In liquid metal alloy [99]

When an induced crack damage broke the conductive pathway, it interrupted the electron flow and simultaneously ruptured the microcapsules. The liquid metal released from the microcapsules and flowed to the crack re-establishing the conductive pathway [99].

Caruso *et al.* [168] synthesized microcapsules containing single walled carbon nanotubes (SWCNT) suspended in organic solvents like Chlorobenzene (PhCl) and Ethyl Phenyl Acetate (EPA)] using oil-in-water *in-situ* emulsion polymerization of urea-formaldehyde. The microcapsules were shown to release SWCNTs in bundle form suspended in the solvents. The SWCNTs used in the suspension, however, did not disperse well in the solvents leading to aggregation of nanotubes as can be seen in the optical micrographs of the microcapsules in Figure 2.20 [43, 168].

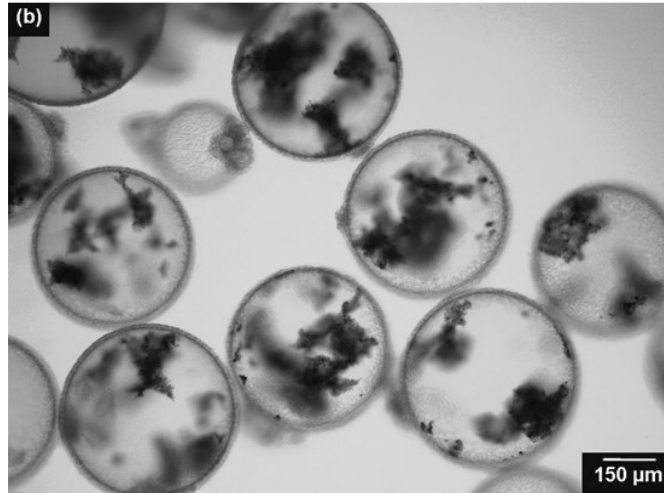


Figure 2.20 Optical micrograph of microcapsules containing SWCNT (0.05 wt%) suspended in EPA [168]

Under applied electric field between two probes submerged in the SWCNT suspension, they [168] showed the migration of SWCNTs which form a bridge between the probes producing a measurable current flow. The result, as shown in Figure 2.21, indicates its applicability to electrical self-healing of materials.

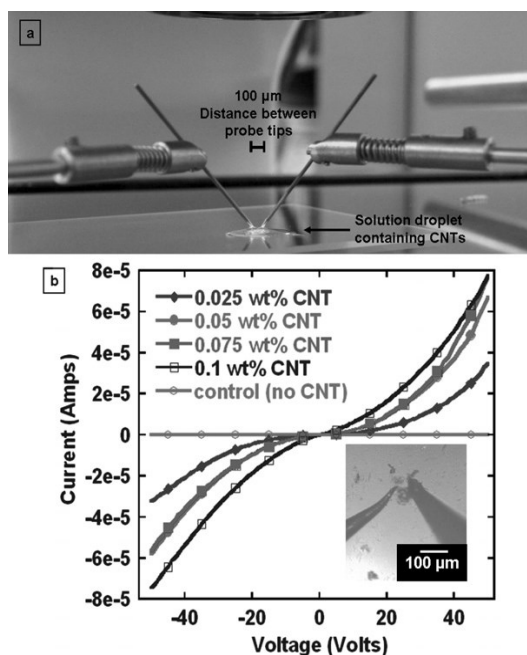


Figure 2.21 Experimental setup showing probe tips submerged into the solution droplet containing SWCNT. (b) current–voltage plots showing conductivity measurements of solutions of capsules containing SWCNT in EPA [168]

In order to limit the problem of dispersibility of SWCNT in a non-polar solvent like chlorobenzene which led to the aggregation of SWCNT in [168], the researchers in the same group in a later work [43] employed a conducting polymer poly (3- hexylthiophene-2, 5-diyl) (P3HT) as an additive to achieve stable SWCNT suspension in a non-polar solvent o-dichlorobenzene. The suspension of SWCNT in o-dichlorobenzene was microencapsulated in PUF shells using *in-situ* polymerization of UF. Using the microcapsules containing the SWCNT suspension, they [43] demonstrated autonomic restoration of electrical conductivity of fractured patterned gold line samples.

Kang *et al.* [97] microencapsulated functionalized carbon black suspended in O-dichlorobenzene using *in-situ* polymerization of urea-formaldehyde. Functionalization of carbon black and addition of core thickeners into the core suspension was shown to improve particle release from microcapsules upon crushing. 100% conductivity restoration of damaged silicon anodes was demonstrated using the microencapsulated carbon black suspension [97].

Pastine *et al.* [170] encapsulated 1 wt.% of multiwall carbon nanotubes (MWCNTs) suspended in toluene inside polyamide shells by interfacial polymerization, which is intended to produce remotely triggerable microcapsules. In these reports [43, 168, 170] however, the majority of core

materials embedded within these microcapsules were solvents, which cannot undergo polymerization reaction for effective self-healing of cracks or damage of a fully cured thermoset polymers like epoxy.

Regarding the healing agent, Bailey *et al.* [92] were able to encapsulate epoxy with high concentration (up to 20 wt.%) of CNTs using ethyl-phenyl acetate (EPA) solvent for conductive coating applications. A conductivity recovery of 64% ($\pm 23\%$) and a structural recovery of 81% ($\pm 39\%$) were measured by *in-situ* electro-tensile tests conducted on coatings and substrate systems. Nevertheless, the healing agent was the epoxy/CNT core material dissolved in a solvent that is not suitable for self-healing applications below 0°C.

Instead of releasing conductive materials from microcapsules, Odom *et al.* [169], in another work, utilized microencapsulated organic solvent, hexyl acetate, alone for the restoration of electrical conductivity of materials. Upon mechanical damage of an electric circuit made of a conductive ink consisting of silver particles, the solvent released from the microcapsules were shown to locally dissolve the polymer binder of the conductive ink. This allowed for the redistribution of the conductive particles in the damaged circuit and restoration of electrical conductivity upon solvent evaporation [169].

Authors in ref. [171] argued that the liquid metal alloy encapsulated in ref. [99] is expensive and the volatile organic solvents used in refs. [43, 92, 168-170] are toxic to human and environment and can form smog limiting their sustainable use in self-healing electronics. They, instead, microencapsulate different conductive aqueous solutions containing poly 3, 4- ethylenedioxythio phene/polystyrenesulfonate, graphene particles, Fe₃O₄ particles or simply running water or deionized water using water-in-oil emulsification polymerization of melamine formaldehyde. The conductivity of the aqueous core of the microcapsules were shown to be sufficient to self-repair electrical circuits [171].

None of these microencapsulated solvents or suspensions used in the above works, however, are capable of undergoing polymerization to effectively recover both electrical and/or mechanical properties of a fully cured thermoset polymer like epoxy-based materials. Also, none of the above works are intended for very low temperature applications such as prevailing in space environment. In our work, CNT suspended in 5E2N is investigated as microencapsulated healing agent for the recovery of electro-mechanical properties of epoxies for targeted aerospace applications at low temperature.

Zamal, Hasna Hena, *et al.* Cure kinetics of poly (5-ethylidene-2-norbornene) with 2nd generation Hoveyda-Grubbs' catalyst for self-healing applications. *Polymer* 153 (2018): 1-8.

<https://doi.org/10.1016/j.polymer.2018.07.082>

CHAPTER 3: INVESTIGATION OF THE POLYMERIZATION KINETICS OF 5E2N INITIATED BY HG2 CATALYST AT LOW TEMPERATURES USING MICRO-RAMAN SPECTRAL ANALYSIS

3.1 Applications and advantages of Raman spectroscopy for our investigation

The current work is related to self-healing polymeric materials systems based on ROMP reaction of microencapsulated self-healing monomer 5E2N initiated by HG2 catalyst. The healing agents (i.e., the monomer and the catalyst) are particularly promising for aerospace industry, but there are still some important challenges related to the temperature effects on the ROMP kinetics and efficiency, to make them suitable for applications in cold environment such as in space. Among the encountered problems, understanding and optimizing the polymerization kinetics at low temperatures represent a key step. These features are investigated in this work using micro-Raman spectroscopy.

Raman spectroscopy is a form of molecular spectroscopy, which is used for the non-destructive materials analysis and identification. The Raman effect is a consequence of the inelastic interaction of light with the electron cloud of molecules, in which a small fraction of the scattered light is shifted in wavelength as compared to the incoming light. This inelastic light scattering results from the fact that as the nuclei of molecules vibrate against each other, the electron cloud is deformed. Thus, Raman scattering can be interpreted as inelastic light scattering from vibrating molecules. Consequently, the wavelength shifts resulting from Raman scattering contain information about the characteristic molecular vibrations and, therefore, about the molecular structure. A Raman spectrum displays the intensity of inelastic light scattering at various wavelength shifts relative to the incident beam on the sample and can thus be seen as a characteristic "spectroscopic fingerprint" of the molecular species within the sample. [172] This phenomenon of inelastic scattering of light was first postulated by Smekal in 1923 and first observed experimentally in 1928 by C.V. Raman along with K.S. Krishnan [173-175].

Raman spectroscopy can be used for both the qualitative and quantitative analysis and for the monitoring of organic, catalytic, and polymeric reaction. Qualitative analysis can be performed by measuring the frequency of scattered radiations while quantitative analysis can be performed by

measuring the intensity of scattered radiations. [176] It also has the added advantage that the spectra are generally unaffected by temperature changes, and that the concentration of the particular species is directly proportional to the intensity of spectral features [174, 177, 178].

This characterization tool was found to be a technique of choice to study the chemistry and kinetics of polymerization reaction at room temperature and above [179-184]. However, employing this powerful and non-destructive approach for studying the kinetics of chemical reactions below 0°C is more challenging due to technical constraints [185, 186]. For example, the formation of ice induces optical scattering effects that deteriorate the signal-to-noise ratio, which complicates both the signal collection and the spectroscopic analysis.

Raman techniques, however, require minimal sample preparation, and it is inexpensive, can be performed on glass or in closed container. Further, it can provide large frequency ranges for spectral observation and due to its scattering process, any types of shapes and sizes can be examined *in-situ* [180, 181, 187, 188].

Further, Raman spectroscopy, as opposed to the traditional ¹H NMR spectroscopy, also allows for the investigation and analysis of solids directly without requiring them to dissolve into a solvent a priori. This provides opportunity for direct evaluation of the activity of the polymeric reaction under simulated cure processing conditions. The underlying chemical changes at the molecular level of the polymers in solid forms can directly be assessed and quantified (if needed) by this method. Further, Raman spectroscopy is a simple, straightforward method that does not require cumbersome sample preparation, it is easy to implement and very powerful and sensitive to molecular level changes of the material even in their solid crystalline forms [189, 190].

3.2 ROMP reaction of 5E2N

The ROMP reaction of 5E2N initiated by HG2 catalyst is depicted in Figure 3.1 below.

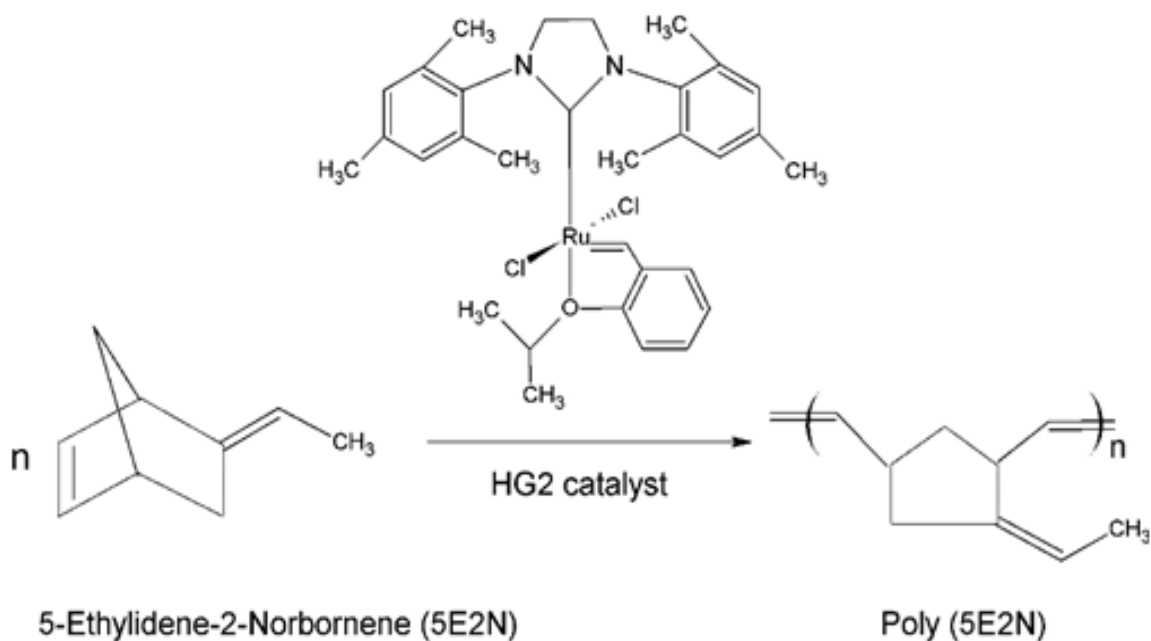


Figure 3.1 ROMP reaction of 5E2N at the presence of HG2 catalyst

The ROMP reaction is a type of olefin metathesis chain growth polymerization of a suitable cyclic olefin. Olefin metathesis is a unique metal-mediated carbon-carbon double bond exchange process. In ROMP reaction, usually a cyclic olefin with high ring strain such as 5E2N monomer is converted to polymeric material in the presence of a suitable catalyst. The catalyst activates the ROMP reaction which is driven from monomer to the formation of the polymer by the release of strain associated with the cyclic olefin. During this process, the double bond present in the reactant monomer takes part in the chemical reaction but remains present in the produced polymer too. This important feature distinguishes ROMP from typical olefin addition polymerization such as the polymerization of ethylene to polyethylene [10].

The ROMP reaction of some cyclic olefins facilitates their polymerization with expansion of volume unlike commonly observed in the other types of polymerization reaction such as condensation polymerization. The extent of the change in volume resulting from the ROMP reaction depends on the size of the ring, the number of the rings per unit volume, and the associated ring strain of the cyclic monomer. Further, for any chain growth polymerization reaction like the ROMP reaction where no by-products are produced, the reaction is always exothermic [191, 192].

The fact that 5E2N monomer can remain liquid at very low temperature down to -80°C [19] makes it suitable to be used as self-healing agent for space applications such as in spacesuits and space vehicles. However, to better characterize and understand the cure reaction of 5E2N monomer in realistic operating environments, the investigation of its polymerization kinetics at low temperatures is essential.

Raimondo and co-workers showed that the self-healing (ROMP) reaction of 5E2N can be triggered at low temperatures (down to -50°C) when initiated by first generation Grubbs (G1) and Hoveyda Grubbs (HG1) catalysts. The reaction was observed to proceed very slowly, taking 1440 min for 52% yields and 450 min for 99% yields, with G1 and HG1 catalysts, respectively [121]. Even if other parameters related to the leakage of the capsules and the diffusion of their core content inside the polymer matrix also contribute to the efficiency of the self-healing process, such a rate is clearly insufficient [181], since a too slow self-healing reaction can cause the diffusion of the healing agent monomer into the matrix material before it polymerizes, resulting in incomplete curing of the material. Hence, measuring and optimizing the cure kinetics of the polymerisation reaction is a crucial step towards implementing any self-healing agent [181], especially for those initiated by HG2 catalyst that shows unprecedented chemical stability, recyclability [163, 193, 194] and fast rates of initial polymerization [161].

Here, we aim to characterize the polymerization kinetics of the 5E2N core with the HG2 catalyst. HG2 is particularly known for its chemical stability [161]. This product can also be handled in air and remain stable when coming into contact with a wide variety of functional groups including esters, amides, ketones, aldehydes and even water, alcohols and acids [158].

For effective self-healing of materials after a damage event, the ROMP reaction of the healing agent must occur quickly, preferably within few minutes depending on the surrounding environment, to prevent further damage or material degradation and to preclude evaporation and diffusion of the monomer from the crack plane [93]. The polymerization kinetics of the healing agents is, thus, one of the most crucial factors for their effectiveness at low temperatures. Its determination is prerequisite for the development of any self-healing system based on ROMP, prior to the optimization of other parameters, such as the concentration, the size and the thickness of the microcapsules, which can also affect the speed and efficiency of the process. In this work, the polymerization kinetics of the core 5E2N initiated by HG2 catalysts has been investigated between -30°C and $+21^{\circ}\text{C}$, to demonstrate the relevance of using these compounds as self-healing agents at low temperatures.

3.3 Experimental

3.3.1 Materials

Commercial 5E2N monomers, mixtures of endo and exo, 99%, containing 100-200 ppm butylated hydroxytoluene (BHT) were purchased from Sigma Aldrich, Canada (Millipore Sigma™). Dichloro [1, 3-bis (2, 4, 6-trimethylphenyl)-2-imidazolidinylidene] (2-isopropoxyphenyl methylene) ruthenium (II) [(HG2) catalyst] were also purchased from the same source. All chemicals were used as received.

3.3.2 Equipment and methods

A Leica Optical System DM LM Raman spectrometer was employed to investigate the ROMP reaction of 5E2N/HG2 agents at low temperatures ranging from room temperature down to -30°C . The set-up is shown in Figure 3.2.

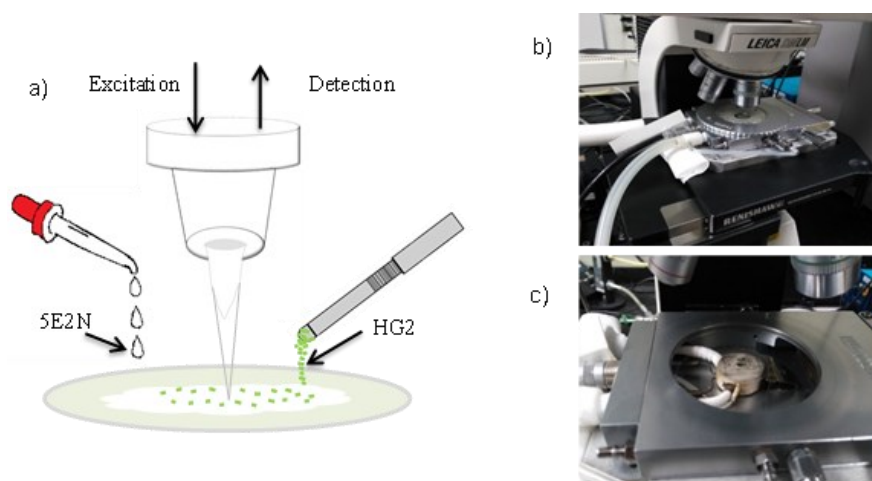


Figure 3.2 a) Schematic of the *in-situ* observation of the ROMP reaction of 5E2N initiated by HG2 catalyst by Raman spectroscopy. b) Raman spectrometer equipped with a thermoelectrically cooled CCD (charge coupled device). Cooling stage equipped with liquid nitrogen is used to maintain the desired temperature for the reaction. C) Sample is placed inside the cooling stage

The system was equipped with LINKAM nitrogen cooling cryostat covered by a transparent window, and a thermoelectrically cooled charge coupled device (CCD) detector protected by a notch filter. Using a diffraction grating of 600 lines/mm positioned at 1250 cm^{-1} , the system can

collect data over a spectral range of approximately 300-3300 cm^{-1} . A 0.5 mW 785 nm laser line was employed for the Raman excitation through an objective lens of x20 numerical aperture from which the Raman signals were collected perpendicularly to the sample stage. Before each set of measurements, the spectrometer was calibrated using the laser excitation line and the 520 cm^{-1} optical phonon peak of crystalline Si, as references.

Initially, a few trial Raman experiments were run to identify the Raman signals generated for the reactant 5E2N monomer and the polymerization product. From the Raman spectra generated during the ROMP reaction, the Raman band related to the characteristic (C=C) functional groups indicating the progress of the reaction was selected for the quantitative analysis.

To study the cure kinetics of the reaction, the measurements were conducted at 21 °C (RT), 1 °C, -5 °C, -10 °C, -20 °C and -30 °C. After cooling down the sample stage of the Raman spectrometer to the desired temperature, the liquid 5E2N monomer was deposited on a glass substrate, which was previously placed on the sample stage. Following thermal stabilization, the HG2 catalyst was added to the 5E2N monomer in a molar ratio of 1:1000, followed by the acquisition of Raman spectra at various time intervals depending on the temperature of the experiment [e.g., 15s (at RT) and 60s (at -30 °C)].

For each temperature, the temporal changes of the Raman spectra were recorded at each interval until saturation after which the intensity of the characteristic Raman band peak, indicating the progress of reaction, does not change significantly. Each of the recorded spectrum is then deconvoluted and fitted with a systematic Levenberg-Marquardt fitting process using two Gaussian functions. Both spectral heights and the integrated areas of the selected Raman peaks are then calculated for each interval and their change with time is incorporated into an Arrhenius type equation to determine the kinetic parameters of the reaction.

The entire method is further described in detail with example in the subsequent sections.

3.4 Results and discussion

3.4.1 Identification of the key Raman phonon peaks

Figure 3.3 shows the Raman spectra recorded initially for the free reactant monomer (5E2N) and during the polymerization reaction (ROMP) immediately after the catalyst particles were added to the monomer.

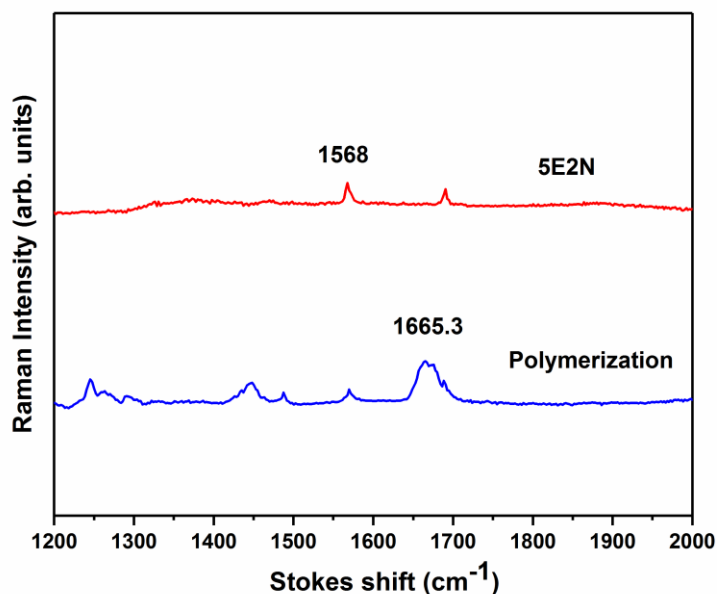


Figure 3.3 Raman spectra recorded for the reactant 5E2N monomer and during the polymerization reaction

The apparent changes in the signal-to-noise ratios reported on the spectra presented in Figure 3.3 are due to the difference in transparency, surface morphology and spectral response of the monomer and the formed polymer. In Figure 3.3, the signal-to-noise ratio can be estimated by the peak height of the Raman signals of interest above the baseline relative to the baseline noise.

The key difference in the Raman spectrum of the liquid unreacted 5E2N and the polymerization spectrum, as can be seen in Figure 3.3, is the appearance of a band peak centered at 1665.3 cm^{-1} . This signal is attributed to the key phonon mode that characterizes the ROMP reaction. Schaubroeck *et al.* [187], assigned this mode to the C=C stretching vibration of the aliphatic double bond of the polymer backbone formed by similar ROMP reaction of DCPD monomer which is another norbornene-based monomer with similar chemical composition of 5E2N. In the current study, the Raman band centered at 1665.3 cm^{-1} (Stokes shifts from 1650.0 to 1680.0 cm^{-1}) is assigned to the same C=C stretching vibration, related to the formation of poly-5E2N, as shown in Figure 3.1.

Schaubroeck *et al.* [187, 188] detected another Raman peak located at 1573.0 cm^{-1} , which was assigned to the vibration of the norbornene ring in the DCPD monomer. A similar Raman signal at 1568 cm^{-1} (i.e., close to 1573.0 cm^{-1}), in the current work,

was also observed in the spectrum of unreacted 5E2N monomer alone, as well as in the polymerization spectrum (see Figure 3.3). Like DCPD, this band centered at 1568 cm^{-1} represents the C=C stretching vibration of the norbornene ring of the 5E2N monomer (See Figure 3.1).

The spectral variations of these two Raman band peaks centered at 1568 cm^{-1} and 1665.3 cm^{-1} over time were monitored and measured for the quantitative kinetic analysis of the ROMP reaction as described in the subsequent sections.

3.4.2 Monitoring the ROMP reaction of 5E2N

The temporal changes of Raman spectra during the first thirty (30) minutes of the ROMP reaction at a temperature of -30°C are reported in Figure 3.4.

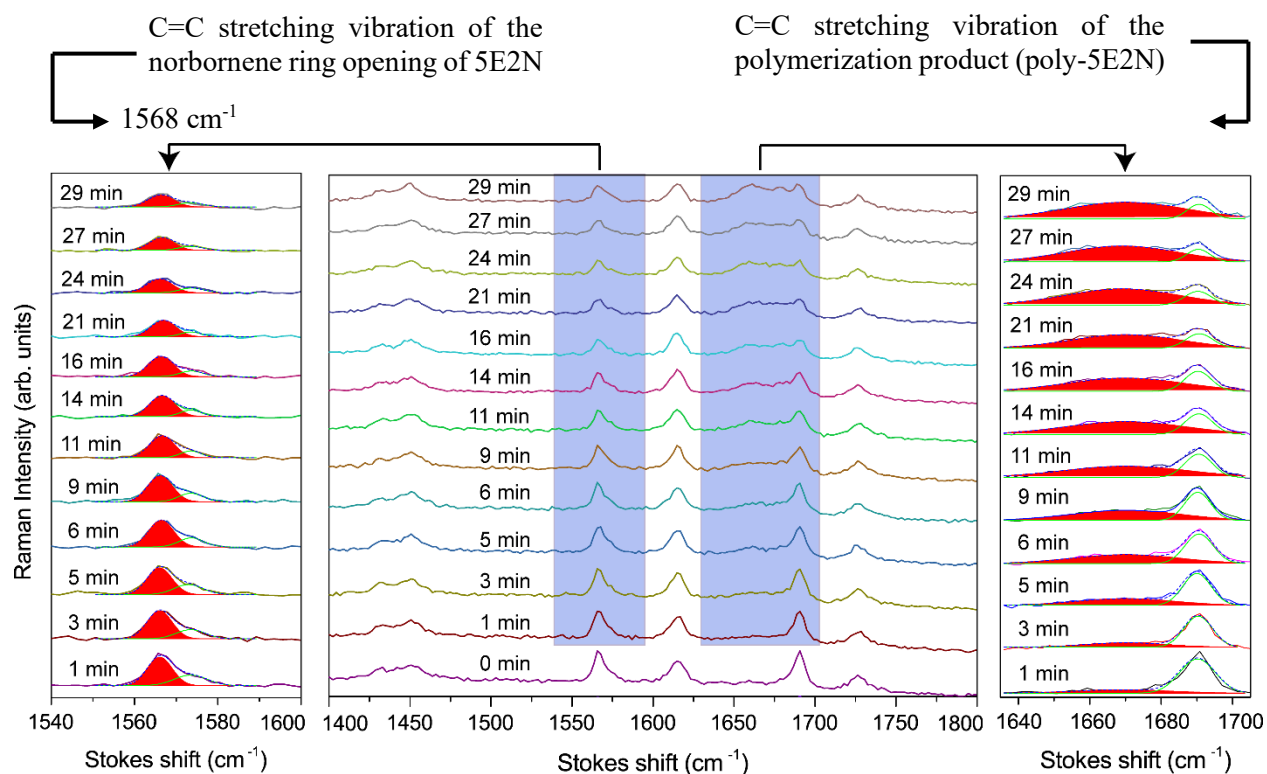


Figure 3.4 Raman spectroscopic observation of the evolution of the polymerization reaction of 5E2N activated by HG2 catalyst at -30°C

Figure 3.4 shows that the intensity of the Raman peak related to the formation of poly-5E2N at 1665.3 cm^{-1} increases with time, while the vibration mode associated with the opening of the norbornene ring of the reactant 5E2N monomer located at 1568.0 cm^{-1} decreases. These two features characterize the progression of the ROMP reaction, in agreement with previous work [187, 195]. Hence, the evolution of either of these two peaks can be monitored to measure the kinetics of the ROMP reaction. In this work, the Raman vibration mode located at 1665.3 cm^{-1} is selected for monitoring and analyzing the progression of the reaction. The saturation time of the polymerization reaction is estimated by calculating the difference of time duration between t_1 , at which the peak of the selected Raman band first appears (i.e., $t_1 = 0$) and t_2 , at which the peak achieves its maximum intensity. After time t_2 , the intensity of the peak does not change significantly. The saturation time for the polymerization reaction at -30°C is calculated to be $t_2 - t_1 = 29\text{ min}$.

The intensities of all peaks are normalized to compare their values across spectra that were recorded at different times. Both the spectral heights and the integrated areas of the Raman signals at 1665.3 cm^{-1} and 1568.0 cm^{-1} are displayed in Figure 3.4, after spectral deconvolution in the $1540\text{-}1600\text{ cm}^{-1}$ and $1640\text{-}1700\text{ cm}^{-1}$ ranges, respectively. To conduct these quantitative analyses, a systematic Levenberg-Marquardt fitting process was performed on each recorded spectrum, using two Gaussian functions. An example of spectral deconvolution is illustrated in the Figure 3.5.

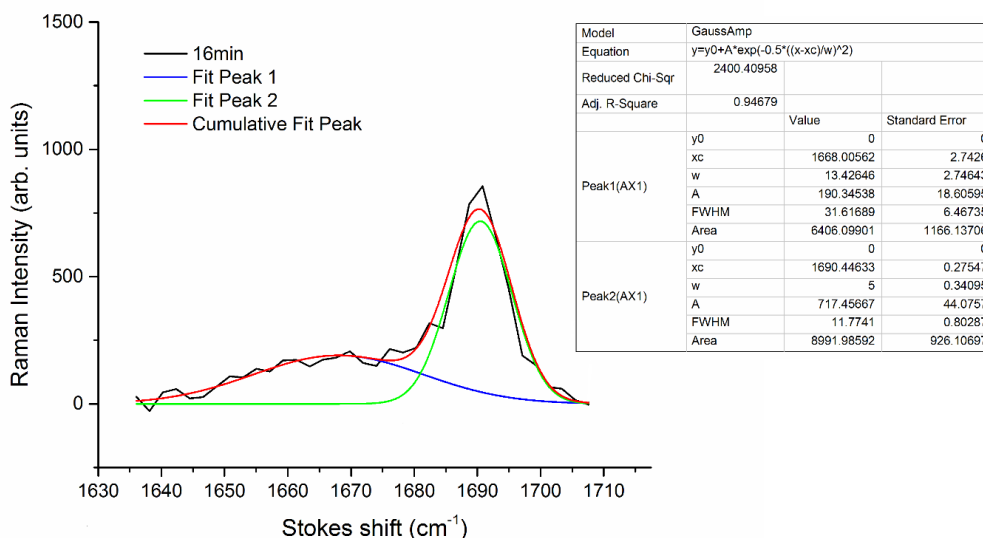


Figure 3.5 Spectral deconvolution of the Raman signal between 1635 and 1705 cm^{-1}

Figure 3.5 illustrates a good fit of the selected Raman band peak with the adjusted R-square value close to unity indicating that the fit error is of the order of the measurement error [196] as desired.

A similar methodology was implemented for the polymerization reaction of 5E2N initiated by the HG2 catalyst at 21°C, 1°C, -5°C, -10°C and -20°C. The saturation times of the ROMP reactions carried out at 1°C, -5°C, -10°C and -20°C were also determined and shown in Table 3.1. For reaction at room temperature, the saturation time was found to be lower than the acquisition time of 15s.

Table 3.1 Saturation times for the reaction at different temperatures

Temperature (°C)	Saturation times
21	Less than 15 sec
1	50 sec
-5	2.5 min
-10	4 min
-20	8 min
-30	29 min

3.4.3 Determination of the kinetic parameters of the reaction

The temperature dependence of reaction rate is typically described by an Arrhenius equation [197] :

$$K_{app} = A \cdot \exp\left(-\frac{E}{kT}\right) \text{-----[Eq. 3.1]}$$

where K_{app} is the apparent rate constant, k is Boltzmann's constant, E is the activation energy, A is the pre-exponential factor and T is the temperature given in Kelvin.

In the absence of any change in laser-matter interaction and optical coupling, the intensity of Raman phonon peaks increases linearly with the concentration of chemical bonds to which they are associated [198]. We used the changes in intensities of the Raman band located at 1665.3 cm^{-1} with time, indicating the formation of poly-5E2N, for the calculation of the kinetic parameters of the ROMP reaction.

The variations in Raman phonon intensity may result from changes in the chemical composition, sample crystallinity, incident light scattering and optical absorption [198, 199]. As these two last effects are mainly due to changes in experimental conditions, their contribution can be minimized by normalizing the collected data with respect to a reference peak. Hence, for non-crystalline poly-5E2N, we infer that most of the observed Raman spectral variations can be associated with changes in material composition.

Denoting the normalized peak intensity at time (t) by A_t and that after the saturation of the reaction by A_s , the integrated rate expression for the simple first order kinetics can be written as [183]:

$$\ln(1 - x)^{-1} = K_{app} t, \text{-----[Eq. 3.2]}$$

where $x = 1 - \frac{A_t}{A_s}$, and t indicates the time.

For each temperature, the calculated changes in normalized intensities of the selected Raman peak at 1665.3 cm^{-1} are plotted over time in Figure 3.6. The apparent differences in signal-to-noise ratios in Figure 3.6 might be due to the different acquisition times employed for collecting the Raman signals at different temperatures.

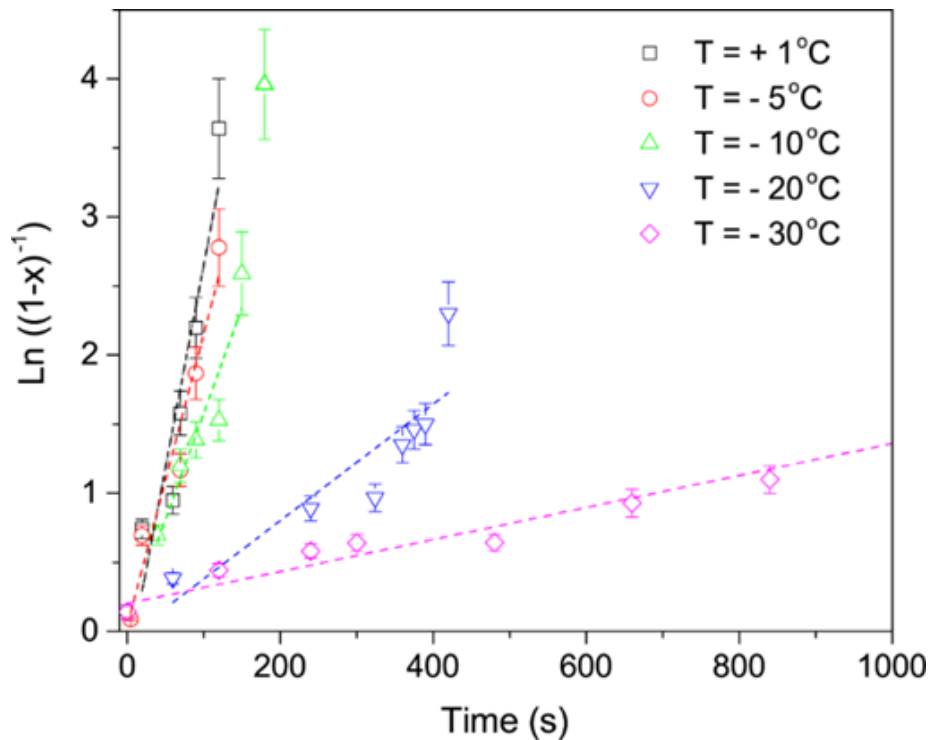


Figure 3.6 Changes in the normalized peak intensities with time for each polymerization temperature

To obtain the apparent rate constants, these data are fitted using a linear regression, shown by dashed lines directly reported on the Figure 3.6. According to Eq. (3.2), the slopes of these lines give the apparent rate constant (K_{app}) for each polymerization temperature. K_{app} values are found to be 2.90×10^{-2} , 2.10×10^{-2} , 1.50×10^{-2} , 4.20×10^{-3} and $1.16 \times 10^{-3} \text{ s}^{-1}$, for reaction temperatures of 1°C , -5°C , -10°C , -20°C and -30°C , respectively. Wilson and co-workers [161] determined the rate constants for the ROMP reaction of DCPD in solution, with G1 and G2, at room temperature, using nuclear magnetic resonance (NMR) experiments. The values of the ROMP rate constants initiated with G1 and G2 catalysts, as determined in ref., [161] are $1.45 \times 10^{-4} \text{ s}^{-1}$ and $4.30 \times 10^{-3} \text{ s}^{-1}$, respectively. By comparison, the rate constant obtained for the ROMP of 5E2N with the HG2 catalyst at 1°C , in the current work, is two orders of magnitude higher [161]. This could be due to the higher reactivity of the HG2 catalyst compared to G1 and G2 catalysts, whose too fast reaction with DCPD did not permit the measurement of the ROMP rate constant at RT in ref. [161].

In Figure 3.7, the rate constants are plotted versus the reaction temperatures (in Kelvin) according to an Arrhenius type function: $\ln(K_{app})$ versus T^{-1} .

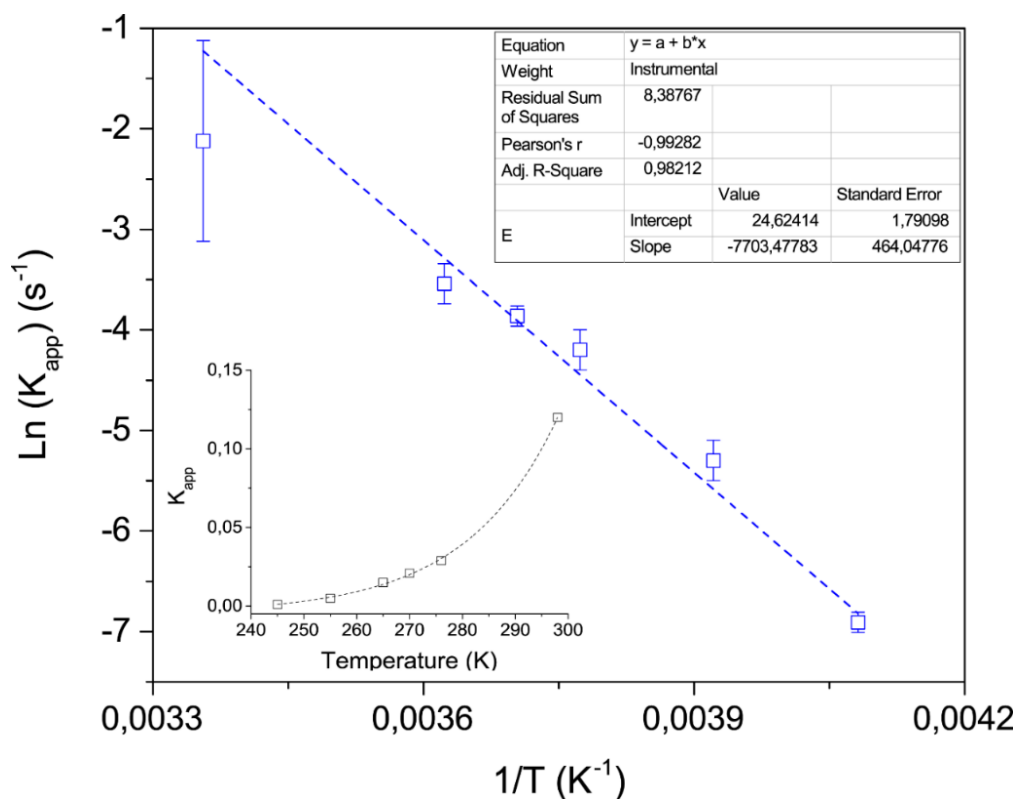


Figure 3.7 Arrhenius plot correlating the apparent rate constants with absolute reaction temperatures for the ROMP reaction of 5E2N/HG2

The value of the function at RT ($T^{-1} = 0.0034 \text{ K}^{-1}$) is estimated by taking a reaction time equal to half of the acquisition time of the Raman measurements, with large errors bars of 50% (Figure 3.7). From the slope of the Arrhenius plot, equals to 7.7 s^{-1} on Figure 3.7, the activation energy of the ROMP reaction is determined to be $64 (\pm 3) \text{ kJ mol}^{-1}$ (0.663 eV). This value is 40 % higher compared to the activation energies obtained by Kessler *et al.* [200] reported between 46 and 51 kJ mol^{-1} depending on the catalyst to monomer ratio, for the ROMP reaction of DCPD triggered by the G1 catalyst. Such a discrepancy may be attributed to small variations of the catalyst concentration and the degree of curing [200]. In the work by Kessler *et al.* [200] the catalyst was also dissolved into the monomer by mixing them vigorously to make a solubilized sample. This later was then used in DSC for the determination of the activation energies [200]. Such a processing is not a suitable scenario for catalyst/monomer pairs in real self-healing conditions. In a realistic situation, when the healing monomer is released from the broken microcapsules and transported to the crack plane of the host matrix, it is likely to meet some catalyst particles present in dispersed state. To mimic such a condition, the catalyst and monomer are not solubilized in our work. This may contribute to the increase of the activation energies extracted from our Raman analyses.

3.5 Concluding remarks

The progress of the ROMP reaction of the 5E2N monomer initiated by the HG2 catalyst at different low temperatures down to -30°C was monitored and analyzed by using a systematic micro-Raman spectroscopic analysis and following a detailed methodology that has been specifically implemented for this investigation. The analysis is based on measuring the changes in the peak intensity and integrated area of Raman phonons related to the characteristic (C=C) functional groups indicating the progress of the reaction with time. The apparent rate constants for the reactions at different low temperatures were determined for simple first order kinetics using the Arrhenius principle. The values of the rate constants are consistent with values found in the literature for similar reactions. Further, although the activation energy of the ROMP reaction of 5E2N/HG2 was found to be relatively consistent with the data available in the literature, it is 40 % higher than the one obtained for similar materials (DCPD/G1). [200] The mean square error and the reliability of the measurements obtained at low temperatures evidence the validity of the methodology developed for the quantitative kinetic characterization of the polymerization reaction. The methodology developed in this work to conduct the quantitative kinetic analysis, thus provides

an opportunity for studying the effects of various factors on the polymerization kinetics for different self-healing systems. It can also be implemented for choosing the materials that are suitable for healing in specific external conditions.

Our analysis also confirms that the combination of 5E2N monomer and HG2 catalyst can be considered as prospective healing agent candidates for low temperature self-healing applications in space. Although additional efforts are needed to use the microencapsulated healing agents in practice, such compounds are promising to develop self-healing materials with optimized healing efficiency.

CHAPTER 4: MICROENCAPSULATION OF CNT/5E2N SUSPENSION, THEIR CHARACTERIZATION AND RECOVERY OF ELECTRICAL CONDUCTIVITY

4.1 Introduction

Investigation of CNT/5E2N as healing agent requires the determination of the type of storage vessel in which they would be integrated into the host material. Microencapsulation of healing agent into polymeric shells is one of the few storage options available which has some advantages over the other extrinsic approaches of self-healing as discussed in chapter 2. The key advantages of microencapsulation of healing agents over the other extrinsic self-healing approaches include ease of integration and better compatibility with the host material as well as easier scalability of the self-healing system [13, 90].

In this chapter we report the successful microencapsulation of multi-walled carbon nanotubes (CNTs) suspended in the self-healing monomer 5E2N into MUF shells through *in-situ* polymerization technique. As the ultimate purpose of our work is to elaborate self-healing polymers offering a fast ROMP reaction, with high recovery rate of electro/mechanical properties, we adapted the established procedures to encapsulate the CNT/5E2N suspension in different weight ratios in polymeric shells and investigated their healing efficiency in polymer.

The physical features of the microcapsules, including their average size, size distribution, shell wall features, and thickness were characterized by optical and scanning electron microscopy. The presence of CNTs inside the core liquid content of microcapsules, as well as their release upon a breaking event are investigated by microscopy and spectroscopy analyses. The effects of the presence of a CNTs in the core liquid 5E2N on the thermal stability of the microcapsules are determined by TGA and DSC. The polymerization activity of the core content extracted from the microcapsules are investigated by Raman spectral analysis to ensure the self-healing capability of the microcapsules.

After the successful microencapsulation of CNT/5E2N suspension, in this chapter, we also demonstrate the ability of this system to restore autonomously the electrical conductivity inside damaged conductive polymer. Electrical conductivity restoration tests of conductive epoxy

polymer incorporated with the microcapsules containing CNT/5E2N showed that they can be used to restore up to 82 % of the electrical conductivity after the conductive path of the self-healing polymer samples was interrupted.

4.2 Experimental

4.2.1 Materials

CNTs were purchased from Bayer Material Science™. These CNTs feature diameters in the 2–20 nm range, and lengths between 1 - 10 µm with 95% purity. The self-healing monomer 5E2N was made from a mixture of endo and exo, 99%, containing 100-200 ppm Butylated hydroxytoluene (BHT). The Grubbs' catalyst, the encapsulating shell materials melamine, formaldehyde, urea, as well as the emulsifying agent polyvinyl alcohol (PVA) and the surfactant sodium lauryl sulphate (SLS) were purchased from Millipore Sigma, Canada. All chemicals were used as received. We also used a conductive commercial silver/epoxy ECCOBOND 56C (Henkel Loctite Ablestik 56C)/Catalyst 9, purchased from Ellsworth Adhesives™, as electrodes for electrical conductivity measurements.

4.2.2 Fabrication of microcapsules

Microcapsules containing CNTs suspended in 5E2N were successfully synthesized by *in-situ* polymerization adapting the process in ref. [20] in a trial-and-error basis. For self-healing materials, one of the most common encapsulation techniques is based on the *in-situ* polymerization method. This latter involves the polymerization reaction of amino resin shell materials such as urea-formaldehyde (UF), melamine-formaldehyde, melamine-urea-formaldehyde etc., with the subsequent formation of shell walls around the droplets of self-healing monomer in an oil-in-water type emulsion. The hydrophilic-hydrophobic balance of the oil-in-water type emulsion is known to play a significant role in the successful formation of the microcapsules through this process [135, 136]. In practice, the suitability of a given material for encapsulation is usually determined empirically [135] due to the diverse physical and chemical nature (viscosity, surface tension, hydrophobicity, solubility, reactivity etc.) of the encapsulating materials.

Further, according to the literature related to self-healing, mostly a single-phase liquid self-healing agent is micro encapsulated through this method. The quality characteristics of the produced microcapsules like their average size, shell wall thickness, morphology, thermal stability etc. are also the results of the synthesis and processing parameters employed [135, 136].

From the key factors that strongly influence the process and the quality characteristics of the microcapsules, the encapsulating material that has been chosen in our work is a two-phase suspension of CNT/5E2N with distinct physical and chemical properties like surface tension, hydrophobicity, pH value etc. To successfully microencapsulate CNT/5E2N into PMUF shells, we employed an empirical trial and error where various parameters such as CNT concentration, stirring speed, amount and concentration of surfactants etc. were varied one at a time, followed by investigations at microscale. The process parameters that led to the successful microencapsulation of 5E2N/CNT is described in section 4.3 in detail.

4.2.3 Characterization

The size and surface morphology of microcapsules were investigated at various magnifications using an Optical Microscope (OM), a field emission JEOL JSM7600F electron microscope (FESEM) at an acceleration voltage of 5kV, and a JEOL JEM-2100F transmission electron microscope (TEM), operating at 200 kV, respectively. The size measurements were obtained using an image analysis freeware (ImageJ).

TGA and DSC analysis were performed to determine the thermal stability of the microcapsules. For the TGA analysis, microcapsule samples were heated from 25 to 700°C under helium environment, using a heating rate of 10°C/min using TGA Q500. For the DSC analysis, microcapsule samples were heated from 0 to 100°C (under nitrogen environment) at a heating rate of 10°C/min using the Mettler Toledo DSC. All the data acquired from TGA, and DSC testing were analyzed using the 'TA Universal Analysis' software. A Leica Optical Systems Series DM LM Raman spectrometer was used to monitor the ROMP reaction ability of the core suspension extracted from the microcapsules. Raman characterization was performed using a confocal Invia Renishaw RM 3000 spectrometer, equipped with a digital camera and a 50× objective lens of 0.75 numerical aperture (NA) to study the relative spectral signatures of microcapsules with and without CNTs.

4.2.4 Fabrication of self-healing polymer samples for electrical conductivity restoration tests

To investigate the ability of the microcapsules to restore electrical conductivity in damaged materials, samples were prepared with conductive silver/epoxy polymer incorporated with the produced microcapsules containing CNT/5E2N. Neat samples (containing no microcapsules) were obtained by mixing ECCOBOND 56C and catalyst 9 in a weight ratio of 100:2.5. The mixture was then spread on a polymer substrate to make a conductive path and cured for 24 hours at room temperature followed by one hour of thermal annealing at 60°C. Two electrical connections were attached to two different points along the conductive path as shown in Figures 4.1 (a) and (c) of the samples.

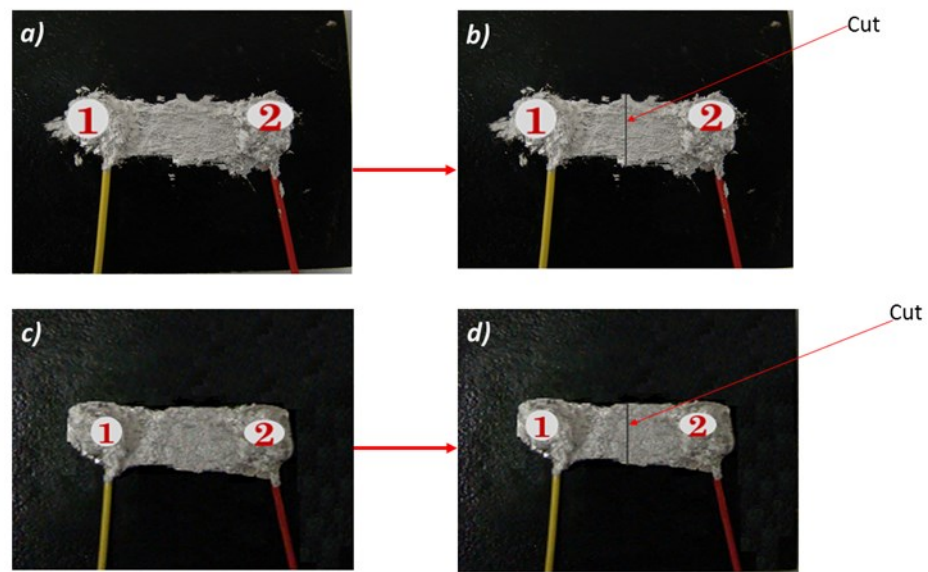


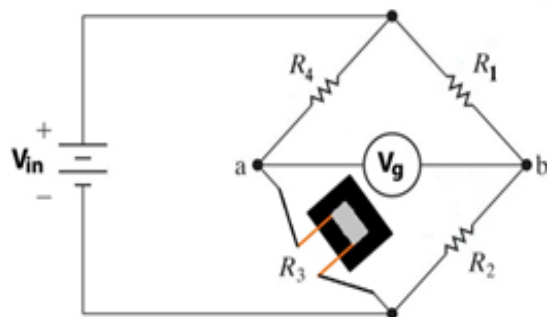
Figure 4.1 Electrical circuits made with conductive silver/epoxy incorporated with microcapsules containing CNT/5E2N and Grubbs' catalyst for the electrical conductivity restoration test. Bridge voltages were measured for the neat (no microcapsules) and self-healing samples (with microcapsules) with a) and c) uncut conductive path; and b) and d) cut between point 1 and 2 and after allowing for healing for 24 hours

The samples were later connected to a Wheatstone bridge circuit for voltage measurements. Wheatstone bridge circuit is a widely used technique for accurate measurements of electrical signals even for a slight change in resistance. The self-healing samples were prepared similarly by mixing and curing a pre-specified amount of ECCOBOND 56C, catalyst 9, microcapsules and

Grubbs' catalyst. After curing, the conductive path of the samples was cut with a razor blade [Figures 4.1 (b) and (d)] disrupting the electrical circuit. The samples were then left untouched for 24 hours at room temperature allowing sufficient time for self-healing of the damaged electrical circuit. The bridge voltage was measured i) at the beginning (uncut sample), ii) immediately after cutting the conductive path, and iii) 24 hours after cutting the conductive path.

4.2.5 Measurement principle and determination of self-healing efficiency:

The restoration of electrical conductivity of the silver/epoxy samples was evaluated in accordance with the procedure described in Ref. [99] The Wheatstone bridge circuit consists of three standard resistors: 100 Ohms (R_1), 10 Ohms (R_2), and 250 Ohms (R_4) resistance, with an input voltage (V_{in}) of 5.0 V. The silver epoxy sample was connected to the circuit as another resistor (R_3), as shown in Figure 4.2. For a slight change in the electrical resistance of the samples connected to the Wheatstone bridge circuit due to the disruption/restoration of the conductive path, the output bridge voltage (V_g) changes accordingly.



The bridge voltage (V_g) for all condition was measured via connection between a-b

Figure 4.2 Circuit diagram of the Wheatstone bridge, the samples were connected in the position of the R3 resistor [99]

Three bridge voltages (V_g , V_c and V_h) were measured. V_g is the initial bridge voltage, V_c is the bridge voltage immediately after the samples were cut and V_h is the bridge voltage after the samples were allowed to heal for 24 hours.

From the circuit analysis, the bridge voltage V_g is given in terms of the resistances as ref. [99] by:

$$V_g = V_{in} [(R_1 / (R_1 + R_2)) - (R_4 / (R_3 + R_4))] \text{-----[Eq. 4.1]}$$

The bridge voltage for the cut samples V_c ,

$$V_c = (V_{in} \times R_1) / (R_1 + R_2) \text{-----[Eq. 4.2]}$$

Autonomic restoration of electrical conductivity (healing efficiency) is assessed in terms of

V_{norm} ,

$$V_{norm} = (V_h - V_c) / (V_g - V_c) \text{-----[Eq. 4.3]}$$

$$= (R_3 + R_4) / (R_h + R_4),$$

where R_h is the resistance of the samples after healing.

In damaged samples, no electrical current pass and the cut bridge voltage is given by Eq. (4.2). For the healed samples, when the current can flow through the circuit, the voltage is dropped and given by Eq. (4.1). Here, the normalized bridge voltage of the samples as calculated by Eq. (4.3) is taken as the percentage of restoration of electrical conductivity, which defines the electrical healing efficiency.

4.3 Results and discussion

4.3.1 Fabrication of microcapsules

A controlled dispersion-emulsification-polymerization-recuperation steps, as depicted in Figure 4.3, were carried out to enable the microencapsulation of CNT/5E2N suspension in PMUF shells.

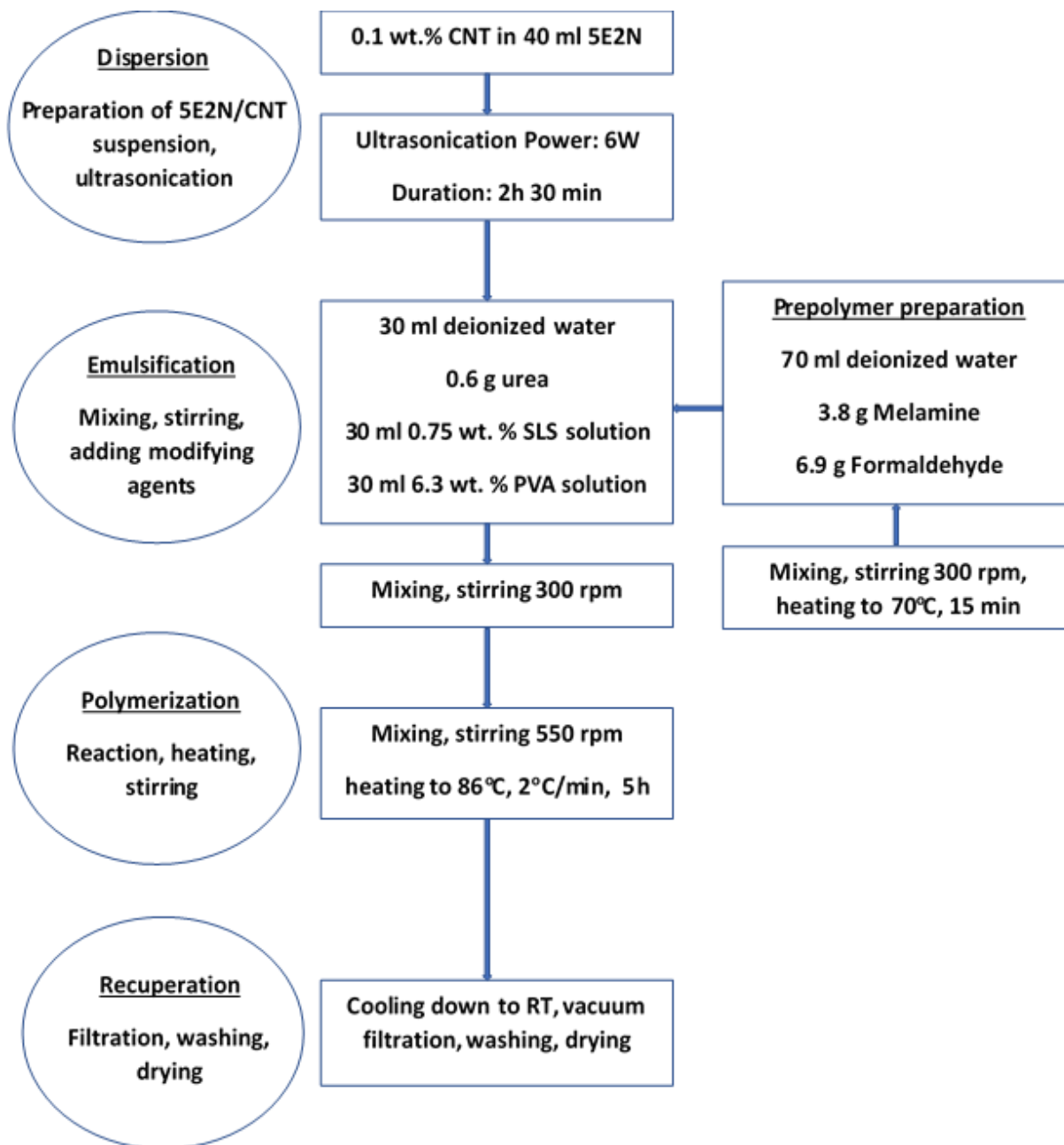


Figure 4.3 Process flow chart for successful microencapsulation of CNT/5E2N in PMUF shells. The process is adapted from ref [20]

The CNTs were first dispersed into the 5E2N monomer using ultrasonication, where the power and duration of ultrasonication were the main controlling factors in obtaining a stable CNT/5E2N suspension with desired characteristics. Occasional visual observations of the final suspension produced confirms that the suspension remains stable for a sufficiently long time, in order of months, as shown in Figure 4.4.

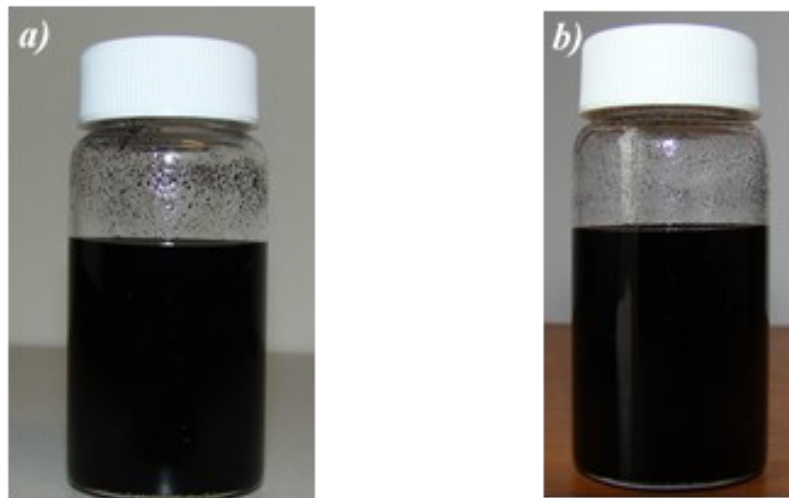


Figure 4.4 CNT/5E2N suspension a) right after the sonication and b) after 1 month

During the emulsification step, pre-specified amount of shell materials (melamine and formaldehyde in the form of a prepolymer and urea), core material (CNT/5E2N suspension), emulsifier (PVA) and surfactant (SLS) were mixed in an aqueous medium using a three-bladed low shear mixer. The stirring speed and the concentration of emulsifier and surfactant were adjusted in this step in every trial as process control parameters until microcapsules were successfully recuperated from the process. For the polymerization step, the emulsion was heated to the final reaction temperature of 86°C at a heating rate of 2°C/min, according to the process presented in Ref. [20] The reaction was then kept running at this temperature for about five hours. During the collection of the microcapsules, the emulsion was first cooled down, rinsed several times with deionized water and acetone, and vacuum filtered. The recuperated microcapsules were then dried in air and stored in glass vials before and in between each characterization. The combination of the major controlling factors that resulted in the successful microencapsulation of CNT/5E2N is presented in Table 4.1.

Table 4.1 Controlling parameters for successful microencapsulation of CNT/5E2N

Parameters	Amounts
CNT	0.05 wt. % and 0.1 wt. %
Sonication power	6W
Sonication time	2 h and 30 min
Stirring speed	550 rpm
PVA	6.3 wt. %, Molecular weight : 85000-124000
SLS	0.75 wt. %

4.3.2 Microscopic investigations

Figure 4.5 (a) shows a typical optical microscope image of the individually separated spherical free-flowing microcapsules. In Figure 4.5 (b), the white circles point CNTs, which have been released within the liquid core upon the crushing of few milligrams of microcapsules. Reference microcapsules that contain only 5E2N (i.e. without CNTs) do not show such features. Further, the liquid core content of the microcapsules is isolated and the released CNTs are seen under SEM, as shown in the inset of Figure 4.5 (b). The white regions seen in Figure 4.5 (b) are dross which results from solid impurities that float on the final emulsion after the microencapsulation process is finished. The dross is removed using micro-sieves before using the microcapsules for the preparation of the samples.

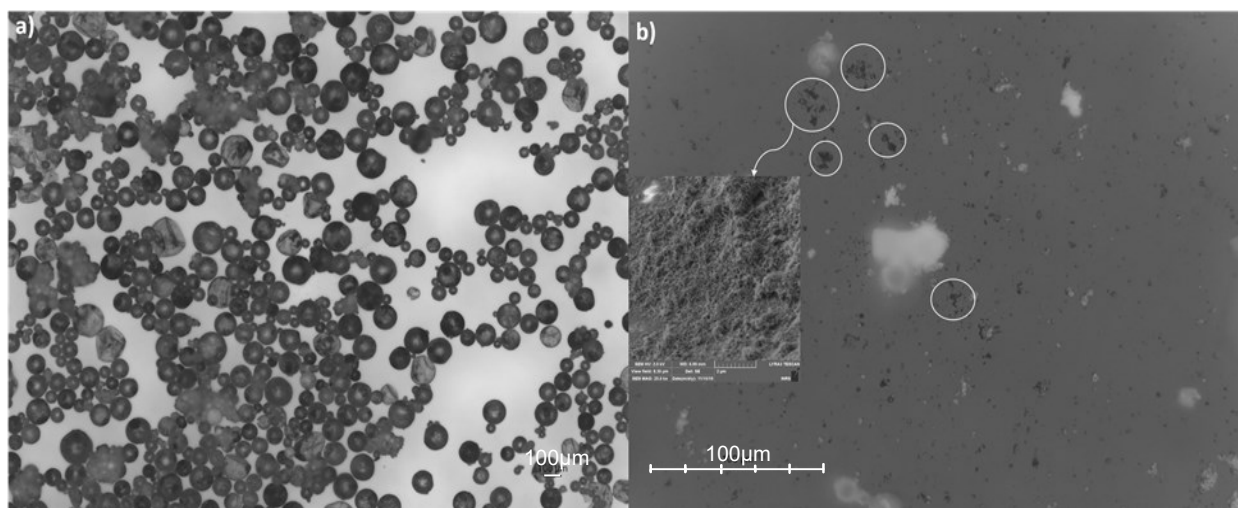


Figure 4.5 (a) Free flowing microcapsules observed under OM (5X). (b) Released CNT particles (encircled) as observed on the glass slide after crushing the microcapsules (OM 50X). The inset shows the high magnification (25000X) image of CNTs released

Figure 4.6 (a-d) shows representative SEM micrographs obtained at various magnifications: x50, x30000, x2300 and x100000, respectively. Individually separated spherical microcapsules are shown in Figure 4.6 (a), with core-shell structure displayed in Figure 4.6 (b) and Figure 4.6 (c). The average shell thickness is found to be around 550 nm. This shell thickness of the microcapsules is sufficiently robust to survive handling and manufacturing of self-healing polymers [133]. The outer shells of the microcapsule walls are observed to be textured, as shown in Figure 4.6 (c), with nanoparticles deposited onto its surface during the *in-situ* polymerization process [133]. The white structures observed in Figure 4.6 (d) and pointed by arrows are CNTs, whose metallic properties make them brighter than the background contrast under electron beam exposure [201].

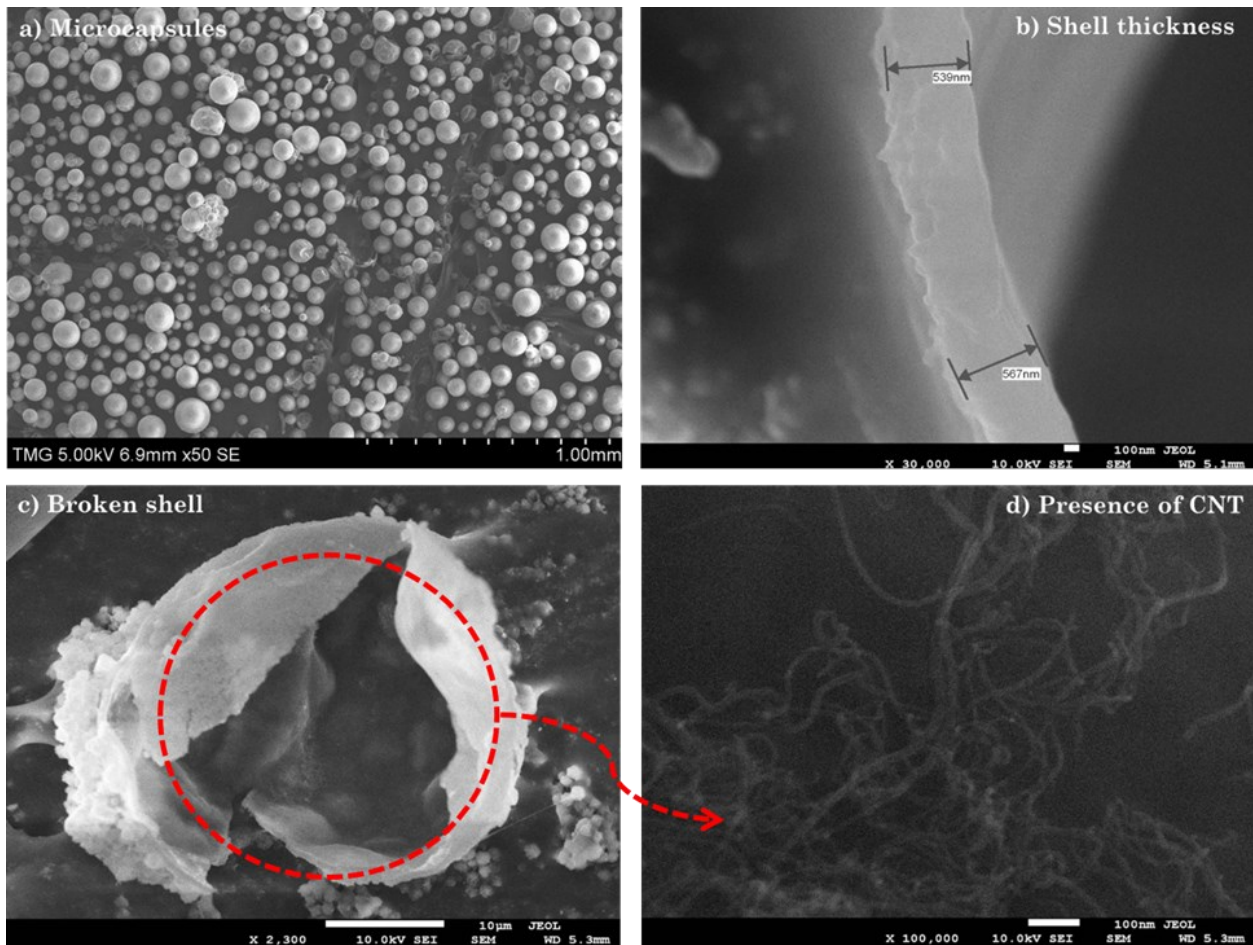


Figure 4.6 SEM observations of (a) individually separated spherical microcapsules (b) shell thickness (c) core-shell structure (d) CNTs inside the core of the microcapsules

Figure 4.7 displays a typical size-distribution of the microcapsules produced at 550 rpm stirring speed. Their diameters vary between 40 and 120 μm , around an average value of 70 μm . Both the dimensions and the size-distribution of the microcapsules are mainly dictated by the stirring speed [20] used during the synthesis process.

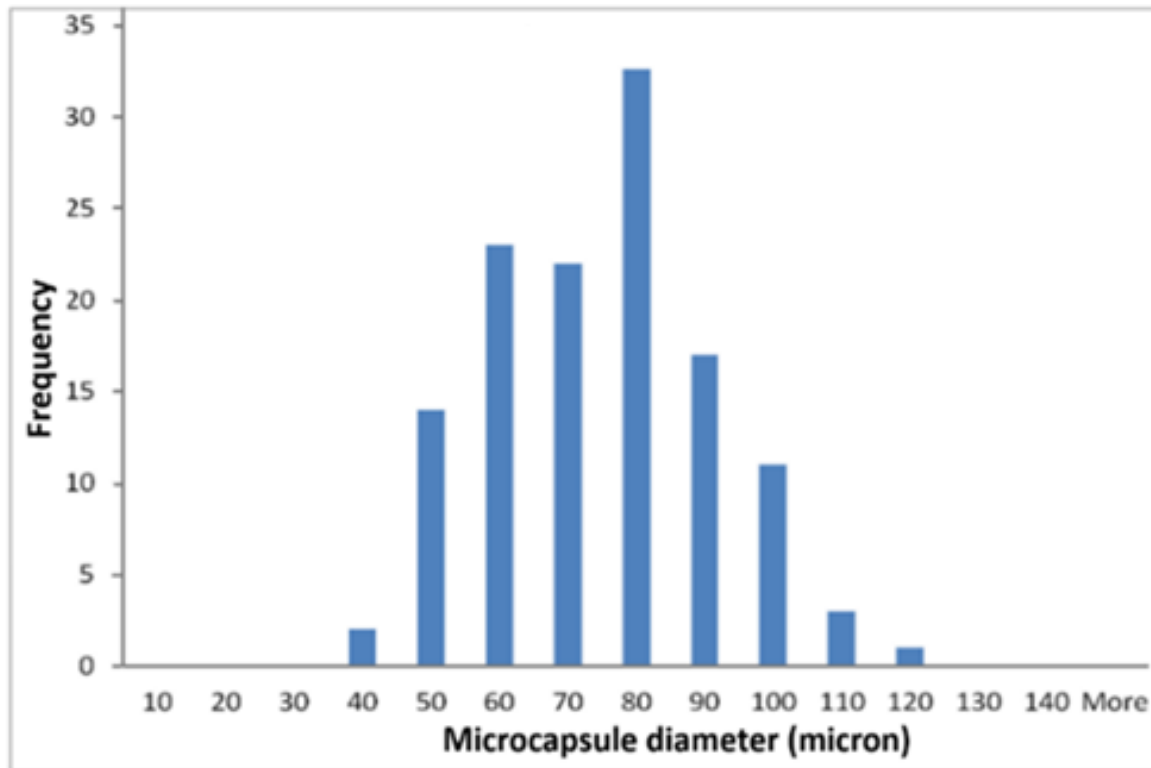


Figure 4.7 Typical distribution of sizes of microcapsules

For TEM observations, we extracted the liquid released from few milligrams of crushed microcapsules and dissolved it into acetone and methanol. A tiny Cu grid with carbon film was then immersed into the solution and dried before placing it into the TEM. The TEM micrographs in Figure 4.8 show the presence of CNTs in the liquid core extracted from the crushed microcapsules. These images further confirms that the processing steps of the synthesis of microcapsules did not cause severe breakage to the CNTs and maintain their original high aspect ratios. Such features are important for maximizing the benefits of incorporating CNT/5E2N into the core of the microcapsules

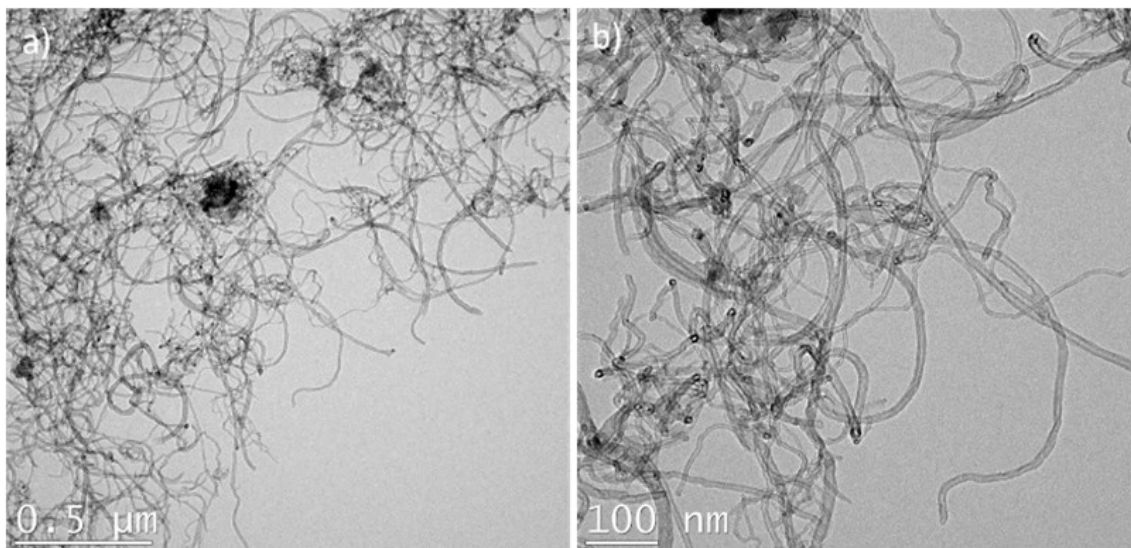


Figure 4.8 TEM observation of CNTs in the core liquid of the microcapsules

4.3.3 Thermal stability analysis

TGA analysis was carried out separately for reference microcapsules containing only 5E2N and microcapsules containing CNT/5E2N suspension. During these experiments, the weight-loss of the samples was measured while the temperature was increased, as reported on Figure 4.9 (a).

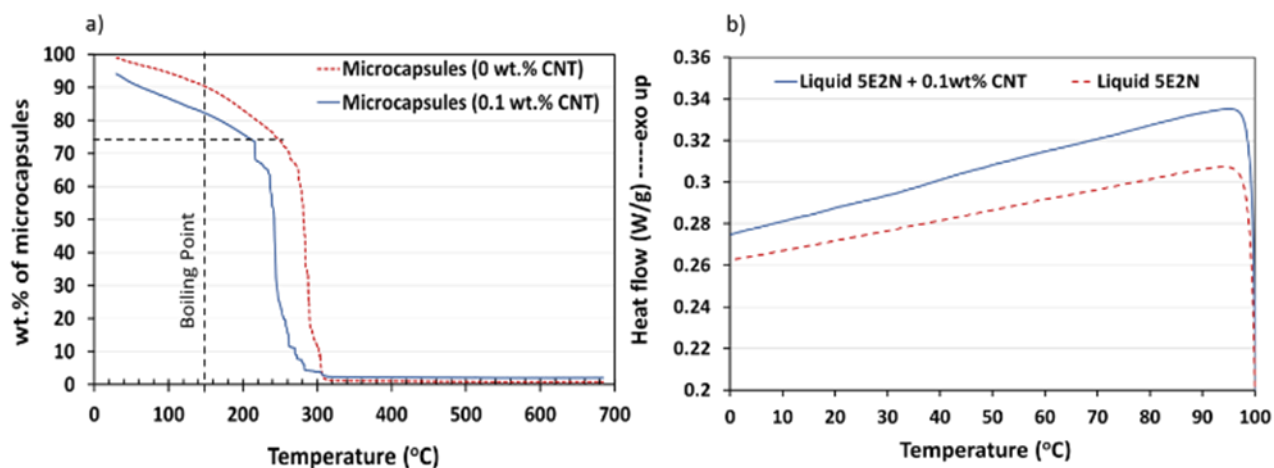


Figure 4.9 a) Comparison of weight loss vs. temperature in TGA for microcapsules containing liquid 5E2N only, and microcapsules containing CNT/5E2N suspension with 0.1 wt. % CNTs. b) Comparison of heat flow vs. temperature of liquid 5E2N and CNT/5E2N suspension with 0.1 wt.% CNTs in DSC

The dashed vertical line drawn reported on Figure 4.9 (a) is connected to the boiling point of 5E2N (148°C) [202], whereas the dotted horizontal line refers to the points on the curves where rapid weight loss begins. According to Liu *et al.* [20] the abrupt drop of the weight loss, observed around 240°C for reference samples, can be associated with the sudden burst of the microcapsule shell. This rupture is caused by the buildup of the vapor pressure inside the microcapsules. The tearing of the microcapsule shells releases the vaporized core materials in the TGA cell, thus resulting in rapid weight loss. For CNT/5E2N microcapsules, this phenomenon also occurs at a bit lower temperatures, around ~ 220°C.

The dispersion of CNTs within the liquid 5E2N was found to slightly affect the thermal stability of the medium. This effect is confirmed by the DSC analysis presented in Figure 4.9 (b), where drops of liquid 5E2N and 0.1 wt.% CNT/5E2N suspension were heated separately from 0 to 100°C. The difference in the slopes of the two lines (Figure 4.9 (b)) indicates the difference in the thermal properties for the 5E2N/CNTs, which possibly causes a slightly quicker build-up of the vapor pressure inside the microcapsules. The presence of 0.1 wt.% CNTs inside the 5E2N liquid slightly decreases the maximum temperature to which the microcapsules can be heated before breaking. However, even if this limit is somehow lower than that of the microcapsules containing only 5E2N, the thermal stability of about 220°C makes the CNT/5E2N microcapsules still suitable for use in the manufacturing of epoxy polymers and their composites, which may require curing at elevated temperatures (up to 180°C) for some applications [122]. On the other hand, the operating temperatures in satellites and other space vehicles do not usually exceed 125°C [179, 182, 197]. This suggests that the CNT/5E2N microcapsules fabricated in our work are stable and operational in the thermal environment of an orbiting spacecraft. The thermal analysis also aids in choosing the appropriate cure schedule (*i.e.* the temperature steps, holding times etc.) for the manufacturing of self-healing polymers.

4.3.4 Qualitative analysis of the core suspension of the microcapsules

Figure 4.10 shows the Raman spectrum of the core liquid extracted from the reference microcapsules and the CNT/5E2N microcapsules, before (Figure 4.10 (a)) and after the polymerization process (Figure 4.10 (b)). The Raman peak observed around 1350 cm⁻¹ (Figure 4.10) corresponds to the spectral signature of the CNT 'D-band'. This mode is related to the presence of disorder in sp²-hybridized carbon systems, whose out-of-plane vibration is more

prominent for CNTs [203]. The phonon peak at 1582 cm^{-1} refers to the ‘G-band’, which is connected to in-plane vibrations of sp^2 -bonded carbon atoms [187, 203-207].

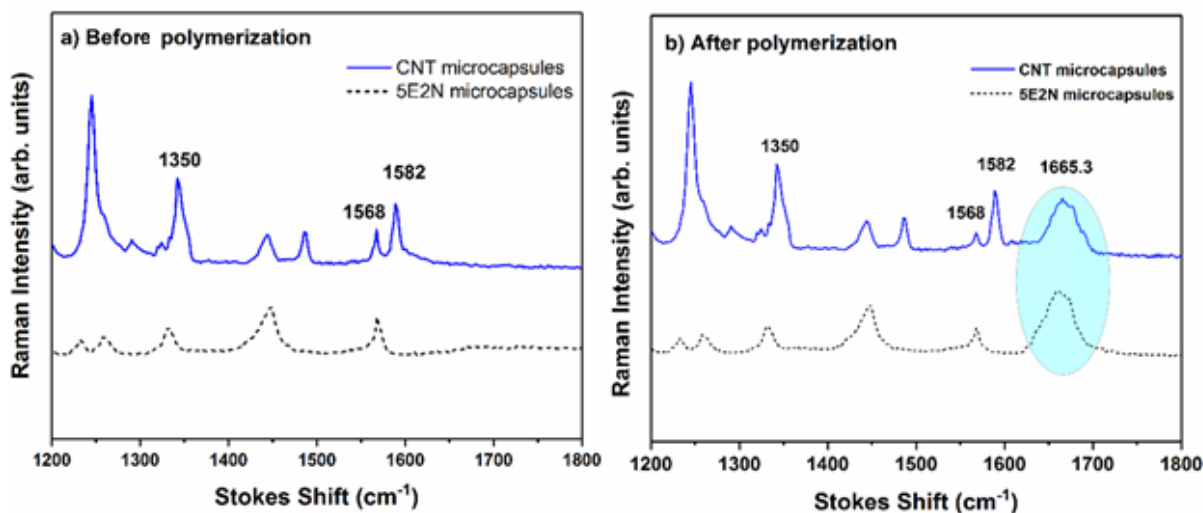


Figure 4.10 Comparison of Raman spectra generated for the core liquid extracted from 5E2N microcapsules and CNT/5E2N microcapsules, before (a) and after (b) polymerization

These two representative Raman signatures confirm the presence of CNTs inside the CNT/5E2N microcapsules. None of the D band and G band peaks have been observed in the reference microcapsules, where the Raman phonon at 1568 cm^{-1} is attributed to the C=C stretching vibration of the norbornene ring of 5E2N [187, 188]. Due to the addition of the catalyst to the core liquid of the microcapsules, another Raman peak appears around 1665.3 cm^{-1} (as indicated within the ellipse in Figure 4.10 (b)). As previously reported, this latter confirms the formation of poly-5E2N after ROMP reaction for the core liquids extracted from both types of microcapsules [208].

4.3.5 Restoration of electrical conductivity

The electrical self-healing ability of CNT/5E2N microcapsules was evaluated using the samples fabricated with electrically conductive epoxy adhesives and incorporated separately with two types of microcapsules. Neat conductive samples without microcapsules were also fabricated as reference. Wheatstone bridge circuits, whose basic principle and operation are presented in the

experimental section of this chapter were installed on the samples. The normalized bridge voltages (see Eq. (4.3) in this chapter) were measured and compared for evaluating the electrical healing efficiency of the CNT/5E2N microcapsules.

The Figure 4.11 demonstrates two types of electrically conductive samples whose conductive paths were first disrupted by introducing a damage/cut (cutting with razor blade) to the conductive path so that no electrical current could pass through it. The samples were then left untouched for 24 hours to allow for self-healing. The samples which did not contain any microcapsules or contain 5E2N-only microcapsules, could not recover the conductivity. The samples which contain the CNT/5E2N microcapsule were found to be able to recover their electrical conductivity, up to 82% of its nominal value as shown in Figure 4.11.

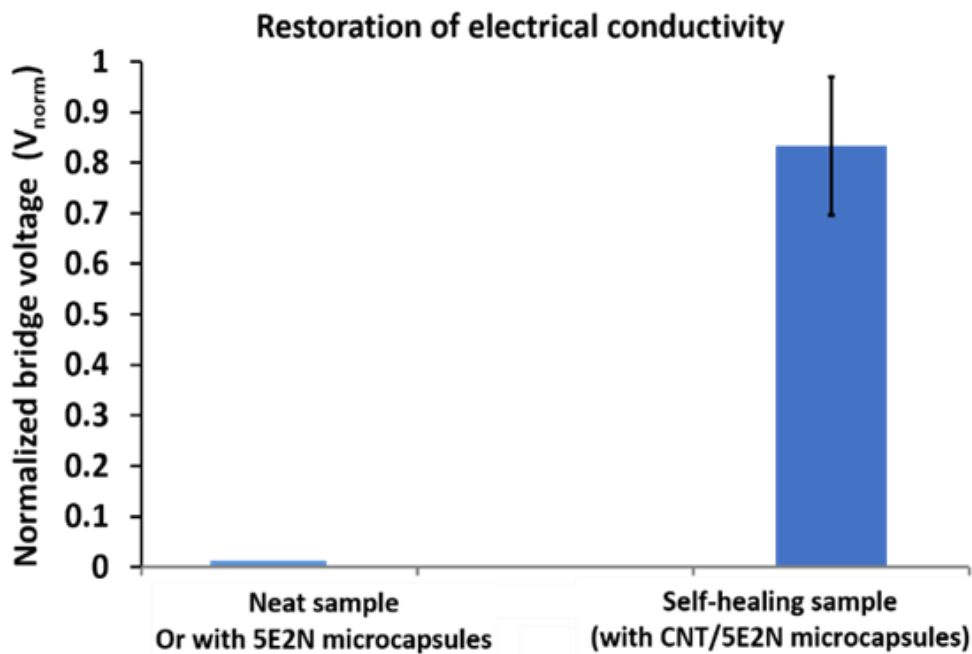


Figure 4.11 Comparison of the restoration of electrical conductivity of the damaged conductive polymer samples with and without CNT/5E2N microcapsules

This makes the incorporation of CNTs into 5E2N monomer relevant to restore the electrical conductivity and/or connections inside damaged electronic circuits. The microcapsules containing such CNTs can thus permit a better repairing/restoring of key electronic components and/or opto-electronic devices used in the advanced aerospace structures.

4.4 Concluding remarks

CNTs suspended in 5E2N self-healing monomer capable of undergoing ROMP reaction were successfully encapsulated using an *in-situ* polymerization technique. An experimental trial and error procedure was used to identify suitable process parameters including the wt.% of CNT, both the power and duration of sonication for dispersion, stirring speed as well as the concentration of emulsifying agent and surfactant that influence the successful formation of the microcapsules. After successful encapsulation of CNT/5E2N suspension, the average dimension, size-distribution, shell-wall topology and thickness of the microcapsules were characterized by microscopic observations. Optical, SEM and TEM images show the formation of microcapsules, as well as the presence of CNTs inside their core and the release of their content upon crushing. As confirmed by Raman analysis, the ROMP reaction is observed for pure 5E2N and mixed CNT/5E2N microcapsules. The structural integrity of these CNT/5E2N microcapsules was investigated up to 600°C, showing that such system can resist to external temperatures of 220–250°C, which makes them suitable to be used in advanced polymer and composites for aerospace. After testing, 82% of the electrical conductivity are found to be autonomically restored inside the conductive epoxy polymer containing CNT/5E2N microcapsules. The microcapsules containing such CNTs can thus permit a better repairing/restoring of key electronic components and/or opto-electronic devices used in the advanced aerospace structures.

CHAPTER 5: FAILURE ANALYSIS OF SELF-HEALING EPOXY USING MICROENCAPSULATED CNT/5E2N

5.1 Evaluation of mechanical self-healing of epoxy

Structural polymers like epoxies are extensively used in many key structures, parts and devices of modern aeroplanes and spacecrafts [1, 101]. These materials serve as matrix for laminated polymer composite parts/structures or as high-performance adhesives in various bonded joints [1-3]. The structural integrity of the parts into which they have been incorporated greatly depends on the mechanical and adhesive properties of the epoxy. During operation, the structures experience different types of mechanical stresses (tensile, compressive, shear etc.) at various locations, depending on their application, geometry, support, nature of loading etc. When the stresses exerted on the polymer/composite parts exceed a critical limit related to the strength of the epoxy, structural damage (or failure) occurs in various forms such as matrix micro-cracking, fracture, yielding, transverse and shear cracking [209, 210]. The triggered damage can accumulate over time inside the epoxy to generate major damage such as delamination or adhesive defects in bonded joints, which can ultimately lead to the structural failure of the whole system [211]. Self-healing epoxies based on microencapsulated monomers and Grubbs' catalysts are relevant to auto-repair the minor damage produced inside various polymer parts and their composites during their operation [9, 13, 102, 125, 126, 212, 213].

Mechanical self-healing efficiencies of microencapsulated healing agents incorporated into the host polymers are generally evaluated by measuring a selected mechanical property of samples before a controlled damage is induced in the samples and after the damage is healed. The extent of recovery of the mechanical properties after healing of the induced damage compared to the control samples are determined by the healing efficiency.

Different methods of loading have been used to induce damage to the host polymers and their composites to evaluate healing efficiencies under the applied loading conditions. Among them, inducing damage through normal mode I fracture loading [90, 112, 214-216], impact loading [217, 218] and tensile-tensile fatigue loading [113, 219] are common. Very few studies, however, reported the healing efficiency of epoxy-based adhesives subjected to shear constraints [127, 220], a feature that must be investigated for potential use in the aerospace industry. Moreover,

the measured healing efficiencies can greatly depend on the type of structural failure that has been generated under various stress conditions. Therefore, the development of any self-healing epoxy materials requires subsequent investigations at the microscale, as well as an accurate evaluation of their self-healing functionality when they are exposed to various types of mechanical stimuli.

In the previous chapter, we have reported successful production of high-quality microcapsules containing a suspension of CNT/5E2N and demonstrated their electrical self-healing capability. In this chapter, we have determined the mechanical self-healing capabilities of the microcapsules incorporated into epoxy samples subjected to two different failure modes. The mechanical resistance of the self-healing epoxies was measured for lap shear and normal fracture mode conducted in agreement with established standards [102, 212, 221], and compared with each other. To extract the effect of the presence of CNTs in the microencapsulated monomer, we also tested two different self-healable epoxy samples: one with epoxy samples containing microencapsulated CNT/5E2N, and another one with microencapsulated 5E2N alone. In each kind of samples, HG2 catalysts were dispersed as initiators of self-healing reaction. Neat epoxy samples that do not contain any microcapsules and catalysts were also prepared, to be used as reference samples. The ultimate objective of this work is to demonstrate, distinctively, the mechanical self-healing capability of the microencapsulated CNT/5E2N as a healing agent, when integrated into epoxies that are subjected to different types of stress conditions. Our results show that, besides acting as an efficient self-healing agent, CNT/5E2N containing microcapsules also improve the robustness of the cured epoxy, much better than the 5E2N containing microcapsules. The mechanical test results are supported by extensive fractographic analysis, Raman measurements and investigation of the contribution of CNTs in improving the mechanical resistance of poly-5E2N produced by ROMP reaction.

5.2 Experimental

5.2.1 Materials, procedures, and equipment

Commercial EPON 828 (a bisphenol-A based epoxide resin) and epicure 3046 (an amidoamine room temperature curing agent) were supplied by Miller Stephenson Chemical Co. Ltd. A wide variety of epoxy formulations is commercially available for aerospace and other advanced applications. We particularly selected this epoxy system to allow for curing at room temperature.

This is to avoid the complexities associated with possible degradation of the Grubbs catalyst (HG2 in the present work) used for self-healing of epoxies [14, 163], especially, when subjected to high temperature processing.

A Leica Optical Systems Series DM LM Raman spectrometer was used to verify the formation of poly-5E2N onto the fractures observed at the material surfaces, for the self-healable samples after their mechanical tests. Raman measurements were performed using a confocal Invia Renishaw RM 3000 spectrometer, a digital camera and a 50× objective lens of 0.75 numerical aperture (NA) to detect the presence of characteristic spectral peaks related to the formation of poly-5E2N resulting from the ROMP reaction of 5E2N released from the broken microcapsules on the fractured surfaces of the samples [208].

5.2.2 Preliminary investigation of the effects of CNTs on the ROMP products of 5E2N

To investigate the contribution of CNTs in enhancing the mechanical resistance of poly-5E2N produced by the ROMP reaction, samples were prepared by dispersing different concentrations of CNTs (0.05 – 1.0 wt.%) into liquid 5E2N monomer using ultrasonication. These CNT/5E2N suspensions were then polymerized at room temperature (RT) through ROMP reactions initiated by HG2 catalyst, in a molar ratio of 1:1000. Micro-indentation and flexural tests under three-point bending arrangements were carried out on the poly (CNT/5E2N) samples to assess the effects of incorporating CNTs on the mechanical properties of the formed polymer.

i) Micro-indentation tests:

The microhardness of the poly (CNT/5E2N) samples incorporated with different concentrations of CNTs (0.05, 0.1, 0.15, 0.2, 0.5 and 1 wt.%) were measured by microindentation test carried out using a Clark Microhardness Tester (model CM-100AT) for an applied load of 200 g. The Vickers hardness is a common measurement of hardness representing the ability of a given material to resist indentation. This value is related to the load, the shape of the indenter and the surface area of indentation [222].

Several indentations normal to the sample were made on different locations of the sample surfaces using the square base pyramid indenter. From the applied loads and impressions of the indenter on the sample surfaces, average hardness values of the samples were calculated. The Clark Microhardness Tester (model CM-100AT) system was equipped with software for automatic

computation of the hardness values from the applied load and the impression geometry of the indenter type used.

ii) Flexural test of the poly (CNT/5E2N) samples:

The flexural test of the poly (CNT/5E2N) samples incorporated with different concentrations of CNTs (0.05, 0.1 and 0.2 wt.%) were carried out according to ASTM D790 [223] standard. The flexural strength and the flexural modulus of the poly (CNT/5E2N) samples were calculated according to the following equations as [223],

Flexural strength

$$\sigma_f = 3pL/2bd^2 \text{ -----[Eq. 5.1]}$$

Where,

σ_f = maximum stress at the outer surface of the test specimen at midpoint, MPa

p = maximum load on the load-deflection curve, N

L = support span, mm

b = width of the beam tested, mm

d = depth of the beam tested, mm

And Modulus of elasticity (bending)

$$E_b = L^3m/4bd^3 \text{ -----[Eq. 5.2]}$$

Where,

E_b = modulus of elasticity in bending, MPa

m = slope of the tangent to the initial straight-line portion of the load-displacement curve, N/mm of deflection.

The load-displacement curves obtained from the experiments provide useful information on the effects of CNT concentration on the strength and stiffness of the poly (CNT/5E2N) samples.

5.2.3 Production of microcapsules and preparation of epoxy mixtures

For the failure analysis of self-healing epoxy incorporated with the microcapsules, two types of microcapsules in PMUF shells were produced using *in-situ* polymerization [20, 133]. One type of

microcapsule only contains the 5E2N monomer and the second one, a suspension of 0.10 wt.% CNT mixed with 5E2N. The micro-encapsulation process and its quality control are described in chapter 4.

For the evaluation of self-healing efficiency and failure analysis, two types of self-healing epoxy samples consisting of epoxy resin (Epon 828), curing agent (epicure 3046), catalyst (HG2) and microcapsules were studied. One type of sample was made with microcapsules that only contain 5E2N as healing agent. The other type of sample was made with microcapsules containing the CNT/5E2N suspension. 1 wt.% of HG2 catalysts and 10 wt.% of microcapsules with average size of $70 \pm 30 \mu\text{m}$ were dispersed into epoxy resin and cured subsequently for the preparation of samples for both the lap shear tests and the mode I fracture tests. Neat epoxy samples made of only epoxy resin and curing agent, without microcapsules and catalyst, were also prepared as reference samples.

5.2.4 Preparation of adhesive joint samples and lap shear test

Adhesive-joint specimens for lap shear tests were prepared according to ASTM D 1002 standard [102, 212]. Each lap-shear specimen consisted of two aluminum plates with dimension $101.6 \times 25.4 \times 1.6$ (in mm). The overlapped area of each aluminum plate was 12.7×25.4 (in mm). Figure 5.1 shows schematic and dimensions of the single lap joint specimen.

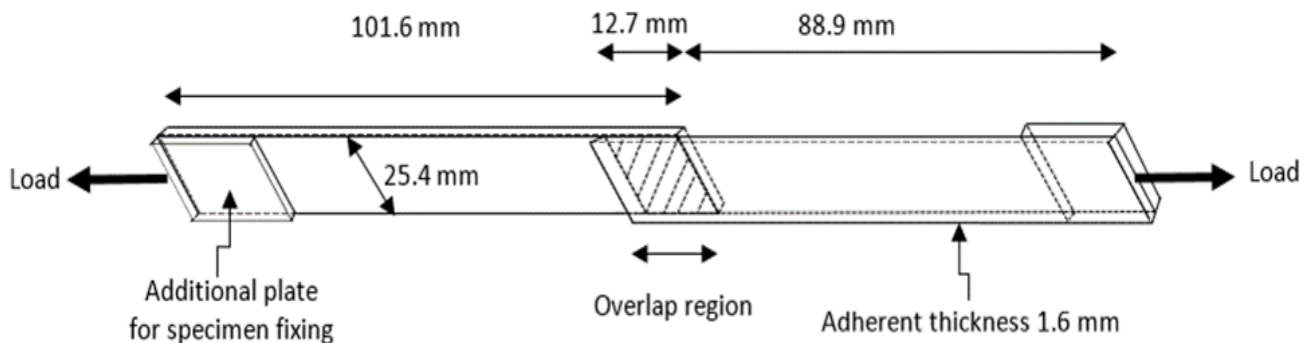


Figure 5.1 Single lap joint configuration used in experiment [221]

First, aluminum plates were cut according to the dimensions in Figure 5.1 above. The adherent surfaces were then manually roughened with sandpaper and cleaned and degreased with MEK (Methyl Ethyl Ketone) to eliminate the dirt and the grease from the surfaces and then rinsed in tap water. Hot air was then blown over the surfaces to make them dry. A self-healing epoxy adhesive was prepared with a 100:47 mixture of EPON 828 and epicure 3046, infused with 10 wt.% of microcapsules and 1 wt.% of HG2. Neat epoxy adhesives were also prepared without the microcapsules and catalyst. A thin layer of the adhesive mixture was applied to the desired area of the overlapped region of the prepared aluminum substrates. The two parts of the specimen were then brought into contact and pressed with modest pressure to squeeze out the excess resin and to achieve a uniform adhesive thickness. The overlapped region of the two aluminum plates were then bonded together by allowing the adhesives to be cured at room temperature for 10 days. This is followed by a post-curing of the samples at 100°C for 4h.

A custom-made rig was used to prepare the test joints in a panel of five bonded samples according to ref. [221]. Further, after placing the adhesives on the substrates on the rig, uniform weight was placed across the samples to ensure uniform bond thickness of the lap shear samples in the same batch. The schematic of the rig and the placement of the loads are shown in Figure 5.2

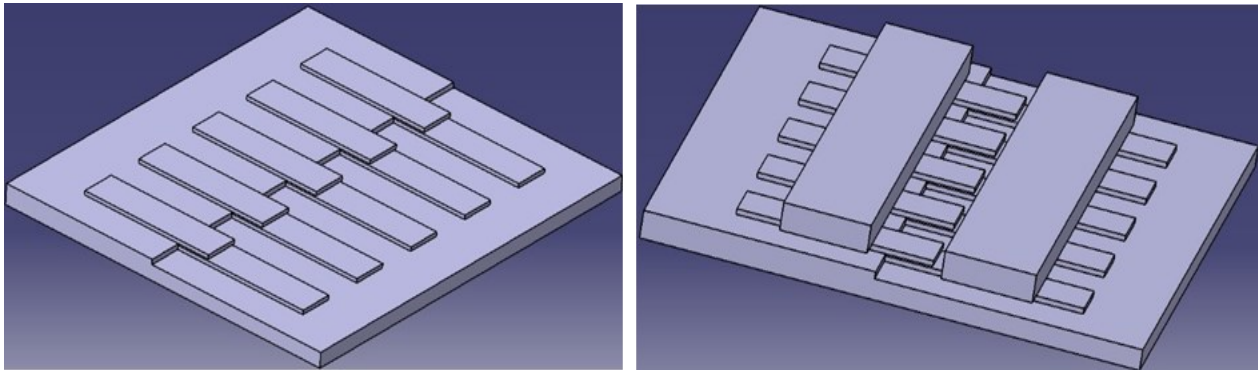


Figure 5.2 Arrangements (not to the scale) for the preparation of lap shear samples to ensure uniform bondline thickness in the same batch

Three types of lap shear adhesive samples were prepared. These are (i) neat epoxy adhesive reference samples, designated as LS (R) and prepared by mixing EPON 828 and epicure 3046 at a concentration of 100:47; (ii) self-healable epoxy adhesive samples with microcapsules containing 5E2N only, designated as LS (5E2N) and prepared by mixing EPON 828 and epicure

3046 at the same concentration and infused with 10 wt.% of 5E2N-only microcapsules and 1 wt.% of HG2; and (iii) self-healable epoxy adhesive samples with microcapsules containing a suspension of CNT/5E2N, designated as LS (CNT/5E2N), prepared using a 100:47 mixture of EPON 828 and epicure 3046, infused with 10 wt.% CNT/5E2N-microcapsules and 1 wt.% of HG2. Lap shear tests were performed by using MTS universal testing machine for a tensile loading using a load cell of 50 KN, at a crosshead speed of 1.27 mm/min. The experimental set up is shown in Figure. 5.3.



Figure 5.3 Experimental set-up for single lap shear test

Five (5) specimens of each type [*i.e.*, LS (R), LS (5E2N) and LS (CNT/5E2N)] were tested in the first loading until failure which is termed as ‘virgin (or original) loading’. The instantaneous loads and displacements were monitored during these experiments. After the first loading, the self-healing samples [*i.e.*, LS (5E2N) and LS (CNT/5E2N)] were kept clamped for 48 hours to allow for the self-healing process to occur at RT before the second loading and measuring the lap shear strengths after healing. It is to be noted that the self-healing ROMP reaction of the 5E2N monomer occurs very fast, in order of minutes, when the monomer comes into contact with the catalyst particles. However, in real application scenario, the healing effect should be stable throughout the

operational time of the parts. Thus, to ensure being on the safe side, we arbitrarily choose a long 48 hours healing time to stabilize the healing effects. We infer that the healing effect obtained after 48 hours is in the steady state condition after which no significant change in the healing effects with time is expected.

The mean lap shear strength is calculated as [222],

$$\tau = P/A, \text{-----[Eq. 5.3]}$$

where P is the maximum load of failure, A is the overlap area of the bonded joint, $A = L \times b$, L is the lapping length (mm) and b is the lapping width (mm). The healing efficiency is given by:

$$\eta_{LS} = \frac{\tau_{healed}}{\tau_{virgin}}, \text{-----[Eq. 5.4]}$$

where, τ_{virgin} is the lap shear strength of the original samples (obtained from the first loading) and τ_{healed} is the lap shear strength of the healed samples (obtained from the 2nd loading).

The original shear strengthening due to the incorporation of microcapsules into the epoxy adhesives can be determined by

$$\Delta\tau_v = \frac{\tau_{vm} - \tau_{vr}}{\tau_{vr}}, \text{-----[Eq 5.5]}$$

where τ_{vm} is the original lap shear strength of the microcapsule-incorporated samples [*i.e.*, LS (5E2N) and LS (CNT/5E2N)] that is calculated for the first (original) loading of the samples, and τ_{vr} is the original lap shear strength of the reference samples [LS (R)] that is determined after the first loading.

5.2.5 Preparation of TDCB samples and mode I fracture test

Figure 5.4 (a) shows the geometry of tapered double-cantilever beam (TDCB) epoxy specimen. Like the preparation of the lap shear test samples, a self-healing epoxy mixture was prepared with a 100:47 mixture of EPON 828 and epicure 3046, infused with 10 wt.% of microcapsules and 1 wt.% of HG2 for the manufacturing of the TDCB samples for mode I fracture test. Neat epoxy mixtures (100:47 mixture of EPON 828 and epicure 3046) were also prepared without the microcapsules and catalyst.

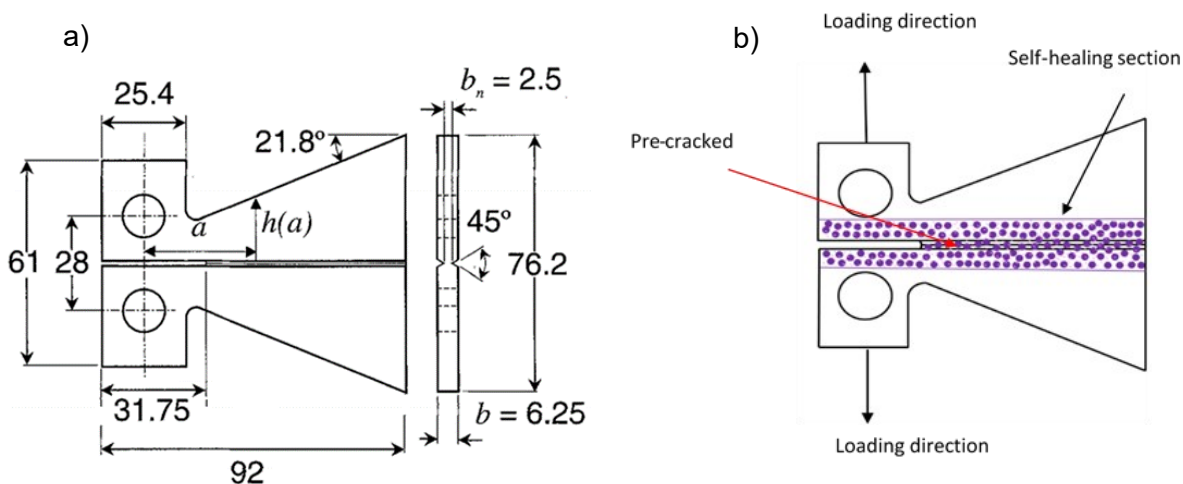


Figure 5.4 a) Tapered double-cantilever beam (TDCB) geometry (dimensions in mm), [12] b) Placement of healing agents and loading direction relative to pre-crack

For the self-healing samples, self-healable mixtures (epoxy, curing agent, catalyst, and microcapsules) were poured only in the mid region of the TDCB samples surrounded by the neat epoxy mixture (containing epoxy and curing agents only) as shown in Figure 5.4 (b). The mid region is the region of interest through which the mode I crack is propagated during the fracture test. This was done to reduce the amount (wt.%) of microcapsules and catalyst required for fabricating the self-healable samples. As before, all epoxy samples were cured at room temperature for 10 days followed by post-curing at 100°C for 4 hours to achieve complete curing.

Similarly, as for the lap shear tests, three types of TDCB epoxy samples were also prepared for the mode I fracture tests. These are (i) neat epoxy reference samples, designated as TDCB (R) and prepared by mixing EPON 828 and episcure 3046 at a concentration of 100:47; (ii) self-healable epoxy samples with microcapsules containing 5E2N only, designated as TDCB (5E2N) and prepared by mixing EPON 828 and episcure 3046 at the same concentration and infused with 10 wt.% of 5E2N-only microcapsules and 1 wt.% of HG2; and (iii) self-healable epoxy samples with microcapsules containing a suspension of CNT/5E2N, designated as TDCB (CNT/5E2N), prepared using a 100:47 mixture of EPON 828 and episcure 3046, infused with 10 wt.% CNT/5E2N-microcapsules and 1 wt.% of HG2.

Mode I fracture tests of TDCB epoxy samples were performed according to the methodology established by White and Sottos for measuring healing efficiencies [102, 212]. Accordingly, the cured samples were first pre-cracked by tapping a razor blade along the centerline of the samples to create a starter notch for ensuring the controlled crack growth along the centerline. [12] The load was then applied by pin loading grips in the perpendicular direction of the pre-crack. These experiments were conducted using a load cell of 1 kN, at a crosshead speed of 0.5 mm/min while monitoring the instantaneous loads and displacements. Figure 5.5 (a) shows a cured self-healing TDCB epoxy sample incorporated with microcapsules and catalyst at the mid-region. Figure 5.5 (b) shows the loading of the sample for the mode I fracture test.

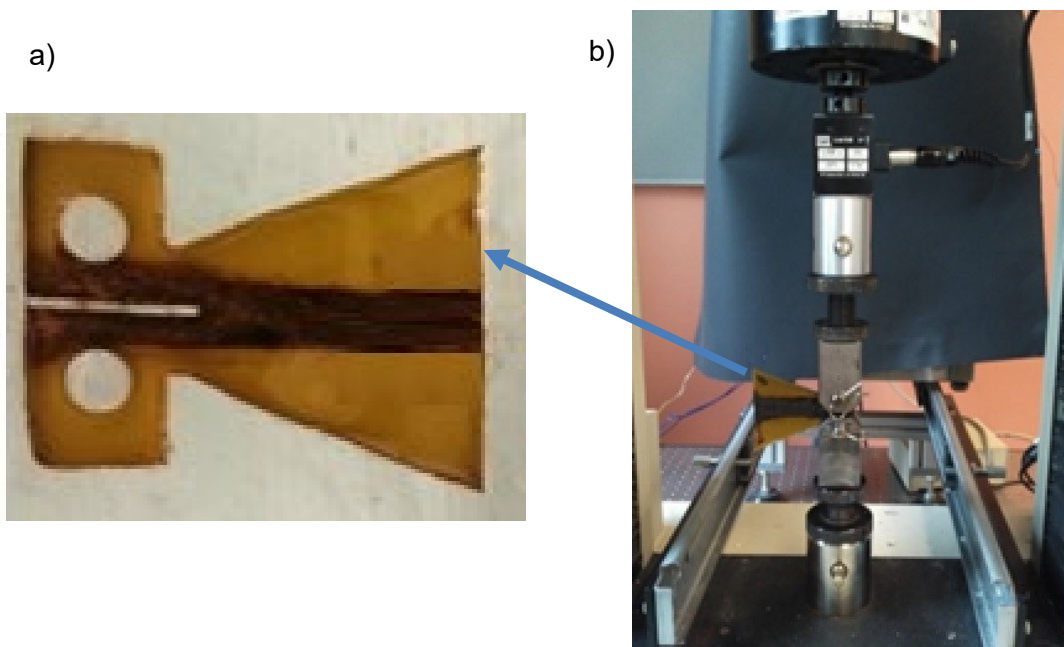


Figure 5.5 a) A cured self-healing TDCB epoxy sample incorporated with microcapsules and catalyst at the mid-region, and b) Loading of the sample for the mode I fracture test

As for lap shear tests, five samples of each type were studied until complete failure, which corresponds to a scenario where the initial cracks have travelled through the centreline of the whole samples, separating them into two halves. The two halves of the samples were then unloaded and immediately brought into contact and clamped for 48 hours to allow for healing process at room temperature. After 48 hours, the healed samples were again loaded into the MTS machine for a second series of fracture tests. Peak failure loads attained during the first loading and second fracture loading were used to calculate the healing efficiency.

The healing efficiency for the TDCB samples, η_I , is defined as the ability of the healed TDCB (5E2N) and TDCB (CNT/5E2N) samples to recover their fracture toughness [6]. This value is calculated according to:

$$\eta_I = \frac{K_{IC_{healed}}}{K_{IC_{virgin}}}, \text{-----[Eq 5.6]}$$

where η_I is the healing efficiency for the mode I fracture of the epoxy samples, $K_{1C_{virgin}}$ is the fracture toughness of the original samples calculated after the first loadings, and $K_{1C_{healed}}$ is the fracture toughness of the healed samples, calculated after the second loading. For TDCB samples, the fracture toughness is shown to be independent of the crack length. According to Refs. [102, 212] the healing efficiency is given by the following equation:

$$\eta_I = \frac{K_{IC_{healed}}}{K_{IC_{virgin}}} = \frac{P_{C_{healed}}}{P_{C_{virgin}}}, \text{-----[Eq 5.7]}$$

where, $P_{C_{virgin}}$ is the load of failure of the original samples during the first loading and $P_{C_{healed}}$ is the load of failure of the healed samples, respectively.

The original fracture toughening due to the incorporation of microcapsules into the TDCB epoxy samples can be determined as follows:

$$\Delta K_{IC_v} = \frac{K_{IC_{vm}} - K_{IC_{vr}}}{K_{IC_{vr}}} = \frac{P_{C_{vm}} - P_{C_{vr}}}{P_{C_{vr}}}, \text{-----[Eq 5.8]}$$

where, $K_{IC_{vm}}$ and $P_{C_{vm}}$ are the original fracture toughness and the corresponding critical failure loads, respectively, both determined after the first loading for the microcapsule-incorporated TDCB (5E2N)] and [TDCB (CNT/5E2N) samples, and $K_{IC_{vr}}$ and $P_{C_{vr}}$ are the original fracture toughness and the corresponding critical failure loads related to the reference TDCB (R) samples after first loadings, respectively.

i) Tg and curing of epoxy

All epoxy samples were cured at room temperature for 10 days. This was followed by a post-curing of the samples at 100°C for 4h. DSC measurement of the cured pure epoxy samples as shown in Figure. 5.6 show no major heat flow event indicating that the epoxy system was sufficiently cured. The Tg of the epoxy was estimated to be around 70°C.

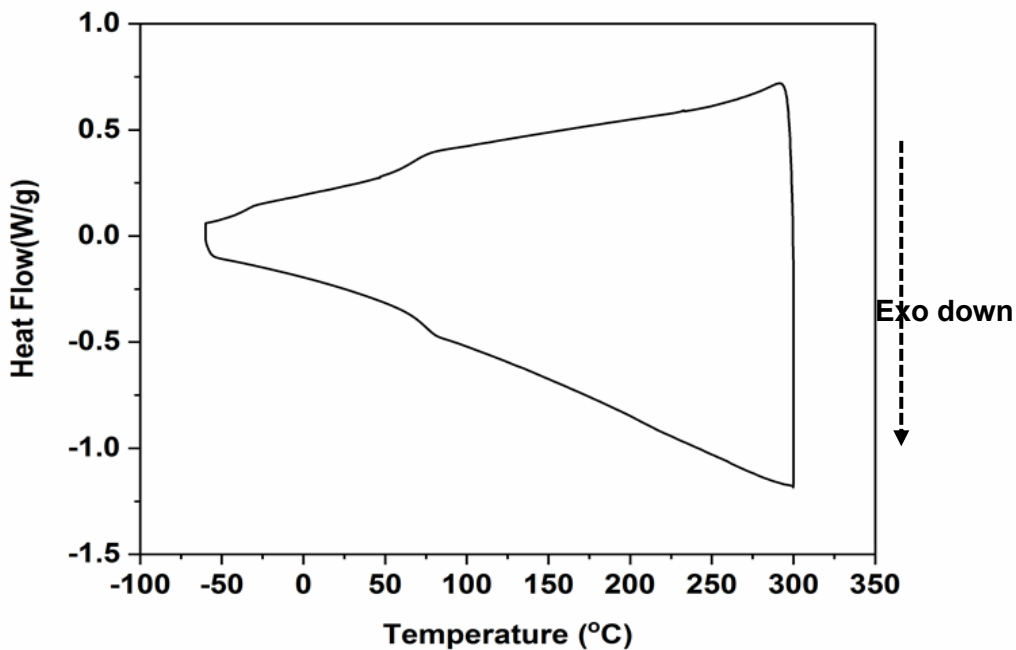


Figure 5.6 Curing and estimation of Tg of epoxy samples

5.3 Results and discussion

5.3.1 Preliminary investigation of the effects of CNTs on the mechanical properties of poly (CNT/5E2N)

To understand the effects of the presence of CNTs in 5E2N monomer on the mechanical properties of poly (CNT/5E2N) produced by the ROMP reaction, poly (CNT/5E2N) samples with different concentrations of CNTs were produced and both their microhardness and their flexural properties were measured in the preliminary investigation.

The effect of CNT concentration in liquid 5E2N monomer on the hardness of the poly (CNT/5E2N) samples is presented in Figure 5.7.

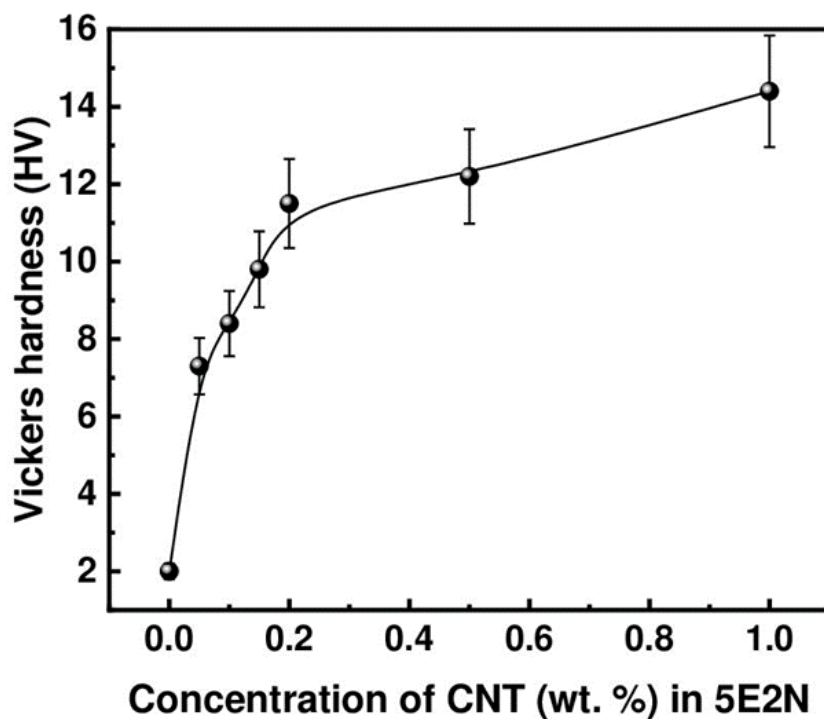


Figure 5.7 Effect of CNT concentration (wt. %) on the hardness of poly (CNT/5E2N) produced by ROMP reaction initiated by HG2. The line is a guide to the eye

The hardness of the neat poly-5E2N samples (0.00 wt.% CNT) is found to be too weak to be quantified. Nevertheless, we observe that a small amount of 0.05 wt.% of CNT dispersed in 5E2N can significantly increase the Vickers coefficients of the formed polymer (Figure 5.7). This hardness increases steeply with the increase of CNT concentration until 0.20 wt.%, above which the slope of the flattened lines exhibits a significant reduction of the hardening rates (Figure 5.7). We infer that the tendency of CNT to aggregate can diminish their effect, for concentrations higher than 0.20 wt.%.

Based on these preliminary measurements, poly (CNT/5E2N) samples were prepared for three concentrations of CNTs: 0.05 wt.%, 0.10 wt.% and 0.20 wt.% for the flexural tests. The representative load-displacement curves obtained after flexural tests are shown in Figure 5.8. In particular, poly-5E2N samples containing no CNT (0.00 wt.%) were found to be so flexible that a three-point bend test could not be performed on these materials (Inset of Figure. 5.8)

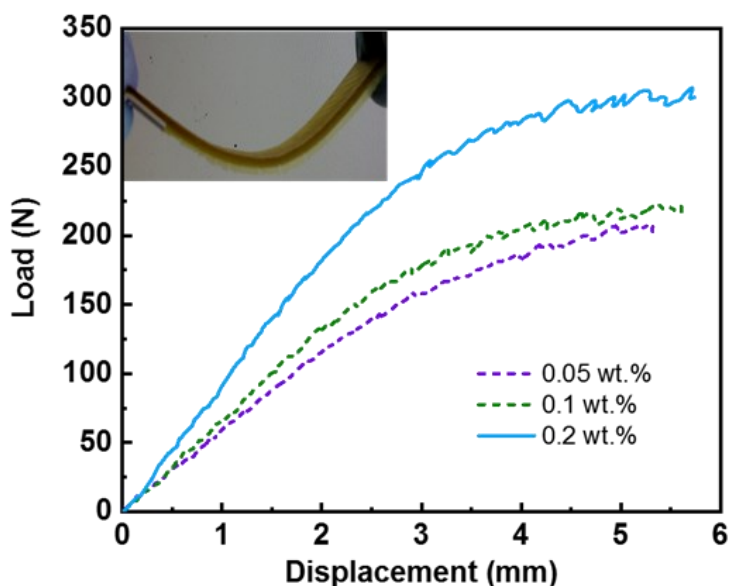


Figure 5.8 Representative load-displacement curves for the poly (CNT/5E2N) samples containing different concentrations of CNTs (0.05, 0.10 and 0.20 wt.%)

Figure 5.8 indicates that increasing the concentration of CNTs in 5E2N up to 0.20 wt.% causes both the material strength and stiffness to increase, as indicated by the maximum loads before failure and by the straight-line portion of the load-displacement curves of the poly (CNT/5E2N) samples, whose slopes increase with CNT content.

According to Ref. [19] incorporating CNT fillers may indeed act as a cross-linking network in poly (CNT/5E2N), however, intercalation of polymer into the CNT is one of the key reinforcing mechanisms of CNT-polymer nanocomposites. These results can be explained by the mechanism where stress is transferred from the matrix to the dispersed rigid phase and large aspect ratio of the nanotubes. Our Raman spectral analysis of the fractured surface of the self-healed epoxy samples, which is shown and discussed later in sections 5.4, confirms this proposition.

Our preliminary results indicate that the presence of CNTs inside poly (CNT/5E2N) improves the material strengthening and, consequently, its self-healing capability. Until now, only the preparation of CNT/5E2N suspension with a CNT concentration of up to 0.10 wt.% has been successfully microencapsulated, due to the agglomeration of CNT at greater contents. [36] Nevertheless, the data reported in Figure 5.8 suggests that such improvements of both the mechanical and the self-healing properties could be enhanced by the implementation of CNT/5E2N suspensions containing more CNTs.

5.3.2 Microcapsules

SEM images of the microcapsules containing only 5E2N and those containing a suspension of CNT/5E2N are shown in Figure 5.9.

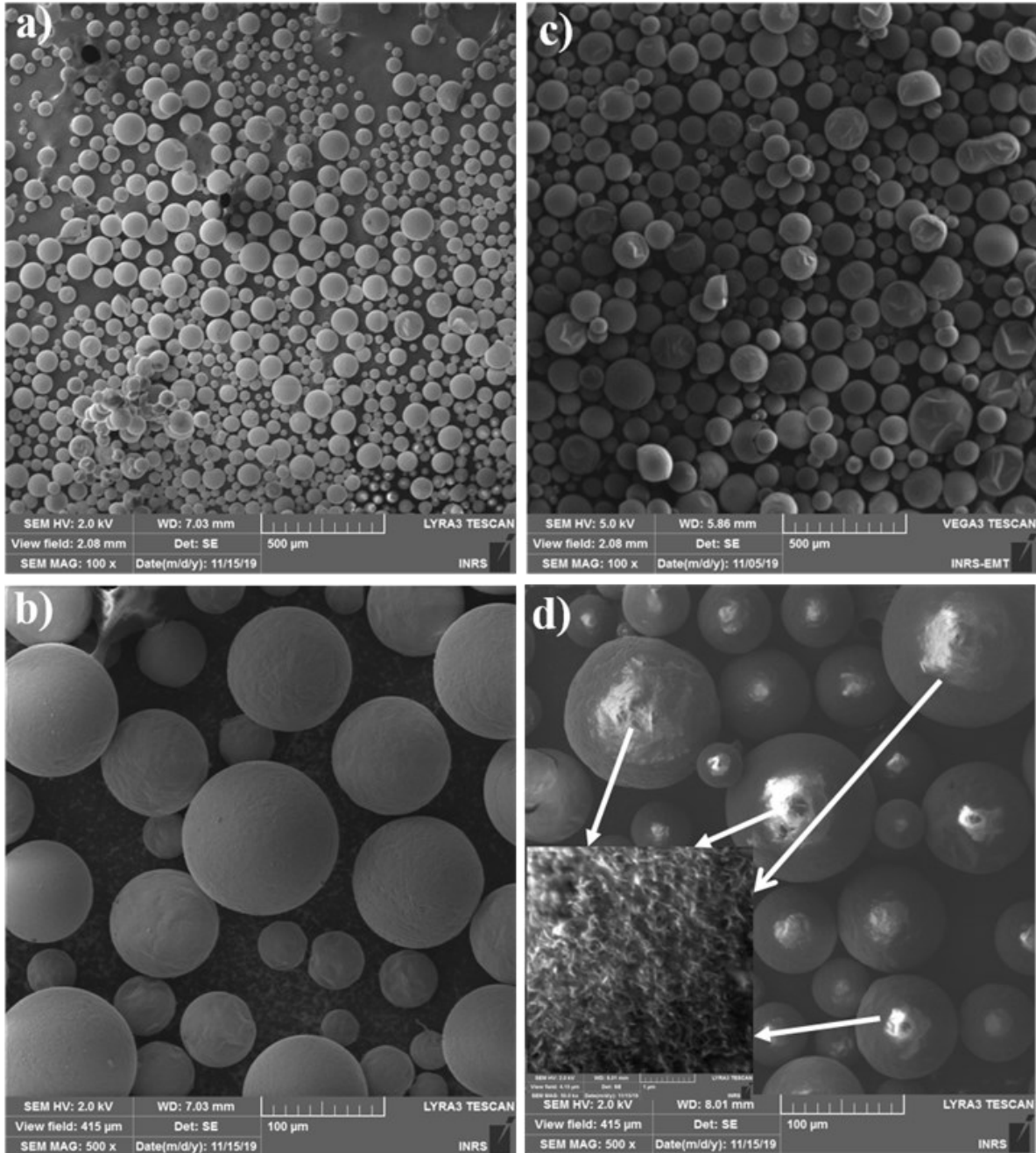


Figure 5.9 SEM micrographs of the two types of microcapsules, containing 5E2N monomer only: a) 100X, b) 500X; containing a suspension of CNT/5E2N: c) 100X and d) 500X, CNTs at the surface of the microcapsules shown in the inset

Figures 5.9 (a) and 5.9 (c) show the spherical shapes of produced microcapsules, and that they are mechanically robust as most of them remain intact not only after incorporating the liquid monomer but also under SEM observations undergoing thereby electron beam. As observed at higher magnification (500X), Figures 5.9 (b) and 5.9 (d) show that the outer surfaces of the microvessels are quite different, due to the presence of irregular nanofiber-like structures (bright). The size, shape and surface roughness of microcapsules may have a significant impact on their bonding to the surrounding polymer matrix [224]. As evidenced in Figure 5.9 (d), the bright microstructures only appear on the surfaces of the CNT/5E2N microcapsules. These very thin nanofiber-like features shown in the inset of Figure 5.9 (d) and pointed by white arrows are associated with CNTs, whose electrical conductivity make them appear brighter than the background image contrast (see inset of Figure 5.9 (d)) [201]. We believe that these CNTs were hanged onto the outer surfaces of the microvessels during the *in-situ* encapsulation process of CNT/5E2N, as evoked later (see section 5.3.3) to explain the changes reported in the mechanical properties of the samples.

5.3.3 Results and analysis of lap shear and mode I fracture tests

The representative load-displacement curves of first loading and second loading (after healing) of the three types of epoxy samples under lap shear and mode I fracture conditions are presented in Figure 5.10. Figure 5.10 (a) refers to the lap shear tests and Figure 5.10 (b) to mode I fracture tests.

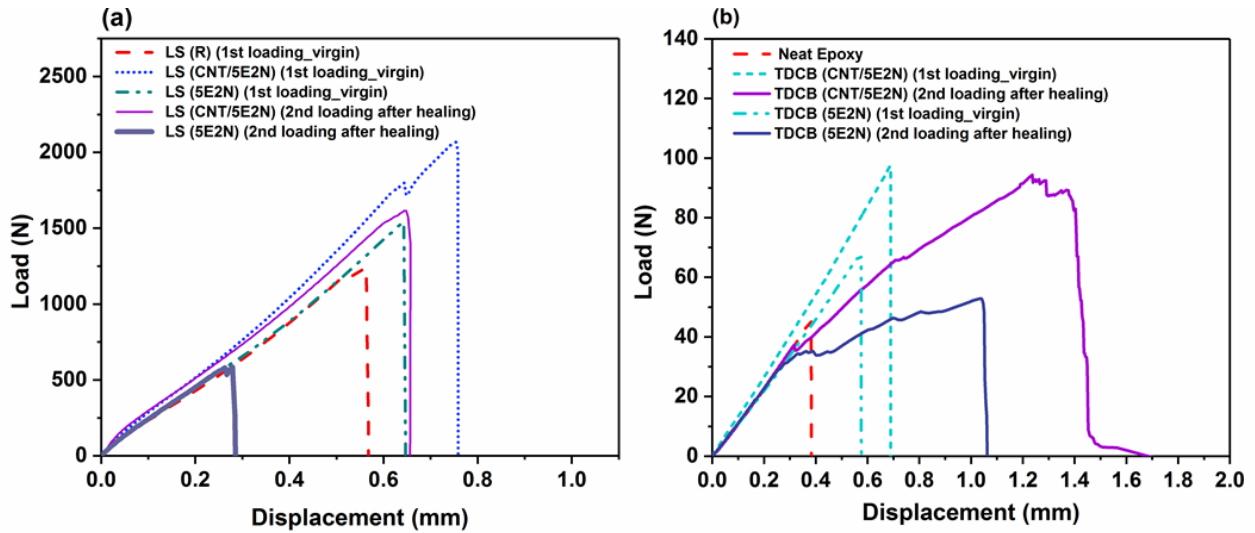


Figure 5.10 (a) Representative load-displacement curves obtained by lap shear tests conducted on LS (R), LS (5E2N) and LS (CNT/5E2N) samples, and (b) mode I fracture tests conducted on TDCB (R), TDCB (5E2N) and TDCB (CNT/5E2N) samples

These data show the general characteristics of the representative load-displacement curves recorded for all the reference [LS (R) and TDCB (R)] and self-healing samples [LS (5E2N) and TDCB (5E2N)], as well as LS (CNT/5E2N) and TDCB (CNT/5E2N)]. During the first loading, often named as ‘virgin loading’ in the literature [12, 13, 102, 133, 138, 167, 212], the samples, in general, undertake proportionately increasing load as the displacement is increased. As the load approaches to the peak, the crack/damage is generated in the epoxy resin and propagates through it leading to its complete failure. At this stage, the sample is separated into two parts and its load carrying capacity drops to zero. The two halves of the damaged sample are then put into contact for 48 hours during which the self-healing reaction occurs. After this period, the two halves of the sample are observed to be glued together. The reassembled samples are then loaded for a second time (referred as ‘2nd loading after healing’ in Figure 5.10) similarly to the first loading, in order to determine its load carrying capacity after healing. No additional loading was performed in the case of reference samples (*i.e.*, LS (R) and TDCB (R)), as these materials were completely fractured during the first loading test and did not undergo any self-healing due to the absence of healing agents. Being able to sustain any load during the second loading of the samples after their initial complete failure implies that self-healing process occurred efficiently.

i) Recovery of strengths

The average lap shear strengths of the three types of pristine (calculated from first loading) and healed (calculated from second loading after healing) adhesive samples are compared in Figures 5.11 (a) and 5.11 (b), respectively. The data reveal that the reference adhesive samples, LS (R), possess an average original lap shear strength of 3.9 MPa without any self-healing property. On the other hand, the LS (5E2N) and LS (CNT/5E2N) samples have greater nominal lap shear strengths of 4.8 and 6.4 MPa, respectively. From complete failure, the LS (5E2N) and LS (CNT/5E2N) samples successfully recover an average lap shear strength of 1.9 MPa and 5 MPa, respectively, after the healing process.

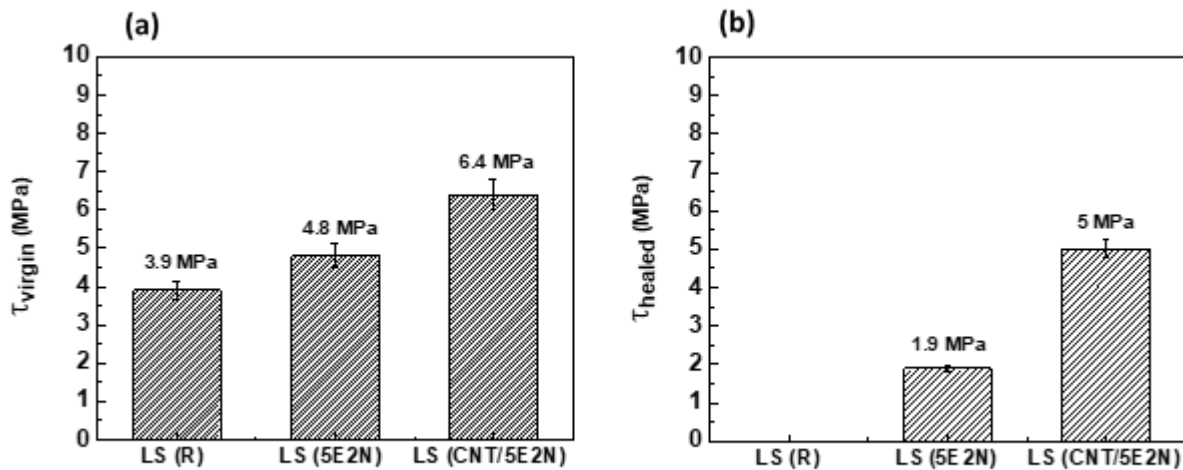


Figure 5.11 Average lap shear strengths of three types of samples in (a) first loading and (b) second loading (after healing)

In the case of TDCB samples, the absolute values of the mode I fracture toughness cannot be simply calculated using the failure loads alone. Such a calculation requires to account for several geometric factors, whose contribution is simplified from Eq. (5.7). These data are discussed later.

ii) Effect of CNT-based microcapsules on mechanical resistance

In agreement with the data reported in Figure 5.11 (a), the reference epoxy adhesive samples without any microcapsules, (*i.e.*, LS (R)), have the lowest nominal lap shear strength. This quantity increases for the samples containing the microcapsules.

Similarly, as evidenced by the load-displacement curves presented in Figure 5.10 (b), the original fracture toughness extracted from the mode I fracture experiments is also found to be higher in the presence of microcapsules. Such improvements with respect to the physical properties of the reference materials are related to the incorporation of 5E2N and CNT/5E2N microcapsules. As defined in Eq. (5.5) and Eq. (5.8), the increase of the material strength is reported for LS and TDCB samples in Figure 5.12, showing improvements by a factor of 3 and 2, respectively.

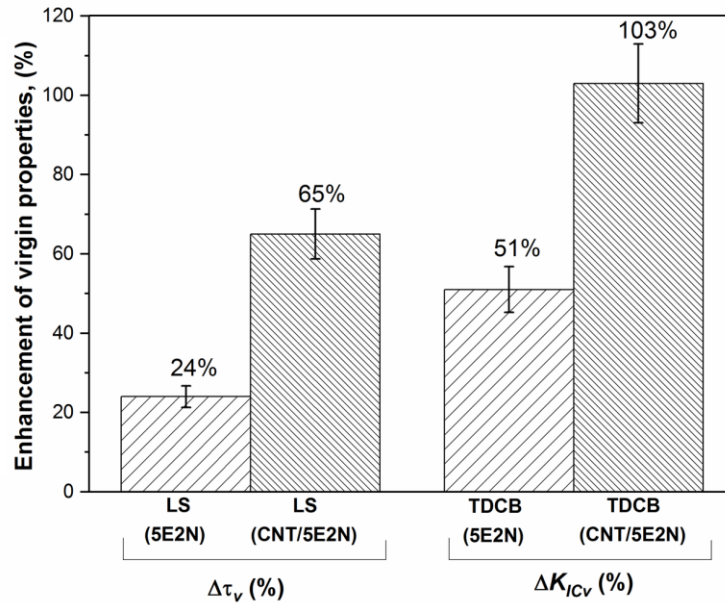


Figure 5.12 Enhancements of original mechanical resistance [$(\Delta\tau_v(\%)$ and $\Delta [K_{IC}]_v (\%)$] due to the incorporation of two types of microcapsules (5E2N-only and CNT/5E2N microcapsules) into the lap shear and TDCB samples

The incorporation of 5E2N containing microcapsules into the LS (5E2N) samples is found to increase the original lap shear strength by $\Delta\tau_v = 24\%$ (Eq. (5.5)), compared to the reference LS (R) samples that do not contain any microcapsules. Similarly, the incorporation of 5E2N-only microcapsules into the TDCB (5E2N) samples increased their original fracture toughness by 51% [$\Delta K_{ICv} = 51\%$, (Eq. (5.8))] compared to TDCB (R) samples. Such effects demonstrate that both LS and TDCB samples containing microcapsules possess greater mechanical resistance to failure. Similar strengthening phenomena resulting from the incorporation of micro-additives into polymers has been previously reported [121, 225], where the size, shape and mechanical properties of the added particles are found to affect the mechanical properties of the polymer composites. [225-231] In self-healing materials containing microvessels, it is suggested that the microcapsules themselves act as additive particles inside epoxy. The crack propagation is

obstructed by the presence of these additional structures so that the strengthening of the composites is enhanced compared to the neat resin [37, 232].

As presented in Figure 5.12, both the average original shear strength and the average original fracture toughness increase by $\Delta\tau_v = 65\%$ and $\Delta K_{IC_v} = 103\%$, with respect to the reference samples for the incorporation of CNT/5E2N microcapsules. The reinforcement of the materials is much higher for the epoxies incorporated with CNT/5E2N microcapsules than for 5E2N-only microcapsules. We believe that such an effect is connected with the presence of CNTs at the outer surface of the microcapsules, as observed in Figure 5.9. The CNT particles attached to the polymeric PMUF shells of the CNT/5E2N microcapsules are suspected to be bonded with the surrounding matrix, thus enhancing the robustness of the host epoxies. This offers better resistance to crack propagation and makes the surrounding epoxy matrix more resistant than for the one of microcapsules that do not have the CNTs.

iii) Self-healing efficiency

To quantify and compare the effectiveness of the self-healing process, we calculated the healing efficiencies according to Eq. (5.4) and Eq. (5.7) for the LS and the TDCB samples, respectively. Figure 5.13 shows that for the lap shear tests, the average healing efficiency achieved by LS (CNT/5E2N) samples was 78% compared to 39% for the LS (5E2N) samples. For the mode I fracture tests, on the other hand, the healing efficiency achieved by TDCB (CNT/5E2N) samples was 97% compared to 76% for the TDCB (5E2N) samples. The average healing efficiencies clearly show that LS (CNT/5E2N) and TDCB (CNT/5E2N) samples have greater self-healing abilities than LS (5E2N) and TDCB (5E2N) samples.

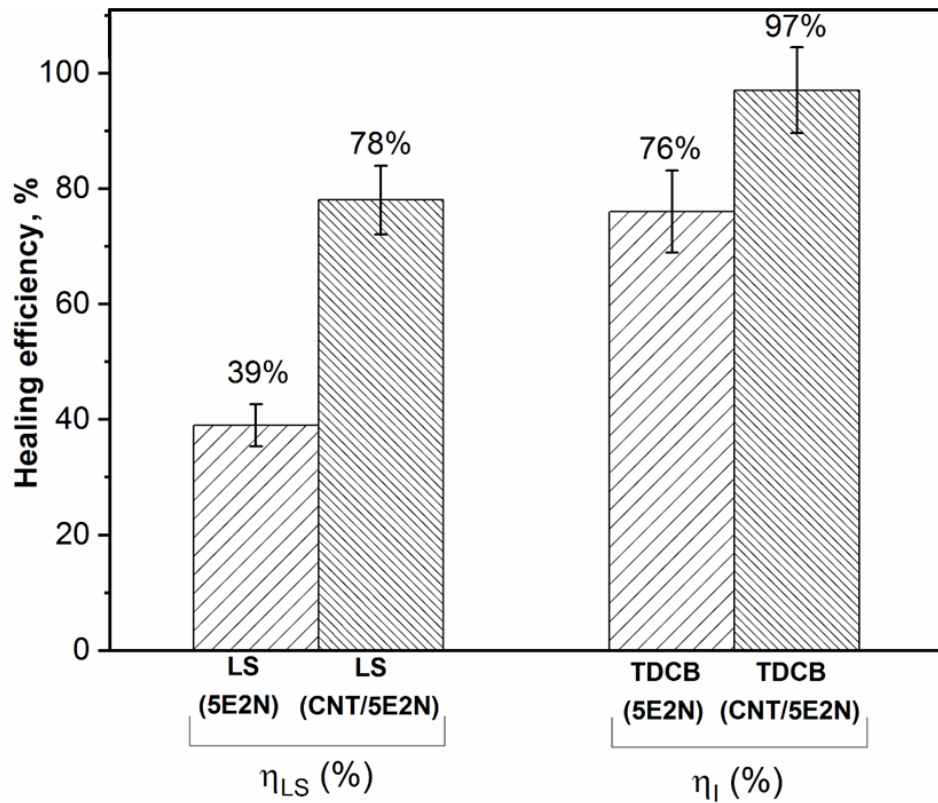


Figure 5.13 Comparison of healing efficiencies of the four types of healed samples, LS (5E2N) (epoxy adhesive samples containing 5E2N-only microcapsules), LS (CNT/5E2N with 0.1 wt.% CNT) (epoxy adhesive samples containing CNT/5E2N microcapsules), TDCB (5E2N) (TDCB epoxy samples containing 5E2N-only microcapsules) and TDCB (CNT/5E2N with 0.1 wt.% CNT) (TDCB epoxy samples containing CNT/5E2N microcapsules)

5.4 Confirmation of self-healing process and contribution of CNTs

SEM imaging of the repaired surfaces of the lap shear and TDCB samples are presented in Figures 5.14 (a) and 5.14 (b). The presence of two distinct polymer layers is evidenced in Figures 5.14 (a) and 5.14 (b), which also show broken microcapsules that have released their core healing agents.

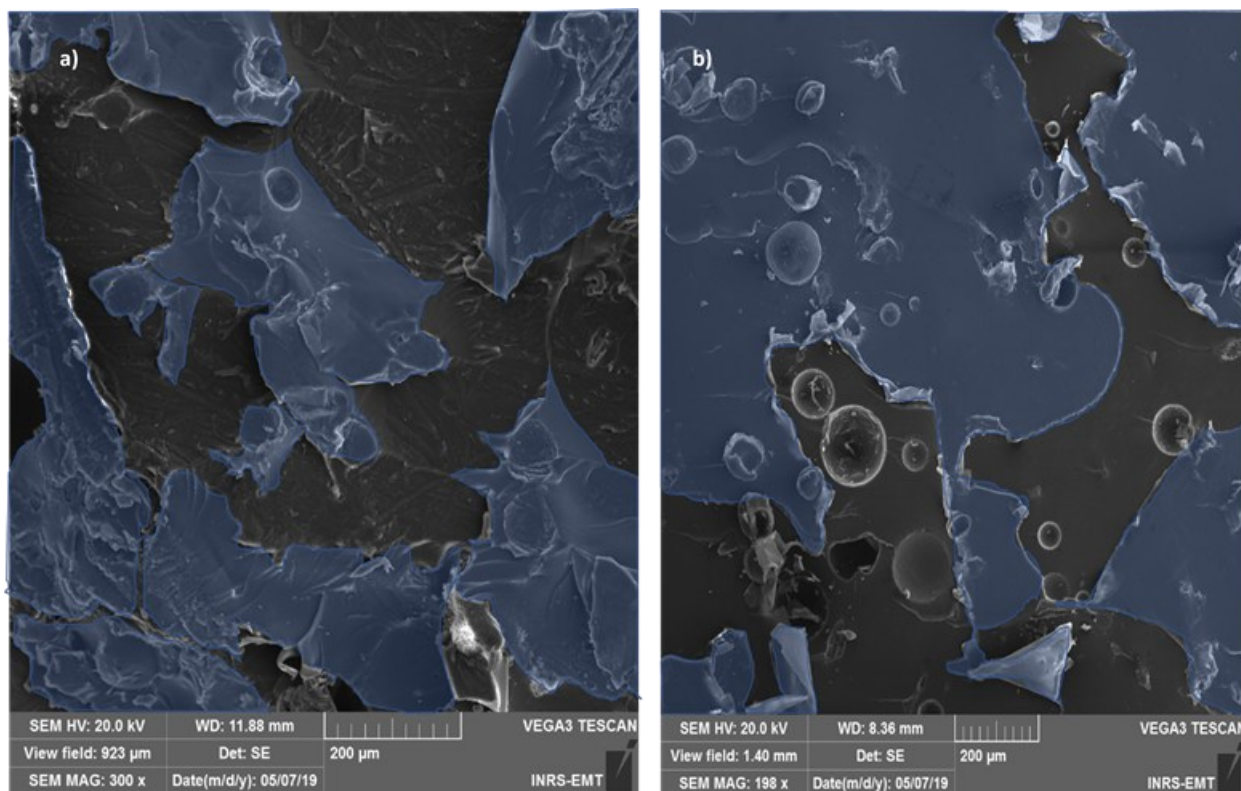


Figure 5.14 Representative SEM micrographs of the fracture surface of the self-healed samples, (a) lap shear sample and (b) TDCB sample. The presence of a self-healed polymer layer (poly-5E2N) is highlighted in blue

As shown by the Raman spectra presented in Figure 5.15 (a), the spectral signature of the layer (highlighted in blue in Figure 5.14) exhibits a characteristic phonon peak at 1665.3 cm^{-1} , which is related to the C=C vibration mode of poly-5E2N [208]. This Raman peak confirms that the collected polymer layers are poly-5E2N, thus indicating that the self-healing reaction (ROMP) was activated at the fracture surface of the tested samples.

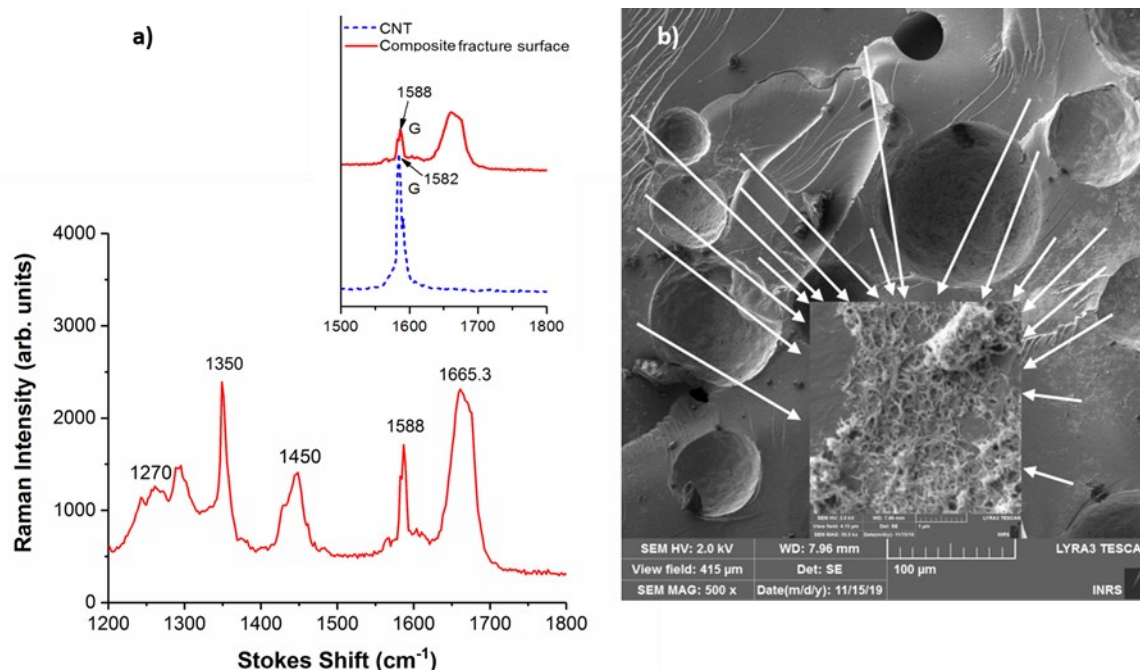


Figure 5.15 (a) Representative Raman spectra generated by the fracture surface of the self-healed epoxy samples. (b) Presence of CNTs at the fracture surface are indicated by arrows and shown in the inset, with magnification of 50000X. The inset shows a slight shift of G-band of the CNTs

The measured Raman bands centered at 1270 cm^{-1} and 1450 cm^{-1} , in Figure 5.15 (a), can be attributed to the C-O stretching mode of epoxide and aromatic ring chain vibration, respectively, of the host epoxy polymer surface [232]. The Raman signal observed around 1350 cm^{-1} corresponds to the CNT D-band, whose out-of-plane vibration is more intense [203]. The slightly shifted G-band of CNT located at 1588 cm^{-1} refers to the in-plane C-C bond stretching vibration [232, 233]. These Raman peaks confirm that the structures observed at the fracture surface of the epoxy samples result from the self-healing process activated by the ROMP reaction of the core liquids (CNT/5E2N suspension) released from the broken microcapsules.

In Figure 5.15 (b), CNTs are also seen inside the poly-5E2N layer at the fracture surfaces of the samples, where microcapsules containing the CNT/5E2N suspension have been incorporated. This, further, verifies that the CNT/5E2N suspension has been released into the fracture surface from the broken microcapsules, and then polymerized through the ROMP reaction initiated by the exposed catalyst particles.

The CNTs present in the CNT/5E2N suspension are also likely to make a stronger interface between the host epoxy and the newly formed poly (CNT/5E2N) nanocomposites. According to

the Raman measurements recorded at the fracture surface of the self-healed epoxy (shown in the inset of Figure 5.15 (a)), it is also observed that inside the repaired sample region, the characteristic G-band of pure CNTs located at 1582 cm^{-1} is slightly shifted to 1588 cm^{-1} . According to Ref. [232] a 6 cm^{-1} shift of the G-band peak towards lower/higher wavenumbers can be associated with the axial elongation/shortening of the C-C bond length inside the nanotube shells. As the value of these characteristic shifts can be correlated with mechanical stress [232, 233], this indicates that the CNTs released into the crack are strained upon loading. We infer that such a situation may facilitate effective load-transfer via the CNT/polymer interface and also explains why the robustness of the self-healing epoxies increases after curing [32, 98, 234, 235]. As stated earlier, the CNTs dispersed within the liquid 5E2N monomer act as reinforcements facilitating stress transfer from the matrix to the dispersed nanotubes when the chemical compounds polymerize into poly (CNT/5E2N) nanocomposites through the ROMP reaction. This mechanism is also consistent with our preliminary investigation discussed in section 5.3.1. It also confirms that a small amount of CNTs dispersed into polymers can significantly increase their mechanical properties like strength and shear modulus [21-23].

According to molecular simulations and elasticity calculations [236], the nature of the interface between nanotubes and their surrounding matrix depends on electrostatic and Van der Waals interactions, as well as on the mechanical interlocking resulting from the internal strain field and the stress/deformation arising from the mismatch between the different thermal expansion coefficients of the CNTs and the polymer. [237, 238] When applied to our materials, the stronger bonding of CNTs with their surrounding matrix translates into a higher healing efficiency for epoxies containing CNT/5E2N microcapsules compared to the ones containing only 5E2N as demonstrated in Figure 5.13.

Additionally, the inclusion of CNT fillers into the cracks may also affect its propagation [239] causing an increase in toughness. To further verify this effect, the fracture surface of the TDCB samples has been closely examined by SEM and a representative SEM image is shown in Figure 5.16.

The fracture surface in Figure 5.16 shows distinct poly-5E2N film and broken microcapsules that have released their core CNTs (shown in the inset). In addition to confirming that the self-healing ROMP reaction is activated at the fracture surface where poly-5E2N films are produced to glue and heal the crack, this figure also shows the presence of tails behind the CNT aggregates, as pointed by arrows at many different locations inside the poly-5E2N layer.

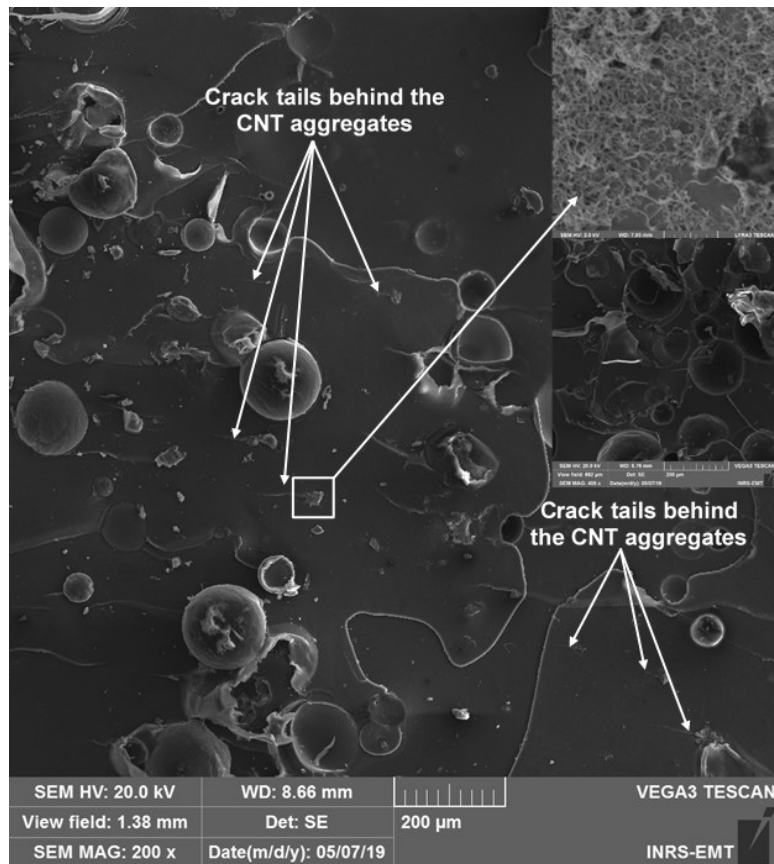


Figure 5.16 Representative SEM micrograph of fracture surface of TDCB samples after the Mode I fracture test. CNT aggregates at the fracture surface are shown in the inset. Presence of crack-tails indicate crack pinning mechanism of toughening by the CNT aggregates

These features of crack are attributed to CNT aggregates, whose effect on the composite toughening can be associated with a crack pinning mechanism [13, 240]. Such a phenomenon is caused by the bifurcation of the crack propagation path in the presence of the filler surface, followed by the subsequent meeting of the previously separated crack fronts [240]. The CNT aggregates in the crack surface thus create the obstruction to the propagation of the crack front causing an increase in toughness of the self-healed samples.

Our fractographic analyses (like in Figure 5.16) further show that the healed poly-5E2N layer is spread substantially over a large area of the host matrix surface, as a consequence of the great wettability of the CNT/5E2N-epoxy system.

This wettability determines the spreading ability of the liquid monomer on the matrix surface to maximize the contact area and the formation of intimate bonds inside the host matrix. The self-healing performance strongly depends on the bond strength between the healed region and its surrounding [8].

As suggested by our mechanical tests, the dispersion of CNTs in 5E2N monomer followed by *in-situ* polymerization favours the formation of CNT/poly-5E2N nanocomposites. It results in a stronger and more active interface between the CNTs and polymer, which is the key for the excellent healing performance of self-healing epoxy incorporated with the microcapsules containing CNT/5E2N.

5.5 Concluding remarks

Excellent mechanical self-healing capabilities by the CNT/5E2N microcapsules are reported for the structural epoxy samples under two different loading modes. For both lap shear mode and mode I fracture tests, the use of CNT/5E2N suspension inside the core of the microvessels is found to improve the original properties of the self-healing epoxies, as well as their healing properties much better than the case of microcapsules containing only 5E2N. The healing efficiency achieved by epoxy adhesive samples made of CNT/5E2N microcapsules with 0.10 wt.% CNT was 78% compared to 39%, for samples with 5E2N alone. When incorporated with 10 wt.% of microcapsules, the original lap shear strength of CNT/5E2N-based epoxies was improved by 64% with respect to the one of neat epoxy, compared to 24% improvement for 5E2N-based samples. The self-healing abilities are found to be even more effective in mode I fracture than in lap shear mode of loading, exhibiting a healing efficiency of 97% for CNT/5E2N microcapsules, compared to 76% for 5E2N microcapsules. We found similar trends for original fracture toughness due to the presence of CNTs in the outer shells of the microcapsules, which contribute to strengthening the host polymers. For mode I fracture tests, we observed an improvement of 103% and 51% in the original fracture toughness of epoxies containing CNT/5E2N and 5E2N microcapsules, respectively. The dispersion of CNTs in 5E2N monomer followed by *in-situ* polymerization results in a stronger and more active interface between the CNTs and polymer, which is the key for the excellent healing performance of self-healing epoxy incorporated with microcapsules containing CNT/5E2N. Our analysis is supported by fractographic observations and characteristic Raman spectral signatures suggesting that the epoxy incorporated with CNT/5E2N microcapsules can serve both as very efficient self-healable matrix material for implementation in high performance laminated composites and self-healable structural adhesives for use as composite bonded joints in aerospace technologies.

CHAPTER 6: CONCLUSIONS, PERSPECTIVES AND RECOMMENDATIONS FOR FUTURE WORKS

6.1 Conclusions and perspectives

Our investigation of CNT/5E2N as microencapsulated healing agents for epoxies for aerospace applications, mainly focuses on three key parts of research. First part is the investigation of the polymerization kinetics of 5E2N initiated by HG2 catalyst at low temperatures using micro-Raman spectral analysis. Second part of the work is related to the encapsulation of CNT/5E2N in polymeric shells and quality characterization of the produced microcapsules. And the final part of this work is dedicated to the determination of the electro-mechanical healing efficiencies of the microencapsulated CNT/5E2N healing agent incorporated into epoxy-based materials.

In our work, an in-depth quantitative analysis of the ROMP reaction kinetics of the 5E2N/HG2 system was systematically conducted from room temperature down to -30°C . By using a Raman spectral analysis that was specifically developed in this framework, the apparent rate constants for the reactions at different low temperatures were determined for the first order kinetics using the Arrhenius principle. The reaction rate constants and the activation energy calculated from our method were found to be consistent with values found in the literature for similar reactions. Our experiments and methodology were specifically designed to enable an efficient monitoring of the ROMP reaction below 0°C . The mean square error and the reliability of the measurements obtained at low temperatures evidence the validity of the methodology developed in this work for the quantitative kinetic characterization of the polymerization reaction. This provides an opportunity for studying the effects of various factors on the polymerization kinetics of different self-healing systems and optimizing them accordingly to make them suitable for specific applications.

Our investigation on the polymerization kinetics of 5E2N confirmed that the ROMP reaction of 5E2N is triggered with the addition of a very low concentration of the HG2 catalyst, and only within several minutes at temperatures as low as -30°C . This condition is representative of a low temperature limit inside satellites and other instruments launched in space. The associated low activation energy of the ROMP reaction implies that the 5E2N/HG2 healing agents can be activated efficiently and, thus, become suitable for self-healing applications in cold environments. However, this feature has to be confirmed well below -30°C , as the temperature at the outer

surface of geostationary satellites in the shadow may fall down to -150°C . Nonetheless, the methodology developed and implemented in this work can be used as a prelude to design and optimize the self-healing function in polymers for advanced applications. We found that the variation of the poly-5E2N phonon intensity around 1665.0 cm^{-1} can be used to determine the activation energy of ROMP reactions at temperatures lower than 0°C . Our data were obtained with a good accuracy (less than 5% deviation), for maximum acquisition times of 30 minutes. In addition to the ease with which the Raman technique can be implemented at low temperatures and for a large variety of catalysts and materials, our results and the methodology we implemented make our experimental approach relevant and complementary to NMR spectroscopy [161] and/or mass spectrometry [241] for measuring various reaction kinetics. The information that can be rapidly collected using this technique can thus be used to inform the direction of mechanistic studies and provide seed technology for further research seeking a molecular-level understanding of the nature of the chemical species and their reaction mechanisms.

In the second part of our work, we successfully microencapsulated CNTs suspended in 5E2N into polymeric shells using *in-situ* polymerization method. An experimental trial and error procedure was used to identify suitable process parameters that influence the successful formation of the microcapsules containing CNT/5E2N with desired characteristics. Extensive thermo-physical characterization of the produced microcapsules was performed by employing various characterization tools including optical, scanning and transmission electron microscopy, thermogravimetric analysis, differential scanning calorimetric analyses, Raman spectral analysis and fractographic analysis. The analyses confirm the presence of CNTs inside the core liquid content of the microcapsules, as well as their release upon breaking event and subsequent polymerization which ensures their efficient self-healing capabilities. The structural integrity of these CNT/5E2N microcapsules was investigated up to 600°C , showing that such system can resist to external temperatures of $220\text{--}250^{\circ}\text{C}$, which makes them suitable to be used in advanced aerospace structures and devices that use structural polymers like epoxies as constituents.

In the final part of our work, we demonstrated efficient recovery of both electrical and mechanical properties of epoxy-based polymer incorporated with the microcapsules containing CNT/5E2N.

For the restoration test of electrical properties, electrical circuits made with conductive epoxy-based polymer incorporated with the microcapsules containing CNT/5E2N were shown to restore autonomically up to 82% of the initial electrical conductivity after the conductive path of the self-healing polymer samples was interrupted. Damaged electrical circuits made with

conductive neat epoxy-based polymer without the microcapsules or with microcapsules containing 5E2N-only did not restore the conductivity autonomously. This makes the incorporation of CNTs into 5E2N monomer relevant to restore the electrical conductivity and/or connections inside damaged electronic circuits. The microcapsules containing such CNTs can thus permit autonomous repairing of key electronic components and/or optoelectronic devices used in advanced aerospace structures.

A comparative analysis of the mechanical self-healing capabilities of two types of microcapsules (i.e., microcapsules containing CNT/5E2N suspension and microcapsules containing 5E2N-alone) incorporated into structural epoxy samples subjected to two different types of mechanical loads (namely lap shear mode and mode I fracture tests) was also performed. Excellent mechanical self-healing capabilities by the CNT/5E2N microcapsules are reported for the structural epoxy samples under both loading modes.

With the CNT/5E2N microcapsules with 0.10 wt.% CNTs incorporated into the epoxy samples, up to 97% of the original fracture toughness was recovered autonomously after their complete failure. 5E2N microcapsules without CNTs, on the other hand, recovered 76% of the original fracture toughness of the epoxy samples. Similarly, 78% of the original adhesive strength of the epoxy samples, compared to only 39%, was recovered with the CNT/5E2N microcapsules. Even the presence of CNTs at the outer shells of the CNT/5E2N microcapsules contributes to the strengthening of the host polymer much better than the 5E2N microcapsules without CNTs at their outer shells.

Extensive fractographic analysis and characteristic Raman spectral signatures obtained at the fracture surfaces of the epoxy samples strongly support the results of our mechanical tests. Our analysis suggests that the dispersion of CNTs in 5E2N monomer followed by *in-situ* polymerization favours the formation of CNT/poly-5E2N nanocomposites. This results in a stronger and more active interface between the CNTs and polymer, which is the key for the excellent healing performance of self-healing epoxy incorporated with the microcapsules containing CNT/5E2N.

In real applications, the self-healing is designed to heal micro-damage. The micro-crack when propagates through the microcapsules, the microcapsules break, and the self-healing process is activated. That is, when a minor damage or a tiny crack form in the part due to some loading/damage event, the self-healing process is activated by releasing the core healing monomer from the broken microcapsules into the crack and polymerize itself to close the

microcrack. Closing of these microcracks enable recovering the minor reduction or loss of properties caused by the creation of the microcracks in the epoxy resin part.

We have demonstrated in our work that with the microencapsulated CNT/5E2N healing agent, the self-healing process is activated and capable of recovering properties significantly even after the complete failure of the epoxy samples. To distinctly identifying the contribution of self-healing process in the recovery of electro-mechanical properties, the microencapsulated CNT/5E2N healing agent is found to recover electro-mechanical properties significantly when the epoxy resin is already completely failed and not capable of sustaining any further electrical/mechanical loads. From this point onward, the healing agent, after the healing reaction, enables the epoxy resin to sustain significant loads again, recovering from zero. This proves the significant healing effectiveness of the microencapsulated CNT/5E2N which is the ultimate objective of the present work. However, in reality, the self-healing is intended to recover the minor reduction or loss of properties of the part due to the formation of some micro cracks in the epoxy resin before they accumulate to lead to the final major failure of the part.

These new CNT/5E2N microcapsules thus offer unique self-healing solutions to devices/structures that require efficient restoration of either or both electrical and mechanical properties at low temperatures. Their ease of being integrated into a great variety of polymeric materials makes them suitable to protect and extend the lifetime of key aerospace structures, space telecommunication equipment and sensors exposed to accidental events and collisions with small debris, as well as against critical ageing effects that can cause their irreversible damage and failure. The use of encapsulated CNT/5E2N could also provide a significant added value to many commercial products and devices requiring long operation periods inside facilities or environments where they cannot be repaired and/or replaced by new ones. Examples of devices and structures in which this technology could be implemented are flexible fluidic antennas, where both electrical conductivity and mechanical properties ensure their efficient functioning, in wireless sensing or monitoring radio systems, switches, radio frequency identification (RFID) tags, conformal circuits for health monitoring etc. Structural polymers like epoxy incorporated with CNT/5E2N microcapsules can also serve as a very efficient self-healable matrix material for use in high performance laminated polymer composites and self-healable structural adhesives employed in aerospace technologies.

6.2 Recommendations for future works

For the future research works, we suggest the following

i) To assess the catalyst/monomer ratio on the cure kinetics of 5E2N/HG2 system

Besides the temperature effect, other parameters like the ratio of monomer to catalyst may significantly influence the reaction kinetics of the 5E2N/HG2 system. These effects should be studied to optimize the reaction kinetics of the healing agents for self-healing applications in space.

ii) To investigate more efficient use of catalyst

Ruthenium is generally scarce in nature and is expensive which might hinder its widespread use in industry. Efforts should be made to find ways to use the Ruthenium-based catalyst more efficiently in the material by reducing its requirements or by recycling after use.

iii) To carry out the electro-mechanical recovery test in low temperature environment

Microencapsulated CNT/5E2N and HG2 system is shown to recover the electro-mechanical properties of polymer significantly at room temperature conditions. The healing agents are also found very active at sub-zero low temperatures. It would be interesting to see how the healing agent system recovers the electro-mechanical properties of polymer in a low temperature environment.

iv) To investigate the CNT/5E2N healing agent for other extrinsic self-healing strategies for polymers including in self-healing epoxies with microvascular network system.

Instead of microencapsulating the CNT/5E2N, the healing agent can be used in self-healing epoxies with embedded microvascular network system with the possibility of replenishing the network with healing agents for the repeated healing of damage at the same location.

AUTHOR CONTRIBUTIONS

This thesis is written as traditional thesis version, based on the INRS Guide-2021, to fulfill the requirement of the PhD program. The first chapter of the dissertation is the introduction, objectives, and methodology. Chapters 2 consists of detailed literature review. Our works, results, and analysis are presented in chapter 3-5. Chapter 6 includes conclusions, perspectives, and recommendations for future works. Following is the authors contribution to Chapters 3-5:

Chapter 3: The result that is discussed in chapter 3, is published as Hasna Hena Zamal, David Barba, Brahim Aissa, Emile Haddad, Federico Rosei; Cure kinetics of poly (5-ethylidene-2-norbornene) with 2nd generation Hoveyda-Grubbs' catalyst for self-healing applications; *Polymer* (2018). I was responsible for experiments and data analysis as well as the primary manuscript composition and revision. David Barba guided me for concept formation, Raman measurement and analysis. He actively participated to the redaction of the MS, the data analyses, and interpretations. Brahim Aissa and Emile Haddad were involved with manuscript composition and review of the manuscript. All authors have read and agreed to the published version of the manuscript.

Chapter 4: The discussed result of chapter 4 is published as Hasna Hena Zamal, David Barba, Brahim Aissa, Emile Haddad, Federico Rosei; 'Recovery of electro-mechanical properties inside self-healing composites through microencapsulation of carbon nanotubes'; *Scientific Reports* (2020). I was responsible for performing the synthesis of microcapsules, sample fabrication, characterization, electrical testing and the thermal and spectroscopy analysis, as well as the manuscript composition. Brahim Aissa guided me for concept formation and arranged for the lab facilities for the experiments. David Barba involved with manuscript composition and review of the manuscript. Emile Haddad assisted in the research activities conducted at MPB Inc. All authors have read and agreed to the published version of the manuscript.

Chapter 5: The chapter discussed about the mechanical testing and the measurement of mechanical self-healing efficiency published as Hasna Hena Zamal, David Barba, Brahim Aissa, Emile Haddad, Federico Rosei; Failure analysis of self-healing epoxy resins using microencapsulated 5E2N and carbon nanotubes; *Smart Mater. Struct.* (2021). I designed the experiments, carried out different types of mechanical testing, spectroscopy measurement, data analysis, wrote the primary manuscript and revised it with suggestions from other co-authors. All authors have read and agreed to the published version of the manuscript.

Prof. Federico Rosei is the main supervisor. He contributed to the training and provided access to his laboratory facilities, as well as financial supports to carry out this project (including scholarships, user fees and the purchase of equipment and chemicals). He also gave directions and guidelines for research, revised all the MS, and contributed to their improvement. He provided critical feedback and helped shape the research.

References

1. Mrazova, M., *Advanced composite materials of the future in aerospace industry*. Incas bulletin, 2013. **5**(3): p. 139.
2. Jakubinek, M.B., et al., *Single-walled carbon nanotube–epoxy composites for structural and conductive aerospace adhesives*. Composites Part B: Engineering, 2015. **69**: p. 87-93.
3. Akpınar, I.A., et al., *Experimental analysis on the single-lap joints bonded by a nanocomposite adhesives which obtained by adding nanostructures*. Composites Part B: Engineering, 2017. **110**: p. 420-428.
4. Rajak, D.K., et al., *Fiber-reinforced polymer composites: Manufacturing, properties, and applications*. Polymers, 2019. **11**(10): p. 1667.
5. Trask, R. and I. Bond, *Biomimetic self-healing of advanced composite structures using hollow glass fibres*. Smart Materials and Structures, 2006. **15**(3): p. 704.
6. Kessler, M., *Self-healing: a new paradigm in materials design*. Proceedings of the Institution of Mechanical Engineers, Part G: Journal of Aerospace Engineering, 2007. **221**(4): p. 479-495.
7. Wool, R.P., *Self-healing materials: a review*. Soft Matter, 2008. **4**(3): p. 400-418.
8. Blaiszik, B.J., et al., *Self-healing polymers and composites*. Annual review of materials research, 2010. **40**: p. 179-211.
9. White, S.R., et al., *Autonomic healing of polymer composites*. Nature, 2001. **409**(6822): p. 794-797.
10. Bielawski, C.W. and R.H. Grubbs, *Living ring-opening metathesis polymerization*. Progress in Polymer Science, 2007. **32**(1): p. 1-29.
11. Nuyken, O. and S.D. Pask, *Ring-opening polymerization—an introductory review*. Polymers, 2013. **5**(2): p. 361-403.
12. Brown, E.N., N.R. Sottos, and S.R. White, *Fracture testing of a self-healing polymer composite*. Experimental mechanics, 2002. **42**(4): p. 372-379.
13. Brown, E.N., S.R. White, and N.R. Sottos, *Microcapsule induced toughening in a self-healing polymer composite*. Journal of Materials Science, 2004. **39**(5): p. 1703-1710.
14. Rule, J.D., et al., *Wax-protected catalyst microspheres for efficient self-healing materials*. Advanced Materials, 2005. **17**(2): p. 205-208.
15. Liu, X., et al., *Characterization of diene monomers as healing agents for autonomic damage repair*. Journal of Applied Polymer Science, 2006. **101**(3): p. 1266-1272.
16. Kessler, M.R. and S.R. White, *Cure kinetics of the ring-opening metathesis polymerization of dicyclopentadiene*. Journal of Polymer Science Part A: Polymer Chemistry, 2002. **40**(14): p. 2373-2383.
17. Lee, J.K., et al., *Characterization of dicyclopentadiene and 5-ethylidene-2-norbornene as self-healing agents for polymer composite and its microcapsules*. Macromolecular Research, 2004. **12**(5): p. 478-483.
18. Aïssa, B., et al., *Self-healing materials systems: Overview of major approaches and recent developed technologies*. Advances in Materials Science and Engineering, 2012. **2012**.
19. Aïssa, B., et al., *Micromechanical characterization of single-walled carbon nanotube reinforced ethylidene norbornene nanocomposites for self-healing applications*. Smart materials and structures, 2012. **21**(10): p. 105028.

20. Liu, X., et al., *Synthesis and characterization of melamine-urea-formaldehyde microcapsules containing ENB-based self-healing agents*. *Macromolecular Materials and Engineering*, 2009. **294**(6-7): p. 389-395.
21. Breton, Y., et al., *Mechanical properties of multiwall carbon nanotubes/epoxy composites: influence of network morphology*. *Carbon*, 2004. **42**(5-6): p. 1027-1030.
22. Li, X., et al., *Nanomechanical characterization of single-walled carbon nanotube reinforced epoxy composites*. *Nanotechnology*, 2004. **15**(11): p. 1416.
23. Szatkowski, P., K. Pielichowska, and S. Blazewicz, *Mechanical and thermal properties of carbon-nanotube-reinforced self-healing polyurethanes*. *Journal of Materials Science*, 2017. **52**(20): p. 12221-12234.
24. Bryning, M.B., et al., *Very low conductivity threshold in bulk isotropic single-walled carbon nanotube–epoxy composites*. *Advanced materials*, 2005. **17**(9): p. 1186-1191.
25. Biercuk, M., et al., *Carbon nanotube composites for thermal management*. *Applied physics letters*, 2002. **80**(15): p. 2767-2769.
26. Choi, E., et al., *Enhancement of thermal and electrical properties of carbon nanotube polymer composites by magnetic field processing*. *Journal of Applied physics*, 2003. **94**(9): p. 6034-6039.
27. Huang, H., et al., *Aligned carbon nanotube composite films for thermal management*. *Advanced materials*, 2005. **17**(13): p. 1652-1656.
28. Chung, D.D.L., *Electrical applications of carbon materials*. *Journal of Materials Science*, 2004. **39**(8): p. 2645-2661.
29. Coleman, J.N., et al., *Small but strong: a review of the mechanical properties of carbon nanotube–polymer composites*. *Carbon*, 2006. **44**(9): p. 1624-1652.
30. Andrews, R. and M. Weisenberger, *Carbon nanotube polymer composites*. *Current Opinion in Solid State and Materials Science*, 2004. **8**(1): p. 31-37.
31. Gojny, F.H., et al., *Influence of different carbon nanotubes on the mechanical properties of epoxy matrix composites—a comparative study*. *Composites Science and Technology*, 2005. **65**(15-16): p. 2300-2313.
32. Thostenson, E.T., C. Li, and T.-W. Chou, *Nanocomposites in context*. *Composites science and technology*, 2005. **65**(3-4): p. 491-516.
33. Thostenson, E.T. and T.-W. Chou, *Processing-structure-multi-functional property relationship in carbon nanotube/epoxy composites*. *Carbon*, 2006. **44**(14): p. 3022-3029.
34. Bandaru, P.R., *Electrical properties and applications of carbon nanotube structures*. *Journal of nanoscience and nanotechnology*, 2007. **7**(4-5): p. 1239-1267.
35. Esawi, A.M. and M.M. Farag, *Carbon nanotube reinforced composites: potential and current challenges*. *Materials & design*, 2007. **28**(9): p. 2394-2401.
36. Jeong, W. and M.R. Kessler, *Toughness enhancement in ROMP functionalized carbon nanotube/polydicyclopentadiene composites*. *Chemistry of Materials*, 2008. **20**(22): p. 7060-7068.
37. Jeong, W. and M.R. Kessler, *Effect of functionalized MWCNTs on the thermo-mechanical properties of poly (5-ethylidene-2-norbornene) composites produced by ring-opening metathesis polymerization*. *Carbon*, 2009. **47**(10): p. 2406-2412.
38. Rosca, I.D. and S.V. Hoa, *Highly conductive multiwall carbon nanotube and epoxy composites produced by three-roll milling*. *Carbon*, 2009. **47**(8): p. 1958-1968.
39. Lin, L. and A.K. Schlarb, *Investigation on morphology and properties of melt compounded polyoxymethylene/carbon nanotube composites*. *Journal of Applied Polymer Science*, 2015. **132**(40).

40. Baughman, R.H., A.A. Zakhidov, and W.A. De Heer, *Carbon nanotubes--the route toward applications*. science, 2002. **297**(5582): p. 787-792.
41. Zamal, H.H.H., S. V. , *Fatigue Damage Behavior of Glass/Epoxy Composites Using Carbon Nanotubes as Sensors*. 2011: p. 189–197.
42. Gao, L., et al., *Coupled carbon nanotube network and acoustic emission monitoring for sensing of damage development in composites*. Carbon, 2009. **47**(5): p. 1381-1388.
43. Odom, S.A., et al., *Autonomic restoration of electrical conductivity using polymer-stabilized carbon nanotube and graphene microcapsules*. Applied Physics Letters, 2012. **101**(4): p. 043106.
44. De Volder, M.F., et al., *Carbon nanotubes: present and future commercial applications*. science, 2013. **339**(6119): p. 535-539.
45. Jones, A.S., et al., *Catalyst morphology and dissolution kinetics of self-healing polymers*. Chemistry of Materials, 2006. **18**(5): p. 1312-1317.
46. Hearn, N., *Self-sealing, autogenous healing and continued hydration: what is the difference?* Materials and structures, 1998. **31**(8): p. 563-567.
47. White, S.R., et al., *Self-healing Polymers and Composites: Capsules, circulatory systems and chemistry allow materials to fix themselves*. American Scientist, 2011. **99**(5): p. 392-399.
48. Yuan, Y., et al., *Self healing in polymers and polymer composites. Concepts, realization and outlook: A review*. Express Polymer Letters, 2008. **2**(4): p. 238-250.
49. Sottos, N.R. and J.S. Moore, *Spot-on healing*. Nature, 2011. **472**(7343): p. 299-300.
50. Diesendruck, C.E., et al., *Biomimetic self-healing*. Angewandte Chemie International Edition, 2015. **54**(36): p. 10428-10447.
51. Bekas, D., et al., *Self-healing materials: A review of advances in materials, evaluation, characterization and monitoring techniques*. Composites Part B: Engineering, 2016. **87**: p. 92-119.
52. Scheiner, M., T.J. Dickens, and O. Okoli, *Progress towards self-healing polymers for composite structural applications*. Polymer, 2016. **83**: p. 260-282.
53. Lee, M.W., *Prospects and future directions of self-healing fiber-reinforced composite materials*. Polymers, 2020. **12**(2): p. 379.
54. Heo, Y. and H.A. Sodano, *Thermally responsive self-healing composites with continuous carbon fiber reinforcement*. Composites Science and Technology, 2015. **118**: p. 244-250.
55. Hia, I.L., V. Vahedi, and P. Pasbakhsh, *Self-healing polymer composites: Prospects, challenges, and applications*. Polymer Reviews, 2016. **56**(2): p. 225-261.
56. Zhang, L., F. Julé, and H.A. Sodano, *High service temperature, self-mendable thermosets networked by isocyanurate rings*. Polymer, 2017. **114**: p. 249-256.
57. Iacono, S.D., A. Martone, and E. Amendola, *Diels-Alder Chemistry to Develop Self-Healing Epoxy Resins and Composites Thereof*, in *Paint and Coatings Industry*. 2018, IntechOpen.
58. Dry, C., *Matrix cracking repair and filling using active and passive modes for smart timed release of chemicals from fibers into cement matrices*. Smart Materials and Structures, 1994. **3**(2): p. 118.
59. Dry, C. and W. McMillan, *Three-part methylmethacrylate adhesive system as an internal delivery system for smart responsive concrete*. Smart Materials and Structures, 1996. **5**(3): p. 297.

60. Dry, C., *Three designs for the internal release of sealants, adhesives, and waterproofing chemicals into concrete to reduce permeability*. Cement and Concrete Research, 2000. **30**(12): p. 1969-1977.
61. Dry, C., *Procedures developed for self-repair of polymer matrix composite materials*. Composite structures, 1996. **35**(3): p. 263-269.
62. Bleay, S., et al., *A smart repair system for polymer matrix composites*. Composites Part A: Applied Science and Manufacturing, 2001. **32**(12): p. 1767-1776.
63. Kousourakis, A. and A. Mouritz, *The effect of self-healing hollow fibres on the mechanical properties of polymer composites*. Smart Materials and Structures, 2010. **19**(8): p. 085021.
64. Motuku, M., U. Vaidya, and G. Janowski, *Parametric studies on self-repairing approaches for resin infused composites subjected to low velocity impact*. Smart Materials and Structures, 1999. **8**(5): p. 623.
65. Pang, J. and I. Bond, *'Bleeding composites'—damage detection and self-repair using a biomimetic approach*. Composites Part A: Applied Science and Manufacturing, 2005. **36**(2): p. 183-188.
66. Trask, R., G. Williams, and I. Bond, *Bioinspired self-healing of advanced composite structures using hollow glass fibres*. Journal of the royal society Interface, 2007. **4**(13): p. 363-371.
67. Pang, J.W. and I.P. Bond, *A hollow fibre reinforced polymer composite encompassing self-healing and enhanced damage visibility*. Composites Science and Technology, 2005. **65**(11-12): p. 1791-1799.
68. Williams, G.J., I.P. Bond, and R.S. Trask, *Compression after impact assessment of self-healing CFRP*. Composites Part A: Applied Science and Manufacturing, 2009. **40**(9): p. 1399-1406.
69. Williams, G., R. Trask, and I. Bond, *A self-healing carbon fibre reinforced polymer for aerospace applications*. Composites Part A: Applied Science and Manufacturing, 2007. **38**(6): p. 1525-1532.
70. Kling, S. and T. Czigány, *Damage detection and self-repair in hollow glass fiber fabric-reinforced epoxy composites via fiber filling*. Composites Science and Technology, 2014. **99**: p. 82-88.
71. Toohey, K.S., et al., *Self-healing materials with microvascular networks*. Nature materials, 2007. **6**(8): p. 581-585.
72. Therriault, D., S.R. White, and J.A. Lewis, *Chaotic mixing in three-dimensional microvascular networks fabricated by direct-write assembly*. Nature materials, 2003. **2**(4): p. 265-271.
73. Toohey, K.S., et al., *Delivery of two-part self-healing chemistry via microvascular networks*. Advanced Functional Materials, 2009. **19**(9): p. 1399-1405.
74. Hansen, C.J., et al., *Self-healing materials with interpenetrating microvascular networks*. Advanced Materials, 2009. **21**(41): p. 4143-4147.
75. Hansen, C.J., et al., *Accelerated self-healing via ternary interpenetrating microvascular networks*. Advanced Functional Materials, 2011. **21**(22): p. 4320-4326.
76. Hamilton, A., N.R. Sottos, and S.R. White, *Pressurized vascular systems for self-healing materials*. Journal of The Royal Society Interface, 2012. **9**(70): p. 1020-1028.
77. Trask, R.S., C.J. Norris, and I.P. Bond, *Stimuli-triggered self-healing functionality in advanced fibre-reinforced composites*. Journal of Intelligent Material Systems and Structures, 2014. **25**(1): p. 87-97.

78. Trask, R. and I. Bond, *Bioinspired engineering study of Plantae vasculae for self-healing composite structures*. Journal of the Royal Society Interface, 2010. **7**(47): p. 921-931.
79. Norris, C., I. Bond, and R. Trask, *Interactions between propagating cracks and bioinspired self-healing vasculae embedded in glass fibre reinforced composites*. Composites Science and Technology, 2011. **71**(6): p. 847-853.
80. Norris, C., I. Bond, and R. Trask, *The role of embedded bioinspired vasculature on damage formation in self-healing carbon fibre reinforced composites*. Composites Part A: Applied Science and Manufacturing, 2011. **42**(6): p. 639-648.
81. Huang, C.-Y., R. Trask, and I. Bond, *Characterization and analysis of carbon fibre-reinforced polymer composite laminates with embedded circular vasculature*. Journal of the royal society Interface, 2010. **7**(49): p. 1229-1241.
82. Esser-Kahn, A.P., et al., *Three-dimensional microvascular fiber-reinforced composites*. Advanced Materials, 2011. **23**(32): p. 3654-3658.
83. Patrick, J.F., et al., *Continuous self-healing life cycle in vascularized structural composites*. Advanced materials, 2014. **26**(25): p. 4302-4308.
84. Farahani, R.D., M. Dubé, and D. Therriault, *Three-dimensional printing of multifunctional nanocomposites: manufacturing techniques and applications*. Advanced materials, 2016. **28**(28): p. 5794-5821.
85. Wu, Q., et al., *3D printing of a self-healing nanocomposite for stretchable sensors*. Journal of Materials Chemistry C, 2018. **6**(45): p. 12180-12186.
86. Therriault, D., S.R. White, and J.A. Lewis, *Rheological behavior of fugitive organic inks for direct-write assembly*. Applied Rheology, 2007. **17**(1): p. 10112-1-10112-8.
87. Qamar, I.P., N.R. Sottos, and R.S. Trask, *Grand challenges in the design and manufacture of vascular self-healing*. Multifunctional Materials, 2020. **3**(1): p. 013001.
88. Vahedi, V., et al., *A facile method for preparation of self-healing epoxy composites: using electrospun nanofibers as microchannels*. Journal of Materials Chemistry A, 2015. **3**(31): p. 16005-16012.
89. Wu, D.Y., S. Meure, and D. Solomon, *Self-healing polymeric materials: A review of recent developments*. Progress in polymer science, 2008. **33**(5): p. 479-522.
90. Kosarli, M., et al., *Microcapsule-based self-healing materials: Healing efficiency and toughness reduction vs. capsule size*. Composites Part B: Engineering, 2019. **171**: p. 78-86.
91. Nordenström, M., et al., *Superamphiphobic coatings based on liquid-core microcapsules with engineered capsule walls and functionality*. Scientific reports, 2018. **8**(1): p. 1-10.
92. Bailey, B.M., et al., *Electrically conductive self-healing polymer composite coatings*. Progress in Organic Coatings, 2015. **85**: p. 189-198.
93. Song, Y.-K. and C.-M. Chung, *Repeatable self-healing of a microcapsule-type protective coating*. Polymer Chemistry, 2013. **4**(18): p. 4940-4947.
94. Li, J., et al., *Self-healing epoxy coating based on tung oil-containing microcapsules for corrosion protection*. Progress in Organic Coatings, 2021. **156**: p. 106236.
95. Zhang, C., H. Wang, and Q. Zhou, *Preparation and characterization of microcapsules based self-healing coatings containing epoxy ester as healing agent*. Progress in organic coatings, 2018. **125**: p. 403-410.
96. Behzadnasab, M., et al., *Evaluation of corrosion performance of a self-healing epoxy-based coating containing linseed oil-filled microcapsules via electrochemical impedance spectroscopy*. Progress in Organic Coatings, 2017. **105**: p. 212-224.
97. Kang, S., et al., *Microencapsulated carbon black suspensions for restoration of electrical conductivity*. Advanced Functional Materials, 2014. **24**(20): p. 2947-2956.

98. Saini, P., *Electrical properties and electromagnetic interference shielding response of electrically conducting thermosetting nanocomposites*. Thermoset Nanocomposites, 2013.
99. Blaiszik, B.J., et al., *Autonomic restoration of electrical conductivity*. Advanced Materials, 2012. **24**(3): p. 398-401.
100. Yadav, R., et al., *Polymer composite for antistatic application in aerospace*. Defence Technology, 2020. **16**(1): p. 107-118.
101. Pastore, R., et al., *Outgassing effect in polymeric composites exposed to space environment thermal-vacuum conditions*. Acta Astronautica, 2020. **170**: p. 466-471.
102. Rule, J.D., N.R. Sottos, and S.R. White, *Effect of microcapsule size on the performance of self-healing polymers*. Polymer, 2007. **48**(12): p. 3520-3529.
103. Patel, A.J., et al., *Autonomic healing of low-velocity impact damage in fiber-reinforced composites*. Composites Part A: Applied Science and Manufacturing, 2010. **41**(3): p. 360-368.
104. Kessler, M., N. Sottos, and S. White, *Self-healing structural composite materials*. Composites Part A: applied science and manufacturing, 2003. **34**(8): p. 743-753.
105. Blaiszik, B.J., et al., *Autonomic recovery of fiber/matrix interfacial bond strength in a model composite*. Advanced Functional Materials, 2010. **20**(20): p. 3547-3554.
106. O'Brien, T.K. and S.R. White. *Assesment of composite delamination self-healing via micro-encapsulation*. in *American society for composites 23rd technical conference proceedings*. Memphis, (TN, USA): DEStech Publications, Inc. 2008.
107. Jin, H., et al., *Fracture and fatigue response of a self-healing epoxy adhesive*. Polymer, 2011. **52**(7): p. 1628-1634.
108. Manfredi, E., et al., *Assessment of solvent capsule-based healing for woven E-glass fibre-reinforced polymers*. Smart Materials and Structures, 2014. **24**(1): p. 015019.
109. Jones, A., et al., *Full recovery of fiber/matrix interfacial bond strength using a microencapsulated solvent-based healing system*. Composites Science and Technology, 2013. **79**: p. 1-7.
110. Jin, H., et al., *Self-healing thermoset using encapsulated epoxy-amine healing chemistry*. Polymer, 2012. **53**(2): p. 581-587.
111. Li, Q., et al., *Effects of dual component microcapsules of resin and curing agent on the self-healing efficiency of epoxy*. Composites Part B: Engineering, 2013. **55**: p. 79-85.
112. He, Z., et al., *Self-healing isocyanate microcapsules for efficient restoration of fracture damage of polyurethane and epoxy resins*. Journal of Materials Science, 2019. **54**(11): p. 8262-8275.
113. Kim, S.Y., N.R. Sottos, and S.R. White, *Self-healing of fatigue damage in cross-ply glass/epoxy laminates*. Composites Science and Technology, 2019. **175**: p. 122-127.
114. Weihermann, W.R., M.M. Meier, and S.H. Pezzin, *Microencapsulated amino-functional polydimethylsiloxane as autonomous external self-healing agent for epoxy systems*. Journal of Applied Polymer Science, 2019. **136**(23): p. 47627.
115. Ahangaran, F., et al., *Development of self-healing epoxy composites via incorporation of microencapsulated epoxy and mercaptan in poly (methyl methacrylate) shell*. Polymer Testing, 2019. **73**: p. 395-403.
116. Sun, T., et al., *A novel strategy for the synthesis of self-healing capsule and its application*. Composites Science and Technology, 2019. **171**: p. 13-20.
117. Ma, W., et al., *Preparation and assessment of a self-healing material based on microcapsules filled with ethyl phenylacetate*. Journal of Applied Polymer Science, 2016. **133**(20).

118. Hia, I.L., et al., *Electrosprayed multi-core alginate microcapsules as novel self-healing containers*. Scientific reports, 2016. **6**(1): p. 1-8.
119. Lee, J., et al., *Fracture behaviour of a self-healing microcapsule-loaded epoxy system*. Express Polymer Letters, 2011. **5**(3).
120. Ghazali, H., L. Ye, and M.-Q. Zhang. *Lap shear strength and healing capability of self-healing adhesive containing epoxy/mercaptan microcapsules*. in *AIP Conference Proceedings*. 2016. AIP Publishing LLC.
121. Raimondo, M., et al., *Healing agent for the activation of self-healing function at low temperature*. Advanced Composite Materials, 2015. **24**(6): p. 519-529.
122. Guadagno, L., et al., *Self-healing materials for structural applications*. Polymer Engineering & Science, 2014. **54**(4): p. 777-784.
123. Guadagno, L., et al., *Healing efficiency and dynamic mechanical properties of self-healing epoxy systems*. Smart Materials and Structures, 2014. **23**(4): p. 045001.
124. Caruso, M.M., et al., *Solvent-promoted self-healing epoxy materials*. Macromolecules, 2007. **40**(25): p. 8830-8832.
125. Caruso, M.M., et al., *Full recovery of fracture toughness using a nontoxic solvent-based self-healing system*. Advanced Functional Materials, 2008. **18**(13): p. 1898-1904.
126. Meng, L.M., et al., *A dual mechanism single-component self-healing strategy for polymers*. Journal of Materials Chemistry, 2010. **20**(29): p. 6030-6038.
127. Yang, G. and J.K. Lee, *Evaluation of 5-ethylidene-2-norbornene with an adhesion promoter for self-healing applications*. Journal of Polymer Science Part B: Polymer Physics, 2016. **54**(12): p. 1170-1179.
128. Ebrahimnezhad-Khaljiri, H. and R. Eslami-Farsani, *The tensile properties and interlaminar shear strength of microcapsules-glass fibers/epoxy self-healable composites*. Engineering Fracture Mechanics, 2020. **230**: p. 106937.
129. Chen, J., et al., *Thermally Crosslinked Functionalized Polydicyclopentadiene with a High T_g and Tunable Surface Energy*. ACS omega, 2016. **1**(4): p. 532-540.
130. Thakur, V.K. and M.R. Kessler, *Self-healing polymer nanocomposite materials: A review*. Polymer, 2015. **69**: p. 369-383.
131. Mauldin, T.C., et al., *Modified rheokinetic technique to enhance the understanding of microcapsule-based self-healing polymers*. ACS applied materials & interfaces, 2012. **4**(3): p. 1831-1837.
132. Lee, J.K., et al., *Thermal analysis of ring-opening metathesis polymerized healing agents*. Journal of Polymer Science Part B: Polymer Physics, 2007. **45**(14): p. 1771-1780.
133. Brown, E.N., et al., *In situ poly (urea-formaldehyde) microencapsulation of dicyclopentadiene*. Journal of microencapsulation, 2003. **20**(6): p. 719-730.
134. Agredo, P., et al., *An Evaluation of the Physicochemical Properties of Stabilized Oil-In-Water Emulsions Using Different Cationic Surfactant Blends for Potential Use in the Cosmetic Industry*. Cosmetics, 2019. **6**(1): p. 12.
135. Nguon, O., et al., *Microencapsulation by in situ polymerization of amino resins*. Polymer reviews, 2018. **58**(2): p. 326-375.
136. Katoueizadeh, E., S.M. Zebarjad, and K. Janghorban, *Investigating the effect of synthesis conditions on the formation of urea-formaldehyde microcapsules*. Journal of Materials Research and Technology, 2019. **8**(1): p. 541-552.
137. Noh, H. and J. Lee, *Microencapsulation of self-healing agents containing a fluorescent dye*. Express polymer letters, 2013. **7**(1): p. 88-94.
138. Hu, J., H.-Q. Chen, and Z. Zhang, *Mechanical properties of melamine formaldehyde microcapsules for self-healing materials*. Materials Chemistry and Physics, 2009. **118**(1): p. 63-70.

139. Cosco, S., et al., *Properties of poly (urea-formaldehyde) microcapsules containing an epoxy resin*. Journal of applied polymer science, 2007. **105**(3): p. 1400-1411.
140. Rochmadi, A.P. and W. Hasokowati, *Mechanism of microencapsulation with urea-formaldehyde polymer*. Am. J. Appl. Sci, 2010. **7**(6): p. 739-745.
141. Yang, G. and J.K. Lee, *Curing kinetics and mechanical properties of endo-dicyclopentadiene synthesized using different Grubbs' catalysts*. Industrial & Engineering Chemistry Research, 2014. **53**(8): p. 3001-3011.
142. Autenrieth, B., et al., *Stereospecific ring-opening metathesis polymerization (ROMP) of endo-dicyclopentadiene by molybdenum and tungsten catalysts*. Macromolecules, 2015. **48**(8): p. 2480-2492.
143. Choi, T.L. and R.H. Grubbs, *Controlled Living Ring-Opening-Metathesis Polymerization by a Fast-Initiating Ruthenium Catalyst*. Angewandte Chemie International Edition, 2003. **42**(15): p. 1743-1746.
144. Fu, G.C., S.T. Nguyen, and R.H. Grubbs, *Catalytic ring-closing metathesis of functionalized dienes by a ruthenium carbene complex*. Journal of the American Chemical Society, 1993. **115**(21): p. 9856-9857.
145. Grubbs, R.H., *Olefin-metathesis catalysts for the preparation of molecules and materials (Nobel lecture)*. Angewandte Chemie International Edition, 2006. **45**(23): p. 3760-3765.
146. Sanford, M.S., M. Ulman, and R.H. Grubbs, *New insights into the mechanism of ruthenium-catalyzed olefin metathesis reactions*. Journal of the American Chemical Society, 2001. **123**(4): p. 749-750.
147. Schrock, R., et al., *Ring-opening polymerization of norbornene by a living tungsten alkylidene complex*. Macromolecules, 1987. **20**(5): p. 1169-1172.
148. Ulman, M. and R.H. Grubbs, *Ruthenium carbene-based olefin metathesis initiators: catalyst decomposition and longevity*. The Journal of organic chemistry, 1999. **64**(19): p. 7202-7207.
149. Nakayama, Y., K. Katsuda, and H. Yasuda, *Ring-opening metathesis polymerization of norbornene with catecholato complexes of tungsten (VI) as effective catalyst precursors*. Polymer journal, 2003. **35**(11): p. 896-900.
150. Goetz, A.E. and A.J. Boydston, *Metal-free preparation of linear and cross-linked polydicyclopentadiene*. Journal of the American Chemical Society, 2015. **137**(24): p. 7572-7575.
151. Ivin, K.J. and J.C. Mol, *Olefin metathesis and metathesis polymerization*. 1997: Elsevier.
152. Romero, P.E., W.E. Piers, and R. McDonald, *Rapidly initiating ruthenium olefin-metathesis catalysts*. Angewandte Chemie, 2004. **116**(45): p. 6287-6291.
153. Liu, J., et al., *The ring-opening metathesis polymerization of dicyclopentadiene with titanocene complexes*. Journal of Molecular Catalysis A: Chemical, 1999. **142**(3): p. 301-304.
154. McCann, M. and A.J. Beaumont, *Catalytic properties of novel chiral polyoxomolybdate (VI) salts: The ring-opening metathesis polymerization (ROMP) of norbornene*. Journal of Molecular Catalysis A: Chemical, 1996. **108**(1): p. 23-27.
155. Balcar, H., A. Dosedlová, and L. Petrusová, *Ring-opening metathesis polymerization of dicyclopentadiene by unicomponent catalysts derived from WCl₆*. Journal of molecular catalysis, 1992. **77**(3): p. 289-295.
156. Li, H., Z. Wang, and B. He, *Ring-opening metathesis polymerization of dicyclopentadiene by tungsten catalysts supported on polystyrene*. Journal of Molecular Catalysis A: Chemical, 1999. **147**(1-2): p. 83-88.

157. Khoury, P.R., J.D. Goddard, and W. Tam, *Ring strain energies: substituted rings, norbornanes, norbornenes and norbornadienes*. Tetrahedron, 2004. **60**(37): p. 8103-8112.
158. Schrodi, Y. and R.L. Pederson, *Evolution and applications of second-generation ruthenium olefin metathesis catalysts*. Aldrichimica Acta, 2007. **40**(2): p. 45-52.
159. Alcaide, B., P. Almendros, and J.M. Alonso, *Ruthenium-catalyzed chemoselective N-allyl cleavage: novel grubbs carbene mediated deprotection of allylic amines*. Chemistry—A European Journal, 2003. **9**(23): p. 5793-5799.
160. Wright, D.L., J.P. Schulte, and M.A. Page, *An imine addition/ring-closing metathesis approach to the spirocyclic core of halichlorine and pinnaic acid*. Organic letters, 2000. **2**(13): p. 1847-1850.
161. Wilson, G.O., et al., *Evaluation of ruthenium catalysts for ring-opening metathesis polymerization-based self-healing applications*. Chemistry of Materials, 2008. **20**(10): p. 3288-3297.
162. Sriram, S.R., *Development of self-healing polymer composites and photoinduced ring-opening metathesis polymerization*. 2002: University of Illinois at Urbana-Champaign.
163. Guadagno, L., et al., *Use of Hoveyda–Grubbs' second generation catalyst in self-healing epoxy mixtures*. Composites Part B: Engineering, 2011. **42**(2): p. 296-301.
164. Keller, M. and N. Sottos. *Effect of microcapsule properties on self-healing composite performance*. in *Proceedings of the 2004 SEM X international congress on experimental and applied mechanics*. 2004.
165. Wilson, G.O., et al., *Autonomic healing of epoxy vinyl esters via ring opening metathesis polymerization*. Advanced Functional Materials, 2008. **18**(1): p. 44-52.
166. Mostovoy, S., *Use of crack-line-loaded specimens for measuring plane-strain fracture toughness*. Journal of materials, 1967. **2**(3): p. 661-681.
167. Keller, M.W. and N.R. Sottos, *Mechanical properties of microcapsules used in a self-healing polymer*. Experimental Mechanics, 2006. **46**(6): p. 725-733.
168. Caruso, M.M., et al., *Microcapsules containing suspensions of carbon nanotubes*. Journal of Materials Chemistry, 2009. **19**(34): p. 6093-6096.
169. Odom, S.A., et al., *A self-healing conductive ink*. Advanced Materials, 2012. **24**(19): p. 2578-2581.
170. Pastine, S.J., et al., *Chemicals on demand with phototriggerable microcapsules*. Journal of the American Chemical Society, 2009. **131**(38): p. 13586-13587.
171. Li, F., et al., *Self-repairing microcapsules with aqueous solutions as core materials for conductive applications*. Green Chemistry, 2021. **23**(2): p. 927-934.
172. Zedler, L., et al., *Monitoring the chemistry of self-healing by vibrational spectroscopy—current state and perspectives*. Materials Today, 2014. **17**(2): p. 57-69.
173. Smith, E. and G. Dent, *Modern Raman spectroscopy: a practical approach*. 2019: John Wiley & Sons.
174. Raman, C. and K. Krishnan, *Polarisation of scattered light-quanta*. Nature, 1928. **122**(3066): p. 169-169.
175. Gegan, E., *The use of raman spectroscopy in the characterization of single walled carbon nanotubes*. 2009.
176. Bumbrah, G.S. and R.M. Sharma, *Raman spectroscopy—Basic principle, instrumentation and selected applications for the characterization of drugs of abuse*. Egyptian Journal of Forensic Sciences, 2016. **6**(3): p. 209-215.
177. Efremov, E.V., F. Ariese, and C. Gooijer, *Achievements in resonance Raman spectroscopy: Review of a technique with a distinct analytical chemistry potential*. Analytica chimica acta, 2008. **606**(2): p. 119-134.

178. Li-Chan, E.C., *The applications of Raman spectroscopy in food science*. Trends in Food Science & Technology, 1996. **11**(7): p. 361-370.
179. Cheatham, C.M., et al., *Kinetics of trifluorovinyl ether cyclopolymerization via Raman spectroscopy*. Polymer international, 1998. **46**(4): p. 320-324.
180. Parnell, S., K. Min, and M. Cakmak, *Kinetic studies of polyurethane polymerization with Raman spectroscopy*. Polymer, 2003. **44**(18): p. 5137-5144.
181. Larin, G., et al., *Rheokinetics of ring-opening metathesis polymerization of norbornene-based monomers intended for self-healing applications*. Polymer Engineering & Science, 2006. **46**(12): p. 1804-1811.
182. Hardis, R., et al., *Cure kinetics characterization and monitoring of an epoxy resin using DSC, Raman spectroscopy, and DEA*. Composites Part A: Applied Science and Manufacturing, 2013. **49**: p. 100-108.
183. Bose, R.K., et al., *A rheological and spectroscopic study on the kinetics of self-healing in a single-component diels–alder copolymer and its underlying chemical reaction*. Journal of Polymer Science Part A: Polymer Chemistry, 2014. **52**(12): p. 1669-1675.
184. Vasiliu, S., et al., *Insights into the mechanism of polymer coating self-healing using Raman spectroscopy*. Applied spectroscopy, 2014. **68**(5): p. 541-548.
185. Sonwalkar, N., S.S. Sunder, and S. Sharma, *Ice/solid adhesion analysis using low-temperature Raman microprobe shear apparatus*. Applied spectroscopy, 1993. **47**(10): p. 1585-1593.
186. Kattel, S., et al. *Strain-Induced Raman Shifts Due to Ice Adhesion*. in *APS March Meeting Abstracts*. 2019.
187. Schaubroeck, D., et al., *Qualitative FT-Raman investigation of the ring opening metathesis polymerization of dicyclopentadiene*. Journal of Molecular Catalysis A: Chemical, 2006. **254**(1-2): p. 180-185.
188. Phadke, A., et al., *Rapid self-healing hydrogels*. Proceedings of the National Academy of Sciences, 2012. **109**(12): p. 4383-4388.
189. Fini, G., *Applications of Raman spectroscopy to pharmacy*. Journal of Raman Spectroscopy, 2004. **35**(5): p. 335-337.
190. Das, R.S. and Y. Agrawal, *Raman spectroscopy: recent advancements, techniques and applications*. Vibrational spectroscopy, 2011. **57**(2): p. 163-176.
191. Perrot, P., *A to Z of Thermodynamics*. 1998: Oxford University Press on Demand.
192. Sadhir, R.K. and R.M. Luck, *Expanding monomers*. 1992: CRC press Boca Raton.
193. Li, Q., T. Zhou, and H. Yang, *Encapsulation of hoveyda–grubbs2nd catalyst within yolk–shell structured silica for olefin metathesis*. ACS Catalysis, 2015. **5**(4): p. 2225-2231.
194. Yang, H., et al., *Encapsulation of an olefin metathesis catalyst in the nanocages of SBA-1: facile preparation, high encapsulation efficiency, and high activity*. ChemCatChem, 2013. **5**(8): p. 2278-2287.
195. Barnes, S., et al., *Raman spectroscopic studies of the cure of dicyclopentadiene (DCPD)*. Spectrochimica Acta Part A: Molecular and Biomolecular Spectroscopy, 2005. **61**(13-14): p. 2946-2952.
196. Gavin, H.P., *The Levenberg-Marquardt algorithm for nonlinear least squares curve-fitting problems*. Department of Civil and Environmental Engineering, Duke University, 2019: p. 1-19.
197. Andronescu, C., et al., *Kinetics of benzoxazine polymerization studied by Raman spectroscopy*. High Performance Polymers, 2013. **25**(6): p. 634-640.
198. Yu, P.Y. and Y. Peter, *M. cardona. Fundamentals of semiconductors*. Physics and Material Properties, 1996.

199. Xu, Z., et al., *Topic review: application of Raman spectroscopy characterization in micro/nano-machining*. *Micromachines*, 2018. **9**(7): p. 361.
200. Kessler MR, W.S., *Cure kinetics of the ring-opening metathesis polymerization of dicyclopentadiene*. *Journal of Polymer Science Part A: Polymer Chemistry*, 2002 **40**(14): p. 2373-83.
201. Li, J., et al., *Direct identification of metallic and semiconducting single-walled carbon nanotubes in scanning electron microscopy*. *Nano letters*, 2012. **12**(8): p. 4095-4101.
202. Ballantyne, B., *In vitro genetic toxicology investigations with 5-ethylidene-2-norbornene*. *Toxic Substance Mechanisms*, 1998. **17**(2): p. 133-151.
203. Bokobza, L. and J. Zhang, *Raman spectroscopic characterization of multiwall carbon nanotubes and of composites*. *Express Polymer Letters*, 2012. **6**(7).
204. Dresselhaus, M.S., et al., *Raman spectroscopy of carbon nanotubes*. *Physics reports*, 2005. **409**(2): p. 47-99.
205. Costa, S., et al., *Characterization of carbon nanotubes by Raman spectroscopy*. *Materials Science-Poland*, 2008. **26**(2): p. 433-441.
206. Dresselhaus, M.S., et al., *Perspectives on carbon nanotubes and graphene Raman spectroscopy*. *Nano letters*, 2010. **10**(3): p. 751-758.
207. Lehman, J.H., et al., *Evaluating the characteristics of multiwall carbon nanotubes*. *Carbon*, 2011. **49**(8): p. 2581-2602.
208. Zamal, H.H., et al., *Cure kinetics of poly (5-ethylidene-2-norbornene) with 2nd generation Hoveyda-Grubbs' catalyst for self-healing applications*. *Polymer*, 2018. **153**: p. 1-8.
209. Mehta, M. and J. Vadher, *A study on different failures of composite materials*. *International Journal of Advance Engineering and Research Development*, 2017. **4**(9): p. 302-307.
210. Jollivet, T., C. Peyrac, and F. Lefebvre, *Damage of composite materials*. *Procedia Engineering*, 2013. **66**: p. 746-758.
211. Mortell, D., D. Tanner, and C. McCarthy, *In-situ SEM study of transverse cracking and delamination in laminated composite materials*. *Composites Science and Technology*, 2014. **105**: p. 118-126.
212. Brown, E., *Use of the tapered double-cantilever beam geometry for fracture toughness measurements and its application to the quantification of self-healing*. *The Journal of Strain Analysis for Engineering Design*, 2011. **46**(3): p. 167-186.
213. Kirkby, E.L., et al., *Embedded shape-memory alloy wires for improved performance of self-healing polymers*. *Advanced Functional Materials*, 2008. **18**(15): p. 2253-2260.
214. Rodriguez, R., et al., *Development of self-contained microcapsules for optimised catalyst position in self-healing materials*. *Polymer*, 2020. **187**: p. 122084.
215. Bolimowski, P., D. Wass, and I. Bond, *Assessment of microcapsule—catalyst particles healing system in high performance fibre reinforced polymer composite*. *Smart Materials and Structures*, 2016. **25**(8): p. 084009.
216. Zhang, H. and J. Yang, *Development of self-healing polymers via amine–epoxy chemistry: I. Properties of healing agent carriers and the modelling of a two-part self-healing system*. *Smart materials and structures*, 2014. **23**(6): p. 065003.
217. Gergely, R.C., et al., *Restoration of impact damage in polymers via a hybrid microcapsule–microvascular self-healing system*. *Advanced Functional Materials*, 2018. **28**(2): p. 1704197.
218. Yuan, Y.C., et al., *Self-healing of low-velocity impact damage in glass fabric/epoxy composites using an epoxy–mercaptan healing agent*. *Smart materials and structures*, 2010. **20**(1): p. 015024.

219. Tan, P., et al., *Healing efficiency characterization of self-repairing polymer composites based on damage continuum mechanics*. Composite Structures, 2019. **208**: p. 367-376.
220. Khan, N.I., S. Halder, and M. Goyat, *Effect of epoxy resin and hardener containing microcapsules on healing efficiency of epoxy adhesive based metal joints*. Materials Chemistry and Physics, 2016. **171**: p. 267-275.
221. ASTM, D., *1002-10*. Standard Test Method for Apparent Shear Strength of Single-Lap-Joint Adhesively Bonded Metal Specimens by Tension Loading (Metal-To-Metal), ASTM International, 2010.
222. Briscoe, B. and S. Sinha, *Hardness and normal indentation of polymers*, in *Mechanical Properties and Testing of Polymers*. 1999, Springer. p. 113-122.
223. ASTM, I., *Standard test methods for flexural properties of unreinforced and reinforced plastics and electrical insulating materials*. ASTM D790-17, 2017.
224. Verbeek, C., *The influence of interfacial adhesion, particle size and size distribution on the predicted mechanical properties of particulate thermoplastic composites*. Materials Letters, 2003. **57**(13-14): p. 1919-1924.
225. Fu, S.-Y., et al., *Effects of particle size, particle/matrix interface adhesion and particle loading on mechanical properties of particulate-polymer composites*. Composites Part B: Engineering, 2008. **39**(6): p. 933-961.
226. Cho, J., M. Joshi, and C. Sun, *Effect of inclusion size on mechanical properties of polymeric composites with micro and nano particles*. Composites Science and Technology, 2006. **66**(13): p. 1941-1952.
227. Nourbakhsh, A., et al., *Effects of particle size and coupling agent concentration on mechanical properties of particulate-filled polymer composites*. Journal of Thermoplastic Composite Materials, 2010. **23**(2): p. 169-174.
228. Kim, B.C. and S.W. Park, *Fracture toughness of the nano-particle reinforced epoxy composite*. Composite structures, 2008. **86**(1-3): p. 69-77.
229. Johnsen, B., et al., *Toughening mechanisms of nanoparticle-modified epoxy polymers*. Polymer, 2007. **48**(2): p. 530-541.
230. Quan, D. and A. Ivankovic, *Effect of core-shell rubber (CSR) nano-particles on mechanical properties and fracture toughness of an epoxy polymer*. Polymer, 2015. **66**: p. 16-28.
231. Ciprari, D., K. Jacob, and R. Tannenbaum, *Characterization of polymer nanocomposite interphase and its impact on mechanical properties*. Macromolecules, 2006. **39**(19): p. 6565-6573.
232. Laurenzi, S., et al., *Fracture mechanisms in epoxy composites reinforced with carbon nanotubes*. Procedia Engineering, 2014. **88**: p. 157-164.
233. Tsai, H.-J., et al., *A competitive binding between O₂ and epoxy with carbon nanotubes*. AIP Advances, 2017. **7**(9): p. 095217.
234. Khan, W., R. Sharma, and P. Saini, *Carbon nanotube-based polymer composites: synthesis, properties and applications*. Carbon Nanotubes-Current Progress of their Polymer Composites, 2016.
235. Zabihi, O., M. Ahmadi, and M. Naebe, *One-pot synthesis of aminated multi-walled carbon nanotube using thiol-ene click chemistry for improvement of epoxy nanocomposites properties*. RSC advances, 2015. **5**(119): p. 98692-98699.
236. Liao, K. and S. Li, *Interfacial characteristics of a carbon nanotube-polystyrene composite system*. Applied physics letters, 2001. **79**(25): p. 4225-4227.
237. Moniruzzaman, M. and K.I. Winey, *Polymer nanocomposites containing carbon nanotubes*. Macromolecules, 2006. **39**(16): p. 5194-5205.

238. Jin, S., *Monitoring the interface of carbon fibre and epoxy microcomposites using Raman spectroscopy with single walled carbon nanotubes as strain sensors*. 2014, University of Manchester.
239. Khoramishad, H. and M. Khakzad, *Toughening epoxy adhesives with multi-walled carbon nanotubes*. *The Journal of Adhesion*, 2018. **94**(1): p. 15-29.
240. Zotti, A., et al., *Fracture toughening mechanisms in epoxy adhesives*. *Adhesives-Applications and Properties*, 2016. **1**: p. 257.
241. Laskin, J., A. Laskin, and S.A. Nizkorodov, *New mass spectrometry techniques for studying physical chemistry of atmospheric heterogeneous processes*. *International Reviews in Physical Chemistry*, 2013. **32**(1): p. 128-170.

ANNEX

Microencapsulation Process in Pictures and Flowcharts:

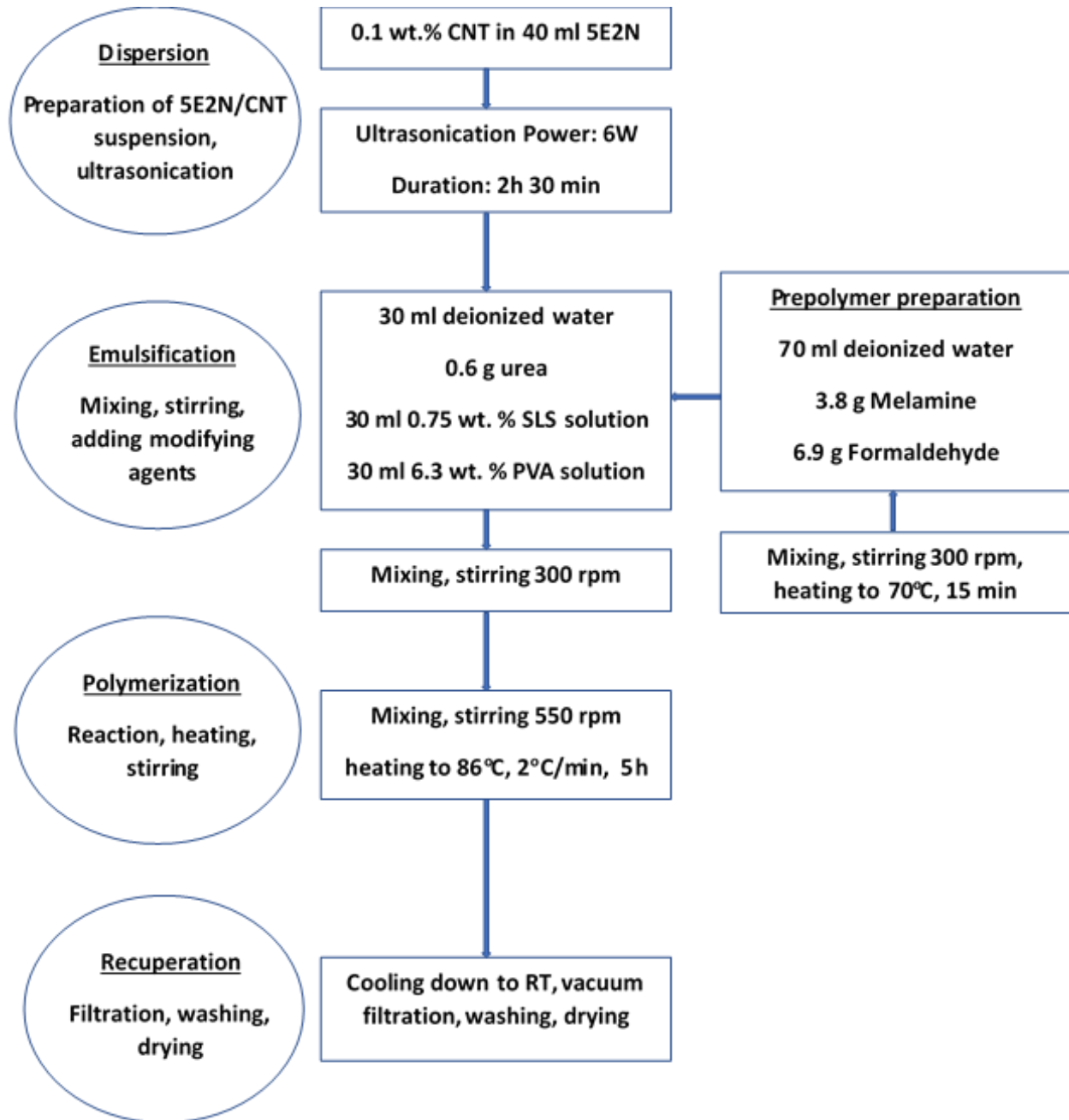
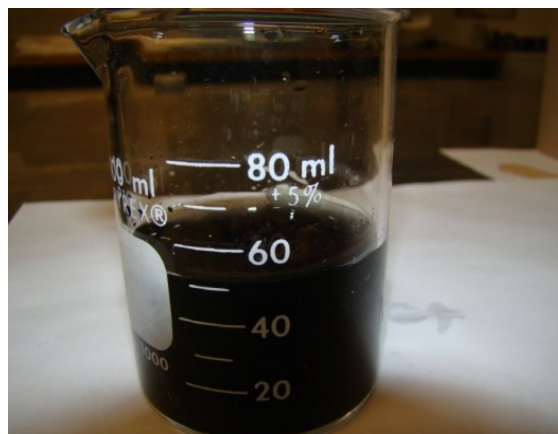


Figure A 1. Process flow chart for successful microencapsulation of 5E2N/CNT in PMUF shells [20]



CNT (0.1 wt.%) in 5E2N before ultrasonication



5E2N/CNT suspension after ultrasonication

Figure A 2. Dispersion of CNT in 5E2N using ultrasonication

a)



b)



Figure A 3. a) Emulsification b) *In-situ* polymerization reaction



Figure A 4. Recuperation step: Vacuum filtration

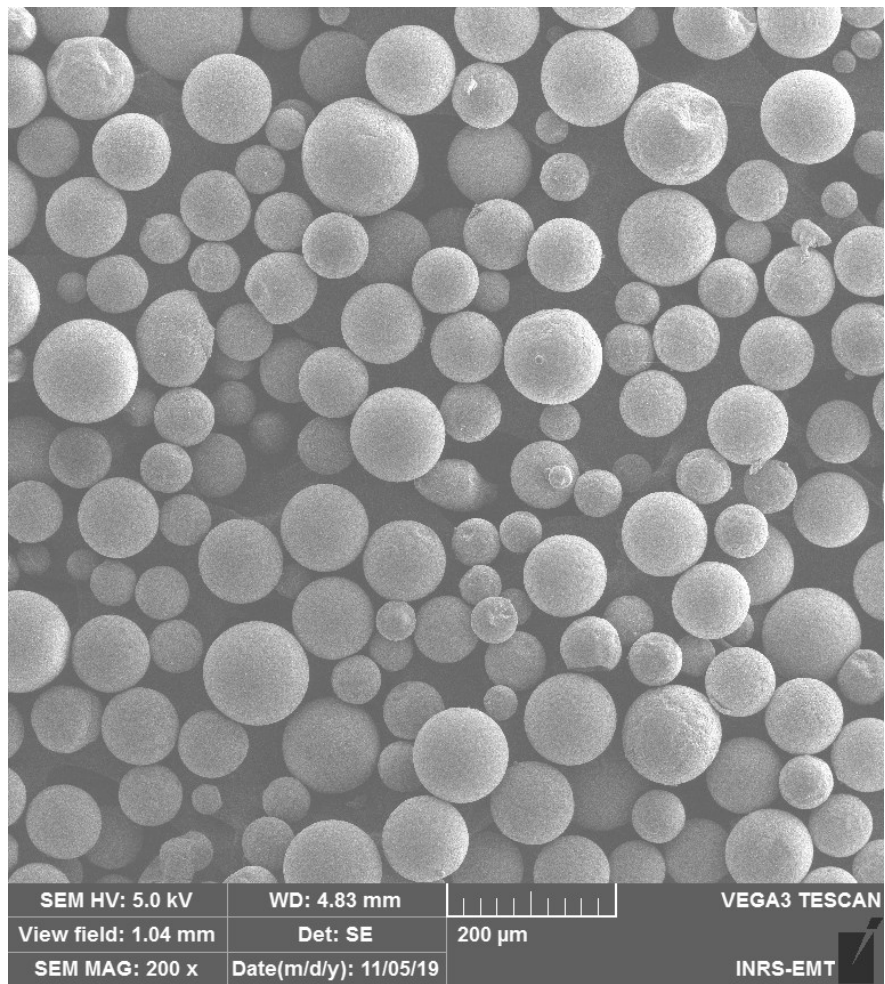


Figure A 5. Microcapsules under SEM

Preparation of molds for self-healing samples in pictures:



a) Mold making Silicone rubber and catalyst



b) Preparation of tools for the desired size of samples. Mold rubber and catalyst in 10:1 ratio are mixed and poured upon these tools, cured at RT for 48 h



c) After curing and demolding the tool, the mold is ready to use.



d) Mold for TDCB samples

Figure A 6. Preparation of molds for different samples

SOMMAIRE RÉCAPITULATIF

INVESTIGATION SUR NANOTUBE DE CARBONE/ETHYLIDENE-5-NORBORNENE-2 COMME AGENT DE GUÉRISON MICRO-ENCAPSULÉ POUR L'ÉPOXY D'AUTO-RÉPARANTS POUR LES APPLICATIONS AÉROSPATIALES

L'introduction :

Les polymères, en particulier les matériaux à base d'époxyde et leurs composites, sont utilisés dans des structures et des dispositifs clés et remplissent de nombreuses fonctions utiles dans les applications civiles et militaires modernes, allant des infrastructures civiles aux applications aérospatiales, automobiles et électroniques. En tant que tels, de nombreuses pièces, structures et dispositifs clés des avions et des engins spatiaux modernes sont constitués de polymères à base d'époxy et de leurs composites [1, 2]. Les époxyes servent de matériaux de matrice pour les composites stratifiés ou d'adhésifs haute performance dans divers joints collés [1, 3, 4]. Des exemples de leurs applications incluent les satellites géostationnaires, les modules spatiaux et les engins spatiaux, le fuselage et les ailes de modèles d'avions de passagers modernes comme le Boeing 787, l'airbus 380, etc. [5]. De plus, l'environnement dans lequel ils fonctionnent peut les soumettre à des températures très basses (jusqu'à -150°C) comme dans l'espace ou dans les régions les plus froides de la terre. Au cours de leurs opérations, les pièces des avions et des engins spatiaux constituées de ces matériaux sont également soumises à des dommages pouvant être causés par diverses charges mécaniques, des collisions avec des débris spatiaux ou tout objet étranger (comme des impacts d'oiseaux) ou d'autres facteurs environnementaux comme le cyclage thermique. L'une des principales préoccupations concernant les pièces en époxy et leurs composites est que même un dommage mineur ou des microfissures dans les sites internes de ces matériaux peuvent sérieusement compromettre [6] leur intégrité structurelle, leurs fonctionnalités et leurs performances prévues. Les microfissures dans les époxyes peuvent se propager pendant l'opération et cela peut finalement conduire à une défaillance des pièces si ces fissures mineures ne sont pas réparées à temps.

Les emplacements éloignés des pièces, comme dans l'espace ou à haute altitude (pour les avions) les rendent également extrêmement difficiles pour la réparation manuelle sur site des dommages. L'une des solutions intelligentes peut être d'auto-réparer ces dommages mineurs sans nécessiter aucune intervention manuelle.

La capacité d'auto-guérison des époxydes utilisés dans les structures et dispositifs spatiaux et aérospatiaux modernes peut atténuer les difficultés, les complexités et les coûts plus élevés associés à la réparation à distance de différents types de dommages. La fonctionnalité d'auto-guérison des époxydes dans leur environnement d'exploitation peut également garantir la sécurité et la fiabilité des équipements de pointe et prolonger ainsi leur durée de vie.

Le concept de polymères auto-cicatrisants comprend des réactifs cicatrisants stockés dans des micro-récipients de stockage (microcapsules) qui sont noyés dans les matériaux polymères. Cette classe de matériaux a été largement étudiée après les travaux pionniers de White et Sottos [9], qui ont montré la récupération efficace des propriétés mécaniques de l'époxyde structural en utilisant des monomères dicyclopentadiène liquide microencapsulés (DCPD) capables de subir une polymérisation par métathèse par ouverture de cycle (ROMP) réaction initiée par le catalyseur Ruthénium Grubbs' [10]. La figure 1 montre le parcours conceptuel du processus d'auto-guérison initialement introduit par White *et al.*[9], utilisant la suspension de CNT/5E2N comme agent cicatrisant microencapsulé.

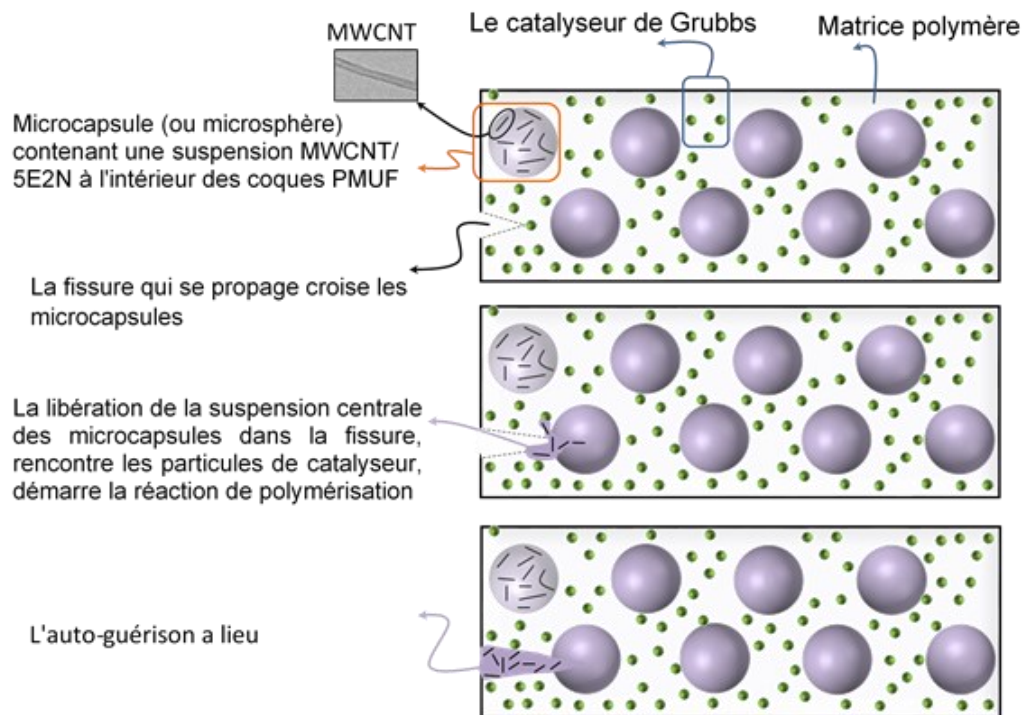


Figure 1. Approche d'auto-guérison basée sur des microcapsules CNT/5E2N

Selon le concept d'auto-guérison, les microcapsules contenant le monomère de l'agent cicatrisant ainsi que le catalyseur de Grubbs sont dispersées à l'intérieur de la matrice polymère.

Lorsque des fissures se forment à l'intérieur de la matrice polymère en raison d'événements de vieillissement ou d'endommagement, elles se propagent vers les microcapsules, de sorte que les parois de l'enveloppe de ces microcapsules se brisent. Cela libère le monomère de l'agent cicatrisant dans la fissure. Une fois que la suspension de CNT/5E2N entre en contact avec le catalyseur de Grubbs dispersé, cette dernière déclenche localement la réaction ROMP. Le nanocomposite CNT/poly-5E2N se forme au niveau du site de fissure, ce qui restaure partiellement la fonctionnalité nominale du matériau.

Plusieurs premiers travaux [9, 12-14] ont démontré la récupération de la ténacité à la rupture d'échantillons d'époxy incorporés avec le catalyseur de Grubbs de première génération (G1) et des microcapsules contenant du DCPD. Jusqu'à 85% d'efficacité de cicatrisation mécanique a été démontrée pour les échantillons incorporés avec 5 à 20% en poids de microcapsules avec 2,5 à 5% en poids de G1 avec un temps de cicatrisation de 48 h à température ambiante (température ambiante). Cependant, pour les applications pratiques, il y a peu d'obstacles avec le système d'agents de guérison DCPD/Grubbs qui doivent être surmontés.

Premièrement, une longue période de guérison, telle que 48h dans les travaux ci-dessus, n'est pas souhaitable. En effet, entre-temps, les dommages peuvent se propager davantage avec le fonctionnement continu de la pièce. Le monomère DCPD libéré des microcapsules brisées, pendant la longue période de cicatrisation, peut également s'évaporer ou se diffuser dans la matrice, réduisant ainsi son efficacité d'auto-guérison.

Deuxièmement, l'exigence d'une grande quantité de catalyseur, jusqu'à 5% en poids dans les travaux ci-dessus, pour une guérison efficace n'est pas non plus souhaitable. De plus, le ruthénium est rare dans la nature et en tant que tel, les catalyseurs au ruthénium sont coûteux. Ainsi, il est essentiel de développer des agents cicatrisants capables de réagir beaucoup plus rapidement avec de faibles besoins en catalyseur [15, 16].

Enfin, le point de congélation du DCPD est d'environ 15°C [17] ce qui limite fortement son utilisation aux basses températures où circulent souvent les véhicules aérospatiaux [18].

De telles contraintes de DCPD incitent à rechercher des monomères d'agents cicatrisants alternatifs qui peuvent être microencapsulés de manière appropriée pour diverses applications d'auto-guérison. Le 5 éthylidène-2-nobornone (5E2N) est l'un d'entre eux qui a un point de congélation autour de -80°C [19]. Il subit une réaction ROMP beaucoup plus rapide avec le catalyseur de Grubbs (de l'ordre de quelques secondes à température ambiante) avec beaucoup moins de charge de catalyseur (jusqu'à 0,1% en poids) par rapport au DCPD [17], ce qui en fait

une alternative curative intéressante agent candidat particulièrement adapté aux applications aérospatiales à basse température.

Le monomère 5E2N seul est microencapsulé dans des coques en poly mélamine urée formaldéhyde (PMUF) en utilisant une technique de polymérisation *in-situ* [17, 20]. Cependant, contrairement au DCPD, le 5E2N produit un polymère mécaniquement plus faible lors de la réaction ROMP, ce qui limite sa capacité à récupérer de manière significative les propriétés mécaniques des époxydes auto-cicatrisants. L'incorporation de nanotubes de carbone (CNT) dans 5E2N a été suggérée pour pallier cet inconvénient [19]. À cette fin, dans ce travail, nous visons à microencapsuler des CNT dispersés dans 5E2N et à étudier la suspension microencapsulée de CNT/5E2N en tant qu'agent cicatrisant pour l'époxy avec des propriétés électromécaniques auto-cicatrisantes pour les applications aérospatiales.

En plus de rendre les polymères plus résistants mécaniquement [30-37], l'intégration de CNT [28, 32, 34, 38-40], dans les polymères peut également être utilisée pour améliorer la conductivité électrique des structures polymères, éviter les étincelles dans les boîtiers de filtre à carburant [40, 41], agir comme des capteurs pour surveiller les dommages [41, 42], améliorer la durée de vie effective des batteries haute performance [43] ou développent des dispositifs électroniques innovants, tels que des circuits imprimés sur des feuilles souples [44]. En tant que tel, une microencapsulation réussie de CNT/5E2N, au lieu du monomère 5E2N seul, peut non seulement surmonter les limitations de la formation d'un polymère plus faible après la réaction ROMP d'auto-guérison, elle peut également conférer les propriétés électriques d'auto-guérison prévues au polymère conducteur/ époxy en rétablissant son réseau électrique après endommagement. La microencapsulation réussie de NTC dispersés dans un monomère auto-cicatrisant, tel que le 5E2N, peut ainsi ouvrir de multiples opportunités pour des applications d'auto-guérison en environnement aérospatial. En soi, le but ultime de ce travail est d'étudier le CNT/5E2N en tant qu'agent cicatrisant microencapsulé pour l'époxyde auto-cicatrisant pour les applications aérospatiales.

Les objectifs :

Les principaux objectifs de ce travail sont

- i) Étude de la cinétique de polymérisation (ou de durcissement) du 5E2N initiée par un catalyseur de ruthénium Grubbs sélectionné à basse température
- ii) Développer des procédures pour permettre la microencapsulation d'une suspension de CNT/5E2N et la caractérisation de la qualité des microcapsules produites

iii) Tester l'efficacité d'auto-guérison mécanique du CNT/5E2N microencapsulé dans différentes conditions de contrainte lorsqu'il est incorporé dans de l'époxy

iv) Test de l'efficacité d'auto-guérison électrique du CNT/5E2N microencapsulé

v) Enquêter sur les effets des NTC présents dans le monomère microencapsulé sur l'efficacité d'auto-guérison

La méthodologie :

L'étude du CNT/5E2N en tant qu'agent cicatrisant microencapsulé pour l'époxyde auto-cicatrisant pour les applications aérospatiales nécessite une compréhension et une mise en œuvre approfondies de certains aspects clés qui influencent fortement le comportement d'auto-cicatrisation et son efficacité. La méthodologie suivie pour atteindre les principaux objectifs de ce travail est discutée comme suit :

i) Comprendre les caractéristiques thermochimiques et le comportement du 5E2N, en particulier la réaction ROMP et la cinétique de sa polymérisation initiée par un catalyseur de Grubbs approprié à basse température.

5E2N, en tant que monomère d'agent cicatrisant, est le principal liquide qui s'écoule vers les fissures, telles qu'elles apparaissent dans les matériaux, qui est ensuite polymérisé par des catalyseurs appropriés pour remplir, fermer et réparer la fissure. Comprendre la caractéristique thermochimique du monomère et son mécanisme de réaction ROMP est donc essentiel pour leurs applications en tant que monomère d'agent cicatrisant. Les principes fondamentaux de ces caractéristiques importantes sont d'abord étudiés de manière approfondie à travers des revues de la littérature. Pour les rendre adaptés aux applications à basses températures telles que dans l'environnement spatial, la compréhension de la cinétique de polymérisation du 5E2N à des températures inférieures à zéro représente une étape clé.

À cette fin, les expériences et la méthodologie sont spécifiquement conçues pour permettre un suivi efficace de la réaction ROMP du 5E2N initiée par le système de catalyseur Hoveyda-Grubbs de 2^e génération (HG2) en dessous de 0°C. Une analyse quantitative détaillée de la cinétique de la réaction ROMP du 5E2N/ Le système HG2 a été conduit de la température ambiante jusqu'à -30°C en utilisant une mesure spectroscopique systématique micro-Raman. L'analyse est basée sur la mesure des changements de l'intensité du pic et de l'aire intégrée des phonons Raman liés aux groupes fonctionnels caractéristiques (C=C) indiquant la progression de la réaction avec le temps. En utilisant cette méthode, les paramètres cinétiques des énergies de réaction et

d'activation sont également déterminés sur la base de l'équation d'Arrhenius typique montrant la dépendance à la température des vitesses de réaction.

ii) Preuve de concept

L'idée clé de microencapsuler le CNT/5E2N au lieu du 5E2N seul en tant qu'agent d'auto-guérison était dérivée de l'espoir que la suspension de CNT/5E2N, lorsqu'elle serait polymérisée par réaction ROMP, produirait un polymère avec des propriétés mécaniques améliorées.

Pour vérifier cela, des échantillons de poly (CNT/5E2N) ont été produits par la réaction ROMP de la suspension de monomères CNT/5E2N avec une concentration variable de CNT. Des échantillons de poly-5E2N ont également été produits, à titre de référence, par la réaction ROMP du monomère 5E2N seul. Des tests de microdureté et des tests de flexion trois points ont ensuite été effectués sur les échantillons et les propriétés mécaniques résultantes ont été comparées.

iii) Microencapsulation de suspension de CNT/5E2N

L'une des parties les plus difficiles de ce travail consiste à déterminer et à établir les paramètres de processus appropriés pour permettre une microencapsulation réussie de CNT/5E2N. Pour résoudre ce problème, la méthode de microencapsulation des monomères d'agents cicatrisants similaires tels que la microencapsulation de DCPD [13] et 5E2N [20] est parfaitement comprise grâce à des revues de la littérature. La méthode standard de microencapsulation est ensuite adaptée pour la microencapsulation de notre monomère de base prévu (CNT/5E2N) selon ses exigences sur une base d'essais et d'erreurs.

iv) Caractérisation de la qualité des microcapsules

Les caractéristiques de qualité des microcapsules peuvent affecter de manière significative leurs performances d'auto-guérison prévues. Les principales caractéristiques de qualité des microcapsules produites qui peuvent affecter leurs performances d'auto-guérison sont étudiées à l'aide de diverses méthodes de caractérisation, notamment la microscopie optique et électronique à balayage (MEB), la microscopie électronique à transmission (MET), l'analyse thermogravimétrique (TGA) et l'analyse spectrale Raman.

v) Évaluation de l'efficacité de cicatrisation des CNT/5E2N microencapsulés intégrés dans les échantillons époxy soumis à différents champs de contraintes

L'efficacité d'auto-cicatrisation mécanique du monomère CNT/5E2N microencapsulé est évaluée en effectuant plusieurs tests mécaniques sur les échantillons d'époxyde incorporés avec les agents cicatrisants. Les protocoles de test largement acceptés utilisés dans la littérature sur

l'auto-guérison pour évaluer l'efficacité de l'auto-guérison sont également suivis dans ce travail. Dans notre travail, les efficacités d'auto-guérison sont évaluées pour les échantillons exposés à deux situations de contraintes différentes, l'une sous un champ de contrainte de rupture de mode I et l'autre sous un champ de contrainte de cisaillement adhésif. En outre, l'efficacité d'auto-guérison électrique du CNT/5E2N microencapsulé incorporé dans les échantillons a été évaluée en utilisant les mêmes principes que les protocoles de test d'auto-guérison.

vi) Enquêter sur les effets des CNT

Pour extraire l'effet des NTC sur les efficacités d'auto-guérison, des échantillons d'auto-cicatrisation sont fabriqués avec les microcapsules contenant 5E2N seul ainsi qu'avec les microcapsules contenant CNT/5E2N. Les efficacités d'auto-guérison des monomères microencapsulés, telles que déterminées par les tests électromécaniques effectués sur les échantillons incorporés séparément avec les deux types de microcapsules, sont ensuite comparées pour extraire l'effet des CNT. Une analyse fractographique et une analyse Raman des surfaces de fracture des échantillons ont également été effectuées pour étayer l'analyse des résultats des tests.

Les résultats et les discussions

Chapitre 3 : Etude de la cinétique de polymérisation du 5E2N initiée par le catalyseur HG2 à basse température en utilisant l'analyse spectrale micro-Raman

Le chapitre 3 rapporte l'étude actuelle de la cinétique de durcissement du poly-5E2N initiée par le catalyseur HG2 à basse température en utilisant une analyse spectrale micro-Raman. Il décrit les procédures détaillées et discute de la méthode développée dans ce travail pour l'enquête.

Pour étudier le comportement de la cinétique de durcissement, les réactions ROMP du 5E2N initiées par le catalyseur HG2 ont été réalisées à différentes basses températures (à 21°C (RT), 1°C, -5°C, -10°C, -20°C et -30°C) dans un spectromètre Raman. Les spectres Raman ont été enregistrés au cours de la progression de la réaction à divers intervalles de temps en fonction de la température de l'expérience [par exemple, 15 s (à TA) et 60 s (à -30°C)].

À partir de la réponse spectrale Raman de la réaction ROMP de 5E2N, comme le montre la figure 2, des bandes Raman caractéristiques liées au processus de polymérisation ont été identifiées par rapport au monomère 5E2N n'ayant pas réagi.

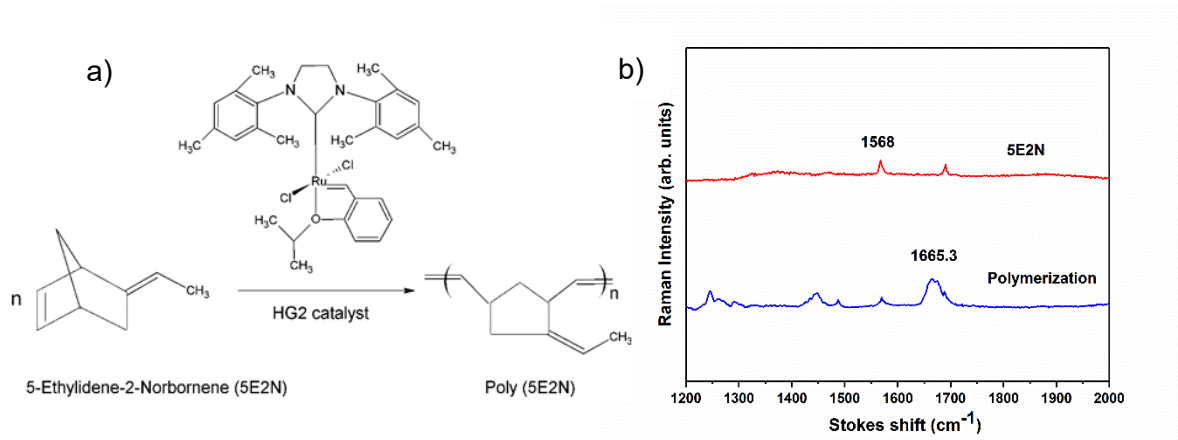


Figure 2. a) schématisation du poly 5E2N formé par la réaction ROMP du 5E2N en présence de catalyseur HG2. b) Spectres Raman produits pour monomère 5E2N n'ayant pas réagi et le polymère formé

A partir des spectres de polymérisation, les bandes Raman centrées à 1665,3 cm⁻¹ et 1568 cm⁻¹ ont été identifiées comme étant les principaux modes de phonons caractérisant la réaction ROMP.

Pour détailler la méthode d'étude du comportement cinétique de durcissement du ROMP de 5E2N, les changements temporels des spectres Raman au cours des trente (30) premières minutes de la réaction ROMP à une température de -30°C sont rapportés sur la figure 3.

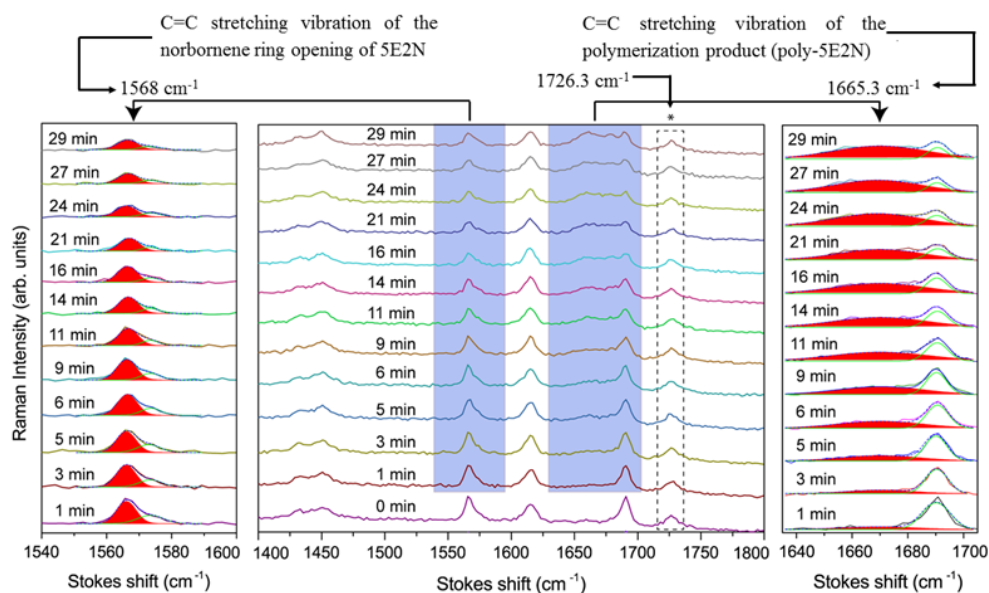


Figure 3. Observation spectroscopique Raman de l'évolution de la réaction de polymérisation du 5E2N activé par le catalyseur HG2 à -30°C

La figure 3 montre que l'intensité du pic Raman lié à la formation de poly-5E2N à 1665,3 cm⁻¹ augmente avec le temps, tandis que le mode de vibration associé à la consommation de réactif monomère 5E2N situé à 1568,0 cm⁻¹ diminue. Ces deux caractéristiques caractérisent la progression de la réaction ROMP, en accord avec des travaux antérieurs [187, 195]. L'évolution de ces pics caractéristiques à différentes températures de réaction a été suivie pour mesurer les paramètres cinétiques de la réaction ROMP.

Les hauteurs spectrales et les zones intégrées des signaux Raman à 1665,3 cm⁻¹ et 1568,0 cm⁻¹ sont affichées sur la figure 3 après déconvolution spectrale dans les gammes 1540-1600 cm⁻¹ et 1640-1700 cm⁻¹, respectivement. Pour effectuer ces analyses quantitatives, un processus d'ajustement systématique de Levenberg-Marquardt a été effectué sur chaque spectre enregistré, en utilisant deux fonctions gaussiennes.

Le temps de saturation de la réaction de polymérisation est estimé en calculant la différence de durée entre t₁, auquel le pic de la bande Raman sélectionnée apparaît pour la première fois (c'est-à-dire t₁ = 0) et t₂, auquel le pic atteint son intensité maximale. Après le temps t₂, l'intensité du pic ne change pas de manière significative. Le temps de saturation pour la réaction de polymérisation à -30°C est calculé comme étant t₂ - t₁ = 29 min.

Une méthodologie similaire a été mise en œuvre pour la réaction de polymérisation du 5E2N initiée par le catalyseur HG2 à 21°C, 1°C, -5°C, -10°C et -20°C. Le tableau 1 montre les temps de saturation des réactions ROMP réalisées à différentes températures.

Tableau 1 Temps de saturation de la réaction à différentes températures

Température (°C)	Temps de saturation
21	Less than 15 sec
1	50 sec
-5	2.5 min
-10	4 min
-20	8 min
-30	29 min

La dépendance à la température de la vitesse de réaction est généralement décrite par une équation d'Arrhenius [197] :

$$K_{app} = A. \exp\left(-\frac{E}{kT}\right), \text{-----[Eq. 1]}$$

Où K_{app} est la constante de vitesse apparente, k est la constante de Boltzmann, E est l'énergie d'activation, A est le facteur pré-exponentiel et T est la température donnée en Kelvin.

En l'absence de tout changement dans l'interaction laser-matière et le couplage optique, l'intensité des pics de phonons augmente linéairement avec la concentration des liaisons chimiques auxquelles ils sont associés.¹⁹⁵ Nous avons utilisé les changements d'intensités de la bande Raman situés à $1665,3 \text{ cm}^{-1}$ avec le temps, indiquant la formation de poly-5E2N, pour le calcul des paramètres cinétiques de la réaction ROMP.

Dénotant l'intensité de pic normalisée au temps (t) par A_t et qu'après la saturation de la réaction par A_s , l'expression de la vitesse intégrée pour la cinétique du premier ordre peut être écrite comme [183] :

$$\ln(1 - x)^{-1} = K_{app} t, \text{ -----[Eq. 2]}$$

Où $x = 1 - \frac{A_t}{A_s}$, et t indique le temps.

Pour chaque température, les changements calculés des intensités normalisées du pic Raman sélectionné à $1665,3 \text{ cm}^{-1}$ sont tracés au fil du temps sur la figure 4 (a)

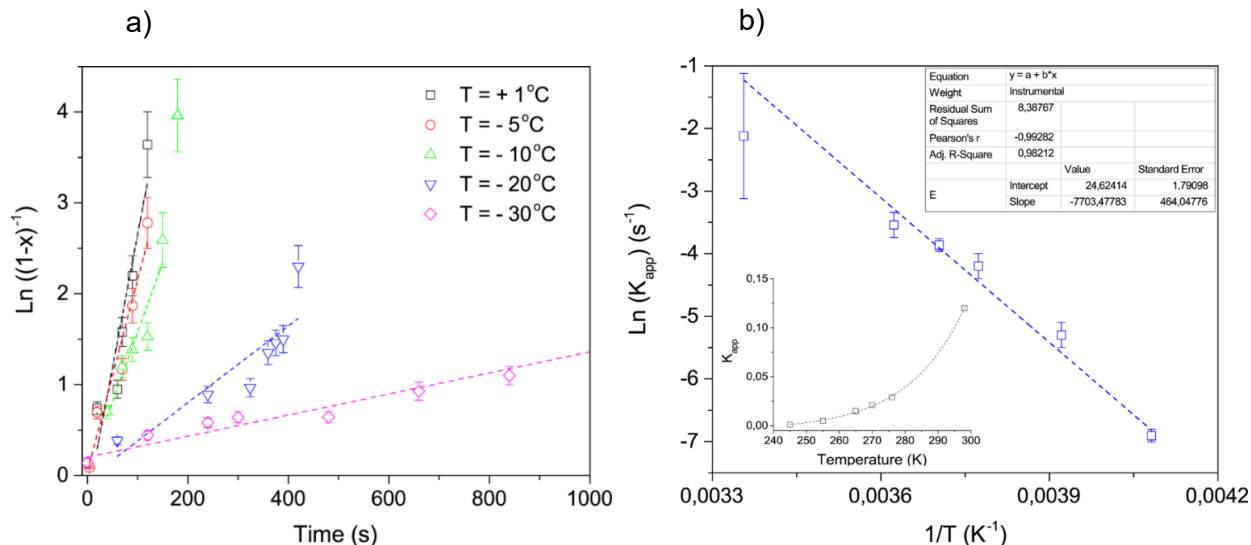


Figure 4. a) Changements dans les intensités de pic normalisées avec le temps pour chaque température de réaction, b) Graphique d'Arrhenius corrélant les constantes de vitesse apparentes avec les températures de réaction absolues pour la réaction ROMP de 5E2N/HG2

Pour obtenir les constantes de vitesse apparentes, ces données sont ajustées à l'aide d'une régression linéaire, représentée par des lignes pointillées directement reportées sur la figure.

Selon l'éq. (2), les pentes de ces droites donnent la constante de vitesse apparente (K_{app}) pour chaque température de polymérisation.

Sur la figure 4(b) les constantes de vitesse sont tracées en fonction des températures de réaction (en Kelvin) selon une fonction de type Arrhenius : $\ln(K_{app})$ en fonction de T^{-1} . D'après la pente du graphique d'Arrhenius, égale à $7,7 \text{ s}^{-1}$ sur la figure 4(b), l'énergie d'activation de la réaction ROMP est déterminée à $64 (\pm 3) \text{ kJ mol}^{-1}$ ($0,663 \text{ eV}$).

Les valeurs des constantes de vitesse et de l'énergie d'activation calculées par cette méthode sont cohérentes avec les valeurs trouvées dans la littérature pour des réactions similaires [161, 200]. La faible erreur quadratique moyenne et la fiabilité des mesures obtenues à basse température témoignent de la validité de la méthodologie développée pour la caractérisation cinétique quantitative de la réaction de polymérisation.

Nos résultats confirment également que la réaction ROMP du 5E2N est déclenchée avec l'ajout d'une très faible concentration du catalyseur HG2, et seulement en quelques minutes pour des températures aussi basses que -30°C . Cette condition est représentative de la température limite à l'intérieur des satellites et autres instruments lancés dans l'espace. La faible énergie d'activation associée à la réaction ROMP implique que les agents cicatrisants 5E2N/HG2 peuvent être activés efficacement et, ainsi, devenir adaptés aux applications d'auto-guérison dans les environnements froids. Néanmoins, une telle caractéristique doit être confirmée bien en dessous de -30°C , car la température à la surface extérieure des satellites géostationnaires dans l'ombre peut descendre jusqu'à -150°C . Néanmoins, la méthodologie développée et mise en œuvre dans ce travail peut être utilisée comme prélude à la conception et à l'optimisation de la fonction d'auto-guérison pour des applications avancées.

Chapitre 4 : Microencapsulation des suspensions de CNT/5E2N, leur caractérisation et récupération de la conductivité électrique

Dans ce chapitre, nous rapportons la microencapsulation réussie de nanotubes de carbone à parois multiples suspendus dans un monomère auto-cicatrisant 5E2N, dans des coquilles de poly mélamine urée formaldéhyde par polymérisation *in-situ*. Les paramètres clés du processus qui ont conduit à la microencapsulation réussie du 5E2N/CNT sont révélés. Il aborde ensuite les différentes caractéristiques importantes des microcapsules et leur contenu central analysé par DSC, TGA, microscopie électronique à transmission (TEM), microscopie électronique à balayage (SEM) et spectroscopie Raman. Enfin, l'efficacité d'auto-guérison électrique des microcapsules est évaluée, et la conception des expériences et le résultat de l'évaluation sont présentés.

Des microcapsules contenant des NTC à parois multiples en suspension dans 5E2N ont été synthétisées avec succès par polymérisation *in-situ* en adaptant le processus dans la réf. [20] sur la base d'essais et d'erreurs. Des étapes contrôlées de dispersion-émulsification-polymérisation-récupération ont été réalisées pour permettre la microencapsulation de la suspension de CNT/5E2N dans des coquilles de PMUF. L'organigramme du processus pour la microencapsulation réussie de 5E2N/CNT dans des coques PMUF est présenté dans la figure 5.

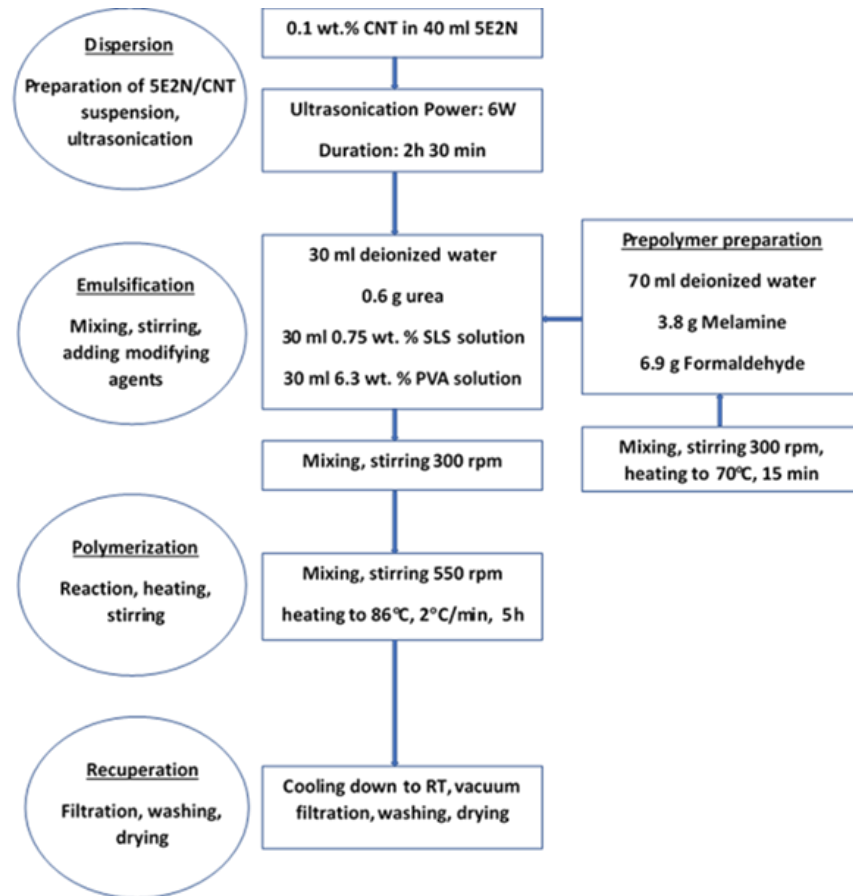


Figure 5. Organigramme du processus pour une microencapsulation réussie de 5E2N/CNT dans des coques PMUF. Le processus est adapté de la réf. [20]

Après avoir récupéré les microcapsules du processus, elles ont été observées au MEB pour leur architecture, leur taille, leurs formes, etc. La figure 6 (a-d) montre des micrographies SEM représentatives obtenues à différents grossissements : x50, x30000, x2300 et x100000, respectivement. Des microcapsules sphériques séparées individuellement sont illustrées à la figure 6 (a), avec une structure cœur-enveloppe illustrée à la figure 6 (b) et à la figure 6 (c). L'épaisseur moyenne de la coque est d'environ 550 nm. Cette épaisseur de coque des

microcapsules est suffisamment robuste pour survivre à la manipulation et à la fabrication de polymères auto-cicatrisants [133].

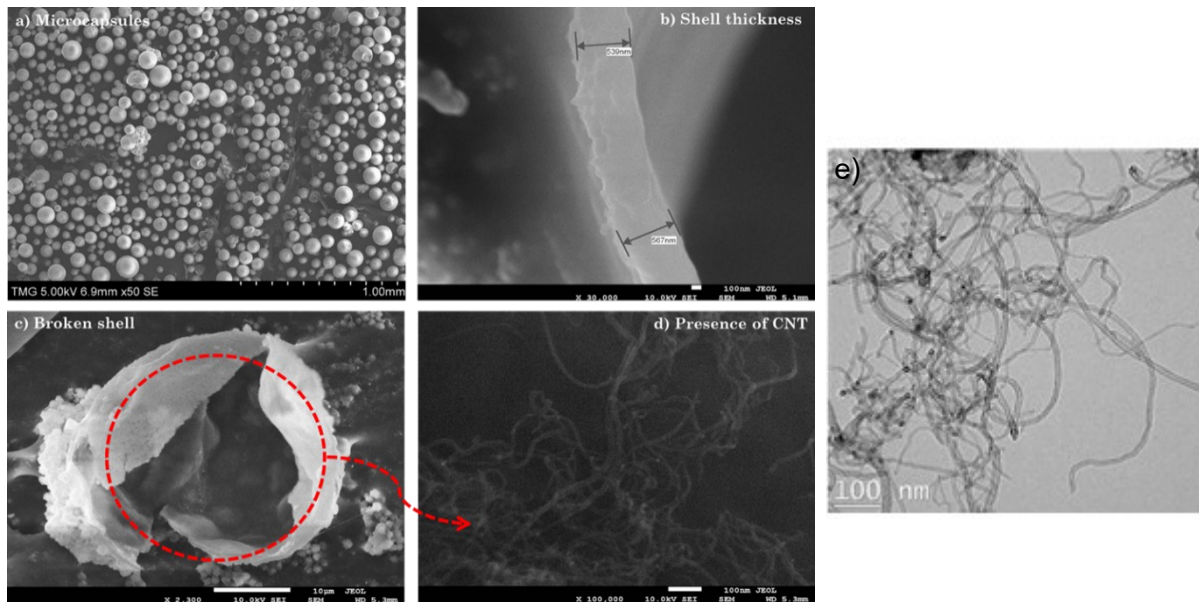


Figure 6. Observations SEM de (a) des microcapsules sphériques séparées individuellement (b) de l'épaisseur de la coque (c) de la structure noyau-coque (d) des NTC à l'intérieur du noyau des microcapsules. e) TEM observation of CNTs in the core liquid of the microcapsules

Les micrographies TEM de la figure 6 (e) montrent la présence de CNT dans le noyau liquide extrait des microcapsules broyées. Ces images confirment en outre que les étapes de traitement de la synthèse des microcapsules n'ont pas causé de rupture grave aux NTC et ont maintenu leurs rapports d'aspect élevés d'origine. De telles caractéristiques sont importantes pour maximiser les avantages de l'incorporation de CNT/5E2N dans le noyau des microcapsules.

Notre analyse thermique des microcapsules par TGA (analyse thermogravimétrique) et DSC (calorimétrie différentielle à balayage) montre que les microcapsules sont stables jusqu'à une température d'environ 220°C, ce qui est bien au-dessus de la limite de température habituelle de fabrication/traitement des polymères avancés et de leur composite aérospatial structure.

La capacité d'auto-guérison électrique des microcapsules CNT/5E2N a été évaluée en utilisant les échantillons fabriqués avec des adhésifs électroconducteurs argent/époxy (Eccobond 56 C) et incorporés séparément avec deux types de microcapsules. Des échantillons d'adhésifs argent/époxy conducteurs purs sans microcapsules ont également été fabriqués comme référence. Des circuits en pont de Wheatstone ont été installés sur les échantillons. Les tensions

de pont normalisées ont été mesurées et comparées pour évaluer l'efficacité de cicatrisation électrique des échantillons.

La figure 7 montre deux types d'échantillons électriquement conducteurs dont les chemins conducteurs ont d'abord été perturbés en introduisant un dommage/coupure (coupe avec une lame de rasoir) sur le chemin conducteur de sorte qu'aucun courant électrique ne puisse le traverser. Les échantillons ont ensuite été laissés intacts pendant 24 heures à température ambiante pour permettre l'auto-guérison.

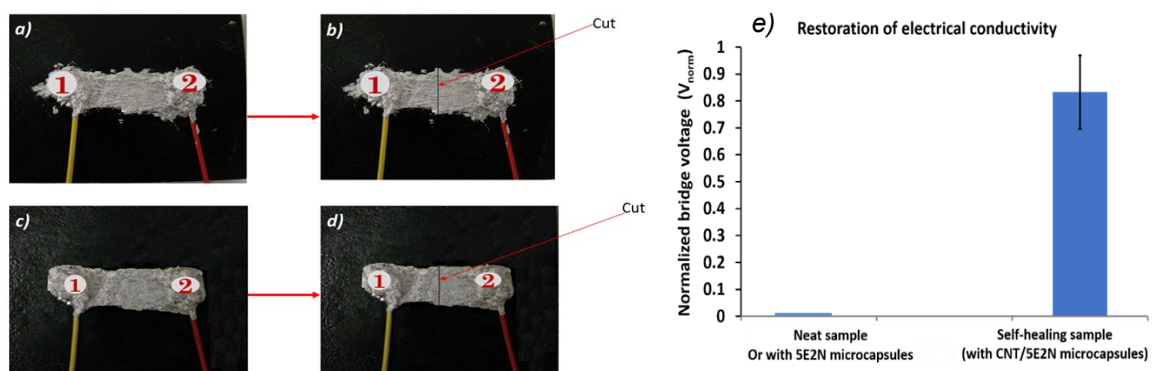


Figure 7. Circuits électriques en argent/époxy conducteur incorporés avec des microcapsules contenant du CNT/5E2N et un catalyseur de Grubbs pour le test de restauration de la conductivité électrique. Les tensions de pont ont été mesurées pour les échantillons purs (sans microcapsules) et auto-cicatrisants (avec microcapsules) avec a) et c) un chemin conducteur non coupé ; et b) et d) coupé entre les points 1 et 2 et après avoir laissé cicatriser pendant 24 heures à TA. e) Comparaison de la restauration de la conductivité électrique

Les échantillons qui ne contenaient pas de microcapsules ou ne contenaient que des microcapsules 5E2N, n'ont pas pu récupérer la conductivité. Les échantillons contenant la microcapsule CNT/5E2N se sont avérés capables de récupérer leur conductivité électrique, jusqu'à 82% de sa valeur nominale comme le montre la figure 7 (e).

Cela rend l'incorporation de CNT dans le monomère 5E2N pertinente pour restaurer la conductivité électrique et/ou les connexions à l'intérieur des circuits électroniques endommagés. Les microcapsules contenant de tels CNT peut ainsi permettre une meilleure réparation/restauration de composants électroniques clés et/ou de dispositifs optoélectroniques utilisés dans les structures aérospatiales avancées.

Chapitre 5 : Analyse de défaillance de l'époxy auto-cicatrisant à l'aide de CNT/5E2N microencapsulé

Dans ce chapitre, nous avons démontré la capacité d'auto-guérison mécanique du CNT/5E2N microencapsulé en tant qu'agent cicatrisant, lorsqu'il est intégré dans des époxyds soumis à deux modes de défaillance mécanique différents. La résistance mécanique des époxyds auto-cicatrisants a été mesurée pour le cisaillement du recouvrement et le mode de fracture normal menés en accord avec les normes établies [101, 209], et comparées les unes aux autres. Les résultats des tests mécaniques sont fortement étayés par une analyse fractographique approfondie, des mesures Raman et une étude préliminaire de la contribution des NTC à l'amélioration de la résistance mécanique du poly-5E2N produit par la réaction ROMP.

L'efficacité d'auto-guérison des polymères structuraux comme les époxyds est généralement évaluée en suivant quelques étapes simples. Premièrement, une propriété mécanique spécifique des échantillons époxy originaux/vierges incorporés avec les agents cicatrisants microencapsulés est évaluée. Ensuite, des dommages sont induits dans les échantillons en appliquant des charges mécaniques. Les dommages peuvent ensuite s'auto-cicatriser et la même propriété mécanique des échantillons est à nouveau évaluée après la cicatrisation. Enfin, l'étendue de la récupération des propriétés mécaniques sélectionnées est déterminée par l'efficacité de cicatrisation en tant que fraction des propriétés d'origine comme suit [222] :

$$\eta_{LS} = \frac{\tau_{healed}}{\tau_{virgin}} \text{-----[Eq. 3]}$$

Où η_{LS} est l'efficacité de cicatrisation pour les échantillons de cisaillement de recouvrement, τ_{virgin} est la résistance au cisaillement de recouvrement des échantillons originaux et τ_{healed} est la résistance de cisaillement de recouvrement des échantillons cicatrisés.

Encore [102, 212],

$$\eta_I = \frac{K_{IC_{healed}}}{K_{IC_{virgin}}} = \frac{P_{C_{healed}}}{P_{C_{virgin}}} \text{-----[Eq. 4]}$$

où, η_I est l'efficacité de cicatrisation pour la fracture de mode I des échantillons époxy avec la géométrie TDCB (Tapered Double Cantilever Beam), $K_{IC_{virgin}}$ est la ténacité à la rupture des échantillons originaux, et $K_{IC_{healed}}$ est la ténacité à la rupture des échantillons cicatrisés. $P_{C_{virgin}}$ est la charge critique de défaillance des échantillons originaux et $P_{C_{healed}}$ est la charge critique de défaillance des échantillons cicatrisés. Pour les échantillons de TDCB, la ténacité à la rupture est indépendante de la longueur de fissure [102, 212].

Pour les essais mécaniques de notre travail, trois types d'échantillons époxy ont été préparés. Pour les tests de rupture de mode I, il s'agit (i) d'échantillons de référence époxy purs, désignés comme TDCB (R) et préparés en mélangeant EPON 828 et épicro 3046 à une concentration de 100:47 ; (ii) des échantillons d'époxy auto-cicatrisables avec des microcapsules contenant du 5E2N uniquement, désignés comme TDCB (5E2N) et préparés en mélangeant EPON 828 et épicro 3046 à la même concentration et infusés avec 10 % en poids de microcapsules de 5E2N uniquement et 1% en poids de HG2 ; et (iii) des échantillons d'époxyde auto-cicatrisables avec des microcapsules contenant la suspension de CNT/5E2N, désigné comme TDCB (CNT/5E2N), préparés à l'aide d'un mélange 100:47 d'EPON 828 et d'épicro 3046, infusé avec 10% en poids de CNT/ 5E2N-microcapsules et 1% en poids de HG2. De même, pour les essais de cisaillement par recouvrement, les échantillons de cisaillement par recouvrement correspondants sont désignés par LS (R), LS (5E2N) et LS (CNT/5E2N) préparés avec la même composition que trois types d'échantillons de TDCB.

Les courbes charge-déplacement représentatives pour le premier chargement (échantillons ininterrompus) et le deuxième chargement (après cicatrisation) des trois types d'échantillons époxy dans des conditions de cisaillement par recouvrement et de fracture de mode I sont présentées à la figure 8. La figure 8 (a) fait référence aux essais de cisaillement par recouvrement et la figure 8 (b) aux essais de rupture en mode I.

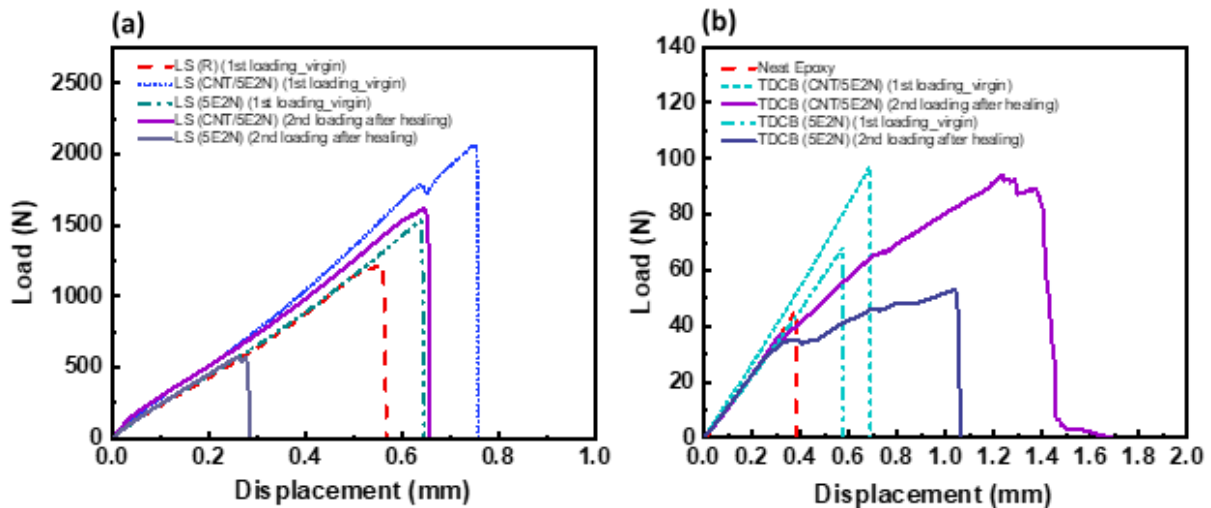


Figure 8. (a) Courbes charge-déplacement représentatives obtenues par des essais de cisaillement par recouvrement menés sur des échantillons LS (R), LS (5E2N) et LS (CNT/5E2N), et (b) des essais de rupture de mode I menés sur TDCB (R), TDCB (5E2N) et TDCB (CNT/5E2N)

Ces données montrent les caractéristiques générales des courbes charge-déplacement enregistrées pour tous les échantillons de référence [LS (R) et TDCB (R)] et auto-cicatrisants [LS (5E2N) et TDCB (5E2N)], ainsi que LS (CNT /5E2N) et TDCB (CNT/5E2N)]. Lors du premier chargement, souvent appelé « chargement vierge » dans la littérature [12, 13, 102, 133, 138, 167, 212], les échantillons, en général, entreprennent une charge proportionnellement croissante à mesure que le déplacement augmente. Au fur et à mesure que la charge approche du pic, la fissure/les dommages sont générés dans la résine époxy et se propagent à travers elle, entraînant sa défaillance complète. A ce stade, l'échantillon est séparé en deux parties et sa capacité de charge tombe à zéro. Les deux moitiés de l'échantillon endommagé sont ensuite mises en contact pendant 48 heures à TA pendant lesquelles la réaction d'auto-guérison se produit. Après cette période, on observe que les deux moitiés de l'échantillon sont collées ensemble. Les échantillons réassemblés sont ensuite chargés une deuxième fois (appelé « 2e chargement après cicatrisation » dans la figure 8 de la même manière que le premier chargement, afin de déterminer sa capacité de charge après cicatrisation. Être capable de supporter n'importe quelle charge pendant le deuxième chargement des échantillons après leur échec complet initial implique que l'auto-guérison s'est produite efficacement.

La figure 9 compare les efficacités de cicatrisation calculées selon l'éq. (3) et l'éq. (4) pour les échantillons LS et TDCB, respectivement.

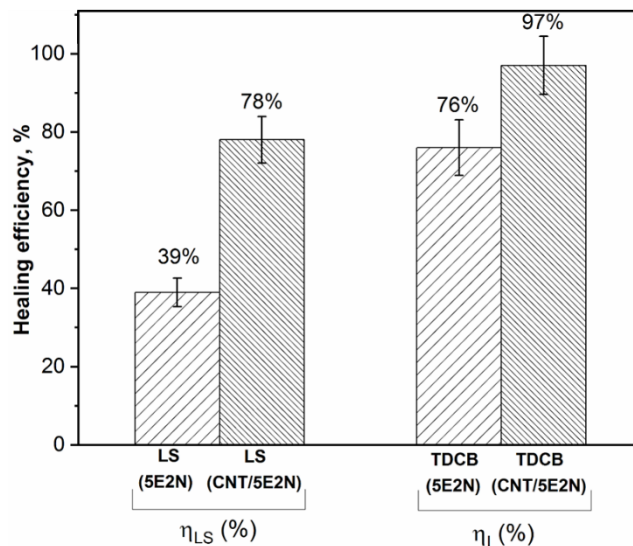


Figure 9. Comparaison des efficacités de cicatrisation des quatre types d'échantillons cicatrisés, LS (5E2N) (échantillons adhésifs époxy contenant des microcapsules 5E2N uniquement), LS (CNT/5E2N avec 0,1 % en poids de CNT) (échantillons adhésifs époxy contenant des microcapsules CNT/5E2N), TDCB (5E2N) (échantillons époxy TDCB contenant des microcapsules 5E2N uniquement) et TDCB (CNT/5E2N avec 0,1 % en poids de CNT) (échantillons époxy TDCB contenant des microcapsules CNT/5E2N)

La figure 9 montre que pour les tests de cisaillement par recouvrement, l'efficacité de cicatrisation moyenne atteinte par les échantillons LS (CNT/5E2N) était de 78% contre 39% pour les échantillons LS (5E2N). Pour les tests de fracture de mode I, en revanche, l'efficacité de cicatrisation atteinte par les échantillons TDCB (CNT/5E2N) était de 97% contre 76% pour les échantillons TDCB (5E2N).

L'imagerie SEM des surfaces réparées des échantillons de cisaillement et de TDCB est présentée dans les figures 10 (a) et 10 (b). La présence de deux canapés polymères distincts est mise en évidence sur les figures 10 (a) et 10 (b), qui ont également brisé leurs microcapsules qui ont libéré des agents cicatrisants du centre.

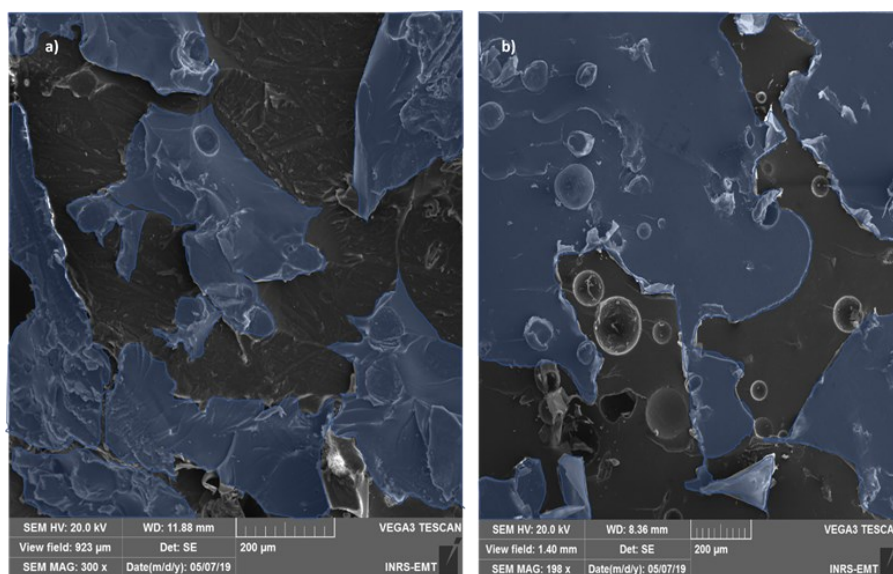


Figure 10. Micrographies SEM représentatives de la surface de fracture des échantillons auto-cicatrisés, (a) échantillon de cisaillement par recouvrement et (b) échantillon TDCB. La présence d'une couche de polymère auto-cicatrisée (poly-5E2N) est surlignée en bleu

Comme le montrent les spectres Raman présentés sur la figure 11 (a), la signature spectrale de la couche (surlignée en bleu sur la figure 10 présente un pic de phonon caractéristique à $1665,3 \text{ cm}^{-1}$, qui est lié au mode de vibration C=C de poly-5E2N [208]. Ce pic Raman confirme que les couches de polymère collectées sont du poly-5E2N, indiquant ainsi que la réaction d'auto-guérison (ROMP) a été activée à la surface de fracture des échantillons testés.

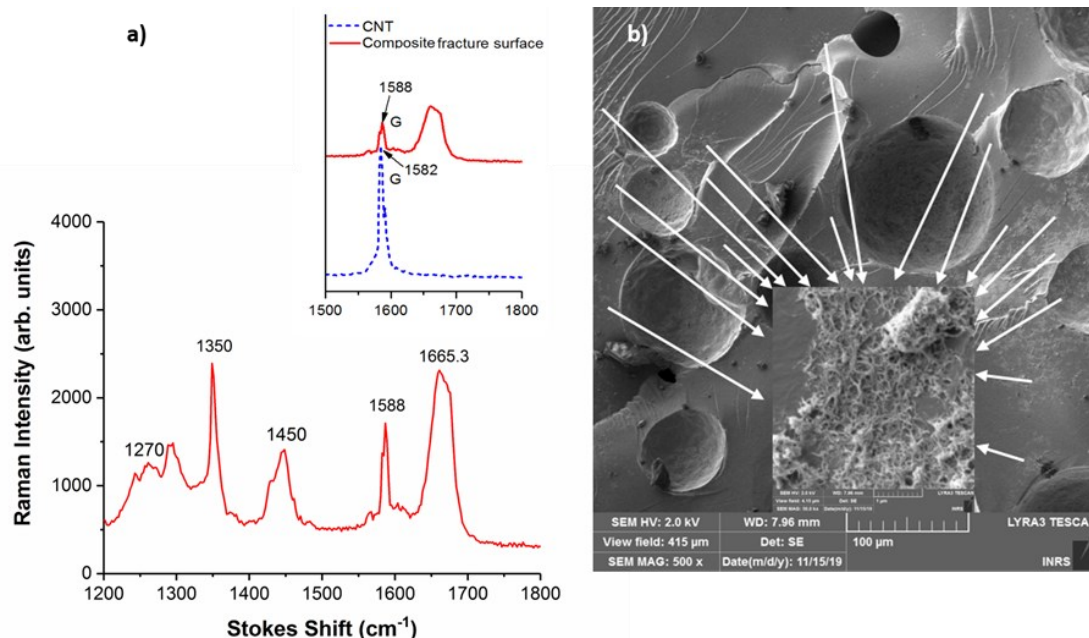


Figure 11. (a) Spectres Raman représentatifs générés par la surface de fracture des échantillons d'époxyde auto-cicatrisés. (b) La présence de CNT à la surface de fracture est indiquée par des flèches et montrée dans l'encart, avec un grossissement de 50000X. L'encart montre un léger décalage de la bande G du CNT

Les bandes Raman mesurées sur la figure 11 (a) peuvent être attribuées au mode d'étirement C-O de l'époxyde (1270 cm⁻¹) et à la vibration (1450 cm⁻¹) de la chaîne cyclique aromatique C=C respectivement, de la surface du polymère époxy hôte [232, 233]. Le signal Raman observé vers 1350 cm⁻¹ correspond à la bande D des CNT, dont la vibration hors plan est plus intense [203]. La bande G légèrement décalée des CNT située à 1588 cm⁻¹ fait référence à la vibration d'étirement de la liaison C-C dans le plan [232, 233]. Tous ces pics Raman confirment que les structures observées à la surface des échantillons époxy résultent du processus d'auto-cicatrisation des microcapsules CNT/5E2N.

Sur la figure 11 (b), des CNT sont également visibles à l'intérieur de la couche de poly-5E2N au niveau des surfaces de fracture des échantillons, où des microcapsules contenant la suspension de CNT/5E2N ont été incorporées. Cela montre que la suspension de CNT/5E2N a été libérée dans la surface de fracture à partir des microcapsules brisées, puis polymérisée avec succès par la réaction ROMP.

D'après les mesures Raman enregistrées à la surface de fracture de l'époxyde auto-cicatrisé (montré dans l'encart de la figure 11 (a), on observe qu'à l'intérieur de la région de l'échantillon

réparé, la bande G caractéristique du CNT pur situé à 1582 cm^{-1} est légèrement décalé à 1588 cm^{-1} . Selon Réf. [232], un décalage de 6 cm^{-1} du pic de la bande G vers les nombres d'onde inférieurs/supérieurs peut être associé à l'allongement/au raccourcissement axial de la longueur de liaison C-C à l'intérieur des enveloppes de nanotubes. La valeur de ces décalages caractéristiques pouvant être corrélée à la contrainte mécanique [232, 233], cela indique que les CNT libérés dans la fissure sont sollicités lors du chargement. Nous en déduisons qu'une telle situation peut faciliter un transfert de charge efficace via l'interface CNT/polymère. Les CNT dispersés dans le monomère liquide 5E2N agissent comme des renforts facilitant le transfert de contrainte de la matrice aux nanotubes dispersés lorsque les composés chimiques polymérisent en poly-5E2N par le biais de la réaction ROMP, qui est la clé de l'excellente performance de cicatrisation de l'époxy auto-cicatrisant incorporé avec des microcapsules contenant du CNT/5E2N. De plus, l'inclusion de charges NTC dans les fissures peut également affecter sa propagation [239] provoquant une augmentation de la ténacité.

D'après des simulations moléculaires et des calculs d'élasticité [236], la nature de l'interface entre les nanotubes et leur matrice environnante dépend des interactions électrostatiques et de Van der Waals, ainsi que des emboîtements mécaniques résultant du champ de contrainte interne et des contraintes/déformations qui en découlent. Du décalage entre les différents coefficients de dilatation thermique du NTC et du polymère [237, 238]. Lorsqu'elle est appliquée à nos matériaux, la liaison plus forte des CNT avec leur matrice environnante se traduit par une efficacité de cicatrisation plus élevée pour les époxy contenant des microcapsules CNT/5E2N par rapport à celles contenant 5E2N uniquement, comme le montre la figure 9.

Les conclusions et les perspectives

Dans notre travail, une analyse quantitative approfondie de la cinétique de réaction ROMP du système 5E2N/HG2 a été systématiquement menée de la température ambiante jusqu'à -30°C . En utilisant une analyse spectrale Raman, les constantes de vitesse apparentes pour les réactions à différentes basses températures ont été déterminées pour la cinétique du premier ordre en utilisant le principe d'Arrhenius. Les constantes de vitesse de réaction et l'énergie d'activation calculées à partir de notre méthode se sont avérées cohérentes avec les valeurs trouvées dans la littérature pour des réactions similaires. L'erreur quadratique moyenne et la fiabilité des mesures obtenues à basse température témoignent de la validité de la méthodologie développée dans ce travail pour la caractérisation cinétique quantitative de la réaction de polymérisation. Cela permet d'étudier les effets de divers facteurs sur la cinétique de

polymérisation de différents systèmes d'auto-guérison et de les optimiser en conséquence pour les rendre adaptés à des applications spécifiques.

Notre enquête sur la cinétique de polymérisation du 5E2N a confirmé que la réaction ROMP du 5E2N est déclenchée avec l'ajout d'une très faible concentration du catalyseur HG2, et seulement en quelques minutes pour des températures aussi basses que -30°C . Cette condition est représentative d'une limite de température basse à l'intérieur des satellites et autres instruments lancés dans l'espace. La faible énergie d'activation associée à la réaction ROMP implique que les agents cicatrisants 5E2N/HG2 peuvent être activés efficacement et, ainsi, devenir adaptés aux applications d'auto-guérison dans les environnements froids.

Dans la deuxième partie de notre travail, nous avons microencapsulé avec succès des CNT en suspension dans 5E2N dans des coques polymères en utilisant une méthode de polymérisation *in-situ*. Une procédure expérimentale d'essais et d'erreurs a été utilisée pour identifier les paramètres de processus appropriés qui permettent la formation réussie des microcapsules contenant CNT/5E2N. Une caractérisation thermophysique approfondie des microcapsules produites confirme la présence de NTC à l'intérieur du contenu liquide central des microcapsules, ainsi que leur libération lors de l'événement de rupture et de la polymérisation ultérieure, ce qui garantit leurs capacités d'auto-guérison efficaces.

Dans la dernière partie de notre travail, nous avons démontré une récupération efficace des propriétés électriques et mécaniques du polymère à base d'époxy incorporé avec les microcapsules contenant CNT/5E2N. Il a été démontré qu'un circuit électrique composé d'un polymère conducteur à base d'époxyde incorporé aux microcapsules contenant du CNT/5E2N restaure de manière autonome jusqu'à 82% de la conductivité électrique initiale après l'interruption du chemin conducteur des échantillons de polymère auto-cicatrisant. Un circuit électrique endommagé réalisé avec un polymère conducteur pur à base d'époxy sans les microcapsules ou avec des microcapsules contenant uniquement du 5E2N n'a pas restauré la conductivité de manière autonome. Cela rend l'incorporation de NTC dans le monomère 5E2N pertinente pour restaurer la conductivité électrique et/ou les connexions à l'intérieur des circuits électroniques endommagés. Les microcapsules contenant de tels CNT peut ainsi permettre la réparation autonome de composants électroniques clés et/ou de dispositifs optoélectroniques utilisés dans les structures aérospatiales avancées.

Pour les tests de rupture en mode cisaillement et en mode I, les microcapsules contenant du CNT/5E2N améliorent les propriétés mécaniques d'origine des époxydes auto-cicatrisants, ainsi que leurs propriétés mécaniques cicatrisées bien mieux que le cas des microcapsules ne

contenant que du 5E2N. Comme l'ont démontré les tests de cisaillement par recouvrement, l'efficacité de cicatrisation mécanique obtenue par les échantillons d'adhésif époxy était de 78% contre 39% pour les échantillons avec 5E2N seul. Les capacités d'auto-guérison s'avèrent encore plus efficaces en cas de fracture de mode I qu'en mode de chargement par cisaillement, affichant une efficacité de cicatrisation de 97% pour les microcapsules CNT/5E2N, contre 76% pour les microcapsules 5E2N uniquement. Notre analyse suggère que la dispersion de CNT dans le monomère 5E2N suivie d'une polymérisation *in-situ* favorise la formation de nanocomposites CNT/poly-5E2N. Il en résulte une interface plus forte et plus active entre le CNT et le polymère, ce qui est la clé des excellentes performances de cicatrisation de l'époxyde auto-cicatrisant incorporé avec des microcapsules contenant du CNT/5E2N. En outre, nous avons trouvé un renforcement significatif du polymère hôte incorporé avec des microcapsules CNT/5E2N en raison de la présence de CNT dans l'enveloppe externe des microcapsules. Nos résultats montrent qu'en plus d'agir comme un agent d'auto-guérison efficace, les microcapsules CNT/5E2N améliorent également la robustesse de l'époxyde durci, bien mieux que les microcapsules 5E2N seules.

Ces nouvelles microcapsules CNT/5E2N offrent des solutions d'auto-guérison uniques aux dispositifs/structures qui nécessitent la restauration de l'une ou des deux propriétés électriques et mécaniques avec un fonctionnement efficace même à basse température. Leur facilité d'intégration dans un grand nombre de polymères et leurs matériaux composites les rendent aptes à protéger et à prolonger la durée de vie des principales structures aérospatiales et des équipements et capteurs de télécommunications exposés à des événements accidentels et à des collisions avec de petits débris, ainsi qu'à des effets de vieillissement critiques qui peuvent causer des dommages et des défaillances irréversibles. L'utilisation de CNT/5E2N encapsulé pourrait également apporter une valeur ajoutée significative aux produits et dispositifs commerciaux nécessitant de longues périodes de fonctionnement à l'intérieur d'installations ou d'environnements où ils ne peuvent pas être réparés et/ou remplacés par de nouveaux. Des exemples de tels dispositifs/structures sont les antennes fluidiques flexibles, où la conductivité électrique et les propriétés mécaniques assurent leur fonctionnement efficace, à utiliser dans les systèmes radio de détection ou de surveillance sans fil, les commutateurs, les étiquettes d'identification par radiofréquence (RFID), les circuits conformes pour la surveillance de la santé ou dans d'autres applications militaires et spatiales.